DEVELOPMENT OF NON-LINEAR NUMERICAL MODELS APPROPRIATE FOR THE ANALYSIS OF JACK-UP UNITS

by

Richard Saint George Thompson

A thesis submitted for the degree of

Doctor of Philosophy

at the University of Oxford

Jesus College, Trinity Term 1996

ABSTRACT

Development of non-linear numerical models appropriate for the analysis of jack-up units

A thesis submitted for the degree of Doctor of Philosophy

Richard Saint George Thompson
Jesus College, Oxford
Trinity Term, 1996

Jack-up units have considerable economic significance because they are used to carry out a large proportion of the world's oil and gas exploration in water depths less than 90.0m. Due to the increase in use of jack-ups in harsher environments, analysis techniques assuming quasi-static and linear structural behaviour have had to be reassessed. This thesis is concerned with non-linear dynamic analysis methods appropriate for a jack-up assessment. Jack-up modelling requires realistic representation of the structure, the foundations and the environmental loading, together with the implementation of appropriate dynamic analysis algorithms. Techniques for each of these aspects of jack-up analysis are reviewed and the implementation of several of the methods in an advanced plane frame analysis program called JAKUP is described. Geometric non-linearity in the structure and work hardening plasticity at the foundations are accounted for in the program. Test cases are presented to verify the implementation of the methods and then some illustrative plane frame quasi-static and dynamic analyses are described. These simple models highlight the importance of accounting for dynamic motions in a jack-up analysis. For the quasi-static analyses, the assumption of pinned footing behaviour is seen to always result in the most conservative displacement and moment predictions. However, the analyses show that this is not always the case when dynamic amplification is accounted for.

ACKNOWLEDGEMENTS

I would like to thank my supervisors, Prof. Guy Houlsby and Dr. Martin Williams, for their invaluable guidance throughout the course of this research.

Special thanks must also be given to Dr. Chris Martin, Dr. Chris Brocklehurst, Dr. Matthew Kernot, Luan Ngo Tran, Dr. Brendan Ruck, Dr. Marcus Rutherford and Nicola Andrews for all their help. I am also indebted to my parents for all their support over the years.

NOTATION

SYMBOLS USED IN THESIS (excluding those only appearing in one location)

A	integration approximation matrix
A	member cross-sectional area
A_s	effective member shear area
B	transformation matrix
b_1, b_2	elastic bowing functions
b'_1, b'_2	derivatives of b_1 and b_2 with respect to q
$\overline{b_1}$, $\overline{b_2}$	modified b_1, b_2 including shear defomation
C	system or element damping matrix
c_{ij}	coefficient of system damping matrix
$\bar{c}$	wave celerity
C_1, C_2, C_3, C_4	footing flexibility coefficients
c_1, c_2	elastic stability functions
c'_1, c'_2	derivatives of c_1 and c_2 with respect to q
$\overline{c_1}$, $\overline{c_2}$	modified c_1, c_2 including shear deformation effects
c_b	length correction factor accounting for deformation due to bowing
$\overline{c_b}$	modified c_b including shear deformation effects
C_d, C_m	drag and inertia coefficient respectively
d	water depth
DA	dynamic amplification factor
e_1, e_2	parameters in yield surface function
E	Young's Modulus
F_s	nodal load vector consistent with the internal state of self stress
f	yield function
$f()$	function with arguments ()
F	force per unit length defined by Morison's equation
F_{wi}	horizontal wind force on block i
G	elastic shear modulus
h	horizontal displacement

H	horizontal load
H_{ult}	maximum horizontal load capacity
H	wave height
H_s	significant wave height
I	member second moment of area
J	Jordan form of A
K	system stiffness matrix
k	element stiffness matrix in local coordinates
k_{ij}	coefficient of system stiffness matrix
k	wavenumber
L	Load operator vector
L	member length
L	wavelength
M	System or element mass matrix
M	moment load
M_{ult}	maximum moment capacity
m_{ij}	coefficient of system mass matrix
N	number of degrees of freedom for the system
N_{c0}	vertical bearing capacity factor with respect to s_{u0}
P	nodal load vector
P	matrix of eigenvectors of A
ΔP^{i}	out-of-balance load vector
Q	member axial force
$q(x)$	distributed load at position x
q	dimensionless member axial force
R	footing radius
R_e	equivalent embedded footing radius
R_x	truncation error
r	modal load value
s	beam length in disturbed position
s_u	undrained shear strength
s_{u0}	undrained shear strength at footing level
S	matrix of local member end forces

$\dot{s}$, $\ddot{s}$	horizontal structural velocity and acceleration at a Gauss point
Sgn	function defining the sign of the drag force in Morison's equation
T	natural period
T	wave period
T_z	zero upcrossing period
t	time station with value t
u	member axial deflection
u	wave particle velocity in the x direction
u_c	current velocity
v	wave particle velocity in the y direction
V_s	shear force
V	vertical load
V_0	pure vertical load capacity
v_s	transverse displacement due to shear
v_{zi}	horizontal wind velocity at centre of block i
w	wave particle velocity in the z direction
x	vector of nodal displacements
x	x-coordinate of a point in a member
$\dot{x}$	vector of nodal velocities
$\ddot{x}$	vector of nodal accelerations
z	vertical displacement
z^e	vertical elastic footing penetration
z^p	vertical plastic footing penetration
α	sign of Sgn function
β	stability parameter in Newmark method
β_1, β_2	parameters in yield surface function
δ	dissipation parameter in Newmark method
Δ	(as prefix) increment in value
ζ_a	association parameter for determining vertical plastic displacement for a footing
η	wave surface elevation
θ	collocation parameter in Wilson-θ method

θ	rotational displacement
θ_{add}	additional member end rotation due to shear deformations
ξ	damping ratio
ξ	scalar determining size of footing plastic displacement increment
λ	eigenvalue
ρ	spectral radius
ρ	density of water
υ	Poisson's ratio
Φ	matrix of grouped eigenvectors
ϕ	potential function
ψ	shape function
ψ	stream function
Ω	frequency ratio
ω	angular forcing frequency
ω_d	damped angular frequency
ω_n	natural angular frequency

Superscripts

t	evaluated at time, t

Subscripts

i	i^{th} value
l	linear
s	secant
T	tangent (global coordinate system)
t	tangent (local coordinate system)

Prescripts

i	i^{th} iteration

CONTENTS

ABSTRACT

ACKNOWLEDGEMENTS

NOTATION

1 INTRODUCTION 1.1
- **1.1 General information on jack-up units** 1.1
- **1.2 Considerations in jack-up structural analyses** 1.3
- **1.3 The need for more research** 1.6
- **1.4 Aims of the present work** 1.7
- **1.5 Structure of thesis** 1.7

2 DYNAMIC ANALYSIS 2.1
- **2.1 Introduction** 2.1
- **2.2 Time domain versus Frequency domain** 2.1
- **2.3 Common direct integration algorithms** 2.3
  - 2.3.1 The central difference method 2.4
  - 2.3.2 The Runge-Kutta method 2.5
  - 2.3.3 The linear acceleration method 2.7
  - 2.3.4 The Newmark method 2.8
  - 2.3.5 The Wilson-θ method 2.9
  - 2.3.6 The Houbolt method 2.10
- **2.4 Stability** 2.11
- **2.5 Accuracy** 2.14
- **2.6 Mode superposition** 2.19
- **2.7 Non-linear analysis** 2.19
  - 2.7.1 Explicit methods 2.20
  - 2.7.2 Implicit methods 2.20
- **2.8 Direct integration in JAKUP** 2.21
  - 2.8.1 Non-linearities encountered in a jack-up analysis 2.22
  - 2.8.2 The linear acceleration method in JAKUP 2.22
  - 2.8.3 Convergence criteria 2.25
- **2.9 Test problems** 2.26
  - 2.9.1 A mass-spring-damper-system 2.27
    - 2.9.1.1 A linear system 2.27
    - 2.9.1.2 A non-linear system 2.31

3 THE STRUCTURAL MODEL 3.1
- **3.1 Introduction** 3.1
- **3.2 The stiffness matrix** 3.1
  - 3.2.1 The linear stiffness matrix 3.2
  - 3.2.2 Large deformation analysis 3.4
    - 3.2.2.1 Geometric non-linearity 3.4
    - 3.2.2.2 The element stiffness matrix 3.6
    - 3.2.2.3 Tracing the load-deflection path 3.7
    - 3.2.2.4 Beam-columns 3.9

3.2.2.5 Incremental formulation of beam-column theory 3.10
3.2.2.6 Deformation due to shear in the incremental formulation 3.14
3.2.2.7 Large deformation under dynamic analysis 3.16
3.3 The mass matrix 3.17
3.4 The damping matrix 3.19
3.4.1 Some common methods of defining a damping matrix 3.20
3.4.2 Damping in JAKUP 3.23
3.5 The Eigensystem 3.24
3.6 Test problems 3.26

4 THE SOIL MODEL 4.1
4.1 Introduction 4.1
4.2 Elastic behaviour of footings 4.2
4.2.1 The 100% fixity and zero fixity conditions 4.2
4.2.2 Partial fixity at the soil-structure interface 4.3
4.2.3 Elastic behaviour in JAKUP 4.7
4.3 Inelastic behaviour of footings 4.8
4.3.1 The Model B work hardening plasticity model 4.12
4.3.1.1 Elastic behaviour 4.13
4.3.1.2 Yield surface 4.13
4.3.1.3 Flow rule 4.15
4.3.1.4 Hardening law 4.16
4.3.2 Incorporation into an incremental structural analysis procedure 4.17
4.4 Performance of Model B 4.23
4.5 Test problems 4.24

5 ENVIRONMENTAL LOADING 5.1
5.1 Introduction 5.1
5.2 Wave theories 5.2
5.2.1 Formulation of the basic equations 5.2
5.2.2 Some common wave theories 5.6
5.2.2.1 Linear theory 5.7
5.2.2.2 Wheeler stretched Airy theory 5.8
5.2.2.3 Stokes finite wave amplitude theories 5.9
5.2.2.4 Stream function theory 5.11
5.2.2.5 Wave theories application 5.12
5.3 Current 5.13
5.4 Hydrodynamic loading 5.16
5.4.1 The formulation of the Morison equation in JAKUP 5.18
5.5 Wind loading 5.21
5.6 Test problems 5.23

6 STRUCTURAL ANALYSIS OF A TYPICAL JACK-UP 6.1
6.1 Introduction 6.1
6.1.1 A representative jack-up 6.1
6.1.2 Soil conditions and preloading of the jack-up 6.2

6.1.3 Environmental conditions and predictions of the jack-up fundamental period 6.4
6.1.4 Structural analyses 6.5
6.2 Analyses at a fixed wave height 6.7
6.2.1 Quasi-static analyses 6.8
6.2.1.1 Hull displacement 6.8
6.2.1.2 Lower guide moments 6.12
6.2.1.3 Conclusions: quasi-static analyses 6.14
6.2.2 Dynamic analyses 6.15
6.2.2.1 Maximum hull sidesway and maximum lower guide moment values 6.15
6.2.2.2 The double amplitude of the hull displacement and lower guide moments 6.19
6.2.2.3 Dynamic amplification of the hull displacement 6.20
6.2.2.4 Analyses with a more detailed finite element model 6.25
6.2.2.5 Conclusions: dynamic analyses 6.28
6.3 Analyses at a fixed wave period 6.28
6.3.1 Variation of the hull displacement with wave height 6.30
6.4 Conclusions: Quasi-static and dynamic analyses 6.32

7 CONCLUDING REMARKS 7.1
7.1 Introduction 7.1
7.2 Main findings 7.1
7.3 Areas for future research 7.5
7.3.1 Extension to 3-dimensions 7.5
7.3.2 Modelling of structural detail 7.5
7.3.4 Modelling cyclic behaviour at the footings 7.6
7.3.5 A footing model in 3-dimensions
7.3.6 Wave theories 7.6

REFERENCES
TABLES
FIGURES

CHAPTER 1

INTRODUCTION

1.1 General information on jack-up units

Self elevating mobile units, or jack-ups as they are commonly known, range in type from the liftboats and workboats, used in the Gulf of Mexico for example, to the more familiar exploration units used worldwide. The exploration units have considerable economic significance because they are used to carry out the majority of exploration for hydrocarbons in water depths less than 90m. The units can be subdivided in two basic categories, those that are mat supported and those that have independent legs. The mat supported units work in areas of soft soil with low bearing pressures and require a fairly level seabed for safe operation. The limiting seabed slope is approximately 1.5^0 (Wu & Chang, 1988). The independent leg units, which are the focus of this study, are used on firm or uneven soil and are fitted with a footing, commonly known as a spudcan, at the end of each leg. Although early designs of jack-ups could have as many as twelve legs (Breeden, 1990), the most common design today is that of the three leg jack-up. An example of such a unit is shown in Fig 1.1 and the side elevations of some typical spudcans are shown in Fig 1.2.

From 1969 to the late 1970s, jack-up design was dominated by the company Marathon Le Tourneau. Due to increasing economic demand, many other designs emerged after this period from such companies as Friede & Goldman and Mitsui. In 1990, the cost of harsh environment rigs ranged from $60 million to $140 million (Breeden, 1990). Bennett & Patel (1987) note that at that time most were designed for water depths up to 300ft (91.4m). Jack-up platforms are a type of gravity platform

because the method of fixation to the seabed is a result of reactions developed due to the rig self weight. The sharp protruding cone at the spudcan base (see Fig 1.2) aids initial location and provides additional horizontal stability. Once a jack-up platform has been towed to site, the legs are jacked down into the seabed until there is adequate bearing capacity for the hull to climb out of the water (Martin 1994). Water is then pumped into ballast tanks to give further soil penetration until the bearing capacity exceeds the maximum vertical reaction expected during the design storm. The process of preloading therefore acts as a proof test of the foundation. After preloading, the ballast tanks are emptied and the hull is jacked clear of the still water level by a distance larger than the maximum expected wave elevation. The distance between the still water level and the underside of the hull during operation is called the airgap and is typically in the region of 20m (NDA, 1987).

Until the early 1980s, these exploration units were only occasionally used as production units (Jensen *et al*, 1989). As a result, the reliability of jack-ups was not regarded as stringently as that of fixed offshore platforms, due to the high mobility and diverse applications of the jack-ups. However, this attitude began to change as jack-up units were increasingly used for year-round drilling. Also, the units began to be used in deeper water such as in the central to northern part of the North Sea, where the environmental conditions are harsher. Although it is likely that deep water fields in the future will be developed by floating production systems in combination with sub-sea systems (Karunakaran *et al*, 1992), the operational range of jack-ups are still being extended to water depths in excess of 100m. Hambly & Nicholson (1991) for example, foresaw a future generation of platforms operating in water depths of approximately 120m. It is therefore essential that a better understanding of their behaviour under environmental loading is gained.

1.2 Considerations in jack-up structural analyses

Before a jack-up is moved to a particular offshore site, a structural analysis must be performed to assess the ability of the unit to withstand a design storm. The loads from this design storm are factored to yield potentially conservative results. This is intended to give minimum factors of safety against certain failure conditions in order to conform to the standards of the regulatory body concerned. Although international standards vary, structural assessment is usually carried out for the 50 year design storm (Hambly & Nicholson, 1991). To perform the structural assessment, a conventional jack-up analysis assumes quasi-static behaviour with no foundation fixity (Hambly *et al*, 1990). Furthermore, linear structural behaviour is often assumed to trace load-deflection paths (Bennett & Patel, 1987). For jack-ups operating in shallow water, this form of simplified analysis can yield acceptable results because there is a significant separation between the natural period of the unit and the period of peak wave energy. Also, the associated wave heights are small compared with those expected in deeper water. This results in small displacements at the hull level. Under these conditions, the safety records of jack-ups have been respectable as the units are rarely subjected to loads approaching the design load.

As the rigs have moved into deeper water the offshore industry has had to reconsider this design approach. Due to the increase in effective leg length there has been an increase in the slenderness and flexibility of the structures, because the axial loads in the lattice legs due to the elevated hull weight causes them to act as beam-columns. This has several important consequences for jack-up structural analyses. The most important effect is that the natural period of the jack-up increases, so that there is a tendency for the principal natural period of the unit to approach that of the

dominant wave period in the seastate. Under these conditions the importance of dynamic amplification on the motions of the rig has to be taken into account. Also, due to the harsher environment, more of the non-linearities in the system have to be accounted for in order to perform a satisfactory structural analysis. These non-linearities can be grouped broadly into structural non-linearities, soil-structure interaction non-linearities and non-linear response induced due to non-linear hydrodynamic loading. Some pertinent issues raised by these additional factors include:

1) Due to the increase in leg flexibility and the eccentricity of the hull with respect to the centroid of the legs, the assumption of small displacement behaviour at the hull level is no longer valid. Furthermore, secondary moments are caused as a result of these hull deflections (the so called P-Δ effect). Chen *et al* (1991) note that two approaches, both based on linear theory, are usually used to account for these effects. The first approach incorporates additional bending moments calculated on the basis of the hull displacement determined through a linear analysis. This method does not account for the change in frequency characteristics of the structure. The second approach involves reducing the stiffness of each leg by the factor $(1 - Q/Q_E)$, where Q is the axial load caused by the hull weight and Q_E is the Euler buckling load. This approach does not account for the secondary moments caused due to the hull deflection. These methods are used in order to reduce the burden on computer time, however, in order to properly trace the load-deflection path, the use of a geometrically non-linear program is required.

2) The attention paid in recent years to the nature of spudcan interaction with the

seabed (*e.g* NDA, 1987; Santa Maria, 1988; Martin, 1994) shows that the assumption of zero foundation fixity is unrealistic. Accounting for foundation fixity also has consequences for jack-up analysis. Moment resistance at the soil-structure interface lowers the natural period of the unit with respect to the pinned model and therefore affects the dynamic characteristics. Also the stability of the jack-up is dependent on the long term moment capacity of the footings. Studies have shown that even conservative modelling of spudcan fixity can give up to a 40% reduction in the critical member stresses relative to the pinned model (Brekke *et al*, 1990). However, Jensen *et al* (1989) note that conventional jack-up analyses still continue to assume that the foundation offers no moment resistance under environmental loading.

3) Hydrodynamic loading on jack-up platforms is drag dominated and therefore of a non-linear nature. This drag dominance occurs due to the slender members used in jack-up leg designs (Karunakaran *et al* 1992). Furthermore the use of non-linear wave theories and free surface effects have an important effect on jack-up response. Nielsen *et al* (1994) note that integrating wave forces up to the instantaneous free surface makes the overturning moment and base shear vary with wave height to a power between 2.5 and 3, *i.e* a linear model is inaccurate. The non-linearities present in the hydrodynamic loading will invoke a non-linear structural response even if the structure itself acts as a linear system (Karunakaran & Spidsoe, 1995). These effects are important because non-linearities with respect to wave height play a large part in the probability of overturning for a jack-up (Jensen *et al*, 1989).

These three concerns only scratch the surface of all the issues involved in

harsh environment jack-up assessments. However, they serve to illustrate the complications in the analysis procedure.

1.3 Review of jack-up analysis procedures

Due to the issues discussed in Section 1.2, there has been an increasing amount of research into the behaviour of jack-ups since the mid 1980s. This section provides a brief review of the state-of-the-art in analysis procedures as applied to various aspects of the jack-up/environment system and some of the papers that give an indication of this position.

Some general comments are required before looking at the detail of analysis procedures. Firstly, it is difficult to divorce advances in jack-up analysis procedures from advances made in analysis techniques for the individual components of the jack-up system. For example, advances made in the geometric non-linear analysis of general space frames are pertinent to the jack-up industry. However, consideration is only given to analysis procedures that have been specifically applied to jack-up analyses.

Secondly, many authors make use of in-house company software which for commercial reasons is not available publicly. As a result, many papers report the various levels of sophistication included in the analysis procedure but do not discuss the method by which the effect was included in the analysis. A third noticeable feature from the literature is that there can be an over-concentration of analysis effort on one part of the system whilst paying scant attention to another part.

As noted in Section 1.2, an instructive jack-up analysis should address:

a) the inclusion of dynamic motions in the procedure

b) the effect of non-linear structural behaviour

c) the effects of foundation fixity and non-linear soil-structure interaction

d) the representation of the water particle kinematics and the effect of drag dominated wave loading on structural behaviour.

Each of these aspects is discussed separately below.

a) The solution of the dynamic equations of motion for the system can be performed in the time domain or the frequency domain. Greeves *et al* (1993) note that analysis in the frequency domain requires the response behaviour to be linearised. This results in the linearisation of the Morison equation, the exclusion of inundation effects and a linear structural and foundation representation. Empirical factors can be applied to approximate the effect of the non-linearities. However, by performing analysis in the time domain many of the non-linearities in the system can be modelled directly. Therefore, time domain methods remain the most robust and widely used analysis procedures (see Chpater 2). The disadvantages of the methods are connected with the burden on computer time and the need to perform multiple simulations for long durations during stochastic analyses.

b) Hoyle (1992) notes that the usual method of jack-up analysis involves the use of a simplified mathematical jack-up model. The term 'simplified' does not relate to the number of non-linear effects included in the procedure but refers to the level of structural detail modelled in the particular analysis (*i.e.* the level of discretization). Papers by Bennett & Patel (1989) and Brekke *et al* (1990) are representative examples of the use of simplified models. Bennet & Patel use a simplified 3-dimensional finite element model calibrated against model tests. Brekke *et al* (1990) calibrate their

model against measurements made on a jack-up operating at the Silver Pit location in the North Sea. Wave kinematics were applied to a detailed leg model and the resulting loads applied to the simplified numerical model. However, the structural behaviour is modelled as linear in both papers.

Due to the increasing power of digital technology, more recent papers have increased the sophistication of simplified numerical models by using a full geometrically non-linear structural algorithm. Such a procedure is used by Karunakaran *et al* (1992) for example. They report the implementation of geometric non-linearity as detailed by Przemieniecki (1968). This method accounts for large deformations as well as the effect of axial loads in the legs. As a result, the system stiffness matrix must be reformulated at each timestep.

There have also been advances in methods of modelling structural detail. Possibly one of the most advanced/detailed models is demonstrated by Lewis *et al* (1992) who use super-element techniques to carry out the analysis procedure. The super-elements are highly detailed finite element models of certain aspects of the structure (*e.g* connecting joints, deck plates) which are slaved to a set of master degrees of freedom. In this way complex finite element geometry are reduced to single specialised elements which reduces the number of degrees of freedom incorporated in the analysis. Lewis *et al* (1992) use a super-element model equivalent to a 4 million element model using standard finite elements, thereby giving a detailed representation of the structure. This method removes much of the uncertainty in defining equivalent stiffnesses for a simplified model because much of this detail is incorporated using the super-element technique. However, although no mention is made of whether the structural model is linear or non-linear, the foundations are represented as pinned joints and in addition, the analysis is quasi-static. The method

therefore represents a high level of structural modelling but neglects the influence of foundation behaviour and inertial effects.

c) As noted in the previous section, the conventional method of accounting for the soil-structure interaction is to model the foundations as pin joints. However, more sophisticated numerical methods of accounting for the soil-structure interaction have been suggested. Hambly *et al* (1990) and Hambly & Nicholson (1991) use a single degree of freedom model to calibrate a numerical simulation procedure against environmental conditions existing at the Arbroath site in the North Sea. The reduction of structural stiffnesses to a single degree of freedom model occurs at each timestep in order to facilitate the incorporation of non-linear vertical and rotational springs at the soil-structure interface. These non-linear springs represent a transition from initially elastic foundation behaviour at low load levels to non-linear foundation behaviour at larger load levels (see Chapter 4). This represents a more realistic representation of foundation behaviour than the use of pinned foundations. However, the structural behaviour is assumed linear in both cases (with the effect of axial load in the legs incorporated by reducing the leg stiffnesses by the factor $(1\text{-}Q/Q_E)$). In addition, although the single degree of freedom model yields results in a computationally efficient manner, certain effects, such as the variation in the height of application of the wave loading due to the varying free surface cannot be incorporated in the model directly, where instead the load is effectively applied at the hull level.

As noted in b), Karunakaran *et al* (1992) use a computer program which is reported to include geometric non-linear behaviour as implemented by Przemieniecki (1968). The program can also implement a kinematic work hardening model (*i.e.* with

nested yield surfaces) at the soil-structure interface. This program therefore has the potential to model all aspects of the system to a high level of sophistication. However, the procedure is applied to a specialised form of jack-up with piled foundations (*i.e.* the jack-up can no longer be classified as a gravity platform). Whilst this possibly represents the future generation of harsh environment jack-ups, the inclusion of piled footings meant that the non-linear footing model was not utilised in the analysis where instead calibrated linear springs were used.

A recent advance in the representation of non-linear foundation behaviour can be found in the work of Martin (1994) (see also Chapter 4). His jack-up analysis procedure incorporated non-linear foundation behaviour based on the principles of work hardening plasticity. His simplified jack-up structural model also incorporated geometric non-linear behaviour. However, the analyses were quasi-static and the environmental load was applied as two single point loads at the mean water level.

d) The inclusion of non-linear hydrodynamic effects such as the variation of the free water surface, relative motion effects and drag dominated non-linear loading are usually addressed by performing analyses in the time domain (Hoyle, 1992) in conjunction with the extended Morison equation (see Chapter 5). In addition, there is a great deal of on-going research dealing with the numerical representation of water particle kinematics and the variation of the free water surface (*e.g.* Tromans *et al*, 1991). However, in the jack-up industry, the two main approaches are the use of regular wave theories and irregular wave theories based on the summation of linear wave components.

If higher order regular wave theories are used (such as Stokes' fifth wave theory), the asymmetry of wave profiles about the mean water level can be accounted

for. However, the stochastic nature of the sea is not modelled. Greeves *et al* (1993) note that random sea-states are normally generated by the summation of linear wave components (thus losing the effect of the wave asymmetry) with randomly generated phase angles and amplitude components derived deterministically from the appropriate wave spectrum. This approach can be found in the work of Karunakaran *et al* (1992) for example. Tucker *et al* (1984) note that this approach does not truly model a random Gaussian process and propose a refined simulation method where the amplitude components are themselves Gaussian distributed random numbers. This hydrodynamic model is incorporated in the analysis procedure of Chen *et al* (1990). This work therefore represents one of the most sophisticated representations of the sea-state. However, as for Hambly *et al* (1990) the jack-up motions are approximated as those of a single degree of freedom oscillator. In addition, the effects of foundation fixity are not included in the model.

These examples demonstrate the advances made in jack-up analysis techniques but also highlight the diversity of non-linear effects accounted for. Concern about the variation of assessment practices around the world motivated the publication of the "Guideline for the Site Specific Assessment of Mobile Jack-up Units" (SNAME, 1993). This was an attempt to standardise assessment procedures in much the same way as the American Petroleum Institute's widely used "Recommended Practice for Planning, Designing and Constructing Fixed Offshore Platforms - Load and Resistance Factor Design" (API, 1993). However, even with these developments, jack-up analyses continue to use very different levels of complexity for different aspects of the analysis procedure. This is one of the issues that this thesis will address.

1.4 The need for more research

Leijten & Efthymiou (1989) cite extracts from the World Offshore Accident Databank and note that the frequency of operational accidents for jack-up platforms is much higher than that of fixed offshore platforms. Also, whereas the accident statistics for fixed offshore platforms have improved with time, those for jack-up platforms have worsened. The degradation in reliability coincided with the increase in use of jack-ups in deeper waters. Of all the accidents resulting in the total loss of a platform, 50% were directly attributable to structural or foundation failure. It is clear that a better understanding of the behaviour of jack-ups is needed. Not only will this avoid some of the catastrophic effects such as accidents, but it will also lead to more confidence in jack-up reliability in harsher environments. This therefore warrants continual evaluation of jack-up analysis techniques.

1.5 Aims of the present work

This thesis is concerned with analysis techniques applicable to the non-linear dynamic analysis of jack-up platforms. Often, jack-up analyses can involve great detail on one aspect of the analysis (*e.g* the structure) whilst ignoring another. One of the major aims of the project was to develop all aspects of the analysis procedure to approximately the same degree of rigour. This thesis describes analysis techniques implemented in an advanced frame analysis program called JAKUP. Several techniques are reviewed for each aspect of the analysis. Then, the methods are applied to the analysis of a simple jack-up numerical model. Although seastates are multidirectional in nature, the present work is limited to plane frame analyses. Therefore, all loading occurs along an axis of symmetry for the jack-up.

1.6 Structure of thesis

Chapter 2 presents an overview of some common methods of integrating the dynamic equations of motion in the time domain. Issues of the stability and accuracy of the methods are raised, and from this discussion two methods are chosen for implementation in JAKUP. The form of the integration methods in JAKUP is then presented and simple test problems are analysed to demonstrate the implementation.

Chapter 3 presents an overview of some different methods of numerically modelling a structure. This is separated into three sections. In the first section, the formulation of the stiffness matrix is discussed. An advanced method for tracing the load-deflection path of a structure undergoing large nodal displacements is described and the resulting forms of the equations in JAKUP are presented. In the second section, some consideration is given to the representation of the inertial properties of a structure. Similarly, the third section details some methods for representing the damping properties of the structure. After these sections the eigensystem is considered. Although uncoupled modal solutions are not sought in this thesis, the initial eigensystem still proves a useful aid to the analysis procedure. Some test problems are then considered to demonstrate the implementation of the equations considered in the chapter.

Chapter 4 presents a brief overview of methods used to trace the load-deflection path at the foundation. Then the equations for a new work hardening plasticity model for clay called Model B (Martin, 1994) are considered in some detail. Some test cases are then demonstrated to validate the implementation.

Chapter 5 discusses the means by which the environmental loads are incorporated into the structural analysis procedure. There are a multitude of possibilities for

predicting the water particle kinematics in a seastate. The present work is however confined to regular wave loading and therefore regular wave theories. Some consideration is also given to wind loading and then some test cases are presented.

Chapter 6 applies all the theories developed numerically in Chapters 2 to 5 to the analysis of a typical jack-up rig operating in 90m water depth. Both quasi-static and dynamic analyses are carried out at a fixed wave height and differing wave periods and a fixed wave period and differing wave heights.

Finally **Chapter 7** discusses the main conclusions from the work and suggests areas requiring further work.

CHAPTER 2

DYNAMIC ANALYSIS

2.1 Introduction

This chapter presents an overview of some of the methods used for direct integration of the equations of motion for a discretized system. The assumptions about the variation of the time derivatives of the nodal displacements during a timestep are presented for some of the most common methods, followed by a discussion of the merits of each method. Further development of the methods used in JAKUP is presented and finally some test results are discussed.

2.2 Time domain versus Frequency domain

The equations of motion for an N degree of freedom dynamic system can be expressed in the form:

$$M^t\ddot{x}^t + C^t\dot{x}^t + K^t x^t = P^t \tag{2.1}$$

where M^t, C^t and K^t are the secant mass, damping and stiffness matrices respectively at time t. The variable P^t is the vector of external applied nodal loads at time t and x^t is the nodal displacement vector. A dot above a variable signifies the differential of that variable with respect to time. Eqn 2.1 represents a set of N coupled second order differential equations. These can represent a linear system (with time invariant coefficient matrices) or a non-linear system (with time varying coefficient matrices). For a linear system, standard procedures for solution exist, usually involving the transformation of the equations into an uncoupled form. This transformation involves a change of basis from the physical coordinate system to the normal coordinate

system. This is achieved by orthogonalizing the equations of motion with respect to a set of N orthogonal vectors which are normally the eigenvectors of the system. Now the response in as many modes as are of interest can be found by a closed form solution (if the nature of the loading permits) or in a numerical manner. If there is sufficient separation between the forcing frequency and a modal frequency, then some of the higher modes can be neglected. This is because these modes will be underexcited and will not contribute significantly to the overall response. The overall response is then found by the linear superposition of the modal responses. The numerical solution can be performed in the time domain, using the Duhamel integral for example. Alternatively, solutions may be obtained in the frequency domain where Fast Fourier Transforms and Inverse Fast Fourier Transforms can be used. For large systems with many degrees of freedom, approximate methods have been developed largely to produce better computational efficiency. However, the key to this modal approach remains the applicability of the principle of superposition which in turn depends on linearity.

For a non-linear system, the eigensystem is constantly changing and the principle of superposition is no longer valid. As a result, much of the elegance of solution is removed. In the frequency domain, linearisation techniques are sometimes employed, for example Borgman linearisation for the drag term in the Morison equation (see Chapter 5) for offshore loading applications. Borgman linearisation replaces the non-linear drag term by a mean value and a sinusoidally varying component. Traditional frequency domain techniques cannot, however, truly model a non-linear system. Vugts (1990) notes that whilst advances in the field of non-linear frequency domain analysis have been made, this still remains an analytical tool of the future.

An analytical approach must therefore be sought that has the capacity to deal with both linear and non-linear equations. The most robust approach involves operating on Eqn 2.1 in the time domain using a direct integration technique. Direct integration methods satisfy Eqn 2.1 at discrete time stations t at intervals Δt, using a numerical step-by-step procedure. The term 'direct' implies that no transformation of the equations into another form is undertaken before the equations are solved. It is this approach that is used in JAKUP.

2.3 Common direct integration algorithms

In the following sections it is assumed that the equations of motion have been solved for the discrete times up to and including time t and that solution is now sought at time $t + \Delta t$. Direct integration methods are derived by assuming some form of variation for displacement, velocity and acceleration within a timestep. This therefore permits approximations to the nodal displacement time derivatives to be made. The variations generally come from two sources. These are, the use of various finite difference formulae and differing truncation points in the Taylor series:

$$f(t+\Delta t) = f(t)+\Delta t\frac{df(t)}{dt} + \frac{\Delta t^2}{2!}\frac{d^2f(t)}{dt^2} + \frac{\Delta t^3}{3!}\frac{d^3f(t)}{dt^3} +... \tag{2.2}$$

Direct integration methods can be classified as either explicit or implicit methods.

Explicit methods result in Eqn 2.1 being formulated at time t. As a result, the stiffness matrix is not a coefficient of the unknown displacement vector and, with certain approximations, efficient solutions can be obtained (see Section 2.3.1). Iteration is not required for non-linear systems.

Implicit methods result in Eqn 2.1 being formulated at time $t + \Delta t$. In this case, the stiffness matrix is a coefficient of the unknown displacement vector. As a

result, implicit methods reduce directly to a quasi-static analysis if C^t and M^t are both null matrices. However, any procedures utilising the pivot points of these null matrices (*e.g* matrix inversion) will have to be eliminated from the solution algorithm during a quasi-static solution. For a dynamic analysis, iteration is required for non-linear systems unless the equations are linearised over the timestep (see Section 2.3.3).

The following sections contain the equations for six common integration methods. These are, the central difference method, the Runge-Kutta method, the linear acceleration method, the Newmark method, the Wilson-θ method and the Houbolt method. Some consideration will then be given to the stability and accuracy characteristics of some of the direct integration methods.

2.3.1 The central difference method

The central difference method (Bathe, 1982; Barltrop & Adams, 1991) is an explicit integration algorithm. It uses the finite difference formulae:

$$\ddot{x}^t = \frac{1}{\Delta t^2}\left(x^{t-\Delta t} - 2x^t + x^{t+\Delta t}\right) \tag{2.3}$$

$$\dot{x}^t = \frac{1}{2\Delta t}\left(-x^{t-\Delta t} + x^{t+\Delta t}\right) \tag{2.4}$$

As the discrete solution is known up to time t, the only unknown in Eqn 2.3 and Eqn 2.4 is the displacement, $x^{t+\Delta t}$. Substituting Eqn 2.3 and Eqn 2.4 into Eqn 2.1 gives the equilibrium equation at time t:

$$M\left[\frac{1}{\Delta t^2}\left(x^{t-\Delta t} - 2x^t + x^{t+\Delta t}\right)\right] + C\left[\frac{1}{2\Delta t}\left(-x^{t-\Delta t} + x^{t+\Delta t}\right)\right] + Kx^t = P^t \tag{2.5}$$

It is assumed in Eqn 2.5 that the system is linear, so that M, C, and K are time

invariant secant matrices. Rearrangement of Eqn 2.5 gives the equation:

$$\left(\frac{1}{\Delta t^2}M + \frac{1}{2\Delta t}C\right) x^{t+\Delta t} = P^t - \left(K - \frac{2}{\Delta t^2}M\right)x^t - \left(\frac{1}{\Delta t^2}M - \frac{1}{2\Delta t}C\right)x^{t-\Delta t} \quad (2.6)$$

A solution for $x^{t+\Delta t}$ can now be obtained from Eqn 2.6. Bathe (1982) notes that the main reason for using this method is for computationally efficient solutions to large systems. However, this efficiency depends on the use of a diagonal mass matrix and the neglect of the system damping matrix. It can be seen from Eqn 2.6 that, under these conditions, because the stiffness matrix is not a coefficient of the unknown displacement vector, only matrix multiplication is needed to obtain a solution. These properties are preserved if a diagonal damping matrix is used. However, this does not allow much control over the system damping. Numerical work conducted by Kreig & Key (1973) suggests that a finer finite element mesh is needed when utilising a diagonal mass matrix as opposed to a consistent mass matrix (see Section 3.3) to preserve the frequency characteristics of the structural system under consideration. Whether this increase in the number of degrees of freedom to be solved is outweighed by increased computational efficiency will obviously vary from analysis to analysis. When using the central difference method the solution at $t = 0$ requires knowledge of the displacement $x^{-\Delta t}$, therefore a special startup algorithm is needed in order to begin the integration. The central difference method is known as a multi-step method for this reason (Nickell, 1973).

2.3.2 The Runge-Kutta method

The Runge-Kutta method (Barltrop & Adams, 1991; Thomson, 1993) is an explicit method. It makes use of the relationships:

$$\ddot{x}^{t+\tau} = M^{-1}\left(P^{t+\tau} - Kx^{t+\tau} - C\dot{x}^{t+\tau}\right) \quad (2.7)$$

$$\dot{x}^{t+\tau} = \dot{x}^{t} + \ddot{x}^{t}\tau \tag{2.8}$$

$$x^{t+\tau} = x^{t} + \dot{x}^{t}\tau \tag{2.9}$$

where $0 \leq \tau \leq \Delta t$. Eqn 2.7 is a rearrangement of the equilibrium equation, Eqn 2.1. Barltrop & Adams (1991) note that for a single degree of freedom system, because each timestep is partially divided, the Runge-Kutta method yields a more accurate solution than the central difference method. Eqns 2.7, 2.8 and 2.9 are all evaluated at the beginning, middle and end of each timestep. Therefore τ takes the values 0, $\Delta t/2$ and Δt respectively. At $\tau = \Delta t/2$, Eqns 2.8 and 2.9 are evaluated in two ways. In the first case:

$$\dot{x}_1^{t+\Delta t/2} = \dot{x}^{t} + \ddot{x}^{t}\Delta t/2 \tag{2.10}$$

$$x_1^{t+\Delta t/2} = x^{t} + \dot{x}^{t}\Delta t/2 \tag{2.11}$$

By substitution into Eqn 2.7 an estimate of the mid-timestep acceleration is found, $\ddot{x}_1^{t+\Delta t/2}$. However, Eqn 2.8 and 2.9 are then re-evaluated giving:

$$\dot{x}_2^{t+\Delta t/2} = \dot{x}^{t} + \ddot{x}_1^{t+\Delta t/2}\Delta t/2 \tag{2.12}$$

$$x_2^{t+\Delta t/2} = x^{t} + \dot{x}_1^{t+\Delta t/2}\Delta t/2 \tag{2.13}$$

which are used to gain another value for acceleration, $\ddot{x}_2^{t+\Delta t/2}$. The values $x_2^{t+\Delta t/2}$, $\dot{x}_2^{t+\Delta t/2}$ and $\ddot{x}_2^{t+\Delta t/2}$ are then used to gain an estimate of displacement, velocity and acceleration values at the end of the timestep (*i.e* $\tau = \Delta t$). Using Simpson's rule, the four values of acceleration (*i.e* one at t, two at $t + \Delta t/2$ and one at $t + \Delta t$) are used to

obtain a better estimate of the velocity change over the timestep. Similarly, the four values of velocity are used to gain an improved estimate of the displacement change over the timestep. The timestep constraint (see Section 2.4) necessary for multi degree of freedom systems is more restrictive than that of the central difference method. However, each timestep requires considerably more calculation, so the additional complexity makes the solution procedure inefficient compared to other methods.

2.3.3 The linear acceleration method

The linear acceleration method (Timoshenko & Gere, 1961; Clough & Penzien, 1975; Boswell & D'Mello, 1993) is an implicit method. It assumes a constant non zero gradient for the acceleration during a timestep. This leads to the assumptions:

$$\dot{x}^{t+\Delta t} = \dot{x}^{t} + \ddot{x}^{t}\Delta t + \frac{\ddot{x}^{t+\Delta t} - \ddot{x}^{t}}{2}\Delta t \tag{2.14}$$

$$x^{t+\Delta t} = x^{t} + \dot{x}^{t}\Delta t + \ddot{x}^{t}\frac{\Delta t^2}{2} + \frac{\ddot{x}^{t+\Delta t} - \ddot{x}^{t}}{6}\Delta t^2 \tag{2.15}$$

Substituting Eqn 2.14 into Eqn 2.15 and rearranging gives:

$$\dot{x}^{t+\Delta t} = [3/\Delta t](x^{t+\Delta t} - x^{t}) - [\Delta t/2]\ddot{x}^{t} - 2\dot{x}^{t} \tag{2.16}$$

Substituting Eqn 2.16 into Eqn 2.14 gives:

$$\ddot{x}^{t+\Delta t} = [6/\Delta t^2](x^{t+\Delta t} - x^{t}) - [6/\Delta t]\dot{x}^{t} - 2\ddot{x}^{t} \tag{2.17}$$

Eqn 2.16 and Eqn 2.17 are in terms of the unknown variable $x^{t+\Delta t}$ and known variables at time t. By substituting Eqns 2.16 and Eqn 2.17 into Eqn 2.1, the equations of

motion are formulated at time $t + \Delta t$, and can be solved for $x^{t+\Delta t}$. Both Clough & Penzien (1975) and Boswell & D'Mello (1993) cast Eqn 2.1, Eqn 2.16 and Eqn 2.17 in an incremental form. This method approximates secant slopes as tangent slopes (see Fig 2.1) and linearises the equations over a timestep. In this way, these analysts apply the algorithm to both linear and non-linear systems without iteration. As will be seen in Section 2.7, other factors must also be taken into account when considering the formulation of direct integration operators in iterative or non-iterative form. The linear acceleration assumptions for a linearized system become:

$$\Delta \dot{x}^t = \ddot{x}^t \Delta t + \Delta \ddot{x}^t \frac{\Delta t}{2} \tag{2.18}$$

$$\Delta x^t = \dot{x}^t \Delta t + \ddot{x}^t \frac{\Delta t^2}{2} + \Delta \ddot{x}^t \frac{\Delta t^2}{6} \tag{2.19}$$

Where Clough & Penzien (1975) differ from some other analysts is that at the beginning of each timestep they reimpose the total equilibrium condition:

$$\ddot{x}^t = M^{-1} (P^t - Kx^t - C\dot{x}^t) \tag{2.20}$$

instead of using:

$$\ddot{x}^t = \ddot{x}^{t-\Delta t} + {}^{(t-\Delta t)}\Delta \ddot{x} \tag{2.21}$$

This process avoids the accumulation of errors from timestep to timestep.

2.3.4 The Newmark method

The Newmark method (Newmark, 1959), is an implicit method. It has variable coefficients β and δ which can be changed to achieve optimum stability, accuracy and

dissipative characteristics (see Section 2.5). The assumptions are:

$$\dot{x}^{t+\Delta t} = \dot{x}^{t} + [(1 - \delta)\ddot{x}^{t} + \delta\ddot{x}^{t+\Delta t}]\Delta t \tag{2.22}$$

$$x^{t+\Delta t} = x^{t} + \dot{x}^{t}\Delta t + [((1/2) - \beta)\ddot{x}^{t} + \beta\ddot{x}^{t+\Delta t}]\Delta t^{2} \tag{2.23}$$

When $\beta = 1/6$ and $\delta = 1/2$, the relationships defined in Eqn 2.22 and Eqn 2.23 correspond to the linear acceleration method. When $\beta = 1/4$ and $\delta = 1/2$, Eqns 2.22 and 2.23 become the unconditionally stable constant acceleration method (Craig, 1981; Timoshenko & Gere, 1961; Barltrop & Adams, 1991). The constant acceleration method is also known as the Newmark $\beta = 1/4$ method. By algebraic manipulations similar to the formulation of Eqns 2.16 and 2.17, the equations of motion can be formulated at time $t + \Delta t$, and solved for $x^{t+\Delta t}$. The method requires no special start-up requirements.

2.3.5 The Wilson-θ method

The Wilson-θ method (Wilson *et al,* 1973) is an implicit method and is directly related to the linear acceleration method. A control variable (θ) is introduced in order to maximise stability and dissipative characteristics. This type of method (first introduced by Wilson and his co-authors) is known as a collocation method. This is because it satisfies the equations of motion outside the time increment at the θ or *collocation* point. A linear variation of acceleration is assumed over an extended time increment, $\theta\Delta t$. This leads to the formulation of the equations:

$$\dot{x}^{t+\tau} = \dot{x}^{t} + \ddot{x}^{t}\tau + \frac{\ddot{x}^{t+\theta\Delta t} - \ddot{x}^{t}}{2}\frac{\tau^{2}}{\theta\Delta t} \tag{2.24}$$

$$x^{t+\tau} = x^{t} + \dot{x}^{t}\tau + \ddot{x}^{t}\frac{\tau^{2}}{2} + \frac{\ddot{x}^{t+\theta\Delta t} - \ddot{x}^{t}}{6}\frac{\tau^{3}}{\theta\Delta t} \tag{2.25}$$

where $0 < \tau < \theta\Delta t$ and $\theta \geq 1$.

Like the Newmark method, no special start up schemes are required as the variables at time $t+\theta\Delta t$ are expressed in terms of quantities at time t only. If $\theta = 1.0$, the method reduces to the linear acceleration method. Normally, the value $\theta = 1.4$ is used for reasons discussed in Section 2.4. A linearly projected load vector is calculated for each extended timestep, *i.e.*:

$$P^{t+\theta\Delta t} = P^t + \theta\,(P^{t+\Delta t} - P^t) \tag{2.26}$$

2.3.6 The Houbolt method

The Houbolt method (Houbolt, 1950) is similar to the central difference method in that it uses finite difference equations. However, unlike the central difference method, it is implicit and unconditionally stable. The two backward difference expansions used are:

$$\ddot{x}^{t+\Delta t} = \frac{1}{\Delta t^2}(2x^{t+\Delta t} - 5x^t + 4x^{t-\Delta t} - x^{t-2\Delta t}) \tag{2.27}$$

$$\dot{x}^{t+\Delta t} = \frac{1}{6\Delta t}(11x^{t+\Delta t} - 18x^t + 9x^{t-\Delta t} - 2x^{t-2\Delta t}) \tag{2.28}$$

By substituting Eqn 2.27 and Eqn 2.28 into Eqn 2.1, a solution for $x^{t+\Delta t}$ can be obtained. The Houbolt method requires a special start-up scheme because the equations of motion formulated at time $t+\Delta t$ require knowledge of variable values at time t, $t-\Delta t$ and $t-2\Delta t$. Therefore, along with the central difference method, it can also be classified as a multi-step method.

2.4 Stability

In Section 2.3.2, it was noted that the Runge-Kutta method has a timestep constraint in order to achieve stability. It is useful at this juncture to consider the implications of stability for the use of the integration methods. In general, explicit direct integration methods are conditionally stable and implicit methods are unconditionally stable. The exception in the methods presented in Section 2.3 is the linear acceleration method. This is an implicit method but is only conditionally stable. It can, however, be modified to unconditional stability as the Wilson-θ method with appropriate selection of θ. If a method is conditionally stable then the length of timestep used for the algorithm is constrained to be a fraction of the smallest natural period of the system. If the timestep is larger than this value then, for a linear system, errors at the beginning of the analysis (due to inaccuracy and round off) will grow without bound and render the solution useless. For some non-linear systems, the loss of the solution stability may not be obvious. This is because the solution may be partly stable and partly unstable, but the solution will be grossly in error. Unconditionally stable algorithms do not have this timestep constraint. Initial errors will not grow without bound during the integration period in all linear cases and in some (but not all) non-linear cases. This does not mean, however, that a solution calculated with an arbitrarily large timestep will necessarily be accurate.

Craig (1981) and Bathe (1982) examine the stability of some of the more common integration methods for a linear system. For a linear system, Eqn 2.1 can be uncoupled, therefore stability can be examined with respect to one row of the orthogonalized equations. A typical equation can be expressed in the form:

$$\ddot{x}^t + 2\xi\omega\dot{x}^t + \omega^2 x^t = r^t \tag{2.29}$$

where ξ is the modal damping ratio, ω is the modal angular frequency and r is the modal load. This equation can be expressed in the form of an integration approximation and a load operator. Therefore:

$$\hat{x}^{t+\Delta t} = A\hat{x}^{t} + L(r^{t+\nu}) \tag{2.30}$$

where, A is the integration approximation matrix, L is the load operator vector and ν is 0, Δt or $\theta\Delta t$ depending on the integration method being reviewed (see Section 2.3). The rows of $\hat{x}^{t+\Delta t}$ are separated from the corresponding row of $\hat{x}^{t}$ by the time interval Δt. Expressed in a recursive form, Eqn 2.30 yields:

$$\begin{aligned}\hat{x}^{t+n\Delta t} = {} & A^{n}\hat{x}^{t} + A^{n-1}L(r^{t+\nu}) + A^{n-2}L(r^{t+\Delta t+\nu}) + \ldots \\ & + AL(r^{t+(n-2)\Delta t+\nu}) + L(r^{t+(n-1)\Delta t+\nu})\end{aligned} \tag{2.31}$$

As an example, the central difference method can be expressed in the integration approximation and load operator form:

$$\begin{bmatrix} x^{t+\Delta t} \\ x^{t} \end{bmatrix} = A \begin{bmatrix} x^{t} \\ x^{t-\Delta t} \end{bmatrix} + Lr^{t} \tag{2.32}$$

where:

$$A = \begin{bmatrix} \dfrac{2 - \omega^2\Delta t^2}{1 + \xi\omega\Delta t} & -\dfrac{1 - \xi\omega\Delta t}{1 + \xi\omega\Delta t} \\ 1 & 0 \end{bmatrix} \tag{2.33}$$

and:

$$L = \begin{bmatrix} \dfrac{\Delta t^2}{1 + \xi\omega\Delta t} \\ 0 \end{bmatrix} \tag{2.34}$$

The stability of the functions is determined by examining the behaviour of the numerical solution for arbitrary initial conditions. If $r^{t} = 0$ in Eqn 2.29, then Eqn 2.31 becomes:

$$\hat{x}^{t+n\Delta t} = A^{n}\,\hat{x}^{t} \tag{2.35}$$

Stability can now be determined by finding the spectral decomposition of A, which takes the form:

$$A^n = P J^n P^{-1} \tag{2.36}$$

where P is a matrix of the eigenvectors of A and J (the Jordan form of A) has the eigenvalues λ_i of A on its diagonal. The spectral radius of A is $\rho(A)$, it is defined as:

$$\rho(A) = \max|\lambda_i| \quad i=1,2,... \tag{2.37}$$

For stability J^n must be bounded for $n \rightarrow \infty$. This will happen if $\rho(A) \leq 1$. Stability therefore depends only on the eigenvalues of the approximation operator and the smaller $\rho(A)$, the more rapid is the convergence of the numerical solution. Fig 2.2 (from Bathe, 1982) shows plots of $\Delta t/T$ *vs.* $\rho(A)$ at $\xi = 0.0$ for the central difference, Newmark $\beta = 1/4$, Wilson-θ and Houbolt methods. (Numerical studies conducted by Weeks (1972) show that small changes in ξ do not generally affect the stability characteristics.) The Newmark $\beta = 1/4$, Wilson-θ and Houbolt methods all demonstrate stability across the entire range of $\Delta t/T$ values considered. These methods are unconditionally stable. For the Wilson-θ method, the value of θ in Fig 2.2 is 1.4. A stability plot of spectral radius against θ shows that the Wilson-θ method is only unconditionally stable if $\theta > 1.37$. The value $\theta = 1.4$ is chosen as this is conventionally considered to give the optimum stability and accuracy characteristics. Fig 2.2 shows that the Houbolt method is the most stable algorithm with the lowest $\rho(A)$ for all $\Delta t/T$ values considered. Similarly, the Wilson-θ method displays lower $\rho(A)$ values than the Newmark $\beta = 1/4$ method over much of the $\Delta t/T$ range considered.

Fig 2.2 also shows that the central difference method exhibits instability for $\Delta t/T > 1/\pi$. As solution is achieved by superposition of modal responses, T must

represent the smallest period of the system. Clough & Penzien (1975) note that the linear acceleration method is also conditionally stable and do not apply a timestep larger than $T/10$. The Runge-Kutta method has a stability range similar to the central difference method (Barltrop & Adams, 1991).

2.5 Accuracy

Bathe (1982) considers the accuracy of the unconditionally stable integration methods considered in Section 2.3. For one row of the uncoupled equations of motion (Eqn 2.29), the initial value problem considered is:

$$\ddot{x}' + \omega^2 x' = 0 \tag{2.38}$$

with:

$$x^0 = 1.0 \quad \dot{x}^0 = 0.0 \quad \ddot{x}^0 = -\omega^2 \tag{2.39}$$

which has the closed form solution, $x' = \cos\omega t$. The variables used to quantify the soluton error are period elongation and amplitude decay (dissipation) and Fig 2.3[a] and [b] show Bathe's plots of these variables against $\Delta t/T$. For the Wilson-θ method, the value $\theta = 1.4$ is used. Fig 2.3[a] and [b] show that the Newmark method (in the constant acceleration form) is the most accurate of the algorithms, introducing the smallest period elongation and no amplitude decay. The Houbolt method yields the least accurate results, introducing the most amplitude decay and period elongation over all values of $\Delta t/T$.

The introduction of amplitude decay is not necessarily disadvantageous. The reason for this is linked to the discretization process which can often model the high modes poorly. Nickell (1973) notes that structural vibration problems are almost always dominated by the low frequency components of the response because the

energy requirements to excite the higher modes is so severe. In a system where the timestep is chosen such that these higher and less important modes are not accurately integrated, amplitude decay acts as a filter to solution errors introduced due to the high frequency response. The Newmark method (*i.e.* with variable β and δ) was deliberately conceived to introduce this inaccuracy into the solution (Hilber & Hughes, 1978). In the Newmark method, δ can be adjusted to give parametric control over the amount of dissipation in the system (Kreig & Key, 1978). The Newmark family become dissipative if $\delta > 1/2$. When $\delta \leq 1/2$, this dissipation is reduced to zero. With the value $\delta = 1/2$, β is adjusted to 1/4 to maintain unconditional stability.

The collocation parameter in the Wilson-θ method similarly affords control over the degree of dissipation. The value, $\theta = 1.4$ is normally used because this gives the optimum collocation position for accuracy and stability amongst the Wilson-θ family. However, unlike the Newmark method, the dissipation in the Wilson-θ method cannot be continuously reduced to zero whilst maintaining unconditional stability (Hilber & Hughes, 1978). In fact the Wilson-θ method with zero dissipation yields the equations for the linear acceleration method (a member of the Newmark family with $\beta = 1/6$ and $\delta = 1/2$) which is conditionally stable. Numerical studies of the Wilson-θ method conducted by Goudreau & Taylor (1973) also show that this method has a tendency to significantly overshoot exact solutions to initial value problems in the early part of the response when large timesteps are involved. This is directly indicative of the behaviour of the higher modes in a multi degree of freedom problem. Due to this effect, the Wilson-θ method is generally seen as unsuitable for the analysis of problems involving impact or suddenly applied loads. Overshoot is an inherent problem in collocation methods of direct integration. It is not highlighted by a conventional stability or accuracy analysis because it is related to the norm of the

integration approximation matrix, A, introduced in Section 2.4. Even though the A matrix can have a small spectral radius, it is still possible for it to have a large norm. Analyses conducted by Hilber & Hughes (1978) show that the effect is absent from the Newmark method.

A noticeable disadvantage of the Houbolt method is that the degree of numerical dissipation is not controllable. Therefore, the numerical decay introduced into finite element problems is somewhat arbitrary. Numerical studies conducted by Hilber *et al* (1977) show that the Houbolt method's numerical dissipation can often affect the low modes too strongly. This aptly demonstrates the trade off between increased stability and reduced accuracy. As noted in Section 2.3, the Houbolt method (like the central difference method) requires a start-up algorithm. Fig 2.3[a] and 2.3[b] were obtained by Bathe (1982) using the closed form solution for the first two timesteps. Hilber & Hughes (1978) note that this need for a start-up algorithm vastly complicates the issue of an accuracy analysis. This is because the starting procedure as well as the solution procedure must be analysed. Furthermore, the interaction of the algorithm with all possible values generated by the starting procedure must be analysed. This is important because the long term accuracy of a step by step integration method is intrinsically linked to the history of the solution up to the present time station. Similarly, no conclusion can be drawn about overshoot for non-self starting algorithms because the effect depends on the interaction with the chosen start-up algorithm.

The discussions so far have concentrated on the 'accuracy' of the unconditionally stable direct integration methods. The available literature tends to view accuracy analysis from the perspective of diminishing the high mode response whilst accurately integrating the low mode response. It is for this reason that there

appears to be little published research investigating the accuracy of conditionally stable methods with respect to unconditionally stable methods. For example, Bathe (1982), Bathe & Wilson (1973), Kreig (1973) and Nickell (1971) examine the stability of conditionally and unconditionally stable methods but eliminate the conditionally stable methods from the ensuing accuracy analyses. The reason for this, as noted earlier, is that there is a trade off between accuracy and stability. The timestep constraint of a conditionally stable method which is linked to the smallest period of the system means that all the modes are automatically integrated with little period elongation or amplitude decay. As a result the type of arguments presented in the preceding paragraphs are now largely redundant in relation to conditionally stable methods. Similarly, the effect of overshoot is not studied in conjunction with explicit integration methods. This is because in the range of timestep values considered, the explicit methods will be operating beyond their stability limits. However, within a very limited timestep range, some comparisons can still be made.

In numerical studies on a damped harmonic oscillator conducted by Weeks (1972) with a timestep $1/25^{th}$ of the fundamental natural period, the central difference method yielded results indistinguishable from the closed form solution whilst the Newmark $\beta = 1/4$ and Houbolt methods both displayed noticeable period elongation. In turn, Barltrop & Adams (1991) note that the Runge-Kutta method is more accurate than the central difference method due to the divided timestep. This divided timestep implies that the algorithm essentially operates at half the user defined timestep. It is this additional computational work that means that methods solving one set of equations per timestep are used in preference to Runge-Kutta type algorithms.

Similarly, Timoshenko *et al* (1974) examine the accuracy of the Newmark $\beta = 1/4$ method with respect to the linear acceleration method. For the Newmark

method, the displacement expansion defined in Eqn 2.23 has $x^{t+\Delta t}$ on the left hand side and $\ddot{x}^{t+\Delta t}$ on the right hand side expanded as Taylor series. By subtraction this leads to a truncation error, R_x. For the Newmark $\beta = 1/4$ method the principal term of the truncation error is:

$$R_x = \frac{\Delta t^3}{12}\frac{d^3x^t}{dt^3} \tag{2.40}$$

A similar process with the linear acceleration method gives the principal term to the truncation error as:

$$R_x = -\frac{\Delta t^4}{24}\frac{d^4x^t}{dt^4} \tag{2.41}$$

This means that the linear acceleration method is more accurate than the Newmark method. As both methods are non-dissipative, the linear acceleration method must therefore introduce less period elongation. This naturally assumes that the linear acceleration method is operating within its stability limit. An increase in $\Delta t/T$ will result in amplification of the high mode response errors as opposed to dissipation (a sign of instability).

From the preceding arguments, it can immediately be seen that the issue of accuracy is not as clearly defined as the issue of stability. Krieg & Key (1973) note that even period elongation or diminution introduced by numerical integration methods can sometimes be used to compensate for errors introduced by the discretization process. They discourage the idea of conducting an accuracy analysis for an integration method remotely from the corresponding finite element discretization. As an example, for a bar equation with a linear shape function field (see Section 3.2.1), they note that the combination of a diagonal mass matrix (see Section 3.3) and the Newmark $\beta = 1/4$ method is disadvantageous because in this case, both the diagonal

mass assumption and the integration assumption underpredict the frequency contents in the modes. Another example with the bar equation shows that the central difference method in conjunction with the diagonal mass matrix gives optimum results when operating at the critical timestep and yields less accurate results as the timestep is reduced. Remseth (1979) argues against the introduction of numerical damping due to the integration algorithm used. The high mode dissipation in his numerical studies is achieved by the control of the structural damping properties. This is discussed further in Section 3.4.

2.6 Mode superposition

As noted in Section 2.2, the equations of motion for a linear system can be uncoupled by orthogonalizing Eqn 2.1 with respect to the system eigenvectors. As a result the response in any mode can be found using any of the direct integration algorithms discussed in Section 2.3. With N uncoupled equations, the integration timestep can be chosen for each mode individually. In a linear system, this is one way to avoid the rigid timestep constraint for conditionally stable methods as the numbers of modes to be integrated is now user defined.

2.7 Non-linear analysis

All of the direct integration algorithms in the preceding sections are also applicable to non-linear analysis. In a non-linear system, the natural periods are themselves a function of time. For conditionally stable methods, the critical timestep must be a fraction of the smallest natural period to be found throughout the entire analysis. Mode superposition will now only work if the eigensystem is found at every timestep. This renders it impractical unless system properties are changing very slowly.

2.7.1 Explicit methods

Explicit algorithms result in the equations of motion being formulated at time t. As a result, these methods do not require iteration.

2.7.2 Implicit methods

Implicit algorithms result in the equations of motion being formulated at time $t+\Delta t$ and therefore iteration is required for a satisfactory solution. It is common to use a form of Newton-Raphson iteration. Bathe (1982) gives the form of the equations of motion for an implicit, modified Newton-Raphson iterative solution for a system with no damping and constant mass. The equations of motion are expressed:

$$M\ {}^{(i)}\ddot{x}^{t+\Delta t} + K_T^t \Delta x^{(i)} = P^{t+\Delta t} - {}^{(i-1)}F_s^{t+\Delta t} \tag{2.42}$$

where:

$${}^{(i)}x^{t+\Delta t} = {}^{(i-1)}x^{t+\Delta t} + \Delta x^{(i)} \qquad {}^{(0)}x^{t+\Delta t} = x^t \tag{2.43}$$

K_T^t is the tangent stiffness matrix at time t, F_s is the vector of nodal loads consistent with the internal state of self stress and the superscript (i) denotes the i^{th} iteration.

As noted in Section 2.3.3, Clough & Penzien (1975), Timoshenko *et al* (1974) and Craig (1981) formulate their implicit equations of motion in a linearized non-iterative form. This is however, directly analagous to stopping the iterative process at $(i) = 1$ and using a timestep small enough so that changes in the system properties over a timestep are minute.

2.8 Direct integration in JAKUP

Of the six methods discussed in Section 2.3, the linear acceleration method and the Newmark method are implemented in JAKUP. For the Newmark method, the parameters $\beta = 1/4$, $\delta = 1/2$ are used (*i.e.* the constant acceleration method). Therefore, JAKUP allows the choice between a conditionally stable and an unconditionally stable algorithm. Where all modal responses are required to high accuracy, the linear acceleration method is used. When the reponse in high modes is not required to high accuracy, the Newmark $\beta = 1/4$ method is used with a suitable choice of timestep. These two algorithms are used because:

1) They are both single-step methods unlike the central difference method and the Houbolt method.

2) They do not suffer from overshoot as does the Wilson-θ method. This is important as some impulse load tests are carried out (see Chapter 6).

3) Because the mass matrix and damping matrix contain non-diagonal terms (see Chapter 3), both methods are computationally more efficient than the Runge-Kutta method.

In light of the preceding comments, however, it should be noted that any single-step method could be implemented in JAKUP in the future without undue difficulty.

Sections 2.8.1-2.8.3 outline the implementation of an integration method within JAKUP to accomodate the non-linearites that are encountered. The arguments are developed for the linear acceleration method only as developments for the Newmark $\beta = 1/4$ method are very similar.

2.8.1 Non-linearities encountered in a jack-up analysis

The main sources of non-linearity in a jack-up analysis are due to the hull deflections which give rise to P-Δ effects, non-linear soil-structure interaction effects and drag dominance in the Morison equation integrated up to the water surface. Large deformation behaviour in JAKUP is implemented as an Eulerian formulation of beam-column theory that results in geometric non-linearity. This is discussed in Chapter 3. Non-linear soil behaviour in JAKUP is implemented as a work hardening plasticity model called Model B. This gives the option of adding 3x3 stiffness matrices at the soil-structure interface representing the stiffness response of a jack-up footing on clay. For a further discussion of the soil-structure interaction, see Chapter 4. Wave loading in JAKUP makes use of some of the regular theories in conjunction with the Morison equation. For a discussion of wave loading, see Chapter 5.

2.8.2 The linear acceleration method in JAKUP

Numerical work conducted by Oran & Kassimali (1976) examines the dynamic geometric non-linear response of a single beam fixed at both ends. The system contains no damping, the mass matrix is diagonal and a point load is applied suddenly at mid-span. The results show that there is a substantial loss of solution accuracy when the equations of motion are solved without iteration. The influence of timestep size is not examined. Numerical work conducted by Weeks (1972) on the same system shows that the inherent stability of unconditionally stable methods in a linear analysis can be retained in a non-linear analysis, provided some form of iteration is performed. For either of the integration methods in JAKUP, there is the option of using it in either iterative or non-iterative form. This can be applied to linear or non-linear analysis with or without Model B footings present. For a purely linear system,

the solution is not improved by iteration during a timestep, but may be improved by a reduction in the size of the timestep. For a non-linear system, a combination of both dictates the accuracy.

The basic equations for the linear acceleration method are given in Section 2.3.3. If iteration is used, the equations of motion are not linearised over the timestep. As both integration methods used are implicit, Eqn 2.1 is formulated at time $t+\Delta t$ which gives:

$$M^{t+\Delta t}\ddot{x}^{t+\Delta t} + C^{t+\Delta t}\dot{x}^{t+\Delta t} + K^{t+\Delta t}x^{t+\Delta t} = P^{t+\Delta t} \tag{2.44}$$

where $M^{t+\Delta t}$ now represents the sum of the linear structural mass and non-linear added mass matrix, and $C^{t+\Delta t}$ is the sum of the linear structural damping matrix and the time varying hydrodynamic damping matrix. Eqn 2.44 assumes that the coefficient matrices are secant matrices. This is true for the mass and damping matrices as the non-linear components arise due to use of the extended Morison equation (see Chapter 5). The stiffness matrix formulation, however, results in the formulation of a tangent stiffness matrix at each timestep. The iterative form of Eqn 2.44 is expressed as:

$${}^{(i-1)}M^{t+\Delta t}\,{}^{(i)}\ddot{x}^{t+\Delta t} + {}^{(i-1)}C^{t+\Delta t}\,{}^{(i)}\dot{x}^{t+\Delta t} + \left[\,{}^{(i-1)}F_s^{t+\Delta t} + {}^{(i-1)}K_T^{t+\Delta t}\,{}^{(i)}\Delta x\right] = P^{t+\Delta t} \tag{2.45}$$

where Δx is the displacement correction vector and:

$${}^{(0)}M^{t+\Delta t} = M^t \tag{2.46}$$

$${}^{(0)}C^{t+\Delta t} = C^t \tag{2.47}$$

$${}^{(0)}K_T^{t+\Delta t} = K_T^t \tag{2.48}$$

and:

$${}^{(0)}F_s^{t+\Delta t} = F_s^t \tag{2.49}$$

Expressing Eqn 2.16 in iterative form gives:

$${}^{(i)}\dot{x}^{t+\Delta t} = [3/\Delta t]({}^{(i)}x^{t+\Delta t} - x^t) - [\Delta t/2]\ddot{x}^t - 2\dot{x}^t \tag{2.50}$$

Similarly, Eqn 2.17 can be expressed as:

$$ {}^{(i)}\ddot{x}^{t+\Delta t} = [6/\Delta t^2]({}^{(i)}x^{t+\Delta t} - x^t) - [6/\Delta t]\dot{x}^t - 2\ddot{x}^t \tag{2.51} $$

By expressing ${}^{(i)}x^{t+\Delta t} = {}^{(i-1)}x^{t+\Delta t} + {}^{(i)}\Delta x$ and substituting Eqn 2.50 and Eqn 2.51 into Eqn 2.45, the iterative equations of motion become:

$$ {}^{(i-1)}M^{t+\Delta t}\left[[6/\Delta t^2]({}^{(i-1)}x^{t+\Delta t} + {}^{(i)}\Delta x - x^t) - [6/\Delta t]\dot{x}^t - 2\ddot{x}^t\right] $$

$$ + {}^{(i-1)}C^{t+\Delta t}\left[[3/\Delta t]({}^{(i-1)}x^{t+\Delta t} + {}^{(i)}\Delta x - x^t) - [\Delta t/2]\ddot{x}^t - 2\dot{x}^t\right] $$

$$ + {}^{(i-1)}F_s^{t+\Delta t} + {}^{(i-1)}K_T^{t+\Delta t}\,{}^{(i)}\Delta x = P^{t+\Delta t} \tag{2.52} $$

which are a set of equations in the base unknown ${}^{(i)}\Delta x$. Because the time-varying components of the mass and damping matrix vary at the wave period, any changes in these matrices during an iteration are small because the change in nodal displacement during a timestep is small compared to the wavelength. Therefore, the Newton-Raphson procedure is applied in a modified form. Using this assumption, the equations of motion can now be rearranged to give:

$$ \left[{}^{(i-1)}K_T^{t+\Delta t} + [6/\Delta t^2]M^t + [3/\Delta t]C^t\right]{}^{(i)}\Delta x = P^{t+\Delta t} + M^t\left[\frac{6}{\Delta t}\dot{x}^t + 2\ddot{x}^t + \frac{6}{\Delta t^2}(x^t - {}^{(i-1)}x^{t+\Delta t})\right] $$

$$ + C^t\left[2\dot{x}^t + [\Delta t/2]\ddot{x}^t + [3/\Delta t](x^t - {}^{(i-1)}x^{t+\Delta t})\right] - {}^{(i-1)}F_s^{t+\Delta t} \tag{2.53} $$

In JAKUP these are solved using Gauss-Jordan elimination to find the first approximation to the new system configuration. It can now be seen that if ${}^{(i)}\Delta x$ is taken as the final solution, the equations above reduce to the linearised incremental form of the equations of motion as used by Clough & Penzien (1975). This is because:

$$ P^{t+\Delta t} - [M^t\ddot{x}^t + C^t\dot{x}^t + F_s^t] = P^{t+\Delta t} - P^t \tag{2.54} $$

2.8.3 Convergence criteria

The first iteration of the displacement vector is found by solving Eqn 2.53 and summing the resulting incremental displacement vector and the existing displacement vector. The internal force vector corresponding to the internal state of self stress can then be computed. This internal load vector must satisfy the relationship:

$$\textit{Internal Load} = \textit{External Applied Load} - \textit{Inertial Load} - \textit{Damping Force} \tag{2.55}$$

In general, however, this equality is not satisfied and an out-of-balance force is computed. This gives the expression:

$$\textit{Out of Balance Load} = \textit{External Applied Load} - \textit{Inertial Load} - \textit{Damping Force} - \textit{Internal Load} \tag{2.56}$$

A new tangent stiffness matrix corresponding to the present system configuration is then formed. This is used in Eqn 2.53 along with the out-of-balance load vector to find a new displacement correction vector ${}^{(i)}\Delta x$. The subroutine that calculates the Model B footing entries to the tangent stiffness matrix is therefore called upon to operate in two modes. In its first mode, a footing matrix is generated depending on the present position of the footing. In its second mode, the incremental changes in the footing loads corresponding to an incremental change in the footing displacements are calculated, together with a new footing stiffness matrix for the present configuration. The importance of at least one iteration can be demonstrated by the case when an elastoplastic footing tries to unload elastically from the yield surface. If an increment is elastoplastic then the subroutine assumes that the next increment will be elastoplastic and calculates an appropriate elasto-plastic footing matrix. If during the first iteration a negative value of ξ (indicating attempted elastic unloading from the yield surface, see Chapter 4) is encountered the footing is allowed to become elastic

again and the initial incremental displacement vector must then be recalculated.

As in Martin (1994) the solution is deemed to have converged when:

$$\sqrt{\frac{\Sigma(\Delta x)^2}{\Sigma(x^2)}} \leq tol \tag{2.57}$$

where, *tol* is a user specified tolerance. The joint rotations and translations are grouped separately and each group must separately satisfy Eqn 2.57. At the beginning of the next timestep the total equilibrium condition is reapplied such that:

$$\ddot{x}^t = M^{-1}[P^t - F_s^t - C\dot{x}^t] \tag{2.58}$$

as opposed to:

$$\ddot{x}^t = \ddot{x}^{t-\Delta t} + \Delta\ddot{x}^{t-\Delta t} \tag{259}$$

This procedure helps to prevent the accumulation of errors. Because the solution accuracy is dictated by the size of the timestep, it is possible that for a particular value of timestep the tolerance cannot be met. In this case, the timestep value must be reduced.

2.9 Test problems

Validating the implementation of a step-by-step integration method is intrinsically linked to the system properties it encounters. Therefore the majority of the numerical tests presented in Chapters 3 to 5 are also to be considered as test problems relevant to this chapter. However, an initial indication of the implementation of the methods can be derived by considering a few simple examples. The tests performed in Section 2.9.1 are not meant to represent a comprehensive stability or accuracy analysis of the linear acceleration or Newmark method. Such work is outside the scope of this thesis.

Instead, the tests performed give an indication of the type of behaviour that can be expected from each method. With confidence established in a particular integration technique, any future integration methods can be validated by comparison with some of the more complex problems presented in later chapters.

2.9.1 A mass-spring-damper system

2.9.1.1 A linear system

A simple but useful mass-spring-damper system to analyse is shown in Fig 2.4. The natural period of the system is 0.2s and all system properties are linear. Under harmonic loading, a closed form solution for the displacement is available. This solution is:

$$x(t) = e^{-\xi\omega_n t}\,(A\,\sin\omega_d\,t + B\,\cos\omega_d\,t) + (P/K)\,D_A^2\,[(1 - \Omega^2)\,\sin\omega t - 2\xi\Omega\,\cos\omega t] \tag{2.60}$$

where, K is the spring stiffness, ω is the forcing frequency, ω_n is the natural frequency, ω_d is the damped natural frequency, $\Omega = \omega/\omega_n$, ξ is the damping ratio and D_A (the dynamic amplification factor) can be expressed as:

$$D_A = \frac{1}{\sqrt{(1 - \Omega^2)^2 + (2\xi\Omega)^2}} \tag{2.61}$$

The coefficients A and B for an arbitrary starting displacement and velocity can be expressed as:

$$A = \frac{(\dot{x}^0 + \xi\omega_n B) - (1 - \Omega^2)(PD_A^2\omega/K)}{\omega_d} \tag{2.62}$$

$$B = (2\xi\Omega PD_A^2/K) + x^0 \tag{2.63}$$

For an overdamped system, $\sin\omega_d t$ and $\cos\omega_d t$ in Eqn 2.60 are replaced by $\sinh(\omega_d t)$

and $\cosh(\omega_d t)$ respectively. Similarly, ω_d changes from $\omega_n(1 - \xi^2)^{1/2}$ for an underdamped system to $\omega_n(\xi^2 - 1)^{1/2}$ for an overdamped system.

Fig 2.5 shows the displacement response for the undamped free vibration problem defined by $P = 0$, $\xi = 0$, $x^0 = 1.0$m and $\dot{x}^0 = 0$. The closed form solution is superposed on the numerical results predicted by both the linear acceleration method and the Newmark $\beta = 1/4$ method implemented in JAKUP. The integration timestep used is 0.005s (*i.e.* $\Delta t/T = 1/40$). Fig 2.5 shows that the linear acceleration method is visually indistinguishable from the closed form solution and that the Newmark method begins to show some period elongation in the latter part of the response. However, this graph indicates that for a small timestep, both methods will converge on the correct solution. Fig 2.6[a] shows the same initial value problem integrated with a timestep of 0.013s ($\Delta t/T = 1/15$). Fig 2.6[b] shows the same responses over a reduced timescale. This graphs demonstrates that the linear acceleration method introduces no amplitude decay but that it does introduce period elongation. However, the Newmark $\beta = 1/4$ method gives rise to a larger degree of period elongation than the linear acceleration method. Figs 2.7[a] and [b] show the response with an integration timestep of 0.02s ($\Delta t/T = 1/10$). The trend in behaviour observed in Fig 2.6 is retained but the period elongation introduced by both methods is now greater. Figs 2.8[a] and [b] show the response at a time step of 0.2 s ($\Delta t/T = 1.0$). Fig 2.8[a] shows that the linear acceleration method has become unstable and the solution rendered useless. Fig 2.8[b] shows that the Newmark method solution has remained bounded, but the results are not accurate although for this particular case, the peak response is quite well predicted every fifth cycle. Both of the curves in Fig 2.8 demonstrate the behaviour of a high mode response in a multi-degree of freedom

problem if the timestep is chosen to be large in comparison to the modal period.

Figs 2.5 to 2.8 are examples of a heuristic approach to timestep selection but serve to demonstrate the expected properties of the integration methods. A quantification of error is now introduced for twenty cycles of forced harmonic loading. The error e is expressed as a percentage of the steady state amplitude, therefore:

$$e = \frac{100(x_{cf}^{t} - x_{n}^{t})}{(P/K)\ D_{A}} \tag{2.64}$$

where, x_{cf}^{t} is the closed form solution and x_{n}^{t} represents the numerical solution. Fig 2.9[a] to [d] show the variation of $|e_{max}|$ with frequency ratio Ω for the linear acceleration method. The variable, $|e_{max}|$ is the modulus of the maximum error occurring in the steady state for twenty cycles of loading. Each plot in Fig 2.9 is evaluated at a different value of damping ratio, ξ. Therefore an indication of the influence of damping on the accuracy characteristics can be gained. Finally, each plot contains response curves at $\Delta t/T$ = 1/10, $\Delta t/T$ = 1/20 and $\Delta t/T$ = 1/40.

Fig 2.9[a] shows the error curve for the underdamped system at ξ = 0.05 This is a typical value of damping for the dominant mode (including hydrodynamic damping) used in conventional jack-up analyses (Chen *et al*, 1990). Fig 2.9[a] shows that the errors increase and reach a maximum at the resonant frequency. After resonance the response curves dip rapidly as the system becomes overexcited. A further rise in errors at higher frequency then occurs. A possible reason for this is that in this ω/ω_n range (*i.e.* $\omega/\omega_n > 1$), the critical period is now the forcing period and not the natural period of the system. Therefore the timestep produces an increasingly poor discretization of the loading function. Fig 2.9[a] also shows that as the timestep decreases, the errors with respect to the closed form solution also decrease.

Fig 2.9[b] shows the error curve at ξ = 0.5, a high value of damping ratio.

Unlike Fig 2.9[a], the response curves do not reach a maximum at the natural frequency. This lack of a peak in the error curves is probably due to the corresponding flattening of the dynamic amplification curves (see Fig 2.10) as the damping ratio increases. Fig 2.9[b] shows that the errors are smaller than those shown by the corresponding curve in Fig 2.9[a].

Fig. 2.9[c] shows the response curves at the critical damping ratio, $\xi = 1.0$. The trend in behaviour observed in Fig 2.9[b] is replicated in Fig 2.9[c]. Once again, the increase in damping ratio has reduced the errors across the entire frequency range considered. Similar comments apply to Fig 2.9[d] which shows the error curves for an overdamped case ($\xi = 1.2$). The error curves all show lower values than the corresponding paths in Fig 2.9[c].

Fig 2.11[a] to [d] shows the corresponding set of error graphs calculated using the Newmark $\beta = 1/4$ method. Fig 2.11 shows that the trend in behaviour for each plot in Fig 2.11 is extremely similar to the corresponding graph in Fig 2.9. It is noteworthy that at each value of $\Delta t/T$, the response curves for the Newmark $\beta = 1/4$ method admit larger errors than the corresponding curve for the linear acceleration method.

Figs 2.9 and 2.11 suggest that the greatest errors from a step-by-step integration method will occur at low damping ratios (where the damped natural frequency and the undamped natural frequency are close). Particular care is needed in the region of the resonant frequency because the resulting displacements are larger than non-resonant responses and the changes in system velocity more rapid. The forcing period should also be considered when setting the timestep, particularly if it is smaller than the system natural period. This is because, as the level of temporal discretization of the load is reduced, there is a greater likelihood of missing the peak

load value. Fig 2.9 and Fig 2.11 also show that as the system damping increases, the errors reduce, therefore, the presence of hydrodynamic damping in the jack-up model is beneficial to the integration process.

2.9.1.2 A non-linear system

As noted in Section 2.9, conclusions about the performance of the integration methods for a non-linear system are difficult to draw without reference to the corresponding non-linearities encountered. Therefore, this aspect of the step-by-step integration methods is best demonstrated by the validation cases in Chapters 3 to 5. However, a simple example is shown in Fig 2.12. Craig (1981) analyses the first 0.55s of response for the system shown in Fig 2.12. Fig 2.13 shows the response calculated by Craig using the Newmark $\beta = 1/4$ method with a timestep of 0.05s (*i.e.* $\Delta t/T = 1/10$), where T is the initial natural period of the system. The responses predicted by JAKUP using the Newmark $\beta = 1/4$ method and the linear acceleration method are also shown. The Newmark $\beta = 1/4$ results predicted by JAKUP are in full agreement with those predicted by Craig, but the results predicted by the linear acceleration method show a slight divergence from the other two solutions as the time increases beyond 0.4s. Because a reduction in spring stiffness means that the natural period of the system becomes larger, the critical timestep for a conditionally stable method increases. Due to this and the arguments of the previous section with respect to the linear system, it is expected that the linear acceleration method yields the more accurate solution. However, the response of a non-linear system is now highly path dependent. Fig 2.14 shows the variation of the spring force over the same time interval considered in Fig 2.13. Due to the size of the timestep, the points at which the stiffness changes value are poorly modelled. Fig 2.15 shows the displacement

response calculated using the Newmark $\beta = 1/4$ method with a timestep of 0.05s and 0.025s. The results from the linear acceleration method for a timestep of 0.025s coincide with those predicted by the Newmark method and are therefore not plotted. Fig 2.15 shows that the response path is now significantly different to that calculated at the larger timestep because the stiffness characteristic of the hysteretic spring is now modelled more accurately.

Fig 2.16 shows the non-linear response and the linear response over an extended time scale using the Newmark $\beta = 1/4$ method at $\Delta t = 0.025$s. Fig 2.16 shows that the non-linear behaviour increases the peak response but reduces the peak to trough displacement with respect to the linear system. Fig 2.17 shows the displacement response of the non-linear system predicted by both the Newmark $\beta = 1/4$ method and the linear acceleration method with $\Delta t = 0.2$s ($\Delta t/T = 0.4$). The solution predicted by the Newmark method remains bounded over the timescale considered. However, Fig 2.17 also shows that the linear acceleration method has become unstable and that the solution is increasing without bound. In this case, the demonstration of the solution error is fortunate because, as noted in Section 2.4, conditionally stable integration methods may not always show obvious signs of instability in a non-linear analysis.

CHAPTER 3

THE STRUCTURAL MODEL

3.1 Introduction

The finite element representation of the structure can be separated into the formulation of a stiffness matrix, a damping matrix and a mass matrix. Some possible matrices will be discussed in this chapter and the eventual equations used in the program JAKUP will be presented. There will also be the presentation of some test results.

3.2 The stiffness matrix

Assembly of the stiffness matrix in JAKUP is a user defined function of the type of analysis to be undertaken. If a small deflection analysis is specified, a stiffness matrix consistent with linear bending theory is formulated. This matrix is time and configuration invariant and can therefore act either as a secant matrix or a tangent matrix. This formulation is discussed further in Section 3.2.1. For large deflections, JAKUP allows the user to specify the use of an incremental formulation of beam-column theory with or without deformation due to shear. Each of these algorithms result in the formulation of a tangent stiffness matrix. Large deflection analysis is discussed in Section 3.2.2.

All of the stiffness methods discussed in this chapter are formulated for the quasi-static problem definition, $K\,x = P$. A brief extension to the dynamics problem represented by Eqn 2.1 is discussed in Section 3.2.2.7. Throughout this chapter, the local coordinate system is defined as that system having its x-axis passing through the centroid (or shear centre) of a local beam element. A global coordinate system is the

axis system shared by the entire finite element assemblage. Therefore, with regards to a stiffness matrix, a lower case k, is the stiffness matrix in the local coordinate system and an upper case K, is the stiffness matrix in the global coordinate system.

3.2.1 The linear stiffness matrix

Linear bending theory assumes that the beam stresses and moments are independent of the deformed configuration of the beam. Therefore calculations for the stresses and displacements are done with respect to the undeformed configuration of the system. Furthermore, the effects of axial loads on the flexural stiffness are ignored. This approach can give acceptable results if the loads only produce small displacements. For the uniform beam of Fig 3.1 the coefficients of the linear stiffness matrix, k_l, are well known (*e.g* Przemieniecki 1968; Livesley, 1975). They are:

$$k_l = \begin{bmatrix} a & 0 & 0 & -a & 0 & 0 \\ 0 & 4b & 3c & 0 & -4b & 3c \\ 0 & 3c & 4d & 0 & -3c & 2d \\ -a & 0 & 0 & a & 0 & 0 \\ 0 & -4b & -3c & 0 & 4b & -3c \\ 0 & 3c & 2d & 0 & -3c & 4d \end{bmatrix} \tag{3.1}$$

where $a = AE/L$, $b = 3EI/L^3$, $c = 2EI/L^2$ and $d = EI/L$. It is the formulation of Eqn 3.1 that is implemented in JAKUP. The coefficients of k_l are found by evaluating the end forces and moments of the beam shown defined in Fig 3.1 in local coordinates in terms of the end displacements. A transformation can then be made to the global coordinate system using a suitable matrix populated with the direction cosines of the beam. Details of this will not be given here.

An alternative method of deriving Eqn 3.1 by virtual work given by Clough & Penzien (1975) is discussed here. This is because the shape functions used in the

derivation are also employed in the formulation of the standard 'consistent' mass matrix (see Section 3.3) and in the evaluation of the equivalent nodal loading due to water particle motions (see Chapter 5). Shape functions are a means of expressing the transverse displacement at some point, x, in a beam in terms of its nodal displacement vector. Under the assumption of linear bending theory, if the beam of Fig 3.1 is subjected to a unit transverse displacement at end 1 with all other end displacements remaining zero, the transverse displaced shape is a cubic Hermitian polynomial which can be expressed:

$$\psi_1(x) = 1 - 3\left(\frac{x}{L}\right)^2 + 2\left(\frac{x}{L}\right)^3 \tag{3.2}$$

Similarly, for a unit rotation (anticlockwise positive) applied at end 1, the transverse displacement at point, x, is:

$$\psi_2(x) = x\left(1 - \frac{x}{L}\right)^2 \tag{3.3}$$

and for a unit axial displacement at end 1 the transverse displacement at point, x, is:

$$\psi_3(x) = 0 \tag{3.4}$$

The corresponding polynomials for unit applied displacements at end 2 are:

$$\psi_4(x) = 3\left(\frac{x}{L}\right)^2 - 2\left(\frac{x}{L}\right)^3 \tag{3.5}$$

$$\psi_5(x) = \frac{x^2}{L}\left(\frac{x}{L} - 1\right) \tag{3.6}$$

and

$$\psi_6(x) = 0 \tag{3.7}$$

By the application of virtual work (Clough & Penzien, 1975) the stiffness matrix coefficients can be evaluated from the equation:

$$K_{ij} = \int_0^L EI(x)\ \psi''_i(x)\ \psi''_j(x)\ dx \tag{3.8}$$

where ψ'' is the second differential of ψ with respect to x.

3.2.2 Large deformation analysis

Due to the presence of significant deck weight often at a large elevation above the seabed, additional jack-up deformations beyond those predicted by linear theory occur. This is because the lines of action of axial loads in the legs do not pass through the centroids of the spudcans. Therefore additional overturning moments are developed due to the load eccentricity. This is termed the P-Δ effect. Also, the presence of the axial loads reduces the flexural stiffness of the legs. Because of these effects, it is necessary to consider the effect of geometric non-linearities and axial loading on jack-up legs. The linear relationship between the applied loads and the nodal displacements assumed in Section 3.2.1 is no longer valid as the elements of the stiffness matrix, K, now depend on the deformed configuration of the structure. Although the expected sidesway of a jack-up hull is small compared to the leg length, this P-Δ effect and reduced leg stiffness is acknowledged to be significant to the overall behaviour of a rig. Due to the increased flexibility of the legs the sway mode natural period of the structure increases. This in turn affects the dynamic amplification under dynamic loading.

3.2.2.1 Geometric non-linearity

Due to the increasing power of digital technology, there has been an increasing amount of research in the last twenty years into methods of accounting for non-linear behaviour in space frame structures. As well as solution techniques for geometric non-linearities, there have also been advances in the formulation of algorithms incorporating material inelastic effects. Kassimali (1983), for example uses a lumped plasticity model to incorporate plastic hinges at the nodes of a beam-column element. In a lumped model, yielding is idealized to occur across the entire beam cross section

at the nodes only. The element between the nodes remains elastic. This is computationally more efficient than trying to account for the movement of plastic hinges and the gradual yielding occurring across a cross section. Kassimali's method is not formulated as a rigorous plasticity model and does not account for load reversals. More recently, Al-Bermani & Kitipornchai (1990) defined yield surfaces for various thin walled sections in conjunction with a lumped plasticity element model. A flow rule was defined (see Chapter 4) and a normality condition constrained incremental nodal forces to be tangential to the yield surface during yield (no work hardening). Yang & Saigal (1984) and Al-Bermani & Kitipornchai (1990) note that the most common load reversal approach is to allow metals to become fully elastic again upon attempted unloading from the yield surface. Although these are significant numerical developments, inelastic effects in the structure are not considered in this thesis. This is because it is not common design practice in the jack-up industry where instead, stresses are compared to an allowable load capacity suitably factored for design. Therefore, in JAKUP, elastic behaviour is assumed for all structural deformations and geometric non-linearities only are considered.

Bazant & El Nimeiri (1973) note that the process of accounting for geometric non-linearities can be separated into two categories. Firstly, the stiffness matrix must be derived at the element level and in conjunction with this a suitable transformation to the global coordinate system defined. Then there must be a method to allow the load-deflection path of the structure to be traced.

3.2.2.2 The element stiffness matrix

The most common approach for deriving the element stiffness matrix for space frames is by using the principle of stationary potential energy (Chan & Kitipornchai 1987 and Kitipornchai & Chan 1987). Here, the potential energy of the loaded element is derived algebraically. By equating the first variation of the potential energy to zero, the nodal force-displacement relationship is obtained. By equating the second variation of the potential energy to zero, the tangent stiffness matrix can be found. Bazant & Cedolin (1991) and Chan & Kitipornchai (1987), use full expressions for strain including non-linear terms in their potential energy formulations to derive the stiffness matrix of a general asymmetric section. For example, the axial strain, ε_{xx}, for an arbitrary point, x, on the member cross section can be expressed:

$$\varepsilon_{xx} = \left(\frac{\partial u_i}{\partial x}\right)_l + \frac{1}{2}\left[\left(\frac{\partial u_i}{\partial x}\right)^2 + \left(\frac{\partial v_i}{\partial x}\right)^2 + \left(\frac{\partial w_i}{\partial x}\right)^2\right]_n \tag{3.9}$$

where u_i, v_i and w_i are the displacements of the point in the x, y, z directions respectively. Subscripts l and n denote linear and non-linear strain components. In order to define the nodal force-displacement relationship the strains at the point x must first be defined in terms of the displacement of the corresponding point along the shear centre. This is because the centroid and shear centre do not coincide for an asymmetric section. The general expression used to relate the two displacements (Remseth, 1979; Chan & Kitipornchai, 1987) is:

$$u_t = u - (y - y_0)\frac{\partial v}{\partial x} - (z - z_0)\frac{\partial w}{\partial x} \tag{3.10}$$

where, u is the axial displacement of the centroid, y and z are the coordinates with respect to the shear centre, y_0 and z_0 are the distance of the shear centre from the principal axis along the y and z axes in the undeformed configuration and v and w are

the shear centre displacements in the y and z directions respectively. The effects of torsion have been omitted from Eqn 3.10. Numerical studies conducted by Remseth (1979) show that for a Lagrangian formulation (see Section 3.2.2.3), Eqn 3.10 is valid for element slope angles of about 15°. However, member sections in JAKUP are assumed to be doubly symmetric, therefore, the centroid and shear centre coincide.

The tangent stiffness matrix, k_t , found from the second variation of potential energy is the sum of the element linear stiffness matrix, k_l, and the geometric stiffness matrix, k_g. Knowledge of this geometric stiffness matrix, k_g , allows the solution for buckling loads by the linearized eigenvalue approach. In this method buckling requires det $|k_l + \lambda k_g| = 0$, where λ is an eigenvalue to be determined. Przemieniecki (1968) notes that this buckling load solution assumes that the prebuckling deflection path is small and ignores the gross deformation that can occur prior to buckling.

As noted in Section 3.2.1, other methods of deriving the element stiffness matrix are by the virtual work equation and by writing equilibrium equations for sections of the element and finding expressions for the end force-displacement relationships. It is this latter approach that gives the greatest physical 'feel' for all the assumptions involved in the derivation process. It is however, not always possible for more general sections (e.g thin-walled asymmetric sections) when the element equilibrium equations may be difficult to derive (due to out of plane warping for example).

3.2.2.3 Tracing the load-deflection path

Bazant & Cedolin (1991) note there are two methods of tracing the load-deflection path of the structure. In the Lagrangian approach, the incremental properties of the element are referred to the natural unstressed state. This method is most suited to

moderately large deflections with large strains (Bazant & El-Nimeiri, 1973). In the Eulerian approach, the incremental properties are referred to the current stress state (or more precisely, the stress state at the beginning of a load step for a numerical procedure). This approach is suited to large deflection analyses with small strains. It is increasingly common to use an updated Lagrangian approach, whereby the nodal coordinates are continuously updated and stresses are referred to this updated state. Oran (1973[b]), notes that this method does not allow arbitrarily large chord rotations in 3-dimensional space. This is because for large displacements, rotations are no longer commutative and cannot be treated as a vector. This therefore limits the large deformation methods of such analysts as Tezcan & Mahapatra (1969), Chan & Kitipornchai (1987) and Bazant & El Nimeiri (1973) where rotations are added vectorially, to chord rotations of about 15^0. It is most common when using the energy methods to derive stiffness matrices to assume a cubic hermitian shape field as in Eqns 3.2-3.7. Bazant & Cedolin (1991) note that in a Lagrangian formulation, these shape functions prevent artificial straining of the neutral axis for rigid body rotations of the element. The above concerns can be avoided by the use of an Eulerian formulation. JAKUP uses an Eulerian formulation of beam-column theory as described by Oran (1973[a] and 1973[b]) and traces the load-deflection path as in Kassimali (1983). For space frames, Oran (1973[b]) makes use of a joint orientation matrix. This matrix represents the orientation of a set of coordinate axes rigidly connected to the beam nodes. In this way rigid body motions can be completely separated from relative member deformations. Remseth (1979) argues that this use of arbitrarily large chord rotations is unnecessary for most space frame structures and certainly in 3-dimensional space, the Eulerian approach is computationally less efficient. This thesis is concerned with plane frames, where rotation occurs about one

axis only, however to allow JAKUP to be used for general purposes in the future, the Eulerian formulation was chosen. Sections 3.2.2.4 to 3.2.2.7 give a brief overview of the incremental beam-column formulation in JAKUP.

3.2.2.4 Beam-columns

This section is included to highlight some of the assumptions pertaining to beam-column theory. Consider Fig 3.2 which is a beam upon which both lateral loads and axial loads act. The forces and displacements in this beam-column are now highly dependent on the eccentricity of the axial load and therefore axial and bending modes are no longer uncoupled. Fig 3.3 (after Chen & Atsuta, 1976) shows the loads acting on an incremental section of the beam. Taking horizontal, vertical and moment equilibrium respectively, Chen & Atsuta derive the equations:

$$H - (H + \frac{dH}{ds}) = 0 \tag{3.11}$$

$$V + \frac{dV}{ds}ds - V - q(x)ds = 0 \tag{3.12}$$

$$M - (M + \frac{dM}{ds}ds) - (V + \frac{dV}{ds}ds)\, ds \cos\theta + q(x)\, ds\, \frac{ds}{2} \cos\theta + (H + \frac{dH}{ds}ds)\, ds \sin\theta = 0 \tag{3.13}$$

$(dV/ds)ds$ and $(dH/ds)ds$ are negligibly small compared to V and H. For small local transverse deflections the assumption is made that $\theta \ll 1$ (radians) and that $dx \approx ds$. Therefore, Eqns 3.11-3.13 reduce to:

$$\frac{dH}{dx} = 0 \quad \Rightarrow H = Q \tag{3.14}$$

$$\frac{dV}{dx} - q(x) = 0 \tag{3.15}$$

$$-\frac{dM}{dx} - V + Q\frac{dw}{dx} = 0 \tag{3.16}$$

Neglecting deformation due to shear, the moment curvature relationship is taken as:

$$M = -EI\frac{d^2w}{dx^2} \tag{3.17}$$

Substituting this into Eqn 3.16 and eliminating V using Eqn 3.15 gives:

$$EI\frac{d^4w}{dx^4} + Q\frac{d^2w}{dx^2} - q(x) = 0 \tag{3.18}$$

Chen & Atsuta (1976) and Bazant & Cedolin (1991) present solutions for Eqn 3.18 for transverse beam deflections. They also present solutions to Eqns 3.11-3.13 using elliptic integrals without making the small deflection assumption. Bazant & Cedolin (1991) note that although a single beam-column with the small transverse deflections assumption cannot model post critical reserve of beam-columns for a Lagrangian formulation, the variation of the large deformation solution from the linearized solution is not too significant until deflections become quite large.

3.2.2.5 Incremental formulation of beam-column theory

Such analysts as Saafan (1963), Connor *et al* (1968) and Tezcan & Mahapatra (1969) have presented incremental beam-column formulations. The Oran (1973[a]) formulation is used in JAKUP because unlike these previous formulations, it contains no assumptions beyond those already contained in conventional beam-column theory. Bhatt (1986) also gives fully consistent beam-column stiffness matrices but gives no method of tracing the load-deflection path in a large deformation analysis. Consideration will first be given to the formulation of a stiffness matrix in local coordinates. Eqn 3.18 is solved for w for the case $q(x) = 0$ as transverse loads in JAKUP are reduced to equivalent nodal loads (see Chapter 5). Fig 3.4 shows the end

forces and displacements for a local beam-column element. Using the moment-curvature relationship defined in Eqn 3.17, the end moments can be expressed in terms of the end rotations (Timoshenko & Gere, 1961; Saafan, 1963) giving :

$$M_1 = \frac{EI}{L}(c_1\,\theta_1 + c_2\,\theta_2) \tag{3.19}$$

$$M_2 = \frac{EI}{L}(c_2\,\theta_1 + c_1\,\theta_2) \tag{3.20}$$

$$Q = EA\,(\frac{u}{L} - c_b) \tag{3.21}$$

If q is defined as:

$$q = \frac{Q}{Q_E} \qquad \Rightarrow q = \frac{QL^2}{\pi^2 EI} \tag{3.22}$$

where Q_E is the Euler buckling load for a column pinned at both ends, then for a compression member ($q > 0$):

$$c_1 = \frac{\phi\,(\sin\phi - \phi\cos\phi)}{2(1-\cos\phi) - \phi\sin\phi} \qquad c_2 = \frac{\phi\,(\phi - \sin\phi)}{2\,(1-\cos\phi) - \phi\sin\phi} \tag{3.23 a:b}$$

where:

$$\phi^2 = \pi^2 q \tag{3.24}$$

For a tension member ($q < 0$):

$$c_1 = \frac{\psi\,(\psi\cosh\psi - \sinh\psi)}{2\,(1-\cosh\psi) + \psi\sinh\psi} \qquad c_2 = \frac{\psi\,(\sinh\psi - \psi)}{2\,(1-\cosh\psi) + \psi\sinh\psi} \tag{3.25 a:b}$$

where:

$$\psi^2 = -\pi^2 q \tag{3.26}$$

For the case of no axial load ($q = 0$) :

$$c_1 = 4\,, \quad c_2 = 2 \tag{3.27 a:b}$$

and Eqns 3.19 - 3.21 reduce to the classical linear bending theory. The variable c_b is a length correction factor accounting for deformation due to bowing. It is not considered in the stiffness matrix derivation of Bhatt (1983), but Saafan (1963) notes that deformation due to bowing may be of the same order of magnitude as the linear extensional term. The length correction factor c_b is given by the expression:

$$c_b = b_1 (\theta_1 + \theta_2)^2 + b_2 (\theta_1 - \theta_2)^2 \tag{3.28}$$

where:

$$b_1 = \frac{(c_1 + c_2)(c_2 - 2)}{8\pi^2 q} \qquad b_2 = \frac{c_2}{8 (c_1 + c_2)} \tag{3.29 a:b}$$

By defining Eqns 3.19 - 3.29, the local member force-displacement relationship has now been completely defined. Enough information is now available to form a secant stiffness matrix k_s (*e.g* Bhatt, 1983). However, in order to trace the load-deflection path, it is necessary have some form of incremental formulation.

In the linearised incremental approach, the base unknown is the vector Δx. The equations of motion for a discrete elastic system can be expressed in the form:

$$f_i (x_1, x_2, ..., x_n) = P_i \qquad i = 1, 2, ..., n \tag{3.30}$$

where f_i are non-linear functions of x_i. In incremental form, we require:

$$\left[\frac{\partial f_i}{\partial x_j}\right] (\Delta x) = (\Delta P) \tag{3.31}$$

where $[\partial f_i / \partial x_j]$ is the tangent stiffness matrix (k_t for local Eulerian coordinates and K_T in global coordinates). Oran (1973[a]) finds the tangent stiffness matrix, k_t for relative member deformations by performing the differentials:

$$[k_t]_{ij} = \frac{\partial S_i}{\partial u_j} + \frac{\partial S_i}{\partial q}\frac{\partial q}{\partial u_j} \qquad i, j = 1, 2, 3 \tag{3.32}$$

where: $S_1 = M_1$, $S_2 = M_2$, $S_3 = QL$, $u_1 = \theta_1$, $u_2 = \theta_2$ and $u_3 = u/L$. By noting that:

$$b_1 = -\frac{c'_1 + c'_2}{4\pi^2} \qquad b_2 = -\frac{c'_1 - c'_2}{4\pi^2} \tag{3.33 a:b}$$

where a prime denotes differentiation with respect to q, the local tangent stiffness matrix is given by:

$$[\,k_t\,] = \frac{EI}{L}\begin{bmatrix} c_1 + \dfrac{G^2_1}{\pi^2 H} & c_2 + \dfrac{G_1 G_2}{\pi^2 H} & \dfrac{G_1}{H} \\ c_2 + \dfrac{G_1 G_2}{\pi^2 H} & c_1 + \dfrac{G^2_2}{\pi^2 H} & \dfrac{G_2}{H} \\ \dfrac{G_1}{H} & \dfrac{G_2}{H} & \dfrac{\pi^2}{H} \end{bmatrix} \tag{3.34}$$

where:

$$G_1 = c'_1\theta_1 + c'_2\theta_2 \tag{3.35}$$

$$G_2 = c'_2\theta_1 + c'_1\theta_2 \tag{3.36}$$

and

$$H = \frac{\pi^2}{\lambda^2} + b'_1\,(\theta_1 + \theta_2)^2 + b'_2\,(\theta_1 - \theta_2)^2 \tag{3.37}$$

where:

$$\lambda = \sqrt{\frac{AL^2}{I}} \tag{3.38}$$

and the differentials c'_1 and c'_2 can be found from Eqn 3.33 without the need for explicit differentiation. Eqn 3.34 now needs to expressed in global coordinates. The incremental global loads and displacements are related by the expression:

$$[\Delta P] = [K_T]\,(\Delta x) \tag{3.39}$$

The global loads are related to the local loads by a 6 x 3 transformation matrix B such that:

$$[P] = [\,B\,]\,[\,S\,] \tag{3.40}$$

The B matrix also relates the local incremental displacements to global incremental displacements, therefore:

$$[\,\Delta u\,] = [\,B\,]^{T}\,[\,\Delta x\,] \tag{3.41}$$

Having specified Eqns 3.38-3.41, Eqn 3.31 can now be expressed:

$$\Delta P = [\,B\,]\,[\,k_{t}\,]\,[\,B\,]^{T}\,(\,\Delta x\,) + [\,\Delta B\,]\,(\,S\,) \tag{3.42}$$

After some algebraic manipulation, [Δ B] (S) can be expressed in the form:

$$[\Delta B]\ (S) = M_1\ [g^{(1)}] + M_2\ [g^{(2)}] + QL\ [g^{(3)}] \tag{3.43}$$

where $g^{(i)}$ are 3 symmetric matrices populated with direction cosines of the rigid body rotation of the element. Therefore, by comparison with Eqn 3.39:

$$[K_T] = [B]\ [k_t]\ [B]^T + M_1\ [g^{(1)}] + M_2\ [g^{(2)}] + QL\ [g^{(3)}] \tag{3.44}$$

Eqn 3.44 is the final goal of the incremental formulation and represents the tangent stiffness matrix in global coordinates. Oran (1973[a]) evaluates the ΔB matrix of Eqn 3.42 (and implicit in Eqn 3.44) assuming that the deformed length, $L\ (1 + \delta) \approx L$, where $\delta = -\ u/L$. Kassimali (1983) evaluates ΔB for the deformed configuration of the beam and retains the terms in δ. Although relative errors between the two formulations are likely to be small, the deformed configuration used by Kassimali is incorporated into JAKUP.

3.2.2.6 Deformation due to shear in the incremental formulation

When considering the shear deformation, the condition that plane sections remain plane is relaxed (Bazant & Cedolin 1991). In the formulations of the previous sections, the shear force is retained but the deformation due to shear is considered negligible compared with that due to bending. Timoshenko & Gere (1961) note that deformation due to shear changes the slope of a deformed beam at a particular point. The gradient induced due to the presence of shear force can be expressed:

$$\frac{dv_s}{dx} = \frac{V_s}{A_s G} \tag{3.45}$$

where A_s is the effective shear area and V_s is the shear force. By considering an element under pure shear, (see Fig 3.5) Bhatt (1986) and Martin (1994) note that the effect of shear on a beam is to produce additional end rotations. Bhatt (1986) derives corrections to his secant stiffness matrix to account for shear but does not consider the effect of beam flexure on axial displacement in his formulation. Martin (1994) modifies equations 3.19 - 3.29 to account for shear in a step-by-step incremental procedure. In an addition to beam-column theory, he also includes the effects of beam flexure in the modification. The value V_{12} (see Fig 3.5) can be expressed as:

$$V_{12} = \frac{(M_1 + M_2)}{L} \tag{3.46}$$

Where the beam length is approximated as the undeformed length L and not the deformed length L - u. Considering deformation due to bending only (in local coordinates), the end moments and axial force give rise to end rotations θ_1 and θ_2. However the end moments will give rise to shear forces as in Eqn 3.46 and additional end rotations due to Eqn 3.45 of :

$$\theta_{add} = \frac{M_1 + M_2}{A_s GL} \tag{3.47}$$

Expressing the total end rotations as $\bar{\theta}_1 = \theta_1 + \theta_{add}$ and $\bar{\theta}_2 = \theta_2 + \theta_{add}$, Martin modifies the stability and bowing functions of Eqns 3.23 - 3.29 to satisfy the conditions:

$$M_1 = \frac{EI}{L} (\bar{c}_1\bar{\theta}_1 + \bar{c}_2\bar{\theta}_2) \tag{3.48}$$

$$M_2 = \frac{EI}{L} (\bar{c}_2\bar{\theta}_1 + \bar{c}_1\bar{\theta}_2) \tag{3.49}$$

$$Q = EA \left(\frac{u}{L} - \bar{c}_b \right) \qquad \bar{c}_b = \bar{b}_1(\bar{\theta}_1 + \bar{\theta}_2)^2 + \bar{b}_2(\bar{\theta}_1 - \bar{\theta}_2)^2 \tag{3.50 a:b}$$

The results, which will just be quoted here, are:

$$\bar{c}_1 = \frac{12c_1 + \beta_s (c_1^2 - c_2^2)}{12 + 2\beta_s (c_1 + c_2)} \tag{3.51}$$

$$\bar{c}_1 = \frac{12c_2 + \beta_s (c_2^2 - c_1^2)}{12 + 2\beta_s (c_1 + c_2)} \tag{3.52}$$

$$\bar{b}_1 = \frac{36b_1}{[6 + \beta_s (c_1 + c_2)]^2} \tag{3.53}$$

$$\bar{b}_2 = b_2 \tag{3.54}$$

and the differentials can be expressed algebraically as:

$$\bar{c}'_1 = \frac{c'_1 - c'_2}{2} + \frac{18 (c'_1 + c'_2)}{[6 + \beta_s (c_1 + c_2)]^2} \tag{3.55}$$

$$\bar{c}'_2 = \frac{c'_2 - c'_1}{2} + \frac{18 (c'_1 + c'_2)}{[6 + \beta_s (c_1 + c_2)]^2} \tag{3.56}$$

$$\bar{b}'_1 = \frac{36}{[6 + \beta_s (c_1 + c_2)]^2} \cdot \left[b'_1 - \frac{2b_1\beta_s (c'_1 + c'_2)}{[6 + \beta_s (c_1 + c_2)]} \right] \tag{3.57}$$

$$\bar{b}'_2 = b'_2 \tag{3.58}$$

where $\beta_s = 12EI/A_sGL^2$. The shear formulation of Martin (1994) is also implemented in JAKUP.

3.2.2.7 Large deformation under dynamic analysis

The incremental stiffness formulation detailed in Sections 3.2.2.5 and 3.2.2.6 are incorporated into a dynamic analysis in the manner described in Section 2.8. Kassimali (1983), uses Newton-Raphson iteration to converge to a solution under static loading. Under dynamic loading, the out-of-balance load vector, ΔP^C, used in a Newton-Raphson type iteration during a timestep is calculated from:

$$\Delta P^C = P^{t+\Delta t} - (M^t {}^{(i)}\ddot{x}^{t+\Delta t} + C^t {}^{(i)}\dot{x}^{t+\Delta t} + {}^{(i)}F_s^{t+\Delta t}) \tag{3.59}$$

where ${}^{(i)}F_s^{t+\Delta t}$ are the nodal forces consistent with the internal state of self stress

corresponding to state ${}^{(i-1)}x^{t+\Delta t} + {}^{(i)}\Delta x$.

3.3 The mass matrix

The simplest form of mass matrix is the lumped mass matrix. The mass is assumed to be concentrated at the beam nodes (usually half of the beam mass per node as in Wu & Chang, 1988) and connected via a massless beam. Przemieniecki (1968) notes that these masses refer to both the translational and rotational inertia of the element, although it is usual to give the concentrated masses zero rotational inertia (Clough & Penzien 1975). The form of the overall system mass matrix is diagonal, with possible zero diagonal terms for the rotational inertia. If there are zero diagonal terms, then those degrees of freedom associated with them will have to be removed from the system equations of motion by, for example, static condensation. This is because zero diagonal terms will prevent such processes as system solution by Gauss-Jordan elimination or mass matrix inversion. The lumped mass matrix is used in practice due to computational advantages gained from its diagonal form. For example, the central difference method for dynamic analysis (see Section 2.3.1) uses the diagonal form to perform considerably fewer operations per timestep than other dynamic solvers. As the lowest level of approximation to the mass matrix, the lumped model can sometimes be less accurate than a consistent mass model and can result in the finite element mesh having to be refined compared to that using a consistent system. However, as noted in Chapter 2, this effect is dependent on the system being analysed.

A consistent mass matrix is evaluated using the same shape functions used to evaluate the stiffness matrix. Clough & Penzien (1975) use the principle of virtual work to derive the coefficients. The resulting equation is:

$$m_{ij} = \int_0^L m(x)\ \psi_i(x)\ \psi_j(x)\ dx \tag{3.60}$$

where $m(x)$ is the mass per unit length at point x. The best known solution to this assumes the cubic Hermitian shape functions of Eqns 3.2-3.7 and the final form of the mass matrix for the beam of Fig 3.1 is (Clough & Penzien, 1975; Livesley, 1975; Przemieniecki, 1968):

$$M = \frac{\bar{m}L}{420}\begin{bmatrix} 140 & 0 & 0 & 70 & 0 & 0 \\ 0 & 156 & 22L & 0 & 54 & -13L \\ 0 & 22L & 4L^2 & 0 & 13L & -3L^2 \\ 70 & 0 & 0 & 140 & 0 & 0 \\ 0 & 54 & 13L & 0 & 156 & -22L \\ 0 & -13L & -3L^2 & 0 & -22L & 4L^2 \end{bmatrix} \tag{3.61}$$

where $\bar{m}$ is the mass per unit length and is here assumed constant along the beam. The choice of shape functions is not limited, however, to cubic Hermitian. Przemieniecki (1968) gives a mass matrix for linear bending shape functions with corrections to approximate shear deformation. Bhatt (1986) for example gives beam-column shape functions (excluding axial deformation due to flexure and deformation due to shear) of:

$$\psi_1(x) = \frac{(1 - c)\ (1 + \cos kx) - s\ (\sin kx - kx + kL)}{D} \tag{3.62}$$

$$\psi_2(x) = \frac{L\ [\ (s/kL - c)\ (1 - \cos kx) + (s - (1 - c)/kL)\ \sin kx - (1 - c)\ x/L]}{D} \tag{3.63}$$

$$\psi_3(x) = 0 \tag{3.64}$$

$$\psi_4(x) = \frac{(1 - c)\ (1 - \cos kx) + s\ (\sin kx - kx)}{D} \tag{3.65}$$

$$\psi_5(x) = \frac{L\ [\ (1 - s)/kL)\ (1 - \cos kx) + (\ (1 - c)/kL)\ (\sin kx - kx)]}{D} \tag{3.66}$$

$$\psi_6(x) = 0 \tag{3.67}$$

where $D = 2\ (1 - c\ ) - skL$, $s = \sin kL$, $c = \cos kL$, $k^2 = Q/EI$ and the axial force is

compressive. Due to the presence of the eccentric axial load in a beam, these shape functions are now dependent on the present configuration of the beam in a step-by-step analysis. This would therefore necessitate the evaluation of Eqn 3.60 at each timestep with iteration within a timestep for the unknown system configuration. However, Remseth (1979), notes that a lower level of approximation for the shape field in the mass matrix is acceptable. This is because the virtual work expression for the mass matrix does not involve differentials of the shape functions which is in contrast to the differentials appearing in a stiffness matrix virtual work derivation. To this end, the mass matrix in JAKUP is a consistent mass matrix using the shape functions of Eqns 3.2-3.7 and given at the element level by Eqn 3.61. For a discussion of the added mass matrix due to water particle motions, see Chapter 5.

3.4 The damping matrix

By direct analogy to Section 3.3, a consistent damping matrix could be derived by using the principle of virtual work. This would give an expression for a damping matrix coefficient of the form:

$$c_{ij} = \int_0^L c(x)\ \psi_i(x)\ \psi_j(x)\ dx \tag{3.68}$$

However, for a real structure, the process of directly measuring a damping property, *c(x)*, analogous to the mass per unit length, for example, is impracticable. If mode superposition is used in the process of solving the equations of motion, then damping can be expressed at the modal level. However, for a direct step-by-step integration method, the elements of the damping matrix must be set explicitly.

3.4.1 Some common methods of defining a damping matrix

Consider a dynamic system with no damping. The equations of motion (Eqn 2.1) reduce to:

$$M\ddot{x} + Kx = P \tag{3.69}$$

If P is a null vector, then Eqn 3.69 represents a free vibration problem. The system has N natural frequencies and N mode shapes, where N is the number of degrees of freedom of the system. If Φ represents the matrix of grouped eigenvectors then the orthogonality conditions are such that:

$$\Phi_r^T M \Phi_r = M_r \tag{3.70}$$

$$\Phi_r^T K \Phi_r = \omega_r^2 M_r \tag{3.71}$$

and:

$$\Phi_r^T M \Phi_s = 0, \qquad \Phi_r^T K \Phi_s = 0, \qquad r \neq s \tag{3.72}$$

where M_r is the modal mass and ω_r is the natural frequency of mode r. For a linear system, this applies at all times t. For a non-linear system, the matrices of Eqn 3.69 vary with time, so Φ represents the instantaneous eigensystem. If the damping matrix satisfies the conditions:

$$\Phi_r^T C \Phi_r = 2M_r \omega_r \xi_r \tag{3.73}$$

$$\Phi_r^T C \Phi_s = 0, \qquad r \neq s \tag{3.74}$$

where ξ_r is the modal damping ratio for mode r, then in a linear system, the complete system of equations of motion can be orthogonalized with respect to the eigenvectors.

This would then allow the solution of the equations at the modal level.

Rayleigh damping is one means by which the damping matrix can be made to satisfy Eqns 3.73 - 3.74 (Clough & Penzien, 1975). The damping matrix is expressed:

$$C = a_0 M + a_1 K \tag{3.75}$$

By application of the orthogonality principle it can be seen that:

$$\xi_r = \frac{1}{2}\left(\frac{a_0}{\omega_r} + a_1 \omega_r\right) \tag{3.76}$$

which allows the damping ratios to be chosen for two modes, usually the lowest and the highest. Selection of a damping ratio in the lowest mode and in a mode close to the lowest mode tends to make the damping in the higher modes artificially high. In a non-linear system the damping matrix could be modified with each change of the stiffness or mass matrix. This would, however, necessitate the decoupling of the eigensystem (or at least the solution of the eigenvalues) at each time step. It would only be practical for systems where the eigensystem did not change significantly from timestep to timestep and some form of iteration for the new eigensystem could be made.

Other methods exist to give greater control over modal damping ratios (Craig, 1981). If :

$$\Phi^T C \Phi = \text{diag}(2\xi_r \omega_r M_r) \equiv \boldsymbol{c} \tag{3.77}$$

then the physical damping matrix can be expressed:

$$C = \Phi^{-T} \boldsymbol{c} \Phi^{-1} \tag{3.78}$$

An alternative expression for the inverse of the eigenvector matrix can be found in terms of the mass matrices. Since:

$$\Phi^T M \Phi = m \tag{3.79}$$

where m = diag M_r then the identity matrix is given by:

$$I = m^{-1}m = m^{-1}(\Phi^T M \Phi) \tag{3.80}$$

therefore:

$$m^{-1}\Phi^T M \Phi = \Phi^{-1}\Phi \tag{3.81}$$

so:

$$\Phi^{-1} = m^{-1}\Phi^T M \tag{3.82}$$

so the physical damping matrix can be expressed:

$$C = (M\Phi m^{-1})\ c\ (m^{-1}\Phi^T M) \tag{3.83}$$

so:

$$C = (M\Phi\ \text{diag}\frac{1}{M_r})\ \text{diag}(2\xi_r\omega_r M_r)\ (\text{diag}\frac{1}{M_r}\Phi^T M) \tag{3.84}$$

which can be expressed in the form:

$$C = \sum_1^N \frac{(2\xi_r\omega_r)}{M_r}\ (M\Phi_r)\ (M\Phi_r)^T \tag{3.85}$$

which satisfies the orthogonality conditions of Eqns 3.73 - 3.74. A damping ratio can now be specified for all modes but this involves the complete solution of the eigensystem. If instead the summation in Eqn 3.85 is taken to some value N_C which is lower than N, the equation is truncated giving zero damping in the modes $N_C + 1$ to N.

It is also possible to solve the eigensystem only up to mode N_C and specify a damping matrix with damping ratios higher than, ξ_{Nc}, in all modes higher than mode N_C. In this case the damping is expressed:

$$C = a_1 K + \sum_1^{N_c - 1} \frac{(2\bar{\xi}_r\omega_r)}{M_r}\ (M\Phi_r)\ (M\Phi_r)^T \tag{3.86}$$

where:

$$a_1 = \frac{2\xi_{N_c}}{\omega_{N_c}} \tag{3.87}$$

$$\bar{\xi}_r = \xi_r - \xi_{N_c} \left(\frac{\omega_r}{\omega_{N_c}}\right) \tag{3.88}$$

and:

$$\xi_s = \xi_{N_c} \left(\frac{\omega_s}{\omega_{N_c}}\right) \tag{3.89}$$

for $s = (N_C + 1) \rightarrow N$. These methods give more control over the damping ratios in a greater number of modes. As before the physical damping matrix could be modified in a non-linear system although, as mentioned earlier, this would probably only be practicable in systems with slowly varying eigensystems or local non-linearities.

3.4.2 Damping in JAKUP

Rayleigh damping is used in JAKUP because it can provide an adequate level of approximation for a jack-up analysis. As noted in Section 3.4.1, setting the damping in two low modes renders the damping in the higher modes artificially high. This is useful because the primary response in a jack-up analysis is in the surge and sway modes. These are the lowest modes, so the larger damping in the higher modes helps to filter out the high mode responses. This also means that non-dissipative step-by-step integration algorithms (see Chapter 2) can be used as freely as dissipative methods. Furthermore, it can be seen from Eqn 3.76 that the lower modes are damped mainly by mass proportional damping and higher modes by stiffness proportional damping. As the structural mass matrix is time invariant, the Rayleigh damping matrix in JAKUP is not altered from timestep to timestep.

Additional system damping occurs due to hydrodynamic damping. This arises directly from the formulation of the Morison equation and is discussed in Chapter 5.

3.5 The Eigensystem

JAKUP also contains subroutines to calculate the eigenvalues and eigenvectors of a dynamic system. In the present study, the eigenvectors are not needed because a mode superposition type of solution to Eqn 2.1 was not sought. The subroutines were included, however, to make JAKUP amenable to future additional solution techniques. An estimate of the eigenvalues is needed in order to set explicit values for the damping matrix of Section 3.4. Press *et al* (1986), note that the most efficient eigensystem solutions are found from the matrix A_1 defined by the eigensystem:

$$A_1 x = \lambda x \tag{3.90}$$

where, A_1, is symmetric and positive definite. The eigensystem of Eqn 2.1 can be expressed in the form:

$$Kx = \lambda Mx \tag{3.91}$$

where $\lambda = \omega^2$. If expressed in the form of Eqn 3.90, then Eqn 3.91 can be written:

$$M^{-1}Kx = \lambda x \tag{3.92}$$

Although M and K are symmetric, the matrix $M^{-1}K$ is in general unsymmetric. Smith & Griffiths (1988 and 1990) note that the symmetry of the problem can be retained by the use of Cholesky decomposition. The mass matrix is expressed in terms of Cholesky factors. This can be expressed mathematically:

$$M = LL^T \tag{3.93}$$

where, L, is lower triangular. Substituting into Eqn 3.91 gives:

$$Kx = \lambda LL^T x \tag{3.94}$$

Therefore:

$$(L^{-1}K)\ (L^{-T}L^{T})\ x\ =\ \lambda L^{T}x \tag{3.95}$$

By defining, $L^{T}x = y$, then the standard eigensystem problem is now available with retained symmetry:

$$(L^{-1}KL^{-T})y\ =\ \lambda y \tag{3.96}$$

Bathe (1982), notes that if the mass matrix is ill-conditioned with respect to inversion, the Cholesky decomposition may yield inaccurate results for the lowest eigenvalues. This may be avoided by carrying out the spectral decomposition of the mass matrix, which involves the complete solution of the eigensystem of the mass matrix. Now the mass matrix is expressed:

$$M\ =\ (RD)(DR^{T}) \tag{3.97}$$

where R is the matrix of grouped eigenvectors of the mass matrix and the matrix product $(D)(D)$, is the diagonal matrix of eigenvalues of M. The matrix RD can now be substituted for, L, in Eqn 3.95.

JAKUP performs Cholesky decomposition and spectral decomposition for the initial configuration of the system. The eigensystem is then solved by the QL algorithm as detailed by Press *et al* (1986).

3.6 Test Problems

The eigensystem provides a useful means of checking structural analysis programs for matrix assembly and orientation effects. Some of the tests were verified using results from the commercial Mathworks program 'Matlab'. Consider the beam of Fig 3.6[a] where all the properties have a value of 1.0. From Eqn 3.61 the mass matrix is:

$$M = \begin{bmatrix} 0.33333 & 0 & 0 \\ 0 & 0.37143 & -0.05238 \\ 0 & -0.05238 & 0.00952 \end{bmatrix}$$

and from Eqn 3.1 the linear stiffness matrix is:

$$K = \begin{bmatrix} 1.0 & 0.0 & 0.0 \\ 0.0 & 12.0 & -6.0 \\ 0.0 & -6.0 & 4.0 \end{bmatrix}$$

The eigensystem, $x = \lambda K^{-1} M x$, can now be solved with a hand calculator by equating, $\det |K^{-1} M - 1/\lambda| = 0$. This yields the three natural periods, $T_1 = 3.628$s, $T_2 = 1.779$s and $T_3 = 0.181$s and the three eigenvectors:

$$x_1 = \begin{bmatrix} 1.000 \\ 0.0 \\ 0.0 \end{bmatrix} \quad x_2 = \begin{bmatrix} 0.0 \\ 0.726 \\ 1.000 \end{bmatrix} \quad x_3 = \begin{bmatrix} 0.0 \\ 0.131 \\ 1.000 \end{bmatrix}$$

Table 3.1 shows the natural periods calculated by Matlab and by JAKUP using Cholesky decomposition and spectral decomposition. The results calculated with Matlab demonstrate that the commercial program was being used correctly. Table 3.1 also shows that the JAKUP results using both types of decomposition are in full agreement with those found by Matlab. Table 3.2 shows the eigenvectors for the corresponding eigenvalues in Table 3.1. Once again, there is full agreement amongst all the methods. The beam of Fig 3.7[a] was then analysed to verify that orientation

effects would not change the eigenvalues. The results, which will not be shown here, were identical to those presented in Table 3.1. Similarly, the beams of Fig 3.6[b] and Fig 3.7[b] were analysed to verify that discretization effects would not affect program performance. The six natural periods found by JAKUP were not affected by beam rotation and matched the Matlab results. The periods are listed in Table 3.3. Table 3.4 shows the eigenvectors corresponding to Fig 3.6[b]. In this table, $O(-n)$ means terms of the order of 10^{-n}. Table 3.4 shows that the Cholesky and spectral decomposition routines have almost modelled the uncoupled axial deformations by forming small numbers ranging downwards from about 10^{-5}. Generally, these numbers are smaller for the spectral decomposition method. A simple subroutine could have been written to set these small vector components to zero, but as no further use was made of the eigenvectors, this was deemed unnecessary. Further eigensystem tests were done for the systems shown in Fig 3.8. These tests provided further proof that discretization and orientation effects did not affect the program. However, results will not be reported here as the vectors become cumbersome as the number of degrees of freedom increases.

These results verify that given masses for the elements of a system with the corresponding stiffness properties and joint coordinates, JAKUP successfully forms the element mass matrix as defined in Section 3.4 and the element stiffness matrix in Section 3.2.1. More importantly, all global matrices are assembled from the individual element matrices within the same subroutine. Therefore the conversion to the global coordinate system has also been verified. Furthermore, the correct eigenvalues are assembled and exported to the Rayleigh damping subroutine when the eigensystem analysis is solved.

It is also necessary to perform tests using the geometric nonlinearity

subroutine. Martin (1994) performs the quasi-static analysis of the cantilever in Fig 3.9 which is subjected to a monotonically increasing end moment. For comparison, he gives the closed form solution. For quasi-static loading, the results are:

$$\frac{u}{L} = 1 - \frac{1}{2\pi\eta}\sin(2\pi\eta); \quad \frac{v}{L} = \frac{1}{2\pi\eta}[1 - \cos(2\pi\eta)]; \quad \frac{\theta}{2\pi} = \eta \quad (3.98a:b:c)$$

where $\eta = ML/2\pi EI$. For analysis in JAKUP, the cantilever was treated as a dynamic system and given an arbitrary value of mass and 2% damping in the first two modes. Fig 3.10 shows the results predicted by JAKUP using two elements with the system loaded slowly compared to the fundamental period in order not to produce dynamic excitation. The deformation causes a total end rotation of 360^0 (*i.e.* the beam is bent round into a circle). It can be seen from this two element case that there is a very good agreement with the closed form solution across the η range considered. The slight deviations from the closed form solution are purely due to inertial effects and could be eliminated by either using the quasi-static solution (as shown by Martin, 1994) or by slower dynamic loading. However, the results shown provide a good test of the method of tracing the load-deflection path during a dynamic analysis.

Frisch-Fay (1962) gives the closed form solution for the post-buckling response of the encastré strut shown in Fig 3.11 by using elliptic integrals. For an ideal strut the critical load is:

$$P_{cr} = \frac{\pi^2 EI}{4L^2} \quad (3.99)$$

and the post-buckling tip deflections are given by:

$$\frac{u}{L} = \frac{2p}{K(p^2)}; \quad \frac{v}{L} = 2 - \frac{2E(p^2)}{K(p^2)} \quad (3.100a:b)$$

where p satisfies:

$$\frac{P}{P_{cr}} = \frac{4[K(p^2)]^2}{\pi^2} \quad (3.101)$$

and $K(p^2)$ and $E(p^2)$ are defined by:

$$K(p^2) = \int_0^{\pi/2} (1 - p^2\sin^2\theta)^{-1/2} d\theta; \qquad E(p^2) = \int_0^{\pi/2} (1 - p^2\sin^2\theta)^{1/2} d\theta \quad (3.102a:b)$$

which are complete elliptic integrals of the first and second kind. Fig 3.12[a] shows the load-deflection path predicted by JAKUP using three beam elements compared with the closed form solution. A small eccentricity ($e = 0.001L$) of the axial load is incorporated in order to initiate instability. To obtain the analytical curves, Eqn 3.101 and Eqn 3.102 were solved using Matlab. Fig 3.12[a] shows that the onset of buckling in the vicinity of the critical load is well predicted and that there is good agreement with the analytical post-buckling response path. To improve the agreement, further subdivisions of the strut would be necessary, but these results serve to demonstrate JAKUP's performance. A sharper transition point at the buckling load could be obtained by reducing the value of the eccentricity. This is demonstrated in Fig 3.12[b] which shows the JAKUP results with the eccentricity reduced by a factor of 10. As predicted, the transition point is now sharper than the bifurcation points shown in Fig 3.12[a]. These results demonstrate that the Oran (1973[a]) formulation has been implemented correctly and that the load-deflection path is properly traced.

An additional test case involving dynamics as well as geometric non-linearity is shown in Fig 3.13. This is an undamped beam, encastré at both ends with the load applied suddenly at midspan. This problem is analysed by Weeks (1972) using the non-linear single degree of freedom equation:

$$M\ddot{x} + C(\dot{x} + a_1\dot{x}^2) + K(x + a_3x^3) = P(t) \quad (3.103)$$

to approximate the equation of motion of the fundamental mode of the system. The variables a_1 and a_3 are constants to account for non-linear terms due to membrane action. The same problem is also analysed over a reduced time scale by Oran & Kassimali (1976) using a two element, three degree of freedom representation of the

system. The mass matrix used is diagonal and the integration timestep is 9.375×10^{-5}s. The results of Weeks are considered first because he produces a response path over a larger time range than Oran & Kassimali. Fig 3.14[a] shows the temporal variation of the midspan vertical displacement predicted by Weeks using the Newmark $\beta = 1/4$ method. The response paths predicted by the Houbolt and central difference methods are also shown. The effects of their use in this particular non-linear system is self explanatory and will not be discussed here. The 'exact' solution is obtained by gradually reducing the timestep until further reductions produce no change in response. Fig 3.14[b] shows the response predicted by JAKUP using two elements and the geometric non-linearity subroutine. The mass matrix used is a diagonal mass matrix and the timestep is 9.375×10^{-5}s as in Oran & Kassimali (1976). Fig 3.14[b] shows that the JAKUP results compare well with those predicted by Weeks. The period of the response matches the Weeks formulation, but the peak response obtained is slightly less than the corresponding response path shown in Fig 3.14[a]. Fig 3.15 shows the predicted path over a limited timescale predicted by Oran & Kassimali. The results of Weeks over this timescale are also shown. A similar reduction in peak response is also predicted and therefore demonstrates that the JAKUP results are fully in character. Fig 3.15 also shows the response path predicted by Oran & Kassimali using a non-iterative solution technique. This shows the importance of equilibrium iterations because the solution displays a substantial drift from the correct solution in the latter part of the response curve.

Weeks also notes that the period of the corresponding linear system is approximately four times that of the non-linear system. Fig 3.16 shows the linear response predicted by JAKUP with the non-linear response also plotted for reference. JAKUP predicts the increase in period but also predicts a large increase in the peak

displacement. However, this is to be expected as demonstrated by Fig 3.17 which shows Weeks' plot of the quasi-static linear and non-linear load-deflection paths. Figs 3.14 to 3.17 demonstrate that the load-deflection path can be traced in a dynamic analysis as well as a quasi-static analysis when the system contains geometric non-linearity.

CHAPTER 4

THE SOIL MODEL

4.1 Introduction

The behaviour of conical and spudcan footings on sand and clay has been the topic of considerable research in recent years. A conventional jack-up analysis models the footing/seabed interaction (from herein referred to as the footing model) as a pin joint (Reardon, 1986, Freize *et al*, 1995). Under this assumption, no moment fixity is allowed to develop at the footings. For a given hull sidesway, stresses in the vicinity of the hull are more conservative (*i.e.* larger) than the stresses derived by modelling the footings as fixed or partially fixed. The economic implications of accounting for footing fixity are considerable. By reducing the stresses in the critical members due to load redistribution to the footings, the jack-up can be used in a harsher environment without the need for upgrading existing rigs or the use of over-designed harsh environment units.

This thesis is concerned with spudcan behaviour on undrained clay. The discussions in this chapter are therefore considered with clay analysis as the overall goal. The program JAKUP can implement pinned or fixed footings or can place linear springs at the soil-structure interface in the vertical, rotational and horizontal senses. There is also the option of using a work hardening plasticity model for clay called Model B (Martin, 1994). The implementation of each of these models is discussed in this chapter, and then some test results are presented.

4.2 Elastic behaviour of footings

When analysing a jack-up, the stability of the footings under combined loading is of the utmost importance. Footing stability depends on the maximum load level a footing can sustain before the failure envelope is reached. The load level on a footing can be uniquely defined in a plane frame analysis by the *V:H:M* force point where *V*, is the vertical footing load, *H* is the horizontal footing load and *M* is the footing moment (see Fig 4.1). In order to trace the path of the *V:H:M* force point for a jack-up footing, it is necessary to make an assumption about the nature of the elastic force-displacement relationship for a footing within the failure envelope. The resulting *V:H:M* force points are then compared to the envelope (see Section 4.3) and in a conventional jack-up analysis, stability is dictated by the first footing to yield (or to commence sliding).

4.2.1 The 100% fixity and zero fixity conditions

The 100% fixity and zero fixity conditions are considered together because they represent two extreme theoretical models of soil-footing interaction. The simplest type of soil-structure interaction to implement is to assume that the footings can be modelled as fixed joints. This is the 100% fixity condition. Although the term 'fixity' applies to the amount of moment resistance only, for this case, infinite stiffness is assumed for all degrees of freedom of the footing. Consequently, there can be no movement in the vertical, horizontal or rotational directions. As the displacement vector for any of the footings is a null vector, all degrees of freedom associated with the footings can be condensed out of the equations of motion. This assumption of footing behaviour allows the largest moment to be developed at the footing level compared to other methods. As a result, in a quasi-static analysis,

stresses developed in the vicinity of the hull in critical leg members will be smaller than those obtained using other assumptions of footing behaviour.

As noted in Section 4.1, footing behaviour within the failure envelope is normally modelled as that of a pinned joint. This is the zero fixity condition. Under a quasi-static analysis, this will give the most conservative results for critical design stresses and displacements. Pinned footings are usually combined with infinite horizontal and vertical stiffness, but have zero rotational stiffness. Therefore rotation is the only allowable displacement at the soil-structure interface. In a structural analysis, the horizontal and vertical degrees of freedom associated with a footing may be condensed out of the equations of motion. This is because as for fixed footings the terms associated with these degrees of freedom in the displacement vector are known to be zero. Fig 4.2 shows a qualitative representation (after Chiba *et al*, 1986) of the distribution of moment between the jack-up footing and the lower guide for a fixed and pinned footing assumption. The diagram also includes a representation of the partial fixity condition (see Section 4.2.2). Fig 4.2 shows that the partial fixity condition leads to an intermediate behaviour compared to that predicted by the 100% and zero fixity assumptions under static loading conditions.

4.2.2 Partial fixity at the soil-structure interface

Elastic behaviour within the yield surface can be modelled by linear springs with finite stiffnesses as shown in Fig 4.3. For short term static footing displacements, the API (1993) recommend the use of solutions for the force-displacement relationships for a rigid circular footing on the surface of a homogeneous elastic half space. For the forces and displacements shown in Fig 4.1, the solutions are:

$$V = \left[\frac{4GR}{1-\nu}\right] z \tag{4.1}$$

$$H = \left[\frac{32GR(1-\nu)}{7-8\nu}\right] h \tag{4.2}$$

$$M = \left[\frac{8GR^3}{3(1-\nu)}\right] \theta \tag{4.3}$$

where z, h and θ are the vertical, horizontal and rotational displacements of the footing respectively (see Fig 4.1). The variable G is the elastic shear modulus of the soil, ν is Poisson's ratio for the soil and R is the radius of the footing. Defining K_{11}, K_{22} and K_{33} using the relationships:

$$K_{11} = \frac{4GR}{(1-\nu)} \qquad K_{22} = \frac{32GR(1-\nu)}{(7-8\nu)} \qquad K_{33} = \frac{8GR}{3(1-\nu)} \tag{4.4a:b:c}$$

then Eqns 4.1 to 4.3 can be formulated in matrix form to give:

$$\begin{pmatrix} V \\ H \\ M/R \end{pmatrix} = \begin{bmatrix} K_{11} & 0 & 0 \\ 0 & K_{22} & 0 \\ 0 & 0 & K_{33} \end{bmatrix} \begin{pmatrix} z \\ h \\ R\theta \end{pmatrix} \tag{4.5}$$

Martin (1994) notes that although these solutions are only applicable to surface footings, they are frequently used to define the behaviour of spudcan footings that have undergone considerable soil penetration. Bell (1991) conducted finite element work on flat circular footings on clay. The results demonstrate that significant increases in soil stiffness occur with increasing footing penetration. The work also highlights the existence of cross coupling between the horizontal and rotational footing displacements. Expressed mathematically, the force-displacement relationship with the cross coupling terms has the form:

$$\begin{pmatrix} V \\ H \\ M/R \end{pmatrix} = \begin{bmatrix} K_1 & 0 & 0 \\ 0 & K_2 & K_4 \\ 0 & K_4 & K_3 \end{bmatrix} \begin{pmatrix} z \\ h \\ R\theta \end{pmatrix} \tag{4.6}$$

where the coefficients K_i are elastic stiffnesses which are now dependent on the amount of plastic footing penetration, z^p. An important output of Bell's work is a set of tabulated K_i values at different embedments depths for flat footings. Additional work conducted by Bell produced tabulated K_i values at differing cone angles for a surface conical footing. Spudcans are normally modelled numerically by considering them as an equivalent conical footing in the manner of Fig 4.4.

For the extreme wave loading event, the rotational stiffness in particular can no longer be realistically modelled as linear elastic. Non-linear elastic models attempt to model the decrease in stiffness as the failure envelope is approached. The Joint Industry Study coordinated by Noble Denton & Associates (NDA, 1987) includes details of experimental work on cohesive clay conducted at Oxford University (Santa Maria, 1988). Experimental investigations examined the behaviour of rotational stiffness with increasing footing rotation angle. A mathematical formulation of the footing stiffness assumes infinite horizontal and vertical stiffnesses and models the nondimesional rotational stiffness, K_r, in the form:

$$K_r = \frac{M}{s_u D^3 \theta} = K_\theta \, f_s \, f_v \, f_h \, f_d \tag{4.7}$$

where D is the footing diameter, s_u is the undrained shear strength of the soil and the empirical factors f_s, f_v, f_h and f_d modify K_θ depending on the footing shape, vertical load, horizontal load and depth of embedment respectively. The variable K_θ is a two parameter hyperbola which can be expressed:

$$K_\theta = \frac{a_1}{a_2 + \theta} \tag{4.8}$$

This hyperbola models the transition from an initially stiff response at low rotations to a more flexible behaviour and limiting moment at large rotations. The parameter a_1 represents the limiting non-dimensionalized moment and a_2 is inversely proportional to the rigidity index, G/s_u. The best fit parameters to the experimental data in NDA (1987) were $a_1 = 0.25$ and $a_2 = 16/(G/s_u)$. The iterative process to define the footing stiffness culminates in the formation of a secant rotational stiffness to define footing behaviour.

SNAME (1993) also detail a method of deriving a secant rotational stiffness for spudcan footings on sand or clay. A reduction multiplier, f_r, is applied to the rotational stiffness as defined by Eqn 4.4[c]. The variable f_r is a function of the size of a defined yield surface and V, H and M. Defining the variable r_f by the expression:

$$r_f = \frac{\left[\left(\frac{H}{AS_u}\right)^2 + \left(\frac{M}{M_0}\right)^2\right]^{1/2}}{4\left(\frac{V}{V_0}\right)\left(1 - \frac{V}{V_0}\right)} \tag{4.9}$$

where, V_0 is the pure vertical load capacity and M_0 is the peak moment load occurring at $V/V_0 = 0.5$ (see Section 4.3), then for a sand analysis:

$$f_r = - r_f / \ln (1 - r_f) \tag{4.10}$$

and for a clay analysis:

$$f_r = (1 - r_f) \tag{4.11}$$

The rotational stiffness is then given by:

$$K_r = f_r K_{33} \tag{4.12}$$

where K_{33} is defined in Eqn 4.4[c]. For clay, the horizontal and vertical stiffnesses are assumed to remain linear elastic throughout the analysis and are defined by K_{11} and K_{22} of Eqn 4.4. Additional empirical factors can be applied to the stiffnesses to account for the depth of embedment. A similar method is outlined by Hambly *et al* (1990) to model non-linear elastic behaviour inside an idealised circular yield surface in (V/V_0):(M/M_0) space (infinite horizontal stiffness is assumed). The transition functions in this case were calibrated to match seabed conditions for a jack-up operating at the Arbroath field in the North Sea. As before, the mathematical implementation leads to the formulation of secant stiffnesses. These stiffnesses are then incorporated into an equivalent single degree of freedom numerical model of a jack-up.

Non-linear elastic models avoid the sharp transition in behaviour that elastic-perfectly plastic models show at yield. However, non-linear elastic models are best suited to modelling monotonic footing responses because the initial load-displacement response is retraced upon load reversal. This is unrealistic compared to a plasticity model. Furthermore, the iterative formation of secant footing stiffnesses is incompatible with the formulation of the tangent stiffness matrix for an incremental structural analysis procedure (see Chapter 3). This is because the secant stiffnesses represent a Lagrangian formulation of system properties whereas the stiffness procedure of Chapter 3 represents an Eulerian system description. Also the formulation of post yield footing behaviour is much more suited to an Eulerian formulation. This is because the flow rule defines plastic increments of displacement.

4.2.3 Elastic behaviour in JAKUP

Elastic behaviour in JAKUP is implemented using a variety of methods. All the

methods assume linear elastic behaviour within the yield surface. Pinned or fixed footings can be implemented by suitable condensation of the null displacement degrees of freedom of the equations of motion (Eqn 2.1). Linear springs can be placed at the soil-structure interface in the manner of Eqn 4.5. Also as a special case of elastic behaviour during a Model B analysis (see Section 4.3.1.1), elastic behaviour with cross coupling between the horizontal and rotational degrees of freedom can also be formulated as in Eqn 4.6. In this manner, the stiffnesses are functions of the depth of embedment. This particular formulation is discussed further in Section 4.3.1 (which deals specifically with the Model B formulation).

4.3 Inelastic behaviour of footings

The failure envelope for a footing on soil using the coordinate system of Fig 4.1, defines a three dimensional surface in V,H,M space within which elastic behaviour can be expected. When the $V{:}H{:}M$ force point reaches the failure envelope or yield surface, further irreversible footing displacements can occur. The envelope therefore defines the bearing capacity of the soil. As noted in Chapter 1, a jack-up is typically loaded to twice its operating weight during preloading. Extensive plastic deformation under the footings can occur resulting in vertical plastic settlement, z^p. As well as being a proof test of the foundation, preloading also dictates the value of the initial pure vertical load capacity, V_0 because the vertical load capacity must balance the applied preload. The pure vertical load capacity is the maximum load that the soil can sustain under purely vertical loading before yielding occurs. The value of V_0 sets the size of the initial failure envelope because when yielding occurs, the yield surface reforms through the new V_0 apex point (Hambly *et al*, 1990). This is shown

qualitatively in Fig 4.5.

Reardon (1986) notes that in a conventional jack-up analysis, footing stability is dictated by the first footing to reach the yield surface. The possibility that stable post yield behaviour may occur leading to advantageous load redistribution is not considered. Although there are numerous bearing capacity solutions for various footing types (*e.g* strip footings, flat circular footings), only a few are commonly used by the offshore industry (Reardon, 1986; API, 1993; SNAME, 1993). In particular, the bearing capacity formulae of Brinch Hansen (1970) and Vesic (1975) are widely used. The Brinch Hansen and Vesic methods are both based on the solution of the vertical bearing capacity for a strip foundation on the surface of a weightless Tresca material:

$$Q/A = (\pi + 2)\, s_u \tag{4.13}$$

where, Q is the vertical bearing capacity of the soil and A is the foundation area in contact with the soil. The Brinch Hansen and Vesic methods modify this relationship with semi-empirical factors to account for differing footing geometries and footing embedments. For a surface circular footing, Brinch Hansen's (1970) yield surface can be expressed:

$$\frac{V}{V_0} = \frac{1 + 0.2B'/L' - 0.5\,(1 - \sqrt{1 - H/A'S_u})\,(1 + 0.4B'/L')}{1.2} \cdot \frac{A'}{A} \qquad (H \le A'S_u) \tag{4.14}$$

and the Vesic (1975) failure envelope can be expressed:

$$\frac{V}{V_0} = \left(1 - \frac{\left(\frac{2 + B'/L'}{1 + B'/L'}\right)H}{(\pi + 2)\,A'S_u}\right)\left(\frac{\pi + 2 + B'/L'}{\pi + 3}\right) \cdot \frac{A'}{A}, \quad H \le A'S_u \tag{4.15}$$

where A', B' and L' will be discussed in due course. The complicated nature of

Eqn 4.14 and Eqn 4.15 arises due to the semi-empirical factors used to account for footing moment and horizontal load. The presence of a moment load is incorporated by considering the statically equivalent eccentric vertical load shown in Fig 4.6. The eccentricity considered in Fig 4.6 is then used to define a footing of reduced area on which the vertical load acts centrally. Therefore, A', B' and L' are functions of the eccentricity, e. No mathematical formulae will be given for them here, but their qualitative meanings are demonstrated in Fig 4.7. The horizontal load is considered as the statically equivalent inclined central load shown in Fig 4.8. Inclination factors are then used to reduce the vertical load at yield. Further corrective factors can be applied to Eqn 4.14 and Eqn 4.15 to account for the depth of embedment of the footing. The Brinch Hansen (1970) and Vesic (1975) methods were primarily intended for use in onshore shallow foundation design. Martin (1994) notes that under these conditions, horizontal loads and moments at the footings are usually small compared to the vertical load. In contrast, relatively large horizontal and moment loads can be developed by a jack-up footing in its operating condition.

Recent research has helped to move away from the empiricism of the Brinch Hansen and Vesic methods. For example, research coordinated by Noble Denton & Associates (1987) (see also Section 4.2.2), includes documentation of work conducted at Cambridge University for predicting the rotational stiffness of spudcan footings on sand. An important result of the experimental work demonstrates that a cigar shaped yield surface previously proposed for strip footings on sand (Butterfield & Ticof, 1979) is also very suitable for predicting the combined load bearing capacity of spudcan footings on sand. This surface is shown qualitatively in Fig 4.9. The yield surface proposed has a much simpler mathematical form than the Brinch Hansen or Vesic surfaces and can be expressed:

$$\left(\frac{H}{V_0}\right)^2 + \left(\frac{M}{D_e V_0}\right)^2 = \frac{1}{4}\left(\frac{V}{V_0}\right)^2\left(1 - \frac{V}{V_0}\right)^2 \qquad (4.16)$$

where D_e is the maximum embedded diameter of the spudcan and the peak horizontal and moment loads occur at $V/V_0 = 0.5$ (although, work conducted by Tan (1990) for conical and spudcan footings on sand demonstrates that peak values occurring at $V/V_0 \approx 0.4$ provides a better description). Furthermore, work conducted by Houlsby & Martin (1992) shows that a cigar shaped yield surface similar to that defined by Eqn 4.16 is also suitable for modelling the failure envelope for spudcans footings on clay. The envelope has the form:

$$\left(\frac{H}{AS_u}\right)^2 + \left(\frac{M}{0.2RV_0}\right)^2 = 16\left(\frac{V}{V_0}\right)^2\left(1 - \frac{V}{V_0}\right)^2 \qquad (4.17)$$

Numerical tests show that this formula is more successful at modelling combined *V*:*H*:*M* interaction loci than either the Brinch Hansen or Vesic methods.

In order to consider the nature of inelastic footing response once the *V*:*H*:*M* force point reaches the yield surface, some means of accounting for irreversible footing displacement is needed. Within the framework of work hardening plasticity, there are several key elements that must be accounted for in order to define a numerical model. As noted earlier, a yield surface must be defined. The size of this yield surface is dictated by V_0. A plot of the variation of V_0 with depth of embedment is called the virgin load-penetration curve. It is important to note that the depth of embedment refers to the vertical plastic penetration z^p and not the total vertical footing displacement. This is because the total vertical footing displacement may contain an elastic component, z^e and V_0 is independent of the size of elastic displacement increments. This immediately raises an important issue. This is that the virgin load-penetration curve allows V_0 to be evaluated at any value of z^p. Therefore

the size of the yield surface is intrinsically linked to the amount of vertical plastic penetration. The variation of V_0 with z^p therefore constitutes a soil hardening law (see Section 4.3.1.4). The other vital element of the model is the flow rule. The flow rule relates the relative magnitudes of plastic vertical, horizontal and rotational displacement increments during an elastoplastic footing response. From this, a new value of z^p can be derived and a yield surface appropriate to the new footing conditions calculated. Previous foundation models have failed to account for some or all of these conditions. For example, the foundation models of SNAME (1993) and Hambly *et al* (1990) mentioned in Section 4.2.2 both define yield surfaces but do not define a hardening law or flow rule which are both essential parts of a soil constitutive model. The work mentioned earlier conducted by Cambridge University on sand (NDA, 1987) does, however, include several plasticity based features. A semi empirical virgin load-penetration curve is defined which allows the peak vertical load V_0 to be calculated at any plastic penetration, z^p. A flow rule is also adopted. However, no mathematical definition of the flow rule is given. This instead takes the form of a series of design curves to estimate the plastic rotational stiffness as the soil-footing behaviour passes into yield. With these considerations in mind however, the work of Martin (1994) represents the first work hardening plasticity model for clay that has been experimentally validated.

4.3.1 The Model B work hardening plasticity model

The Model B work hardening plasticity model for clay was the culmination of recent experimental work conducted at Oxford University (Martin, 1994) investigating the behaviour of spudcan footings on clay. It was developed to eliminate certain deficiencies in existing numerical models for foundations on clay. The aims of the

work were to investigate the shape of the yield surface for spudcan footings on clay, to provide a hardening law and to investigate the applicability or otherwise of associated flow (see Section 4.3.1.3) during an elastoplastic displacement increment. The model was formulated in numerical form to facilitate its inclusion in an incremental analysis of a footing. In the following sections, an overview of the main features of Model B as implemented in JAKUP is presented.

4.3.1.1 Elastic behaviour

Investigation of the elastic response within the yield locus was not a priority of the Model B investigations. For Model B the behaviour within the yield surface is as defined by Eqn 4.6 (after Bell, 1991). This can be expressed incrementally as:

$$\begin{pmatrix} \Delta V \\ \Delta H \\ \Delta M/R \end{pmatrix} = \begin{bmatrix} K_1 & 0 & 0 \\ 0 & K_2 & K_4 \\ 0 & K_4 & K_3 \end{bmatrix} \begin{pmatrix} \Delta z \\ \Delta h \\ R\Delta\theta \end{pmatrix} \tag{4.18}$$

The stiffness factors K_i are dependent on the depth of embedment (z^p) and take account of the increase in undrained strength with depth. Eqn 4.18 represents a classical elasticity approach with a sudden transition from elastic to elastoplastic response at the yield surface. The spudcan footings are treated as equivalent cones in the manner already described in Fig 4.4. As noted in Section 4.2.2, the tabulated K_i values for conical footings are evaluated at the soil surface only. Embedded K_i are evaluated by assuming the same variation with depth as those of the tabulated K_i values for flat circular footings.

4.3.1.2 Yield surface

As noted in Section 4.3, recent research on conical and spudcan footing behaviour

suggests that a cigar shaped yield surface is a sensible interaction locus for modelling the combined *V:H:M* load bearing capacity for spudcan footings on clay. Initially a similar shape for the Model B surface was adopted to assist in identifying the type of physical testing to be undertaken. This yield surface can be expressed in the form:

$$\left(\frac{H}{AS_u}\right)^2 + \left(\frac{M}{M_0}\right)^2 = 16\left(\frac{V}{V_0}\right)^2\left(1-\frac{V}{V_0}\right)^2 \tag{4.19}$$

When defining a flow rule (Section 4.3.1.3), the Δz^p:Δh^p:$R\Delta\theta^p$ axes are plotted coincident with the (V/V_0):(H/H_0):$(M/R)/(M_0/R)$ axes, where Δh^p and $\Delta\theta^p$ are the horizontal and rotational plastic displacement increments during an elasto-plastic footing response. By symmetry, at $V/V_0 = 0$ and $V/V_0 = 1$, the incremental plastic displacement vectors are directed along the Δz^p: (V/V^0) axis (*i.e.* plastic displacements are purely in the vertical direction at the apex points of the yield surface). The disadvantage of Eqn 4.19 is that a uniquely defined normal vector does not exist at these points. This is because the tips of the yield surface defined by Eqn 4.19 are pointed. Martin (1994) shows that a yield surface of the form:

$$f\left(V\ ,\ H\ ,\ M/R\right) = \left(\frac{H}{H_0}\right)^2 + \left(\frac{M/R}{M_0/R}\right)^2 - 2\left[e_1 + e_2\left(\frac{V}{V_0}\right)\left(\frac{V}{V_0} - 1\right)\right]\left(\frac{H}{H_0}\right)\left(\frac{M/R}{M_0/R}\right) -$$

$$\left[\frac{(\beta_1+\beta_2)^{\beta_1+\beta_2}}{(\beta_1)^{\beta_1}(\beta_2)^{\beta_2}}\right]^2\left(\frac{V}{V_0}\right)^{2\beta_1}\left(1-\frac{V}{V_0}\right)^{2\beta_2} = 0 \tag{4.20}$$

provides a good fit to his experimental data. The tips of the yield surface represented by Eqn 4.20 are rounded. Therefore a unique normal vector exists at the two points $V/V_0 = 0$ and $V/V_0 = 1$. From the physical tests, the best fit parameters are given by:

$$H_0/V_0 = 0.127 \text{ and } M_0/RV_0 = 0.166$$

and:

$$\beta_1 = 0.764: \quad \beta_2 = 0.882: \quad e_1 = 0.518: \quad e_2 = 1.18.$$

A final adjustment is needed to Eqn 4.20 to allow f to be evaluated at values of $V/V_0 > 1$. This is achieved by raising the expression to the power of $1/(2\beta_2)$. Therefore, f is now redefined as:

$$f(V, H, M/R) = \left[\left(\frac{H}{H_0}\right)^2 + \left(\frac{M/R}{M_0/R}\right)^2 - 2\left[e_1 + e_2\left(\frac{V}{V_0}\right)\left(\frac{V}{V_0} - 1\right)\right]\left(\frac{H}{H_0}\right)\left(\frac{M/R}{M_0/R}\right)\right]^{\frac{1}{2\beta_2}} -$$

$$\left[\frac{(\beta_1 + \beta_2)^{\beta_1 + \beta_2}}{(\beta_1)^{\beta_1}(\beta_2)^{\beta_2}}\right]^{\frac{1}{\beta_2}}\left(\frac{V}{V_0}\right)^{\frac{\beta_1}{\beta_2}}\left(1 - \frac{V}{V_0}\right) = 0 \qquad (4.21)$$

It is physically impossible for V to exceed V_0. However it is necessary to evaluate f for $V/V_0 > 1$ during the numerical process to determine whether an increment is elastoplastic or not. The yield surface function f is not defined for $V/V_0 < 0$ unless β_1/β_2 happens to be an integer value.

4.3.1.3 Flow rule

Another essential feature of a work hardening plasticity model is the flow rule. The flow rule defines the relative magnitudes of the plastic displacement vectors during an elastoplastic increment. The assumption of associated flow implies that displacement increments are normal to the yield surface when plotted coincident with the V:H:M/R axis system. This can be expressed mathematically:

$$\begin{bmatrix} \Delta z \\ \Delta h \\ R\Delta\theta \end{bmatrix}^p = \xi \begin{bmatrix} \partial f/\partial V \\ \partial f/\partial H \\ \partial f/\partial (M/R) \end{bmatrix} \qquad (4.22)$$

where ξ defines the magnitudes of the displacement increments. Retrospective numerical simulations of the experimental data demonstrated that the assumption of

associated flow leads to an overprediction of the vertical plastic footing displacements during yield. A non-associated flow rule requires the formulation of a plastic potential function, g. The plastic potential function defines the relative plastic displacement vector as a function of V/V_0. However, Martin (1994) notes that experimental evidence supports the assumption of associated flow in the $H{:}M/R$ plane. Model B therefore uses an altered version of Eqn 4.22 with a correction factor for the vertical plastic displacement increment. The flow rule can now be expressed:

$$\begin{bmatrix} \Delta z \\ \Delta h \\ R\Delta\theta \end{bmatrix}^p = \xi \begin{bmatrix} \zeta_a \cdot \partial f / \partial V \\ \partial f / \partial H \\ \partial f / \partial (M/R) \end{bmatrix} \tag{4.23}$$

where ζ_a, the association parameter, takes the values:

$\zeta_a = 0.580$ when $V/V_0 < 0.464$

$\zeta_a = 0.639$ when $V/V_0 \geq 0.464$

At $V/V_0 = 0.464$, $\partial f/\partial V = 0$ and plastic displacement increments occur normal to the V/V_0 axis (ie no increase in vertical plastic displacement occurs). Eqn 4.23 retains associated flow in the $H{:}M/R$ ($\Delta h^p{:}R\Delta\theta^p$) plane but reduces the magnitude of the vertical plastic penetration increments.

4.3.1.4 Hardening law

As noted in Section 4.3, the pure vertical load capacity dictates the size of the yield surface. The vertical load capacity is related to the bearing capacity factor, N_{c0}, by the expression:

$$V_0 = N_{c0}\, \pi\, R^2\, s_{u\,0} \tag{4.24}$$

The bearing capacity factors N_{c0} are tabulated for different embedment depths z^p. The N_{c0} values are lower bound values and were calculated numerically by Martin (1991)

using the FORTRAN program FIELDS written by Prof. G. T Houlsby at Oxford University. The variable s_{u0} is the undrained shear strength at the embedded level z^p. Because s_u varies with depth, s_{u0} is calculated as the average strength over a depth of R_e below the spudcan. R_e is the maximum embedded radius of the spudcan's equivalent cone. Although, the N_{c0} values are tabulated, Eqn 4.24 directly implies that the pure vertical load capacity is a function of vertical plastic penetration, z^p.

4.3.2 Incorporation into an incremental structural analysis procedure

Chapter 2, Section 2.8 outlines the manner in which non-linearities are included in the iterative modified Newton-Raphson type solution of the dynamic equations of motion. In order to include Model B type footings into the structural analysis procedure, the Model B subroutine must return to the main program a 3x3 footing tangent stiffness matrix corresponding to the present configuration of the system. In the global coordinate system shown in Fig 4.10 the incremental footing force-displacement relationship can be expressed:

$$\begin{bmatrix} \Delta H \\ \Delta V' \\ \Delta M' \end{bmatrix} = \begin{bmatrix} A_{11} & A_{12} & A_{13} \\ A_{21} & A_{22} & A_{23} \\ A_{31} & A_{32} & A_{33} \end{bmatrix} \begin{bmatrix} \Delta h \\ \Delta z' \\ \Delta \theta' \end{bmatrix} \tag{4.25}$$

where the A matrix is the footing tangent stiffness matrix and H, V' and M' are the horizontal, vertical and moment loads respectively in the global coordinate system. H is unaltered from Fig 4.1 because it acts in the same sense in both the local and global coordinate system. The flexibility analogue of Eqn 4.25 is also needed during the iterative process to calculate the change in the footing loads due to a calculated iterative change in the displacement vector. The footing loads are then incorporated into the vector of internal loads consistent with the internal state of self stress of the

system. As described in Section 2.8 and 3.2.2.7, an out-of-balance load for the system can then be calculated. The Model B subroutine must therefore operate in two modes. One mode operates under load control, and the other mode is under displacement control. To follow the development of the mathematical model (which follows the procedure in Martin (1994) closely) it is convenient to return to the local coordinate system of Fig 4.1. The overall incremental form of Model B is first expressed in the form:

$$\begin{bmatrix} B_{11} & B_{12} & B_{13} & B_{14} & B_{15} & B_{16} & B_{17} \\ B_{21} & B_{22} & B_{23} & B_{24} & B_{25} & B_{26} & B_{27} \\ B_{31} & B_{32} & B_{33} & B_{34} & B_{35} & B_{36} & B_{37} \\ B_{41} & B_{42} & B_{43} & B_{44} & B_{45} & B_{46} & B_{47} \\ B_{51} & B_{52} & B_{53} & B_{54} & B_{55} & B_{56} & B_{57} \\ B_{61} & B_{62} & B_{63} & B_{64} & B_{65} & B_{66} & B_{67} \\ B_{71} & B_{72} & B_{73} & B_{74} & B_{75} & B_{76} & B_{77} \end{bmatrix} \begin{bmatrix} \Delta V \\ \Delta H \\ \Delta M/R \\ \Delta z \\ \Delta h \\ R\Delta\theta \\ \xi \end{bmatrix} = \begin{bmatrix} inc_1 \\ inc_2 \\ inc_3 \\ 0 \\ 0 \\ 0 \\ 0 \end{bmatrix} \tag{4.26}$$

where the 7x7 B matrix will be discussed in due course. The vector on the right hand side of Eqn 4.26 is a control vector that specifies if an increment is under load or displacement control. Therefore, [inc_1, inc_2, inc_3] = [ΔV, ΔH, $\Delta M/R$] under load control and [inc_1, inc_2, inc_3] = [Δz, Δh, $R\Delta\theta$] under displacement control. The B_{ij} coefficients are then adjusted accordingly. Because, the flow rule defines displacement increments, it is more convenient to approach the formulation of the B matrix in terms of flexibility instead of stiffness. To define the B matrix it is necessary to consider the elastic and elasto-plastic behaviour of the footing.

During an **elastic** increment, $f < 0$ and the combined $V{:}H{:}M$ force point lies inside the yield surface. Eqn 4.18 reformulated in terms of flexibility can be expressed:

$$\begin{bmatrix} \Delta z \\ \Delta h \\ R\Delta\theta \end{bmatrix} = \begin{bmatrix} C_1 & 0 & 0 \\ 0 & C_2 & C_4 \\ 0 & C_4 & C_3 \end{bmatrix} \begin{pmatrix} \Delta V \\ \Delta H \\ \Delta M/R \end{pmatrix} \tag{4.27}$$

where:

$$C_1 = \frac{1}{K_1}; \quad C_2 = \frac{K_3}{K_2 K_3 - K_4^2}$$

$$C_3 = \frac{K_2}{K_2 K_3 - K_4^2} \quad C_4 = \frac{K_4}{K_4^2 - K_2 K_3} \tag{4.28a-d}$$

During an **elastoplastic** increment, $f = 0$. The force point lies on the yield surface and remains on the envelope during yielding increments. The value of z^p will change (unless the plastic potential happens to be normal to the Δz^p axis as discussed in Section 4.3.1.3). The yield surface will expand or contract depending on the particular value of V/V_0. The **elastic** component of the elastoplastic increment is defined by Eqn 4.27. However, the elastic coefficients C_1 to C_4 are dependent on the plastic vertical footing displacement z^p. For example, consider the qualitative plot of the vertical footing displacement with vertical footing load shown in Fig 4.11. If there is an increment in vertical displacement, the new unload gradient is different to that at the start of the increment. The new flexibility coefficient is:

$$C_1^{new} = C_1 + (dC_1/dz^p)\Delta z^p \tag{4.29}$$

Therefore from Fig 4.11, the new elastic displacement is:

$$z^e = (V + \Delta V)\,(C_1 + (dC_1/dz^p)\Delta z^p) \tag{4.30}$$

As a result the increment in elastic displacement is:

$$\Delta z^e = z^e - C_1 V \tag{4.31}$$

From the above argument it can be seen that there are additional elastic coupled displacements during an elastoplastic footing increment above those shown in Eqn

4.27. These additional effects can be expressed in the form:

$$\begin{bmatrix} \Delta z \\ \Delta h \\ R\Delta\theta \end{bmatrix}^{coup} = \Delta z^p \begin{bmatrix} dC_1/dz^p & 0 & 0 \\ 0 & dC_2/dz^p & dC_4/dz^p \\ 0 & dC_4/dz^p & dC_3/dz^p \end{bmatrix} \begin{bmatrix} V + \Delta V \\ H + \Delta H \\ M/R + \Delta M/R \end{bmatrix} \tag{4.32}$$

The **plastic** component of the elastoplastic displacement increment is described by the flow rule of Eqn 4.23 *i.e.:*

$$\begin{bmatrix} \Delta z \\ \Delta h \\ R\Delta\theta \end{bmatrix}^p = \xi \begin{bmatrix} \zeta_a \cdot \partial f/\partial V \\ \partial f/\partial H \\ \partial f/\partial(M/R) \end{bmatrix} \tag{4.33}$$

Due to the formulation of Eqns 4.27 to 4.33, there is now enough information available to define the incremental displacement vector during an elastoplastic footing response. This can be found by summing Eqn 4.27, Eqn 4.32 and Eqn 4.33. Therefore, the displacement increment can be expressed:

$$\begin{bmatrix} \Delta z \\ \Delta h \\ R\Delta\theta \end{bmatrix}^{ep} = \begin{bmatrix} C_1 & 0 & 0 \\ 0 & C_2 & C_4 \\ 0 & C_4 & C_3 \end{bmatrix} \begin{pmatrix} \Delta V \\ \Delta H \\ \Delta M/R \end{pmatrix} + \xi \begin{bmatrix} \zeta_a \cdot \partial f/\partial V \\ \partial f/\partial H \\ \partial f/\partial(M/R) \end{bmatrix} +$$

$$\xi \cdot \zeta_a \cdot \frac{\partial f}{\partial V} \begin{bmatrix} dC_1/dz^p & 0 & 0 \\ 0 & dC_2/dz^p & dC_4/dz^p \\ 0 & dC_4/dz^p & dC_3/dz^p \end{bmatrix} \begin{bmatrix} V + \Delta V \\ H + \Delta H \\ M/R + \Delta M/R \end{bmatrix} \tag{4.34}$$

where $\Delta z^p = \xi . \zeta_a . \partial f / \partial V$ (from Eqn 4.33). An additional condition is needed to define ξ. This arises by noting that the force point must remain on the yield surface during yielding. This is called the consistency condition and is represented mathematically by:

$$\delta f = 0 \tag{4.35}$$

Applying this to Eqn 4.21 and rearranging the terms, the consistency equation

becomes:

$$\frac{\partial f}{\partial V}\Delta V + \frac{\partial f}{\partial H}\Delta H + \frac{\partial f}{\partial (M/R)}\Delta(M/R) +$$

$$\xi \cdot \zeta_a \cdot \frac{\partial f}{\partial V}\left[\frac{\partial f}{\partial V_0}\cdot\frac{dV_0}{dz^P} + \frac{\partial f}{\partial H_0}\cdot\frac{dH_0}{dz^P} + \frac{\partial f}{\partial (M_0/R)}\cdot\frac{d(M_0/R)}{dz^P}\right] = 0 \quad (4.36)$$

With the formulation of Eqn 4.27 to Eqn 4.36 there is now enough information available to formulate the B matrix introduced in Eqn 4.26. The 7x7 matrix can be expressed in the form:

$$\begin{bmatrix}
1 \text{ or } 0 : & 0 : & 0 : & 0 \text{ or } 1 : & 0 : & 0 : & 0 \\
0 : & 1 \text{ or } 0 : & 0 : & 0 : & 0 \text{ or } 1 : & 0 : & 0 \\
0 : & 0 : & 1 \text{ or } 0 : & 0 : & 0 : & 0 \text{ or } 1 : & 0 \\
C_1 : & 0 : & 0 : & -1 : & 0 : & 0 : & \zeta_a \frac{\partial f}{\partial V}\left(1 + [V + \Delta V]\frac{dC_1}{dz^P}\right) \\
0 : & C_2 : & C_4 : & 0 : & -1 : & 0 : & \frac{\partial f}{\partial H} + \zeta_a \frac{\partial f}{\partial V}\left[[H + \Delta H]\frac{dC_2}{dz^P} + [M/R + \Delta M/R]\frac{dC_4}{dz^P}\right] \\
0 : & C_4 : & C_3 : & :0 : & :0 : & -1 : & \frac{\partial f}{\partial M/R} + \zeta_a \frac{\partial f}{\partial V}\left[[H + \Delta H]\frac{dC_4}{dz^P} + [M/R + \Delta M/R]\frac{dC_3}{dz^P}\right] \\
B_{71} : & B_{72} : & B_{73} : & B_{74} : & B_{75} : & B_{76} : & B_{77}
\end{bmatrix} \quad (4.37)$$

where the seventh row of B is: [0 : 0 : 0 : 0 : 0 : 0 : 1] during an elastic increment or:

$$\left[\frac{\partial f}{\partial V} : \frac{\partial f}{\partial H} : \frac{\partial f}{\partial (M/R)} : 0 : 0 : 0 : \zeta_a \frac{\partial f}{\partial V}\left(\frac{\partial f}{\partial V_0}\cdot\frac{dV_0}{dz^P} + \frac{\partial f}{\partial H_0}\cdot\frac{dH_0}{dz^P} + \frac{\partial f}{\partial (M_0/R)}\cdot\frac{d(M_0/R)}{dz^P}\right)\right]$$

(which represents the consistency condition) during an elastoplastic increment. The first three rows of the B matrix are adjusted to the left hand option or the right hand option (*i.e.* a 1 or 0) depending on if the control vector specifies load or displacement control. The 3x3 flexibility matrix in local coordinates can now be specified by considering appropriate terms in Eqn 4.37. Therefore the incremental flexibility relationship in local coordinates can be expressed:

$$\begin{bmatrix} \Delta z \\ \Delta h \\ R\Delta\theta \end{bmatrix} = \frac{1}{B_{77}} \begin{bmatrix} B_{41} - B_{71} \cdot B_{47} : B_{42} - B_{72} \cdot B_{47} : B_{43} - B_{73} \cdot B_{47} \\ B_{51} - B_{71} \cdot B_{57} : B_{52} - B_{72} \cdot B_{57} : B_{53} - B_{73} \cdot B_{57} \\ B_{61} - B_{71} \cdot B_{67} : B_{62} - B_{72} \cdot B_{67} : B_{63} - B_{73} \cdot B_{67} \end{bmatrix} \begin{bmatrix} \Delta V \\ \Delta H \\ \Delta M/R \end{bmatrix} \quad (4.38)$$

Inverting the flexibility matrix of Eqn 4.38 and adjusting the moment rotation terms gives the incremental force-displacement relationship in local coordinates. This can be expressed in the form:

$$\begin{bmatrix} \Delta V \\ \Delta H \\ \Delta M \end{bmatrix} = \begin{bmatrix} S_{11} & S_{12} & S_{13} \\ S_{21} & S_{22} & S_{23} \\ S_{31} & S_{32} & S_{33} \end{bmatrix} \begin{bmatrix} \Delta z \\ \Delta h \\ \Delta\theta \end{bmatrix} \quad (4.39)$$

where the S matrix is essentially the inverse of the flexibility matrix in Eqn 4.38. Therefore, the incremental force-displacement relationship in global coordinates introduced in Eqn 4.25 can now be expressed:

$$\begin{bmatrix} \Delta H \\ \Delta V' \\ \Delta M' \end{bmatrix} = \begin{bmatrix} S_{22} & -S_{21} & -S_{23} \\ -S_{12} & S_{11} & S_{13} \\ -S_{32} & S_{31} & S_{33} \end{bmatrix} \begin{bmatrix} \Delta h \\ \Delta z' \\ \Delta\theta' \end{bmatrix} \quad (4.40)$$

Eqn 4.40 is the goal that was set by the form of Eqn 4.25.

The Model B subroutine can return a 3x3 footing stiffness matrix consistent with the present configuration of the system. It can also return the incremental changes in the footing loads (ΔV:ΔH:ΔM) consistent with the incremental displacements (Δv:Δh:$\Delta\theta$) calculated during the iterative process. At the beginning of a time increment, an elastic footing stiffness matrix is returned if the combined V:H:M force point yields a value of $f < 0$. If yielding is detected during one of the iterations, then the footing is forced to remain elastoplastic for all further iterations during that timestep even if negative ξ values are found whilst solving Eqn 4.36. If $f = 0$ at the beginning of a time increment, then an elastoplastic footing stiffness

matrix is returned. If a positive ξ value is calculated in the first iteration, then the footing is again forced to remain elastoplastic for all subsequent iterations during that timestep. A footing is only allowed to become elastic again (and unload from the yield surface) if a negative ξ value is found in the first equilibrium iteration.

4.4 Performance of Model B

Martin (1994) performs several retrospective numerical simulations of some of his physical experiments using the Model B description of footing behaviour. The numerical simulations show that the Model B formulation gives excellent predictions of the variation of the vertical bearing capacity of the soil with depth. As noted in Section 4.3, the pure vertical load capacity dictates the size of the yield surface because the failure envelope forms through the V_0 apex point. This agreement in vertical capacity predictions is important because Martin's experiments show that although the yield surface undergoes significant expansion with increasing penetration, the overall shape remains nearly constant allowing the normalised surface given by Eqn 4.21 to be defined. Because the variation of the apex point with depth is well predicted, Model B therefore gives a good prediction of the failure envelope over a considerable range of depths.

Some of the simulations show that Model B occasionally underpredicts the elastic stiffnesses within the yield surface. However, this behaviour is more dependent on the selection of a suitable rigidity index (G/s_u) than any specific shortcoming of the Model B algorithm. As noted in Section 4.3.1.1, Model B assumes linear elastic behaviour at all load values within the yield surface. As a result, Model B cannot predict the gradual decrease in stiffness as the yield surface is approached shown by the physical experiments. Instead, there is a sharp transition from linear elastic to

non-linear inelastic behaviour at the yield surface. As noted in Section 4.2.2, the effect of gradual yielding is what the non-linear elastic models attempt to simulate by the use of transition functions applied to the initial elastic stiffnesses.

Martin's experimental work was primarily directed towards the prediction of monotonic loading. Therefore the numerical prediction of load reversals by Model B is not considered in depth. However, one experimental test, involving a complete large amplitude moment/rotation cycle at constant V/V_0 suggests that the effect of gradual yielding is even more marked upon load reversal. The corresponding Model B simulation predicts the same elastic stiffness upon unloading from the yield surface (constant V/V_0 in this case) as in the primary load path. Therefore, the numerical unload cycle matches the physical path poorly in this isolated case. However, in the same simulation Model B does make a good prediction of the ultimate moment reached in the physical test when the footing rotation returns to zero. It should be noted that this type of response is still more realistic than the unload path that would be obtained from a non-linear elastic model. Martin notes that small amplitude cycles of load reversal would probably be well modelled numerically by Model B. An additional consideration is that time dependent effects such as creep and consolidation are not modelled. However, this cannot detract from the fact that Model B demonstrates that a rational work hardening plasticity model can be formulated for footings on clay. Furthermore, this formulation can be included in an advanced structural analysis procedure.

4.5 Test problems

Martin (1994) analyses the preloading of a single jack-up footing using a computer implementation of Model B called OXSPUD. The footing (shown in Fig 4.12) is

preloaded to 100MN. As the program JAKUP must have a structure attached to the footing, the analogous problem is considered by using the system of Fig 4.13. For this case, the 100 MN weight of the single beam is applied slowly at the footing level in order to avoid inducing excessive dynamic response. Under these circumstances bouncing can occur in the early part of the response path to which the soil subroutine reports a loss of soil contact. Fig 4.14[a] shows Martin's plot of the variation of footing displacement with footing load. The corresponding undrained shear strength profile used is also shown. Fig 4.14[a] shows that under full preload, the footing undergoes 14.945m of vertical penetration. Fig 4.14[a] also shows the effect of unloading to the operating load (half the preload in this case). This portion of the load-displacement path shows that there is 0.128m of elastic recovery. A separate test not shown graphically but reported in the text notes that complete removal of the load results in an ultimate footing penetration of 14.689m. This value represents the amount of vertical plastic penetration that occurs during the simulation. Fig 4.14[b] shows the load-displacement path predicted by JAKUP. Fig 4.14[b] shows that JAKUP correctly predicts the vertical displacement due to preload when load is applied slowly using a dynamic system description. The unload path also matches the amount of elastic recovery predicted by OXSPUD. However, the initial portion of the response curve in Fig 4.14[b] differs from that shown in Fig 4.14[a]. This is because JAKUP starts loading the spudcan with the maximum equivalent cone radius having just become fully embedded in the soil. Therefore, the equivalent radius in contact with the soil does not change throughout the response path in Fig 4.14[b]. The initial part of the response curve shown in Fig 4.14[a] represents loading with the tip of the spudcan just about to penetrate the soil.

This one simulation with the Model B algorithm is a severe test of the validity

of implementation of the soil stiffness subroutine. Not only does it test that the elastic behaviour is correct, but because there is over 14.0m of continuous yielding, the yield surface is incrementally expanded at each timestep and appropriate incremental elasto-plastic displacements formed in order to arrive at the end point. In practice a dynamic solution to this problem would not be sought, because the number of timesteps needed to load the footing slowly is larger than the number of load increments needed with a static analysis.

Martin (1994) also performs a pushover analysis of a typical jack-up unit on Model B type foundations using the simplified jack-up model shown in Fig 4.15. Fig 4.16[a] shows Martin's plot of the vertical, horizontal and moment loads predicted under a static analysis using the Model B footings. Fig 4.16[a] shows that the windward and leeward footings yield simultaneously at 4.32 MN. After this there is a gradual loss of moment fixity and a catastrophic sliding failure occurs at an environmental load of 7.74 MN. Once again, this is a severe test of the algorithm due to the interaction with the structural analysis procedure. Also the loading causes the foundation to be driven to failure. Fig 4.16[b] shows the corresponding plot of the footing loads predicted by JAKUP under a gradually increasing environmental load using the same numerical model of the jack-up shown in Fig 4.15. In addition the hull mass used is 15.3×10^6 kg, the individual leg mass is 1.3×10^6 kg and 2% damping is placed in the sway mode. Fig 4.16[b] shows that JAKUP correctly predicts the simultaneous onset of yield for both footings. The elastic region of Fig 4.16[b] differs slightly from that shown in Fig 4.16[a]. This is due to some dynamic excitement of the jack-up and could be eliminated by slower loading. The catastrophic failure of the foundation is predicted at a slightly higher environmental load than that shown in Fig 4.16[a]. This is because as the footings approach failure, the jack-up hull begins to

accelerate. Therefore internal loads consistent with the state of self stress are now in balance with an increasingly significant inertial (and damping) load. This can be seen more clearly from Fig 4.17 which shows the horizontal hull acceleration during the simulation. The disturbance in the vicinity of the origin in Fig 4.17 is due to a small impulse response upon initial load application. A similar pattern in behaviour is seen at first yield due to the sudden loss in moment fixity.

Because the action of regular waves produces harmonic loading, it is also necessary to demonstrate that a solution can be obtained under a sinusoidally varying point load. Fig 4.18 shows the variation of vertical footing displacement for the windward footing of Fig 4.15, due to sinusoidally varying the point load, H_{env}. The excitation period is 12.5s which is approximately twice the natural period of the unit and the amplitude of H_{env} is 9.0MN. Fig 4.18 shows that due to continual yielding and unloading from the yield surface, the amount of vertical plastic penetration for the windward footing increases with each cycle. The yielding process can be seen more clearly from Fig 4.19 which shows the non-linear vertical load-displacement path for the windward footing. Fig 4.20 shows the resulting horizontal hull displacement. Figs 4.18 to 4.20 simply act to demonstrate that Model B can be incorporated into a dynamic analysis procedure with cycles of loading as well as with monotonic load variations.

CHAPTER 5

ENVIRONMENTAL LOADING

5.1 Introduction

The environmental loading on a jack-up is due to the combined action of wave, current and wind loading. The process of defining the wave loading for an offshore structure can be divided into two stages: the use of a suitable wave theory to estimate the water particle kinematics, and the calculation from these motions of loads on the structure. In this thesis, the first operation will make use of regular wave theories in two dimensions. Section 5.2.1 contains a discussion of the governing equations for regular wave theories applicable to jack-up platforms. Some of the solutions to these equations are then presented in Sections 5.2.2.1 to 5.2.2.4. The second operation makes use of the Morison equation. This is discussed in Section 5.4.

Currents vary slowly compared to the natural periods of jack-up oscillations. Similarly, the main wind energy is associated with periods considerably larger than jack-up natural periods (SNAME, 1993). Both of these will therefore be considered as steady phenomena. Current and wind loading will be considered in Sections 5.3 and 5.5 respectively. Finally some test results for environmental loading are presented in Section 5.6.

5.2 Wave theories

Ocean waves are random in nature, but in order to provide engineering solutions, the use of regular wave theories is common. Regular waves have a fixed profile with respect to an axis system translating at the wave celerity and can provide useful results in offshore analysis. They are often used together with a design wave for a significant return period, typically 50 years in the jack-up industry (100 years in the jacket industry, Freize *et al,* 1995) to define particle kinematics for a site specific structural assessment. There are numerous regular wave theories, many involving complex iterative solutions which are only feasible because of increasingly powerful computational technology. However, only a few theories are widely used in offshore engineering (SNAME 1993). Some of the most widely used are Airy theory, Wheeler stretched Airy theory, Stokes' theory and stream function theory. Each of these will be discussed in Section 5.2.2. As this thesis is concerned with a plane frame idealization of a jack-up, these theories are all applied to two-dimensional flow. Only theories based on stream functions are invalid for multidirectional wave theories.

All regular wave theories used for gravity platform analysis represent attempts to solve the same set of governing equations. These equations are discussed in Section 5.2.1.

5.2.1 Formulation of the basic equations

Rahman (1995) notes that real water waves propagate over viscous oceans with irregular rough bottoms of varying permeability. However, he notes that the main body of fluid motion in real oceans is nearly irrotational (such that viscosity may be ignored) and incompressible. Therefore, the main assumptions used when defining the governing equations for regular wave theories applicable to jack-up assessment are:

1) The flow is assumed to be incompressible.

2) The flow is assumed to be inviscid so that shear forces are negligible.

3) The flow is considered to be irrotational.

Two additional assumptions are also made, these are:

4) The seabed is even and impermeable.

5) The free surface is considered uncontaminated implying that surface tension effects are negligible and that there is constant pressure over the free surface.

Barltrop & Adams (1991) describe the formulation of the governing equations in the x,y,z Cartesian coordinate system. **Incompressibility** for a flow means that the flow into any elemental volume must equal that out of the elemental volume. The mathematical formulation of this condition leads to the continuity equation:

$$\frac{\partial u}{\partial x} + \frac{\partial v}{\partial y} + \frac{\partial w}{\partial z} = 0 \tag{5.1}$$

where u, v and w are the wave particle velocities in the x, y and z directions respectively.

Inviscidity implies that the rate of rotation for a group of particles is constant. This gives the equations:

$$\frac{1}{2}\left(\frac{\partial w}{\partial y} - \frac{\partial v}{\partial z}\right) = \omega_x \tag{5.2}$$

$$\frac{1}{2}\left(\frac{\partial u}{\partial z} - \frac{\partial w}{\partial x}\right) = \omega_y \tag{5.3}$$

$$\frac{1}{2}\left(\frac{\partial v}{\partial x} - \frac{\partial u}{\partial y}\right) = \omega_z \tag{5.4}$$

where ω_x, ω_y and ω_z are constants. For **irrotational** flow:

$$\omega_x = 0 \quad \omega_y = 0 \quad \omega_z = 0$$

The equations of motion for an elemental volume are formulated by considering the forces necessary to accelerate an infinitesimal element. This leads to the equations of dynamic equilibrium. These are:

$$\frac{Du}{Dt} = \frac{f_x}{\rho} - \frac{1}{\rho}\frac{\partial P}{\partial x} \tag{5.5}$$

$$\frac{Dv}{Dt} = \frac{f_y}{\rho} - \frac{1}{\rho}\frac{\partial P}{\partial y} \tag{5.6}$$

$$\frac{Dw}{Dt} = \frac{f_z}{\rho} - \frac{1}{\rho}\frac{\partial P}{\partial z} \tag{5.7}$$

where ρ is the density of water, P is the fluid pressure and f_x, f_y and f_z are body forces in the x, y and z directions respectively. Here, the z axis is coincident with the direction of the acceleration due to gravity g and so f_x and f_y are typically zero and $f_z = -\rho g$. The differentials Du/Dt, Dv/Dt and Dw/Dt are the total particle accelerations in the x,y,z directions respectively. These can be expressed in Eulerian form as:

$$\frac{Du}{Dt} = \frac{\partial u}{\partial t} + u\frac{\partial u}{\partial x} + v\frac{\partial u}{\partial y} + w\frac{\partial u}{\partial z} \tag{5.8}$$

$$\frac{Dv}{Dt} = \frac{\partial v}{\partial t} + u\frac{\partial v}{\partial x} + v\frac{\partial v}{\partial y} + w\frac{\partial v}{\partial z} \tag{5.9}$$

$$\frac{Dw}{Dt} = \frac{\partial w}{\partial t} + u\frac{\partial w}{\partial x} + v\frac{\partial w}{\partial y} + w\frac{\partial w}{\partial z} \tag{5.10}$$

where $\partial u/\partial t$, $\partial v/\partial t$ and $\partial w/\partial t$ represent the acceleration of the flow in the x,y and z directions at some point in space. The other terms in Eqns 5.8 to 5.10 are the convective terms of the total particle acceleration.

Wave theories are developed by defining a velocity potential ϕ or a stream function ψ. The velocity potential is related to the velocity by the equations:

$$u = \frac{\partial \phi}{\partial x} \quad v = \frac{\partial \phi}{\partial y} \quad w = \frac{\partial \phi}{\partial z} \tag{5.11 a:b:c}$$

These expressions for ϕ satisfy the irrotationality condition. Substitution of Eqns 5.11 a:b:c into the continuity equation (Eqn 5.1) leads to the formulation of the Laplace equation.

$$\nabla^2\phi = \frac{\partial^2\phi}{\partial x^2} + \frac{\partial^2\phi}{\partial y^2} + \frac{\partial^2\phi}{\partial z^2} = 0 \tag{5.12}$$

The stream functions are orthogonal to the velocity potentials, but can only satisfy the irrotational condition in two-dimensions. Therefore:

$$u = \frac{\partial \psi}{\partial y} \qquad v = - \frac{\partial \psi}{\partial x} \tag{5.13 a:b}$$

Further development, is now given in terms of velocity potential only. Combining the irrotationality condition with the Eulerian dynamic equilibrium condition leads after some manipulation, to the unsteady form of the Bernoulli equation:

$$\frac{\partial \phi}{\partial t} + \frac{1}{2}(u^2 + v^2 + w^2) + gz + \frac{P}{\rho} = C(t) \tag{5.14}$$

For steady flow $\partial\phi/\partial t = 0$, and $C(t)$ is constant. If the axis system is defined to be moving at the wave celerity, $\overline{c}$, then for a regular wave, flow in that axis system is steady. An expression for ϕ is developed by satisfying the Laplace equation and the boundary conditions. The boundary conditions are:

1) No flow through the seabed. Therefore:

$$\frac{\partial \phi}{\partial z} = 0 \qquad \text{at } z = - d \tag{5.15}$$

where d is the water depth.

2) Constant pressure over the free surface. From the Bernoulli equation, this gives:

$$\frac{\partial \phi}{\partial t}\Big|_{z = \eta} + g\eta + \frac{1}{2}(u_\eta^2 + v_\eta^2 + w_\eta^2) = constant \tag{5.16}$$

where η is the z-coordinate of the surface. For a two dimensional flow in the x-z plane with an axis system translating at the wave celerity, $\partial\phi/\partial t = 0$ and Eqn 5.16 can be expressed in the form (Rahman, 1995):

$$\eta + \frac{1}{2g}[(u_\eta - \overline{c})^2 + w_\eta^2] = Q \tag{5.17}$$

where Q, the Bernoulli constant, represents the total energy along the free surface. Note that Eqn 5.16 and Eqn 5.17 represent the same boundary condition. It is referred

to as the dynamic free surface boundary condition.

3) The final condition is that particle velocities at the surface must equal the free surface velocity itself. (When the surface particle velocities exceed the free surface velocity, the wave is said to have reached its breaking limit and particles are ejected from the crest.) This condition is expressed mathematically by making the resultant free surface velocity vector everywhere tangential to the free surface: this is the kinematic free surface condition. Therefore:

$$\frac{\partial \eta}{\partial x} = \frac{w_\eta}{u_\eta - \bar{c}} \tag{5.18}$$

Eqns 5.15 to 5.18 present considerable difficulty in solution due to the free surface boundary conditions. The equations are non-linear and are applied at the free surface boundary, η, which is unknown until the equations have been solved. It is the different methods of approximating the free surface boundary conditions that lead to the development of differerent wave theories. Section 5.2.2 presents the results for some of the most frequently used theories in the jack-up industry for flow in two dimensions (x-z plane).

5.2.2 Some common wave theories

The wave theories are presented with respect to the axis system of Fig 5.1 where the elevation, z, is measured from the still water level. For reasons discussed in Section 5.4, only horizontal kinematics are presented.

5.2.2.1 Linear Theory

Linear theory was formulated by Airy (Airy, 1845) using velocity potential, ϕ. Eqns 5.16 and 5.18 are linearized by assuming that the wave heights are small compared to the wavelength and the depth. Therefore $\eta + d \approx d$ and $u^2 + w^2 \approx 0$. The free surface boundary conditions of Eqns 5.16 and 5.18 are now applied at $z = 0$. Furthermore, the normal to the free surface is assumed to be vertical, so the kinematic free surface boundary condition (Eqn 5.18) is expressed:

$$\frac{\partial \eta}{\partial t} = \frac{\partial \phi}{\partial z}\Big|_{z=0} \tag{5.19}$$

Linear theory can also be understood to be a first order Stokes solution (see Section 5.2.2.3). In view of the assumptions in its derivation, the theory is not valid above the still water level. The results needed for an engineering analysis are:

$$\eta(x,t) = \frac{H}{2}\cos A \tag{5.20}$$

$$u(x,z,t) = \frac{\pi H}{T}\frac{\cosh(k(z+d))}{\sinh(kd)}\cos A \tag{5.21}$$

$$\dot{u}(x,z,t) = \frac{2\pi^2 H}{T^2}\frac{\cosh(k(z+d))}{\sinh(kd)}\sin A \tag{5.22}$$

where:

$$A = 2\pi\left(\frac{x}{L} - \frac{t}{T}\right) \tag{5.23}$$

and u and $\dot{u}$ are the horizontal water particle velocity and local flow acceleration respectively. The wavenumber k is found from:

$$k = \frac{4\pi^2}{gT^2}\left[\tanh\left(\frac{2\pi d}{L}\right)\right]^{-1} \tag{5.24a}$$

which reduces to:

$$k \approx \frac{4\pi^2}{gT^2} \tag{5.24b}$$

in deep water.

5.2.2.2 Wheeler stretched Airy Theory

As mentioned in Section 5.2.2.1 linear theory is not theoretically valid above the mean water level. However, linear theory is often extrapolated above the mean water level. Although linear theory is thought to overpredict particle kinematics in the crest, this is justified on the grounds that the difference in velocity predictions above the mean water level between linear and higher order theories (such as Stokes fifth theory) is often small in certain circumstances such as in deep water (Gudmestad & Connor, 1986).

Linear theory forms the basis for linear random theory which involves the summation of sinusoidal waves of different frequencies. The overprediction of crest velocities increases without bound as the wave frequency increases (Gudmestad, 1990). As a result of this, several empirical corrections to linear theory exist, with Wheeler stretching (Wheeler, 1970) being one of the most widely used (SNAME, 1993). It involves an empirical alteration of the depth decay function formulated on the basis of comparison with wave tank results in both the velocity and acceleration terms. Although Wheeler stretching violates the Laplace equation locally, satisfying an average flow condition instead, its application lowers the crest velocities and raises the trough velocities. The wave elevation remains as in Eqn 5.21 but the kinematics are now modified to:

$$u(x,z,t) = \frac{\pi H}{T} \frac{\cosh\left(\frac{k(z+d)}{1+\eta/d}\right)}{\sinh(kd)} \cos A \tag{5.25}$$

$$\dot{u}(x,z,t) = \frac{2\pi^2 H}{T^2} \frac{\cosh\left(\frac{k(z+d)}{1+\eta/d}\right)}{\sinh(kd)} \sin A \tag{5.26}$$

5.2.2.3 Stokes finite wave amplitude theories

Two years after Airy proposed his linearized water wave theory (Airy, 1845), Stokes extended the analysis to finite amplitude waves (Stokes, 1847). Here all terms are retained in the non-linear free surface boundary conditions of Eqns 5.16 (or 5.17) and 5.18. The theory is based on the fact that for steady flow, there are an infinite set of potentials of the form:

$$\phi_n = B_n \cosh[nk(z + d)] \sin(nkx) \tag{5.27}$$

for n = 1, 2...∞, that satisfy the Laplace equation (Eqn 5.12). Rahman (1995) notes that the better known solutions were attempted by making use of a small perturbation parameter ε, related to H/L. The total steady state velocity potential is expressed:

$$\phi = \sum_{n=1}^{\infty} \varepsilon^n \phi_n \tag{5.28}$$

Similarly, wave elevation, wave celerity and wave energy are expressed in the forms:

$$\eta = \sum_{n=1}^{\infty} \varepsilon^n \eta_n \qquad \overline{c} = \sum_{n=1}^{\infty} \varepsilon^n \overline{c_n} \qquad Q = \sum_{n=1}^{\infty} \varepsilon^n Q_n \tag{5.29 a:b:c}$$

As before, the wave surface elevation, η, is unknown before the system of equations is solved. To achieve a solution, the free surface boundary conditions of Eqns 5.17 and 5.18 are satisfied by expanding the variables of Eqns 5.28 and 5.29 as Taylor series about $z = 0$. For example, the velocity potential is expanded to give the form:

$$\begin{aligned} \phi[x,\eta(x)] &= \phi(x,0) + \eta \left(\frac{\partial \phi}{\partial z}\right)\Big|_{z=o} + \ldots\ldots \\ &= (\varepsilon\phi_1 + \varepsilon^2\phi_2 + \ldots.) \\ &+ (\varepsilon\eta_1 + \varepsilon^2\eta_2 + \ldots.) \times \left(\varepsilon\frac{\partial \phi_1}{\partial z} + \varepsilon^2\frac{\partial \phi_2}{\partial z} + \ldots.\right) \end{aligned} \tag{5.30}$$

By equating terms with the same power of ε in the surface boundary condition equations, progressively higher order solutions can be obtained in terms of lower order

solutions. If n in Eqns 5.28 and 5.29 is taken to N instead of ∞, then this gives an N^{th} order approximation to the solution. As N increases, this necessitates the calculation of a large number of complicated coefficients (20 for N = 5). Barltrop & Adams (1991) note that due to the large number and complex nature of the coefficients for higher order solutions, small algebraic errors can occur in calculation so that results reported by different analysts tend to vary. If N = 1, then linear theory is recovered. Solutions to third order have been developed (*e.g* Skjelbreia, 1959) but are seldom used in the offshore industry today. Results taken to fifth order are most commonly used in the offshore industry and particularly in the solution by Skjelbreia & Hendrickson (1960). The fifth order results needed for slender member force calculation are:

$$\begin{aligned} k\eta(x,t) = {} & \gamma\cos\Phi + (\gamma^2 B_{22} + \gamma^4 B_{24})\cos 2\Phi + (\gamma^3 B_{33} + \gamma^5 B_{35})\cos 3\Phi \\ & + \gamma^4 B_{44}\cos 4\Phi + \gamma^5 B_{55}\cos 5\Phi \end{aligned} \tag{5.31}$$

$$\begin{aligned} u(x,z,t) = {} & \bar{c}\,(\gamma A_{11} + \gamma^3 A_{13} + \gamma^5 A_{15})\cosh\sigma\cos\Phi \\ & + 2\bar{c}\,(\gamma^2 A_{22} + \gamma^4 A_{24})\,\mathit{cosh}2\sigma\cos 2\Phi \\ & + 3\bar{c}\,(\gamma^3 A_{33} + \gamma^5 A_{35})\,\mathit{cosh}3\sigma\,\mathit{cos}3\Phi \\ & + 4\bar{c}\,(\gamma^4 A_{44})\,\mathit{cosh}4\sigma\,\mathit{cos}4\Phi \\ & + 5\bar{c}\,(\gamma^5 A_{55})\cosh 5\sigma\cos 5\Phi \end{aligned} \tag{5.32}$$

$$\begin{aligned} \dot{u}(x,z,t) = {} & k\bar{c}^2\,(\gamma A_{11} + \gamma^3 A_{13} + \gamma^5 A_{15})\cosh\sigma\sin\Phi \\ & + 4k\bar{c}^2\,(\gamma^2 A_{22} + \gamma^4 A_{24})\cosh 2\sigma\sin 2\Phi \\ & + 9k\bar{c}^2\,(\gamma^3 A_{33} + \gamma^5 A_{35})\,\mathit{cosh}3\sigma\,\mathit{sin}3\Phi \\ & + 16k\bar{c}^2\,(\gamma^4 A_{44})\cosh 4\sigma\,\mathit{sin}4\Phi \\ & + 25k\bar{c}^2\,(\gamma^5 A_{55})\,\mathit{cosh}5\sigma\sin 5\Phi \end{aligned} \tag{5.33}$$

where $\sigma = k\,(z + d)$ and $\Phi = k\,(x - \bar{c}t)$. The coefficients A_{ij}, B_{ij} and C_i (see Eqn 5.35) are functions of d/L and are listed by Skjelbreia & Hendrickson but are also

summarized in Patel (1989) and Prince-Wright (1988) for example. The values of k and γ are found by simultaneous solution of the equations:

$$\frac{\pi H}{d} = \frac{2\pi}{kd}\left[\gamma + \gamma^3 B_{33} + \gamma^5 (B_{35} + B_{55})\right] \tag{5.34}$$

and

$$\frac{2\pi d}{gT^2} = \frac{kd}{2\pi}\tanh[kd(1 + \gamma^2 C_1 + \gamma^4 C_2)] \tag{5.35}$$

The wave celerity is given by the expression:

$$\overline{c}^2 = \overline{c_0}^2 (1 + \gamma^2 C_1 + \gamma^4 C_2) \tag{5.36}$$

where $\overline{c_0}$ is the linear wave celerity. (Note that Skjelbreia & Hendrickson's expression for C_2 was subject to a minor correction by Nishimura *et al* (1977) in that the term in c^8 should be -2592 c^8 and not +2592c^8.)

5.2.2.4 Stream function theory

Stream function theory was first developed by Dean (1965) and is applicable to two dimensional flow. Dean's stream function has the form:

$$\psi(x,z) = \frac{X_1}{T} z + \sum_{n=2}^{N} X_n \sinh(nk(z + d)) \cos(nkx) \tag{5.37}$$

where N represents the order of the theory (originally taken to 19). The kinematic free surface boundary condition (constant pressure along the surface) means that the surface value of the stream function is a constant. Therefore:

$$\psi_\eta = \frac{X_1}{T}\eta + \sum_{n=2}^{N} X_n \sinh(nk(\eta + d)) \cos(nkx) \tag{5.38}$$

The coefficients X_n are found iteratively by minimizing the mean square error, E, in the fit with the dynamic free surface boundary condition. Therefore:

$$E = \frac{1}{I} \sum_{i=1}^{I} (Q_i - \bar{Q})^2 \qquad (5.39)$$

where i takes values from 1 to I as x takes values spanning a wavelength. The variable Q_i is the Bernoulli constant at the i^{th} position of x and $\bar{Q}$ is the average value of the Bernoulli constants. The wave height, H, is not a specific input to the iterative process, so once any solution has been found, further iterations on complete solutions are performed until the wave height is close to the desired wave height. Sarpkaya & Isaacson (1981) note that as the process is essentially a Fourier expansion of the surface elevation, it gives the best fit to the surface boundary conditions compared to linear theory and the Stokes fifth order theory. Barltrop & Adams (1991) note that the theory is valid for a wide range of wave heights in deep water but breaks down in shallow water (as does Stokes' theory). It can also be very slow to converge to a solution in deep water.

5.2.2.5 Wave theories application

Wave theories can be assessed from a theoretical viewpoint or by comparisons with experimental values. Sarpkaya & Isaacson (1981) note that all wave theories (without empirical corrections) satisfy the Laplace equation (Eqn 5.12) and the seabed boundary condition. Therefore, the fit of the wave theory to the free surface boundary conditions is generally used as a measure of error. However, they also note that suitability from a theoretical viewpoint does not necessarily correspond to a better fit with experimental data. Also, due to difficulties in obtaining the data, experimental comparisons for steep waves are largely unavailable. Modern computer methods can provide a good fit to the surface boundary conditions numerically. However, they

are in excess of typical engineering requirement when compared to the other assumptions used in analysis of an offshore structure.

Of the methods discussed in Section 5.2.2, stream function theory provides the best fit to the free surface boundary conditions. Barltrop & Adams (1991) note that the theory is valid for most water depths and wave heights encountered by offshore structures. They also note that a high order stream function can successfully model the kinematics of steep deep water breaking waves (spilling breakers). However, Sarpkaya & Isaacson (1981) note that the results of Stokes theory at fifth order overlap with those of stream function theory in deep water ($d/gT^2 > 0.01$). Several selection diagrams for wave theories have been published (*e.g* Dean, 1970; SNAME, 1993) and these are discussed further in Section 6.2 at the time of application. The theories implemented in JAKUP are linear theory, Wheeler stretched linear theory and Stokes' theory at fifth order. The choice of theory is user defined.

5.3 Current

When assessing a jack-up for site suitability, a current associated with the wave for the return period must also be specified. Vugts (1990) notes that there is more uncertainty involved in selecting an appropriate return period current than with selecting a design wave. This is because there is a shortage of data concerning the joint probability of occurrence of waves and current. Once a current has been selected, however, further complications arise in defining the nature of the wave-current interaction. These concerns can be grouped into two categories. Firstly, the influence of current on the wave particle velocities must be defined. Secondly, the manner in which hydrodynamic forces due to current are accounted for must be considered.

Several theories exist for defining particle kinematics in the presence of current. In reality, when a wave encounters a current propagating in the wave direction, the wave amplitude decreases and the wavelength increases and *vice versa* when the current propagates against the wave direction. Barltrop & Adams (1991) modify the use of regular wave theories by Doppler shifting the wave kinematics. An apparent wave period T_0 is defined which is the wave period seen by an observer translating at the current velocity, u_c. If the actual period is T (*i.e* relative to a stationary axis system), a first order solution is obtained by simultaneous solution of the equations:

$$\frac{L}{T} = \frac{L}{T_0} + u_c \tag{5.40}$$

which defines the wave celerity in the stationary axis system, and:

$$\frac{gT_0^2}{2\pi} = \frac{L}{\tanh(2\pi d/L)} \tag{5.41}$$

which is the full linear dispersion equation. Thus, the celerity in the fixed reference frame is based on the actual period T, whilst the particle kinematics are calculated on the basis of the apparent wave period, T_0. Eqn 5.40 is only theoretically correct for regular waves based on potential flow in the presence of a current profile uniform with depth. A non-uniform profile implies rotational flow. The API (1993) suggest a third empirical simultaneous equation to define an equivalent steady current, u_c, in the presence of a non-uniform current, $U_c(z)$. This can be expressed:

$$u_c = \frac{4\pi/L}{\sinh(4\pi d/L)} \int_{-d}^{0} U_C(z) \cosh\left[\frac{4\pi(z + d)}{L}\right] dz \tag{5.42}$$

Current also has an impact on wave spectra for irregular seas. For example, Bennet & Patel (1987) found that in model tests in a wave tank on a scaled jack-up, if wave amplitudes were to be matched to those found in the zero current case, the

input wave spectrum to the wave generator had to be modified in the presence of current. Eatock Taylor & Rajagopalan (1983) modify the wave spectrum in the presence of current using the equation:

$$S_{\eta\eta}(\omega) = \frac{4S^{*}_{\eta\eta}(\omega)}{\left[1 + \sqrt{1 + \frac{4u_c\omega}{g}}\right]^2 \sqrt{1 + \frac{4u_c\omega}{g}}} \tag{5.43}$$

where $S_{\eta\eta}{}^{*}(\omega)$ is the zero current wave spectrum and $S_{\eta\eta}(\omega)$ is the modified spectrum that accounts for the change in wave height in the presence of current. $S_{\eta\eta}(\omega)$ is limited by an upper limit due to wave breaking.

Further issues are raised concerning the applicability of the Morison equation (see Section 5.4) to combined wave-current kinematics. Sarpkaya & Isaacson (1981) note that there is little information on the effect of current and wave interaction on hydrodynamic loading. Vugts (1990) suggests that in the presence of current, the drag coefficient may be reduced. His explanation of this is that currents carry away drag induced vortices shed from the structure before wave cycling can move them back onto the structure. Although recent research suggests that combined wave-current forces should be found from separate applications of the Morison equation (Freize *et al*, 1995), it is still normal practice for jack-up assessments to add the current and wave kinematics before applying the Morison equation (Patel, 1989). The conventional method of including the current effects on wave loading is by vectorially superimposing the current profile and the wave velocity field generated in the absence of current (Sarpkaya & Isaacson, 1981). Vugts (1990) notes that this is almost certainly too simplistic a model. However, together with the use of drag and inertia coefficients (see Section 5.4) defined for the zero current case, this approach will in general lead to conservative predictions of in-line forces. This approach is used by

such analysts as Loseth *et al* (1990) and Nielsen *et al* (1994) for example. It is also the approach adopted by SNAME (1993).

The influence of currents on wave particle kinematics is not considered in this thesis. Therefore, wave-current kinematics are found by the superposition of the two velocity fields as in SNAME (1993). This introduces a steady state offset into the loading and provides additional harmonic content into the wave loading (see Section 5.4).

5.4 Hydrodynamic loading

The Morison equation (Morison *et al*, 1950; O'Brien & Morison, 1952) is still the main tool used in the calculation of hydrodynamic loads on slender members in waves. It was originally proposed to calculate the horizontal hydrodynamic loading on a vertical pile in harmonic flow. It consists of a non-linear drag term proportional to $u|u|$ due to vortices caused as the flow passes the member and an inertia term due to the pressure gradient in an accelerating fluid. It is expressed mathematically by the equation:

$$F(x,z,t) = (1/2)C_d \rho D u|u| + C_m \rho A \dot{u} \qquad (5.44)$$

where $F(x,z,t)$ is the horizontal force per unit length on the vertical cylinder, ρ is the density of water, D is the member diameter, A is the member cross-sectional area and C_d and C_m are the drag and inertia coefficient respectively. Vugts (1990) notes that the inertia term is valid only if there is negligible disturbance of the incoming wave due to the presence of the member. The drag term is entirely empirical. Generally, the equation is applied if the ratio of wavelength to reference diameter is greater than 5.

Empirical modifications have been made to the equation to account for current and relative movement between the structure and the fluid. The extended Morison equation incorporating relative motions is expressed in the form:

$$F(x,z,t) = (1/2)C_d\rho D(u_t - \dot{s})|u_t - \dot{s}| + C_m\rho A\dot{u} - (C_m - 1)\rho A\ddot{s} \quad (5.45)$$

where u_t is the vector sum of the current and wave velocities resolved normal to the member axis. The variables $\dot{s}$ and $\ddot{s}$ are the structural velocity and acceleration respectively at point (x,z). The drag term is now proportional to $(u_t - \dot{s})|u_t - \dot{s}|$ and therefore directly formulates the system hydrodynamic damping. The non-linear drag term also introduces harmonics into the loading time history. This is because the term, $\cos\omega t\,|\cos\omega t|$ (introduced by the cyclic variation of the particle kinematics), has a Fourier component at 3ω, where ω is the wave angular frequency. Therefore, structures may be excited by wave components at three times their natural period. In the presence of a current, the 3ω component is reduced and a 2ω component appears. The components are approximately equal if the current velocity is 20% of the wave orbital velocity (Barltrop & Adams, 1991).

For hydrodynamic loading due to regular waves, SNAME (1993) suggest the use of the extended Morison equation incorporating the relative motion effects. For a random wave analysis, SNAME (1993) state that the extended Morison equation should only be used if :

$$\frac{uT_n}{D_i} \geq 20 \quad (5.46)$$

with:

$$u = u_c + \frac{\pi H_s}{T_z} \quad (5.47)$$

where u is the particle velocity, D_i is the reference diameter of a chord, H_s is the significant wave period, T_z is the zero-up crossing period, T_n is the fundamental period

of the jack-up and uT_n/D_i represents the Keulegan-Carpenter parameter of the flow. As this thesis is concerned with regular wave loading, the relative motion formulation of Eqn 5.45 is used in JAKUP.

A further question is raised due to the presence of particle accelerations in Eqn 5.45. Sarpkaya & Isaacson (1981) note that the particle acceleration term in the Morison equation is often applied without the convective terms (*i.e* the flow acceleration is used). For example, Barltrop & Adams (1991) and Patel (1989) omit convective terms in their Morison equation formulations. SNAME (1993) state that $\dot{u}$ is the particle acceleration, but does not explicitly say whether convective terms are to be applied or neglected. Hahn & Sangvi (1994) for example, also use the term 'particle acceleration' but then employ flow accelerations in their formulations. The API (1993) note that although some papers advocate the use of convective acceleration terms (*e.g* Madsen, 1986), these are all based on the assumption that the flow does not separate from the cylinder. They state that this is only true for very small amplitude oscillations. Furthermore, the convective acceleration only exceeds 15% of the local acceleration in extreme seas. Chen *et al* (1990) observe that jack-up response is drag rather than inertia dominated for much of the wave frequency range of interest, and that the drag dominance increases with increasing wave height. Thus, acceleration terms in JAKUP are used without convective terms when applied to the Morison equation.

5.4.1 The formulation of the Morison equation in JAKUP

In modelling jack-up platform legs, the lattice leg bay sections are often replaced by a single beam running vertically through their plan centroids. Although the P-Δ effect is important in terms of the additional loads incurred due to the hull weight and

eccentricity, the actual leg deflections are considered small in comparison to the wavelengths of waves found in deep water. Therefore in JAKUP particle kinematics are calculated at the undeflected beam position and because no inclined submerged members are modelled, only horizontal water motions are considered.

For JAKUP Eqn 5.45 is expanded as follows:

$$F(x,z,t) = (1/2)\alpha C_d \rho D\ (u_t^2 - 2u_t\dot{s} + \dot{s}^2) + C_m \rho A\dot{u} - (C_m - 1)\rho A\ddot{s} \quad (5.48)$$

where α is +1 for $u_t > \dot{s}$ and -1 for $u_t < \dot{s}$. Using the sign convention shown in Fig 5.2, consider the distributed load in terms of the corresponding beam shape functions of Eqns 3.2 - 3.7 (Clough & Penzien 1975). For the 3 degree of freedom problem shown, the distributed load can be expressed:

$$\begin{aligned} F(x,z,t) = (1/2)C_d\rho D\ (\mathrm{Sgn}(u_t - [\psi_{xl},0,\psi_{\theta 1}] \begin{bmatrix} \dot{x}_1 \\ \dot{z}_1 \\ \dot{\theta}_1 \end{bmatrix})\ (u_t^2 - 2u_t[\psi_{xl},0,\psi_{\theta 1}] \begin{bmatrix} \dot{x}_1 \\ \dot{z}_1 \\ \dot{\theta}_1 \end{bmatrix} \\ + \left([\psi_{xl},\ 0,\ \psi_{\theta 1}] \begin{bmatrix} \dot{x}_1 \\ \dot{z}_1 \\ \dot{\theta}_1 \end{bmatrix} \right)^2) \\ + C_m\rho A\dot{u} - (C_m - 1)\rho A[\psi_{xl},0,\psi_{\theta 1}] \begin{bmatrix} \ddot{x}_1 \\ \ddot{z}_1 \\ \ddot{\theta}_1 \end{bmatrix} \end{aligned} \quad (5.49)$$

Where ψ_{ij} should be understood to mean $\psi_{ij}(z)$, the shape function evaluated at a particular point, z. The function, Sgn, is the resulting sign of, $u_t - [\psi_{xl},0,\psi_{\theta 1}] \begin{bmatrix} \dot{x}_1 \\ \dot{z}_1 \\ \dot{\theta}_1 \end{bmatrix}$.

An equivalent nodal load is found via the integration of the distributed load function with the corresponding shape function. Therefore P_{ij} at time t is found from:

$$P_{ij} = \int_{length} \psi_{ij}(z)\ F(x,z,t)\ dz \tag{5.50}$$

This integral is found by 7 point Gauss integration. For the 3 degree of freedom case in Fig 5.2, Eqn 5.50 can be expanded to give:

$$P_{ij} = \rho \sum^{gp} \kappa_{gp} \psi_{ij}(z_{gp}) \left(\underbrace{\frac{C_d D \alpha u_t^2(z_{gp})}{2}}_{(a)} + \underbrace{C_m A \dot{u}(z_{gp})}_{(b)} \right.$$

$$\underbrace{- C_d D \alpha\ u_t(z_{gp})\ \ [\psi_{xl}(z_{gp}),\ 0,\ \psi_{\theta 1}(z_{gp})] \begin{bmatrix} \dot{x}_1 \\ \dot{z}_1 \\ \dot{\theta}_1 \end{bmatrix}}_{(c)} \tag{5.51}$$

$$\underbrace{- (C_m - 1)\ A\ [\psi_{xl}(z_{gp}),\ 0,\ \psi_{\theta 1}(z_{gp})] \begin{bmatrix} \ddot{x}_1 \\ \ddot{z}_1 \\ \ddot{\theta}_1 \end{bmatrix}}_{(d)}$$

$$\left. \underbrace{+ \frac{C_d D \alpha}{2} \left[[\psi_{xl}(z_{gp}),\ 0,\ \psi_{\theta 1}(z_{gp})] \begin{bmatrix} \dot{x}_1 \\ \dot{z}_1 \\ \dot{\theta}_1 \end{bmatrix} \right]^2}_{(e)} \right)$$

where the Gauss weights are κ_{gp}, z_{gp} is the z value at a Gauss point and the summation ($\sum^{gp}$) is performed over the number of Gauss points. (Each term in Eqn 5.51 is assigned a letter for convenience so that reference can be made to the appropriate term in a discussion in Section 5.6.) In a plane frame assemblage with more than one beam connected to any particular node, P_{ij} is added to any other terms that may contribute to the nodal load. In general, for a plane frame assemblage, the load vector due to hydrodynamic loading takes the form:

$$P = fn(u^2) + fn(\dot{u}) - H_y\dot{x} - A_m\ddot{x} + (fn(\dot{x}^2)) \qquad (5.52)$$
$$(1) \quad (2) \quad (3) \quad (4) \quad (5)$$

Terms (1) and (2) of Eqn 5.52, represent the force on a rigid element as defined by the original Morison equation without relative motion effects. Term (3) of Eqn 5.52 consists of a matrix H_y premultiplying the nodal velocity vector and represents the component of the system hydrodynamic damping linear in the structural motions. This term can be taken to the left hand side of the system equations of motion (Eqn 2.1) where H_y is added to the structural damping matrix. Similarly, term (4) can be taken to the left hand side of Eqn 2.1 where A_m, the added mass matrix, can be added to the structural mass matrix. Term (5) represents the non-linear component of the hydrodynamic damping and is retained as a load on the right hand side of the equations of motion. In JAKUP, these squared nodal velocities are expanded as Taylor series about the beginning of the timestep.

5.5 Wind Loading

Wind forces are time-varying in nature and for certain types of structure (*e.g* long suspension bridges, masts), the dynamic response to these fluctuations is critical to the structural design. For offshore structures, Vugts (1990) notes that the wind-induced forces are generally small compared with the hydrodynamic forces. They account for about 15% of the total environmental loading on a structure under extreme conditions (Patel, 1989) and are a minor contributor in relatively shallow water (< 10 % according to the API, 1993). Furthermore, the main wind force variations have a frequency range appreciably below that of the fundamental natural frequencies of most offshore structures (Vugts, 1990; SNAME, 1993). The forces should not be ignored however, as they can have an effect on the overturning moment due to the large lever

arms developed as the water depth increases.

To proceed with wind loading calculations, a reference wind velocity associated with the return period for the site must first be specified. These reference velocities are specified at a specific elevation above the mean water level. (Normally 10m in the offshore industry.) Patel (1989) notes that there are two types of wind velocity considered in offshore engineering analyses. These are the sustained velocity over a length of time greater than 60 seconds, and the gust velocity averaged over a time less than 60 seconds (usually 3 seconds). The gust velocity accounts for the fact that within long durations, there will be short durations with higher mean speeds. SNAME (1993) recommend the use of the sustained velocity over 1 minute as the reference velocity for jack-up assessments. The API (1993) note that because gust velocities are only coherent over short distances, they affect the smaller elements on a platform and should be used for calculating the maximum static load on individual members.

The wind force, F_{wi} on a projected area can be expressed in the form (SNAME, 1993, API, 1993):

$$F_{wi} = \frac{1}{2}\rho_a \, C_s \, A_i \, v_{zi}^2 \tag{5.53}$$

which is similar to the drag loading term in the Morison equation. The variable A_i is the projected area of block i perpendicular to the direction of the wind, C_s is the shape coefficient for the projected area, ρ_a is the density of air and v_{zi} is the wind velocity at the centre of block i. For leg sections subjected to wind loading, $C_s = C_d$.

Due to air particle contact with the sea surface, wind velocities vary with elevation. If v_{ref} is the reference velocity (*i.e.* the 1 minute sustained velocity for the appropriate return period at an elevation, z_{ref}, of 10m above the mean water level), then at an elevation z, v_{zi} is given by the relationship:

$$v_{zi} = v_{ref}\left(\frac{z}{z_{ref}}\right)^{1/N} \tag{5.54}$$

Patel (1989) notes that Eqn 5.54 is semi-empirical and subject to constant revision. He suggests the value $1/N = 0.113$ for offshore engineering assessments. SNAME (1993) suggest $1/N = 0.1$ and the API (1993) use $1/N = 0.125$, although this latter value is used in conjunction with a sustained reference wind velocity averaged over one hour. Wind force values are normally input directly at the relevant nodes in numerical analysis procedures. It is this approach that is incorporated in JAKUP.

5.6 Test problems

Gudmestad & Connor (1986) present tables of particle velocities for different wave theories in order to compare with their formulation of an engineering approximation for non-linear waves. For a wave with the characteristics, T = 17s, H = 30m and d = 300m, Fig 5.3[a] shows the crest velocities for a linear wave calculated by JAKUP compared with those given by Gudmestad & Connor. Fig 5.3[a] shows that predicted velocities are in full agreement with the reference velocities. (Note that Gudmestad & Connor do not give the trough velocities for the linear case.) Gudmestad & Connor also give a linear wave particle velocity at an elevation of 16.6 m. This is because their surface elevation is based on Stokes' second theory which produces an asymmetric profile about the mean water level. JAKUP does not reproduce this value because linear wave theory predicts a symmetric wave profile about the mean water level. (*i.e* JAKUP returns a zero value for particle kinematics if a Gauss point lies above the free water surface.)

For the same environmental conditions as Fig 5.3[a], Fig 5.3[b] shows the JAKUP and Gudmestad & Connor predictions for the crest and trough velocities of

a Wheeler stretched Airy wave. Once again, there is excellent agreement and it can be seen that Wheeler stretched Airy theory lowers the crest velocities compared to those predicted by linear theory.

Fig 5.3[c] shows the results predicted for a Stokes fifth order wave for the same wave condition considered in Fig 5.3[a] and [b]. Once again, Gudmestad & Connor base their surface elevation (but not the kinematics) on Stokes' second order theory. For these conditions, Stokes fifth order theory predicts a slightly lower crest and a slightly lower trough than Stokes second order theory. However, the velocity predictions by JAKUP and Gudmestad & Connor shown in Fig 5.3[c] again coincide. Fig 5.3[d] shows the predictions for a 17 s, 30m wave for a water depth of 150m. The particle velocities above the mean water level are slightly higher than those in the 300m water depth case. Once again, there is full agreement between the JAKUP predictions and the Gudmestad & Connor results. These results help to verify that the simultaneous equations defined by Eqn 5.34 and Eqn 5.35 are solved correctly in a Stokes fifth analysis. Further evidence of this was provided by the results of Skjelbreia & Hendrickson (1960) who tabulate the values of all 20 coefficients for their solution of Stokes' fifth theory for the wave condition, d = 30ft, H = 18.667ft and T = 7.72s. The coefficients generated by JAKUP were checked against their values and were found to be in full agreement.

Particle kinematics generated by the wave theories are then passed to a subroutine that calculates equivalent nodal loading due to the extended Morison equation. As noted in Section 5.4, JAKUP formulates equivalent nodal loading at each timestep by performing 7 point Gauss integration on the distributed hydrodynamic load on a beam. In order to check the formulation of nodal loads, some tests were done for a uniform linear beam submerged in water.

Consider the beam of Fig 5.4 which is acted upon by a uniform current of 1.5 m/s. The beam properties used are, I = 20 m^4, A = 0.4 m^2, L =120 m, E = 210 GPa, D = 0.71 m and M = 1930,000 kg. Also C_d = 1.0, C_m = 2.0 and 10% damping is placed in the principal mode. For a uniform current, the distributed load due to water particle motions is $1/2(C_d \rho D u_t^2)$. With the values stated above this results in a distributed load of 798.75 N/m. The static end deflection for a linear beam due to a uniform distributed load (w) is:

$$\delta_{static} = \frac{wL^4}{8EI} \tag{5.55}$$

and the static end rotation is:

$$\theta_{static} = \frac{wL^3}{6EI} \tag{5.56}$$

So for the uniform current of 1.5 m/s:

$$\delta_{static} = 4.93 \times 10^{-3} \text{ m}$$

$$\theta_{static} = -5.48 \times 10^{-5}$$

Reference is now made to Eqn 5.51 which has a letter assigned to each term in the Morison formulation. If term (a) of Eqn 5.51 has been formulated correctly then the steady state solution after the initial transient response should converge to the static values. Fig 5.5[a] shows the variation of the lateral displacement with time at the tip node. Similarly, Fig 5.5[b] shows the variation of the end rotation (anticlockwise positive) with time at the top node. These figures show that convergence to the values of δ_{static} and θ_{static} does occur. The test was also done for the beams shown in Fig 5.6 in order to check for any orientation errors. The arrows in the elements in Fig 5.6 show if the beam was specified from node 1 to 2 (*i.e.* 0° to the vertical) or vice versa (180° to the vertical). The output traces obtained from these tests were identical to Fig 5.5[a] and [b] and will therefore not be shown here.

The tests were then repeated for the beam idealized as 2 linear elements as

shown in Fig 5.7[a], [b] and [c] and as 3 linear elements as shown in Fig 5.7[d]. Convergence to the static values defined by Eqn 5.55 and Eqn 5.56 also occurred. Fig 5.8, for example, shows the tip sidesway for the 3 element case of Fig 5.7[d].

In order to check the formulation of term (b) of Eqn 5.51, JAKUP allows the purely artificial scenario of a uniform water particle acceleration to be applied to a structure with no water particle velocity, *i.e*:

$$\dot{u} = 1.5ms^{-2} \quad u_t = 0$$

In this case, the distributed load perpendicular to the beam axis is:

$$w = C_m \rho A \dot{u} \tag{5.57}$$

and from Eqn 5.55 and Eqn 5.56:

$$\delta_{static} = 7.41\text{x}10^{-3} \text{ m}$$

$$\theta_{static} = -8.23\text{x}10^{-5}$$

This case was applied to the orientations of Fig 5.6[a] and [b]. Fig 5.9 shows a typical sidesway (corresponding to Fig 5.6[a]) which shows that the correct steady state value is obtained. Similarly, the 4 noded beam of Fig 5.7[d] was analysed. The resulting sidesway also converged to the static values and will not be included here, but Fig 5.10 shows the resulting temporal variation of end rotation.

For a beam fully submerged in water, the matrix in term (d) of Eqn 5.51 is constant whilst that in term (c) varies with the wave period. However, the term (c) matrix is constant in the presence of a uniform current. For the six degree of freedom problem in Fig 5.11[a] and a constant current, the matrix in term (c) takes the form:

$$C_d \rho D \alpha u_t \begin{bmatrix} \int \psi_1(z)\psi_1(z) & 0 & \int \psi_1(z)\psi_3(z) & \int \psi_1(z)\psi_4(z) & 0 & \int \psi_1(z)\psi_6(z) \\ & 0 & \int \psi_2(z)\psi_3(z) & \int \psi_2(z)\psi_4(z) & 0 & \int \psi_2(z)\psi_6(z) \\ & & \int \psi_3(z)\psi_3(z) & \int \psi_3(z)\psi_4(z) & 0 & \int \psi_3(z)\psi_6(z) \\ & & & \int \psi_4(z)\psi_4(z) & 0 & \int \psi_4(z)\psi_6(z) \\ & & & & 0 & \psi_5(z)\psi_6(z) \\ \textit{symmetric} & & & & & \int \psi_6(z)\psi_6(z) \end{bmatrix} \tag{5.58}$$

and the matrix in term (d) takes the form:

$$(C_m - 1)\rho A \begin{bmatrix} \int \psi_1(z)\psi_1(z) & 0 & \int \psi_1(z)\psi_3(z) & \int \psi_1(z)\psi_4(z) & 0 & \int \psi_1(z)\psi_6(z) \\ & 0 & \int \psi_2(z)\psi_3(z) & \int \psi_2(z)\psi_4(z) & 0 & \int \psi_2(z)\psi_6(z) \\ & & \int \psi_3(z)\psi_3(z) & \int \psi_3(z)\psi_4(z) & 0 & \int \psi_3(z)\psi_6(z) \\ & & & \int \psi_4(z)\psi_4(z) & 0 & \int \psi_4(z)\psi_6(z) \\ & & & & 0 & \psi_5(z)\psi_6(z) \\ \textit{symmetric} & & & & & \int \psi_6(z)\psi_6(z) \end{bmatrix} \tag{5.59}$$

where the integrals are taken over the beam length. For a fully submerged beam with a constant current, it is possible to evaluate the matrices using a hand calculator. For the configuration of Fig 5.11[b] and a current of 1.5 m/s, the damping matrix in term (c) gives:

$$(c) = \begin{bmatrix} 23734.285 & 0 & 200828.57 & 8215.7143 & 0 & -118671.12 \\ 0 & 0 & 0 & 0 & 0 & 0 \\ 200828.57 & 0 & 2190857.2 & 118671.12 & 0 & -1643129.7 \\ 8215.7143 & 0 & 118671.12 & 47468.562 & 0 & 0 \\ 0 & 0 & 0 & 0 & 0 & 0 \\ -118671.12 & 0 & -1643.129.7 & 0 & 0 & 4.3817\times10^6 \end{bmatrix}$$

and the added mass matrix in term (d) is:

$$(d) = \begin{bmatrix} 8914.2856 & 0 & 75428.572 & 3085.7143 & 0 & -44571.312 \\ 0 & 0 & 0 & 0 & 0 & 0 \\ 75428.572 & 0 & 822857.16 & 44571.312 & 0 & -617137.92 \\ 3085.7143 & 0 & 44571.312 & 17828.568 & 0 & 0 \\ 0 & 0 & 0 & 0 & 0 & 0 \\ -4457.312 & 0 & -617137.92 & 0 & 0 & 1.6457\times10^{6} \end{bmatrix}$$

The matrices generated by JAKUP for this test case were outputed to a file for a significant number of timesteps. The values were then checked and were in full agreement with the values calculated by hand. The test was repeated with a current of 2.5 m/s. The added mass matrix was unchanged as would be expected and the coefficients of the hydrodynamic damping matrix increased by a factor of 1.67 (*i.e* 2.5/1.5). This meant that given the correct water particle kinematics, terms (c) and (d) of Eqn 5.51 were formulated correctly.

Term (e) of Eqn 5.51 does not lend itself to the type of analysis described for the previous terms. This is because the vector of nodal velocities is not separable from the rest of the term as in terms (c) and (d). However, JAKUP calculates terms (c) and (e) at the same time having made one calculation for $C_d\rho D\alpha$. As noted in Section 5.4.1, the nodal velocities are expanded as Taylor series about the beginning of the timestep. (This can be performed to different truncation points in the series). The velocity response of a jack-up is generally small compared to the water particle velocity except for a narrow bandwidth bracketing the natural frequency, so it can be predicted that the contribution of term (e) (featuring the square of the structural velocity) to a jack-up analysis is small if not negligible. However, it is expedient to check that, with no structural damping and still water conditions, the response to an impulsive load dies away due to the formulation of term (e). The beams of Fig 5.12 were analysed under these conditions. Fig 5.13[a] shows the response of the beam of

Fig 5.12[b] to an impulsive load. The drag coefficient, C_d is raised to 10.0 to highlight the effect. This figure shows that the decay does occur in the absence of structural damping. The noise on the response path of Fig 5.13[a] is due to the excitation of high frequency mode response. This can be seen more clearly from Fig 5.13[b] which shows the same response path over a reduced timescale. For comparison, Fig 5.14 shows the same test case incorporating 10% structural damping. Results obtained from the beam of Fig 5.12[a] were very similar to those shown in Fig 5.13 and are therefore not included here.

In view of the considerations described thus far, the results of passing a wave of finite height with zero current past the 3 degree of freedom beam idealization was used as the basis to check finer discretizations of the leg. With damping reduced to 2% in the fundamental mode, Fig 5.15 shows one such test case. Fig 5.16 shows the variation of lateral tip displacement with time with results superimposed for all four test cases. As would be expected, the traces show good agreement because inundation effects on the leg are not a factor in the test. These results show that increasing discretization of the leg does not affect the computation of nodal loads in JAKUP.

CHAPTER 6

STRUCTURAL ANALYSIS OF A TYPICAL JACK-UP

6.1 Introduction

The numerical procedures detailed in the preceding five chapters and incorporated into the program JAKUP are now used to perform structural analyses for a simplified rig. The analyses presented in this chapter by no means represent survival design analyses which would involve significantly more finite element modelling and a large burden on computer time. Instead, the range and versatility of JAKUP is demonstrated in the manner of a case study.

6.1.1 A representative jack-up

Fig 6.1 shows the initial numerical model used to represent a plane frame discretization of a typical jack-up. The leg spacing in side elevation of 51.96m indicates that the legs form the nodal points of a 60° equilateral triangle of side 60m when viewed in plan. An equivalent beam model is used, where the actual jack-up legs are each replaced by a discretized single beam passing through the leg centroid with equivalent stiffness and hydrodynamic properties. For this plane frame reduction, the hull is also represented by a beam element. The leg weights are applied as point loads at the nodes, in the same distribution as the mass matrix. However, even with the application of leg self weight, P-Δ effects are in general dominated by the hull weight due to its elevation and eccentricity. An allowance for buoyancy is also included in the nodal load distribution. For the purpose of design it would be desirable to include some form of non-linear leg/hull interaction. This is not,

however, considered here, and the leg-hull connection is assumed rigid.

Although the model is relatively simple, it is adequate to show the trend in behaviour of the jack-up as the environmental loads considered in this chapter vary. In an actual jack-up analysis, an equivalent beam model could not be used to fulfil all of the design requirements for an operational rig. However, the equivalent beam approach is a powerful and computationally efficient way of establishing global loads and displacements which can then be applied, for example, to a detailed leg model or jacking system model. A mixed model can go one step further in providing design data. A mixed numerical model has equivalent legs below the mean water level and a detailed finite element mesh above the mean water level in the vicinity of the hull. The global responses obtained will be similar to those calculated using the simpler approach. However, due to the increased number of degrees of freedom, there will be a reduction in computational efficiency. The values used in Fig 6.1 were derived after considering the properties of 'typical' rigs analysed by Martin (1994), SNAME (1993), Jensen *et al* (1989), NDA (1987) and Nielsen *et al* (1994). Detail above the deck level is not modelled as this increases the number of degrees of freedom and hence the number of poorly discretized high frequency modes. This in turn places greater constraints on the step-by-step integration method. A value of 2% structural damping is placed in the dominant mode (sway mode).

6.1.2 Soil conditions and preloading of the jack-up

The undrained strength profile considered for the clay seabed has the values s_{um} = 50.0 kPa, and ρ = 2.0 kPa/m, where, s_{um} is the undrained shear strength at the mudline level and ρ is the rate of undrained shear strength increase with depth. These values are typical for a North Sea deep water environment (Martin, 1994). The

rigidity index is G/s_u = 100. The spudcans have a 10.0 m radius which is typical of some harsh environment rigs existing today. Fig 6.2 shows a side elevation of the spudcans attached to the jack-up. For simplicity, the spudcan of Fig 6.2 will be represented graphically by the footing shape shown in Fig 6.1.

With the preceding conditions and the jack-up data of Section 6.1.1 specified, there is now enough information to predict the footing penetration under preload. This is accomplished by using the Model B description of footing behaviour. The rig has an operating weight of 206.7 MN (including buoyancy), therefore the jack-up is preloaded to twice this weight as a proof test of the foundation. To accomplish this each footing is preloaded to 137.8 MN, after which the load is reduced to its operating value of 68.9 MN per footing. Fig 6.3 shows the load-penetration path for a preload of 137.8 MN followed by complete removal of the footing load. This Figure shows that there is a total penetration of 5.4m at full preload. When the load is reduced to its operating value, there is a small amount of elastic recovery leading to a total footing settlement of 5.2m from the mudline. Fig 6.3 also shows that when the load is completely removed, there is 5.1m of plastic penetration remaining. This initial plastic penetration, Δz_p^i, can now be used as an input to the soil stiffness subroutine in JAKUP (see Chapter 4) to avoid preloading the rig from the soil surface for each analysis. To be consistent with the Model B prediction of preload penetration, test cases with footings modelled as pinned joints and fixed joints, (0% and 100% moment fixity respectively), have the fixity point 5.2m below the mudline. In JAKUP, it is assumed that the soil does not backfill above the spudcan after the preloading operation occurs. The cavity caused by preloading is therefore modelled as stagnant water.

6.1.3 Environmental conditions and predictions of the jack-up fundamental period

A variety of wave heights and periods are considered in Section 6.2 and Section 6.3 but the water depth is maintained at 90.0 m. This water depth is indicative of the upper range of depths for rigs existing today (Karunakuran *et al*, 1992). After consideration of such environmental design conditions as those used by Brekke *et al* (1990), Hambly *et al* (1990), Karunakuran *et al* (1992) and SNAME (1993), the current velocity (assumed here as a block profile) is taken as 1.0 m/s. A wind velocity of 42.0 m/s is chosen as being representative of a 50 year sustained wind velocity for the North Sea. Using the formulation of Chapter 5 and using an average shape coefficient of 1.0, this wind velocity results in a horizontal load of 3.23 MN. As mentioned in Chapter 5, this is applied directly at the nodes. The wind load is applied at the level of the hull in Fig 6.1.

Barltrop & Adams (1991) note that jack-up analyses are sensitive to the values of drag and inertia coefficient used. In a full assessment analysis, the values would be derived by calibration from either a physical model test or field observations. However, the literature on analyses of harsh environment rigs show a fairly consistent range of values for the hydrodynamic coefficients used for an equivalent leg analysis. The values used in this analysis are based on the leg bay section shown in Fig 6.4 (from Nielsen *et al*, 1994). Therefore, C_{de} = 2.23 and C_{me} = 2.0, where C_{de} and C_{me} are the average equivalent drag and equivalent inertia coefficients respectively. The hydrodynamic equivalent diameter and area are D_e = 2.14m and A_e = 3.5m^2. Note that an equivalent beam model cannot provide any information on the nature of internal wave cancellation effects within a single lattice jack-up leg (see Section 6.2).

Having specified the information in Sections 6.1.1-6.1.3, it is now necessary to gain an estimate of the natural period of the dominant mode of the jack-up. A

solution of the complete linear eigensystem is done by JAKUP prior to integration of the equations of motion in order to give an indication of the magnitude of timestep needed to maintain accuracy and/or stability. The fundamental periods found for the linear system were 7.0s, 5.6s and 3.4s for analyses with pinned, Model B (based on the pseudo-elastic footing stiffnesses after preloading) and fixed footings respectively. For the non-linear system, impulse tests were done to give an estimate of the response in the fundamental mode. Figs 6.5[a], [b] and [c] show the response to a 10.0 MN load applied for 0.01s at the hull level for a rig with pinned footings, Model B footings and fixed footings respectively. The natural periods are 8.3s, 6.6s and 4.6s respectively, showing as expected that the greater the fixity, the shorter the natural period and that the presence of axial loads in the legs reduces their flexural stiffness.

6.1.4 Structural analyses

In the analyses presented, loading is considered along an axis of symmetry with a single leg to windward. However, this does not imply that this combination of jack-up orientation and sea direction will lead to the most critical loading case. The stiffness matrix used accounts for geometric non-linearity including deformation due to shear as detailed in Chapter 3. The Stokes fifth order wave theory in the Skjelbreia & Hendrickson (1960) solution is used to model the water particle kinematics and the extended Morison equation is used to define fluid loading (see Chapter 5). All variables are considered with respect to steady state conditions (*i.e.* transient motions are ignored). The Newmark β = 1/4 method is used to integrate the equations of motion. The size of the timestep used in all analyses is 2.0×10^{-3}s. This value was chosen on the basis of the Model B algorithm. The smallest period of the linear

system incorporating Model B footings (based on the pseudo-elastic footing stiffnesses after preloading) was approximately 2.0×10^{-2}s. The timestep is approximately one tenth of this value. The stability and accuracy arguments of Chapter 2 were based on the response of a linear system. However, as noted in Section 2.8.2, the inherent stability of an unconditionally stable method can be retained in a non-linear system by the use of iteration. Although a larger timestep could be used whilst maintaining stability, it was found that the timestep chosen was needed to adequately trace the path-dependent nature of the Model B solution and maintain accuracy. Similary, a larger timestep could have been used for the analyses with pinned and fixed footings. However, it was decided not to introduce differences into the analyses based on the timestep. The option of using the linear acceleration method was not used. As noted in Chapter 2, the stability limit in a linear system using this method is approximately one tenth of the smallest system natural period. However, for the non-linear solution incorporating Model B footings, this value had to reduced by a factor of about 2. This would have resulted in a smaller timestep than that used with the Newmark β = 1/4 method.

There are a multitude of response variables that can be considered. However, as this is not a design analysis, consideration of each of them does not aid the qualitative understanding of the jack-ups' behaviour. As a result, the response variables considered are the maximum and double amplitude of the hull displacement and the maximum and double amplitude of the lower guide moments. The double amplitude (or peak to trough value) of a variable is the difference between its maximum and minimum value. The maximum value of a response is of interest because the extreme value of stresses in critical members is directly related to the structural stability of the unit. The double amplitude of a response is important from

a fatigue standpoint and influences the unstable propagation of cracks. Nielsen *et al* (1994) note that crack propagation in most steel structures undergoing time varying loading cannot be prevented in the longrun because flaws are inherent in most metallic structures. Therefore a reliable estimate of the onset of unstable crack propagation is highly desirable.

The analyses are divided into two sections. In the first section, computer simulations are carried out at a fixed wave height. These fixed wave height analyses are themselves divided into quasi-static analyses and dynamic analyses. Quasi-static solutions are briefly considered because they form the basis of future dynamic amplification factor comparisons. The quasi-static responses obtained also force consideration of the variation of the loading on the jack-up. Such results are not readily visible by considering dynamic analyses in isolation.

In the second section, analyses are carried out at a fixed value of wave period, but at different values of wave height.

6.2 Analyses at a fixed wave height

In order to display the importance of dynamic amplification on the response of a jack-up rig, analyses are carried out at varying values of period but at a set value of wave height. Fig 6.6 shows the diagram (from SNAME, 1993) of the regions of applicability of wave theories and the regions of limiting wave steepness. Similar figures can be found, for example, in Dean (1970) (see Fig 6.7) and the API (1993). The bounded area for a particular solution technique varies slightly from analyst to analyst. The regions do not represent areas where one method is correct and another

method incorrect. Instead, the boundaries represent guidelines on the divergence of results obtained with one technique from those obtained utilizing a higher order solution technique. Table 6.1 shows a list of wave periods and the wave height, H_d, at which the Stokes fifth solution diverges from a stream function solution. The wave height of limiting wave steepness, H_{max}, is also shown. The wave periods below 9.0s in Table 6.1 bracket the range of fundamental natural periods for the jack-up as detailed in Section 6.1.3. Some of the d/gT^2 values are beyond the scale of Fig 6.6. Fig 6.7 has a slightly more extensive d/gT^2 range. Although the border construction is based on a slightly different criterion than Fig 6.6 (based on the mean square errors to the fit with the free surface boundary conditions), it can be seen that for large d/gT^2, the H/gT^2 values at the borders become constant. Table 6.1 is not a comprehensive list, but it shows that longer periods are associated with a larger limiting wave height than smaller periods.

In order to provide a wave height that can be applied across a wide period range, the wave height of 13.0m is chosen for the fixed height computer simulations. For the 13.0m wave (acting in conjunction with the wind and current condition of Section 6.1.3), the period range considered is from 5.8s to 20.0s. SNAME (1993) note that the periods of most waves are contained in the 2.0-20.0s range. The 5.8s lower limit of the range is a representative point beyond which convergence difficulties are found for the Stokes fifth solution, at the prescribed wave height of 13.0m. These convergence difficulties occur because the second harmonic of the solution becomes significant with respect to the fundamental. Also, the initial wavelength value used in the iteration for a Stokes fifth solution is derived from linear theory. In the (H/gT^2):(d/gT^2) range considered above, the two theories can differ significantly. This

issue is discussed further in Section 6.2.1.1. From Table 6.1 it can be seen that at lower periods, this 13.0m wave height is slightly beyond the limiting wave height region. Therefore some separate analyses are undertaken at a reduced wave height of 6.0m to investigate responses at low periods. The associated period range is 4.6-9.0s.

6.2.1 Quasi-static analyses

A quasi-static analysis involves applying the environmental load incrementally to the jack-up structure whilst ignoring dynamic effects. The quasi-static response is the solution of the stiffness expression:

$$^{(i-1)}F_s + K_T \Delta x^{(i)} = P \qquad (6.1)$$

This is solved using the same Gauss-Jordan subroutine that solves for displacement increments during a dynamic analysis.

6.2.1.1 Hull displacement

For the 13.0m wave in a 90.0m water depth acting in conjunction with the wind and current condition of Section 6.1.3, Fig 6.8[a] shows the maximum sidesway of the hull over a 5.8-20.0s period range for the footings modelled as pinned joints, Model B footings and fixed joints. This Figure shows that as expected, over the full period range considered the pinned footings give the largest displacements and fixed footings the smallest. This can be seen more clearly from Fig 6.8[b] which shows the maximum displacements as a percentage of the corresponding pinned footing analyses, where the fixed footings analyses are typically 30% and the Model B analyses 63% of the pinned footings results.

Fig 6.8[c] shows the variation of the double amplitude of lateral hull displacement over the same period range as Fig 6.8[a]. The relative positions of the

curves due to the three different assumptions of footing behaviour is the same as that of Fig 6.8[a]. Again, this can be demonstrated more clearly by Fig 6.8[d] which shows the responses as percentages of the corresponding pinned footings analysis results.

The turning point for the response paths in Fig 6.8[a] and [c] occur at different periods. Fig 6.8[a] shows that the turning point for the maximum hull displacement curves occurs at a period of about 11.0s. The paths in Fig 6.8[c] (the peak to trough hull displacements) display two turning points. The first occurs at a period of about 7.6s. After this period the response paths remain fairly uniform until a small reduction in response culminates in a second turning point at a period of about 9.0s. The reasons for these results are linked to several interacting effects occurring in the 7.6s to 11.0s period range. These effects can be attributed to the phase of the hydrodynamic loading on the legs and the vertical distribution of loading along each leg.

The period of the Stokes fifth wave that results in the hydrodynamic loading on the windward and leeward legs occurring in antiphase is about 7.6s. At this period, the half wavelength of the wave is approximately equal to the side elevation leg spacing of the jack-up. The first turning point on the response curves of Fig 6.8[c] can be observed to be in the vicinity of this period. This period does not represent a cancellation period due to the presence of harmonics in the load spectrum (see Section 6.2.2.1) and due to the fact that there is a single windward leg and two leeward legs. However, partial cancellation effects occur in the vicinity of this wave period.

The distribution of loading along each leg is also an important factor in the quasi-static response. This can be demonstrated by considering the hydrodynamic

loading on a single leg. Fig 6.9[a] shows the variation of the maximum and double amplitude of horizontal load on a single leg (excluding wind load). Both of the response paths have a turning point at a period of about 10.0s. Because internal cancellation effects within a leg are not modelled, this turning point must occur due to the variation of the vertical distribution of particle kinematics. If the fundamental term in Stokes fifth wave theory is approximated by a linear wave, then by consideration of Eqn 5.21 and Eqn 5.22, the particle velocity can be expressed:

$$u(x,z,t) \approx \frac{\pi H}{T} \frac{\cosh(k(z + d))}{\sinh(kd)} \cos A \tag{6.2}$$

and the flow acceleration by:

$$\dot{u}(x,z,t) \approx \frac{2\pi^2 H}{T^2} \frac{\cosh(k(z + d))}{\sinh(kd)} \sin A \tag{6.3}$$

As the period increases at a set wave height, the factors $\pi H/T$ and $2\pi^2 H/T^2$ decrease, which results in a decrease in the force per unit length at a particular point (see Eqn 5.50). However as the period increases, the wavelength also increases. Therefore the decay with depth of the particle kinematics due to the factor, $\cosh(k(z + d))/\sinh(kd)$, becomes less marked as the period increases. This results in greater loading over the lower portions of the jack-up leg. At the turning point of Fig 6.9[a], this exponential change in the depth decay factor becomes dominant over the decrease in kinematics with period. This effect can be seen more clearly from Fig 6.9[b] which shows that although the total horizontal load on a leg increases after the period of 10.0s, the hydrodynamic overturning moment on the leg continues to decrease after this period due to the vertical distribution of load on the leg. Fig 6.9[b] shows that the moment response only begins to increase after a period of about 14.0s.

The behaviour shown in Fig 6.9[a] and Fig 6.9[b] is not mirrored by the global platform base shear and the global platform overturning moment. Fig 6.9[c] shows

the variation of the maximum and double amplitude of base shear across the period range considered. Strictly for the purposes of Fig 6.9, the contribution of the wind load to the base shear is not included so that the turning points for the maximum and double amplitude variables may be more easily compared. As opposed to Fig 6.9[a] each response path in Fig 6.9[c] has a different turning point. The double amplitude of base shear has a minimum at a period of about 7.6s. As noted earlier, this value is in the vicinity of the period at which the windward and leeward leg loads occur in antiphase. The maximum value of base shear has a minimum value at a period of about 9.0s. Even though this period is larger than 7.6s (and therefore the phase difference between loading on the leeward and windward legs decreases), the maximum value of load on a single leg is still decreasing (see Fig 6.9[a]). The interaction of the two effects leads to a turning point at 9.0s. This demonstrates the importance of phase on the quasi-static response but does not fully explain the shape of the hull displacement variables. This is linked to the global overturning moment. Fig 6.9[d] shows the variation of the maximum and double amplitude of global overturning moment on the platform (excluding the contribution of the wind load) which, as for the base shear, does not match the pattern of behaviour shown for a single leg (see Fig 6.9[b]) due to similar arguments of phase differences of the moment loading on each leg. Fig 6.9[d] shows that most of the features in these curves are mirrored in the response of the hull displacement variables shown in Fig 6.8[a] and 6.8[c]. This can be seen more clearly from Fig 6.10 which shows the variation of the hull displacement variables with the corresponding global overturning moment variable (including wind load). The response paths display a linear relationship with a slight change of slope at the turning point period shown in Fig 6.9[a].

For a 13.0m wave with a full wavelength of 51.96m, wave crests would arrive at the windward and leeward legs in phase. However, considerable difficulty is found in trying to get Stokes fifth theory to converge to a solution for this wavelength due to reasons discussed in Section 6.1.4. Estimating a period using linear theory results in an approximate value of about 5.8s. However, Fig 6.11 shows that for large H/gT^2, linear theory can give up to a 20% difference in wavelength prediction compared to the Stokes fifth theory. To gain an indication of the behaviour of the jack-up unit at low periods, the wave height is reduced to 6.0m. Fig 6.12 shows the variation in wavelength for a 6.0m wave and a 13.0m wave over a 4.6-9.0s period range. Due to the reduction in wave height from 13.0m to 6.0m, the period/wavelength relationship will alter when using the Stokes fifth theory. For example, at a wave height of 6.0m, the period at which the leg loads are in antiphase increases slightly to about 8.0s and a reinforcement period can now be defined at 5.42s. Fig 6.13[a] shows the variation of the maximum hull displacement for the 6.0m wave over a limited number of data points in the 4.6-9.0s period range. As predicted, each response curve shows a maximum at the reinforcement period. Fig 6.13[b] shows that the maxima for the double amplitude of hull displacement also occur at the reinforcement period.

6.2.1.2 Lower guide moments

Fig 6.14[a] shows the variation of the maximum value of lower guide moment for the windward leg. The wave height is 13.0m and the period range considered is the same as in Fig 6.8[a]. As for the variation of maximum lateral hull displacement the assumption of pinned footing behaviour results in the largest lower guide moment at all periods and the assumption of fixed footing behaviour yields the smallest results across the entire period range. It is interesting to note that the trend in behaviour

demonstrated in Fig 6.8[a] is not mapped directly onto the response curves for the maximum windward lower guide moment. There is a high degree of correlation between the hull displacement and moment for the assumption of pinned footing behaviour. However, the paths for the assumption of partial fixity and total fixity display a marked flattening of the response in the higher period range (some 10.0-20.0s).

Fig 6.14[b] shows the variation of the double amplitude of the lower guide moment for the windward leg. (The abbreviation 'l.g.m' on the ordinate axis means, lower guide moment.) In comparison with the double amplitude of the lateral hull displacement, much the same comments as those used in the previous paragraph apply. The pinned analyses show a high correlation with an increasing flattening of the response as the degree of foundation fixity increases.

Any turning points in the lower guide moment paths displayed in Fig 6.14[a] and [b] are fully consistent with those shown in Fig 6.8. As a result low period effects at the reduced wave height of 6.0m are not included here for the moment response, as no new information can be obtained outside that gained from the displacement response. The flattening of the responses as seen in Fig 6.14[a] and Fig 6.14[b] is linked to the variation of the lower guide moment at the leeward legs. Fig 6.14[c] shows the variation of the maximum lower guide moment for one of the leeward legs and Fig 6.14[d] shows the variation of the corresponding double amplitude of the lower guide moment. The shapes of the response paths in Fig 6.14[c] and Fig 6.14[d] are broadly similar to those for the windward leg variables, therefore arguments about the phase and vertical distribution of loading are applicable to the leeward leg variables also. However, the variation of moment between the leeward and windward lower guide moments is not linear. This can be seen more

clearly from Fig 6.15[a] which shows the variation of the maximum windward lower guide moment with the maximum leeward lower guide moment. Similarly, Fig 6.15[b] shows the variation of the double amplitude of windward lower guide moment with the double amplitude of the leeward lower guide moment. Each of the response paths in Fig 6.15[a] and [b] form an angled 'u' shape. The lowest point on each curve corresponds to the period when the vertical distribution of particle kinematics becomes dominant over the decrease in particle kinematics at a particular point (see Fig 6.9[a]). Generally, the windward leg has a larger maximum value and double amplitude of lower guide moment than the leeward legs. It is also noticeable, particularly for the unit with fixed footings, that there is a transfer of moment to the leeward leg after the minimum point on the response path is reached. For example, the double amplitude of windward lower guide moment for the fixed footing unit reaches a minimum value of 45MNm and then remains fairly constant at this value whilst the leeward moment increases from 30 MNm to 40 MNm.

6.2.1.3 Conclusions: quasi-static analyses

The quasi-static response of a jack-up is seen to give the largest response variables for analyses assuming pinned footing behaviour. Similarly, the smallest results occur when fixed footing behaviour is assumed. Analyses with footings modelled as Model B (partial fixity) footings result in intermediate responses at all periods. The phase difference between loading on the windward and leeward legs is seen to be an important effect whereby design conditions should not be chosen to coincide with minimum loading on the jack-up. The trend in behaviour between the hull displacement and the lower guide moment is seen to have a high correlation for pinned analyses with a gradual reduction in correlation as the degree of fixity

accounted for increases. Depth decay factors are also seen to play an important role in the determination of jack-up responses.

6.2.2 Dynamic analysis

Dynamic effects are now included in the analyses of Section 6.2.1. Hydrodynamic loading is calculated using the extended Morison equation. As a result of this formulation, additional non-linear effects occur, including a time varying mass matrix, non-linear hydrodynamic damping and relative motion effects between the water and the structure.

6.2.2.1 Maximum hull sidesway and maximum lower guide moment values

The first two response variables considered are the maximum lateral hull displacement and the maximum lower guide moment for the windward leg. Fig 6.16 shows the variation of the maximum hull sidesway over the 5.8-20.0s period range considered in Fig 6.8[a]. Two regions of significant dynamic amplification can be seen on each response path in Fig 6.16. Considering the jack-up analysed with pinned footings as an example, the first turning point occurs in the vicinity of its natural period at 8.5s. The distribution of data points is such as to detect a slight shift in natural period (by about 0.2s) for the pinned footing unit. This shift is due to the combined effects of added mass and hydrodynamic damping. The second maximum (at 17.0s for the discrete data of Fig 6.16) occurs at about twice the natural period. Fig 6.17[a] shows the temporal variation of the hull displacement for a pinned footing analysis at a wave period of 17.0s and Fig 6.17[b] shows the amplitude spectrum of this hull displacement trace. This Figure shows that there is a strong response at half of the applied wave period (twice the applied frequency). This second harmonic is due to

two main effects. Firstly, the Stokes fifth wave theory has a component at twice the fundamental wave frequency. Secondly, as noted in Chapter 5, the current velocity introduces harmonics into the drag loading at twice the fundamental frequency when vectorially added to the wave particle velocity in the Morison equation. This effect can be seen more clearly from Fig 6.17[c] which shows the amplitude spectrum of the total horizontal hydrodynamic load on the jack-up (excluding relative motion effects) for a 17.0s wave period. The presence of the second harmonic in the load spectrum means that a resonant response is induced when the jack-up is excited by waves at twice its natural period (half its natural frequency).

Fig 6.16 shows that there is a similar trend in behaviour for the response curve of the jack-up analysed with Model B footings. The period range considered is such that resonant responses due to wave excitation at approximately twice and three times the natural period are visible for the Model B analyses. The response due to wave excitation in the vicinity of three times the natural period, results in the slight rise in response at the 20.0s wave period. For the analyses with footings modelled as fixed joints, the fundamental natural period does not fall within the period range considered, but resonance due to wave excitation in the vicinity of twice the natural period is clearly visible, bracketing the 8.0-10.0s period range. Any resonance due to the third harmonic of loading is not clearly visible.

Fig 6.16 clearly demonstrates the importance of accounting for dynamic motions in a jack-up structural analysis. The most important observation from these analyses is that the assumption of pinned footing behaviour does not result in the largest prediction of maximum hull displacement across the entire period range considered. This can be seen more clearly from Fig 6.18 which shows the maximum hull displacements as a percentage of the corresponding analysis assuming pinned

footing behaviour. In a period range bracketing the natural period of the unit analysed with Model B footings (some 6.0-7.0s), the assumption of partial fixity results in the largest hull displacement estimate. Also, considering the 13.5s wave period, the 35% reduction in hull displacement predicted by the quasi-static analysis (see Fig 6.8[b]) is reduced to 0% in Fig 6.18. Over the entire 5.8-20.0s period range, the assumption of fixed footing behaviour still results in the smallest estimate of the maximum hull displacement, although this might not be the case for other sets of parameters.

Because the 6.0-7.0s period range is slightly beyond the range of applicability of the Stokes fifth solution, it is expedient once again to reduce the wave height and briefly examine some low period effects. Fig 6.19 shows the variation of the maximum lateral hull displacement for a 6.0m wave over the 4.6-9.0s period range considered in Fig 6.13[a]. As noted in Section 6.2.1.1, the period/wavelength relationship is now slightly altered. For example, from Fig 6.12 it can be seen that the natural period of the unit with pinned footings is now slightly closer to the period resulting in the leg loads occurring in antiphase. Similarly, the natural period of the unit analysed with Model B footings is now slightly further away from this period. However, Fig 6.19 supports the contention that the pinned footing analysis is no longer the most conservative hull displacement estimate across the 6.0-7.0s period range. Similarly, for a small period range near the resonant period of the unit analysed with fixed footings (about 4.6-4.8s) the Model B analyses yield the least conservative hull displacements.

It is worth noting that the use of linear wave theory or stream function theory for example, would result in significantly different predictions of resonance due to the second harmonic of loading. This is because linear theory does not have harmonics above the fundamental wave frequency. A stream function solution can have a large

number of harmonics (although it is unusual to have more than nineteen), therefore, the contribution of the second harmonic would be significantly reduced compared to that of a Stokes fifth solution. In the wave period range commonly used for design wave applications (12.0-18.0s), Fig 6.16 shows that the response can be dominated by second harmonic effects when using a regular Stokes' fifth wave theory analysis. Fig 6.20 shows the maximum hull displacement for the three different assumptions of footing behaviour for a Stokes fifth solution with the current velocity reduced to zero. This shows that the resonant response due to wave excitation at approximately twice the natural period is reduced compared to Fig 6.16, but that it is still present and significant.

Fig 6.21[a] shows the variation of the maximum lower guide moment for the windward leg. The first noticeable feature is that the trend in behaviour for each moment-period path directly mirrors that of the corresponding displacement-period path shown in Fig 6.16. Therefore the addition of dynamic behaviour has a correlating effect on the hull displacement and lower guide moment compared to a quasi-static analysis. However, in conjunction with the quasi-static analyses, the relative positions of the response curves show a slight deviation from those of Fig 6.16. This can be seen more clearly from Fig 6.21[b] which shows the maximum lower guide moments as a percentage of the corresponding analysis modelling the footings as pinned joints. More importantly, Fig 6.21[b] also shows that for a small wave period range bracketing twice the natural period of the jack-up analysed with fixed footings (in the 9.0s region), the assumption of 100% fixity does not result in the smallest prediction of maximum lower guide moment. In this region, the Model B footing assumption leads to the smallest estimate.

The variation of the lower guide moment at the leeward legs has not been

discussed in detail because the trend in behaviour directly mirrors that displayed by the moment at the windward leg. This can be seen more clearly from Fig 6.21[c] which shows the variation of the maximum lower guide moment for one of the leeward legs. Fig 6.21[d] shows the variation of the maximum leeward lower guide moment for one leg with the corresponding windward leg variables. With some numerical scatter, all of the response paths define an approximately linear relationship.

6.2.2.2 The double amplitude of the hull displacement and lower guide moments

Fig 6.22[a] and [b] show the double amplitude of lateral hull displacement and the double amplitude of lower guide moment for the windward leg. Once again, these variables can be considered together due to the extreme similarity in behaviour. Fig 6.22[a] and Fig 6.22[b] show that there are now two period ranges where the assumption of Model B footing behaviour results in the largest values for double amplitude variables. These period ranges bracket the fundamental natural period (6.0-7.0s) and twice the natural period (13.0-14.0s) of the jack-up analysed with Model B footings. Similarly, there is an 8.5-9.5s period range where the assumption of Model B footing behaviour results in the least conservative (smallest) results for the double amplitude variables. This region brackets twice the natural period of the unit analysed assuming fixed footing behaviour. Similar comments apply to the variation of the double amplitude of moment at a leeward leg therefore these results will not be discussed in detail, but are shown in Fig 6.22[c]. Similarly Fig 6.22[d] shows the variation of the leeward double amplitude of lower guide moment with the corresponding windward variable. As for the maximum lower guide moments, the moment at the windward legs is slightly larger than that at the windward leg.

6.2.2.3 Dynamic amplification of the hull displacement

Sections 6.2.2.1 and 6.2.2.2 show that the trend in behaviour of responses related to the lateral hull displacement (*i.e.* maximum values and peak to trough values) are directly indicative of the behaviour of the corresponding responses related to the lower guide moment. The similarity in behaviour is more marked than that displayed by a quasi-static analysis. As a result of this hull displacement variables are used as a representative response to consider in terms of dynamic amplification.

Fig 6.23[a] shows the maximum hull displacement of Fig 6.16 non-dimensionalized with respect to the corresponding maximum quasi-static hull displacement (see Fig 6.8[a]). The abscissa is maintained as a period scale. This non-dimensionalized displacement does not represent dynamic amplification in the conventional sense because the response on which it is based is not a zero mean process. However it is an important variable to consider as it represents the amplification of an extreme value above that predicted by a quasi-static solution. Similarly, Fig 6.23[b] shows the variation of the peak to trough dynamic hull sidesway non-dimensionalized with respect to the corresponding peak to trough quasi-static response (see Fig 6.8[c]). Unlike Fig 6.23[a], this can be taken as more representative of a conventional dynamic amplification factor because it automatically accounts for any variations in the mean value of the loading. The period scale of Fig 6.23[a] and [b] will obviously now have to be non-dimensionalized also, but it is still useful to retain Fig 6.23[a] and [b] so that amplification effects can be explained relative to their absolute position in the period range considered.

Fig 6.24[a] shows the variation of the non-dimensionalized maximum hull displacement with frequency ratio, Ω. (The abbreviation 'max.' on the ordinate axis means, maximum.) The non-dimensionalized maximum hull displacement will from

now on be referred to as the maximum hull displacement amplification factor. The frequency ratio Ω is the ratio of the forcing wave angular frequency to the angular natural frequency of the jack-up unit. Therefore, $\Omega = T_n/T$, where, T_n is the jack-up natural period and T is the wave forcing period. Similarly, Fig 6.24[b] shows the variation of the non-dimensionalized double amplitude of hull displacement with frequency ratio. The non-dimensionalized double amplitude of hull displacement will be referred to as the double amplitude amplification factor. For the analyses with footings modelled as fixed joints, the amplification curves of Fig 6.24 do not extend into the $\Omega > 0.8$ region because this represents the low period area below 5.8s shown in Fig 6.23. Fig 6.24 more clearly demonstrates the similarity in behaviour for the analyses with each assumption of footing behaviour. A large amplification factor peaking in the region of the unity frequency ratio eventually leads to a secondary resonance induced by the second harmonic of loading in the vicinity of $\Omega = 0.5$. Assuming a greater degree of fixity for the footing model does not necessarily result in a smaller amplification factor. For example at $\Omega \approx 1.0$ for analyses modelling the footings as Model B joints, the maximum hull displacement amplification factor at resonance is 21% larger and the double amplitude amplification factor 17% larger than the corresponding amplification factor at resonance for analyses modelling the footings as pinned joints. The response for analyses with fixed footings at $\Omega \approx 0.5$ is slightly higher than the analyses with Model B and pinned footings and is a consequence of the level of discretization. This is discussed further in Section 6.2.2.4

The Model B behaviour appears to be somewhat anomalous in the 0.7 to 0.8 Ω range compared to the other analyses, with an arched response in Fig 6.24[a] and a flattened response in Fig 6.24[b]. From Fig 6.23[a], this frequency ratio range corresponds to a period range from about 7.6-10.0s. From Section 6.2.1.1, it will be

recalled that cancellation effects occur in the vicinity of 7.6s and that the load on a single leg reached its turning point (see Fig 6.9[a]) at about 10.0s. This anomalous behaviour can possibly be attributed to the preceding two factors.

In order to extend the range of some of the response curves in Fig 6.24[a] and Fig 6.24[b], it is necessary to consider the low period effects in the range below 5.9s shown in Fig 6.19. Figs 6.25[a], [b] and [c] show the maximum hull displacement amplification factors for each type of footing assumption with superposed results for the 13.0m wave height and the 6.0m wave height. As would be expected, the general pattern of the responses is similar with some minor variation in values at the different wave heights. Similarly, Figs 6.26[a], [b] and [c], show the variation of the double amplitude amplification factors for analyses with each assumption of footing behaviour. Once again the results for a 13.0m wave and the low period 6.0m wave are superposed. Fig 6.26[a] and Fig 6.26[c] show that in the region of overlap for the two wave heights, the amplification factors are very similar for the pinned footing and fixed footing analyses. Fig 6.26[b] shows that for the Model B footing analyses, the variation in values across the two wave heights is slightly more significant than the analyses assuming pinned and fixed footing behaviour. As the wave height increases, the behaviour becomes closer to the analyses with pinned footings. This is possibly due to the cross coupling between the horizontal and rotational footing stiffnesses in conjunction with greater loading over the lower portions of the leg at the larger wave height.

Some parallels can be drawn between the double amplitude curves and the dynamic amplification curves for a linear single degree of freedom system. As noted in Chapter 2, the dynamic amplification factor for a linear single degree of freedom system can be expressed as:

$$D_A = \frac{1}{\sqrt{(1 - \Omega^2)^2 + (2\xi\Omega)^2}} \qquad (6.4)$$

This assumes that the load has only one frequency component. Fig 6.27 shows the amplification curves for the double amplitude of hull displacement at H = 13.0m plotted together with two curves defined by Eqn 6.4. The values of damping ratio used are ξ = 0.07 which passes through the extreme point of the Model B analyses and ξ = 0.087 which matches the extreme value of the pinned footings analysed at the fundamental frequency. These curves bound the two extreme values of double amplitude amplification factor for the jack-up analyses and implies that the hydrodynamic damping varies between 5 and 6.7%. The different values of damping ratio occur because the hydrodynamic damping is related to the magnitude of the structural velocities which are larger for the analyses with pinned footings at resonance associated with the first load harmonic.

The model with excitation at a single frequency defined by Eqn 6.4 does not fully explain the shape of the response curves seen in Fig 6.24[a] and [b] due to the additional harmonics in the load spectrum. In order to predict the shape of the curves, some indication of the ratio of harmonics in the loading is needed. As an illustrative example, Fig 6.28 shows the amplitude spectrum of the hydrodynamic leg load at a period of 16.0s which shows that for this particular load case, the first three harmonics are the dominant terms. These harmonics occur in the approximate ratio (0.7:0.25:0.05). This implies that a more suitable form of the dynamic amplification curve takes the form:

$$D_A = \frac{n_1}{\sqrt{(1 - \Omega^2)^2 + (2\xi\Omega)^2}} + \frac{n_2}{\sqrt{(1 - (2\Omega)^2)^2 + (2\xi(2\Omega))^2}} +$$

$$+ \frac{n_3}{\sqrt{(1 - (3\Omega)^2)^2 + (2\xi(3\Omega))^2}} + \ldots\ldots \tag{6.5}$$

where the n_i values (all < 1.0) represent the contribution of the i^{th} harmonic to the amplitude spectrum and $\sum n_i = 1$. This particular period is considered because it is in the region where phase effects identified in Section 6.2.1.1 do not significantly affect the response. Using the ratio of the first three harmonics in Fig 6.28, Fig 6.29 shows the double amplification values of Fig 6.24[a] plotted together with two amplification curves defined by Eqn 6.5. The numerical results are represented by data markers only for clarity. The damping ratios used are $\xi = 0.05$ which passes through the peak response of the Model B analyses and $\xi = 0.061$ which matches the peak response of the pinned footing analyses. This attributes approximately 3% and 4.1% respectively to the hydrodynamic damping. These damping ratios are slightly lower than those used in Fig 6.27. Although the curves of Fig 6.29 do not match the numerical results exactly, they demonstrate that the double amplification factor is built up from responses at different harmonic components. The differences between Eqn 6.5 and the double amplitude factors occur because the ratio of the magnitudes of the harmonics in the loading does not stay constant across the entire period range considered. This is partly due to the solution of Stokes fifth theory at a particular period and partly due to the phase of the loading on the legs. The hypothetical curve of Eqn 6.5, does not account for the phase difference of loading between the windward and leeward legs if the n_i coefficients take fixed values. However, the form of Eqn 6.5 suggests that if the harmonic content of the load at each period is known, together with a suitable damping ratio, then the double amplitude amplification curves could be estimated on a point by point basis.

6.2.2.4 Analyses with a more detailed finite element model

Before concluding this section it is useful to briefly consider the effect of the level of finite element modelling on the response variables. The numerical model shown in Fig 6.1 was used partly because it is adequate to show the trend in behaviour of the jack-up response, but also because it is possible to obtain solutions within a reasonable timescale. Fig 6.30 shows a more detailed numerical model used to reanalyse a limited number of points in the Ω range considered in Fig 6.24[a] and [b]. It should be noted that with this numerical model, run times on a Sun ELC incorporating Model B footings could be in excess of sixteen hours with no other large processes running.

As for the numerical model shown in Fig 6.1, the natural period of the more detailed model was found by applying a 10.0MN load at the deck level for 0.01s. The natural periods obtained for each assumption of footing behaviour were unchanged from the previously derived values, therefore no graphs for the temporal variation of hull displacement are presented here. However, this demonstrated that the fundamental period of the jack-up unit is predicted well using relatively few Oran (1973[a]) elements.

Analyses with the more detailed model are carried out with each footing model at two values of frequency ratio. The frequency ratios are $\Omega \approx 0.5$ (which is an extreme point in terms of response to the second load harmonic) and $\Omega \approx 0.6$ (where the amplification curves vary rapidly with frequency ratio). In addition, analyses are carried out at set period of 16.0s because this value is used for analyses at a fixed period in Section 6.3. The response variables considered are the quasi-static and dynamic hull displacement variables and the corresponding amplification factors.

Table 6.2 shows the difference in response between the simpler model and the more detailed model, expressed as a percentage. For example, a value of 1.6 means

that the response predicted by the simpler model is 1.6% larger than that of the more detailed model. Table 6.2 shows that the simpler model generally underpredicts the quasi-static responses but can overpredict the dynamic values in the vicinity of a resonant response. Also, in general, the analyses with pinned footings show the smallest variations whilst those with fixed footings show the largest. For example, at $\Omega \approx 0.5$, the pinned footing analyses show up to a 2% overprediction for the dynamic hull displacement variables and up to a 3.3% underprediction of the quasi-static variables. The Model B analyses at $\Omega \approx 0.5$ show a 4.4% overprediction of the maximum hull displacement and an 8.7% overprediction of the dynamic double amplitude of the hull displacement. The quasi-static responses for the Model B analyses show up to a 2% underprediction with the simpler model. The worst results are shown by the analyses with fixed footings, with a 14.5% overprediction of the dynamic double amplitude of hull displacement and an 8% underprediction of the corresponding quasi-static response.

At $\Omega \approx 0.6$, the dynamic analyses with pinned footings show a slight decrease in accuracy with the maximum hull displacement, for example, being overpredicted by about 8%. However, the quasi-static responses show a smaller variation than the corresponding variables at $\Omega \approx 0.5$. In contrast, the dynamic Model B analyses show a smaller variation compared to results obtained at $\Omega \approx 0.5$ with the double amplitude of response being underpredicted by about 2.5%. Simultaneously, the quasi-static values show a slightly increased variation compared to the more detailed model. Similar comments apply to the fixed footing analyses at this frequency ratio.

The responses at the period T = 16.0s which is in the range of periods used for an assessment analysis are generally captured well by the simpler model with each footing type. The largest variation is for the fixed footing analyses with a 4.6%

overprediction of the double amplitude of hull displacement but only a 0.79% overprediction of the maximum value. The pinned and Model B analyses show a smaller variation in double amplitude than the fixed footing analyses but have a larger variation in maximum value with the Model B analyses showing a 2% variation.

The consequences to the amplification values are most severe where an overpredicted dynamic response is divided by an underpredicted quasi-static response. Once again, the worst prediction is given by the analyses with fixed footings at $\Omega \approx 0.5$. The double amplification factor is overpredicted by 25% and hence reduces to a value of 4.0 which shows a much closer correlation to the pinned and Model B analyses. Similarly, the double amplitude amplification factors for the pinned and Model B analyses are overpredicted by about 5% and 10% respectively at this resonant peak.

In general however, the response variables predicted by the simpler model provide a good prediction of trends in behaviour. There is inevitably some variation due to the level of finite element modelling used. For a more detailed analysis for a site specific assessment, an investigation of the convergence to a solution due to the finite element mesh would have to be undertaken. The results shown here show that the simpler model is quite successful in modelling the response of the Model B and pinned analyses, but that a slightly more detailed discretization is necessary to reduce errors for the fixed footings analyses. This is possibly because the fixed footings rig has the most complicated deformed leg shape (with a point of contraflexure) compared to the pinned or Model B analyses. This leg shape is more accurately modelled with a finer distribution of elements.

6.2.2.5 Conclusions: dynamic analyses

Dynamic analyses have been presented for the environmental conditions detailed in Section 6.1. The presence of inertia and damping is seen to have a correlating effect between response variables related to the hull displacement and the corresponding variables related to the lower guide moment. Under a dynamic analysis, the assumption of pinned footing behaviour is seen to yield the most conservative responses only in certain period ranges. Similarly, the assumption of fixed footings does not always culminate in the least conservative responses. The jack-up behaviour is seen to be dominated by the second harmonic of wave loading in a large region of the period range considered and some concern is raised as to the correlation of this effect with other wave theories.

6.3 Analyses at a fixed wave period

Analyses at a fixed value of wave period but with a varying value of wave height are now briefly considered. The fixed period chosen is 16.0s because, it is in the period range typically used for an assessment analysis and it allows a wide variety of wave heights to be used that are below the limiting wave height (see Table 6.1). It is also outside the 7.6-11.0s period range that results in the smallest values of jack-up loading. The wave height range considered is from 7.0m to 30.0m. The density of Gauss points in the vicinity of the mean water level is increased slightly by using the numerical model shown in Fig 6.31. Quasi-static and dynamic analyses are considered together and the hull displacement is used as a representative response variable.

Fig 6.32[a] and [b] show the variation of the maximum hull displacement with wave height for quasi-static and dynamic analyses respectively. Each plot contains

results for footings modelled as pinned joints, Model B footings and fixed joints. For this period, both the quasi-static and dynamic analyses predict that the assumption of pinned footing behaviour results in the largest hull displacements and that of fixed footing behaviour the smallest. Both the quasi-static and dynamic analyses with Model B footings display anomalous behaviour compared to the pinned and fixed footing analyses in the upper wave height range (25.0-30.0m). There is a marked increase in the rate of change of hull displacement with wave height. This effect is due to yielding at the footings and immediately highlights the advantage of incorporating Model B type footings in a jack-up structural analysis. This is because a direct indication of footing yield is obtained, which is in contrast to a conventional jack-up analysis where the combined force point for each footing must be compared to a failure envelope (see Chapter 4). One further consideration can be highlighted by the Model B analyses. As an example, Fig 6.33 shows the temporal variation of hull displacement for the dynamic analyses with Model B footings at a wave height of 25.0m. This shows that the hull displacement reaches a steady state where the double amplitude and maximum value of hull displacement do not continue to increase with each cycle of loading. Therefore, for this particular case, yielding at the foundation occurs in a stable manner and the failure envelope expands due to the increase in vertical footing penetration. Similar comments apply to the dynamic analysis with Model B footings at a wave height of 28.0m and the quasi-static analyses with yielding foundations. Yielding at the leeward footings occurs and is eventually stabilised by work hardening at the soil-structure interface. These results are in contrast to the dynamic analysis with Model B footings at a wave height of 30.0m. Fig 6.34 shows the temporal variation of the hull displacement for this particular case. Within the timescale of this analysis (200s), the footing does not

reach a steady state and can be considered as an unstable foundation for this wave condition. The data point on Fig 6.32[b] corresponding to this analysis is therefore somewhat artificial in that it represents the maximum hull displacement attained within the considered timescale.

Fig 6.35[a] and [b] show the double amplitude of hull displacement for each assumption of footing behaviour for quasi-static and dynamic analyses. As for the maximum hull displacements, the assumption of pinned footing behaviour gives the largest results and the assumption of fixed footings the smallest for both the quasi-static and dynamic analyses. The Model B analyses do not show anomalous behaviour in the upper wave height range. However, this is solely due to the sample length used to capture response variables in the steady state. Fig 6.36[a] and [b] show the dynamic hull displacement variables non-dimensionalized with respect to the corresponding quasi-static solution. For this particular period, both of the amplification factors show only minor variations across the wave height range considered for each assumption of footing behaviour.

6.3.1 Variation of hull displacement with wave height

For a purely drag loaded structure with no current or relative motion effects, and with wave forces integrated to the mean water level, Eqn 5.44 shows that the wave forces would vary with the square of the wave height. However, the presence of inertia, relative motion effects and integration to the free surface complicates this process. In order to consider the variation of jack-up response variables with wave height, Chen *et al* (1990) use a power index, J_x defined by:

$$J_x = (H/X)(\mathrm{d}X/\mathrm{d}H) \tag{6.6}$$

where H is the wave height, and X is the jack-up response variable considered. The

power index is used because if a response variable varies with wave height to the power n, then:

$$X = AH^n \tag{6.7}$$

where A is a constant and n varies with wave height. Differentiating Eqn 6.7 gives the relationship:

$$dX/dH = nAH^{(n-1)} \tag{6.8}$$

From Eqn 6.7:

$$AH^{(n-1)} = X/H \tag{6.9}$$

therefore, by comparison with Eqn 6.6,

$$J_x = n \tag{6.10}$$

This concept is used to give an indication of the variation of the hull displacement variables considered in Section 6.3.

Fig 6.37[a] and [b] show the variation of the power index for the quasi-static maximum and double amplitude of hull displacement respectively. The differential in Eqn 6.6 is found by fitting cubic polynomial functions to the data points using Matlab and finding the differential of the polynomial at the data points. For the analyses with Model B footings, the data points associated with yielding at the foundation are not included in the power index calculations. Fig 6.37[a] and [b] show that, as expected, the response increases in non-linearity as the wave height increases. In general, the variation of power index for each assumption of footing behaviour is very similar. The responses based on the double amplitude of hull displacement reach a higher power index value than those based on the maximum value. This is a consequence of the mean value of hull displacement introduced by the wind and current load.

Fig 6.38[a] and [b] show the power index for the dynamic maximum hull displacement and the double amplitude of hull displacement respectively. Unlike the quasi-static analyses, the response paths for each assumption of footing behaviour are slightly different. This difference is most marked for the double amplitude of dynamic hull displacement. The power index values reach a slightly higher value for dynamic analyses with Model B and fixed footings compared to the corresponding quasi-static values. However, the reverse is true for the pinned footing analyses where instead the quasi-static results display a higher degree of non-linearity in the upper wave height range. Because the quasi-static power index values are so similar, this suggests that the frequency ratio is a factor in the hull displacement's variation with wave height.

It is important to note that these results are highly dependent on the drag and inertia coefficient used and would vary for different sets of these parameters. However, the general trend in behaviour is from an initial linear response to a non-linear drag dominated response as the wave height increases.

6.4 Conclusions: Quasi-static and dynamic analyses

Quasi-static and dynamic analyses have been presented in this chapter for a simple model of a jack-up unit. The analyses were intended to show the trend in behaviour of the jack-up for different assumptions of footing behaviour and a number of wave conditions. The importance of accounting for dynamic motions in a jack-up analysis has been demonstrated because analyses with the assumption of pinned footing behaviour do not give the most conservative results at all period values. In addition to this, the feasibility of incorporating a work hardening plasticity model at the foundation has been demonstrated with a direct indication of footing yield being given

for analyses at varying values of wave height. The consequences of finite element discretization have not been examined in detail, but preliminary studies indicate that some quantitative variations will inevitably occur, but that the qualitative meaning of the results is unaltered.

CHAPTER 7

CONCLUDING REMARKS

7.1 Introduction

Jack-up platforms are conventionally used for short durations in water depths less than 90.0m to drill exploratory and production wells for hydrocarbons. However, in recent years the operational range of jack-ups has increased due to commercial pressure, resulting in extended periods of use in deeper and more exposed areas such as the central to northern part of the North Sea. As a result, accident statistics for jack-ups have worsened. In order to provide a fuller understanding of jack-up behaviour, the potential influence of dynamic amplification and non-linearities in the system must be considered in an assessment analysis. The purpose of this project was to review analysis techniques applicable to the non-linear dynamic analysis of jack-ups, and to demonstrate the feasibility of their application by combining several of the techniques studied in a structural analysis procedure. This was achieved by implementing the methods in an advanced plane frame analysis program called JAKUP written specifically for the project. One aim of the project was to develop each aspect of the analysis to approximately the same level of rigour. The main findings of the work are summarised in this chapter and then some areas for future work are suggested.

7.2 Main findings

The equations for several common step-by-step integration methods for analysis in the time domain were presented, and the issues of stability and accuracy governing their use were discussed. Several desirable features for a step-by-step method were

identified. These are:

1) Only one set of equations should be solved per timestep.

2) The solution scheme should be self starting.

3) Any algorithmic dissipation should be parametrically controllable.

4) The methods should not produce overshoot.

5) The method should be unconditionally stable.

On this basis, two methods were selected and implemented in JAKUP. These are the 'linear acceleration method' which is only conditionally stable but displays many desirable properties, and the Newmark method in the form of the unconditionally stable 'constant acceleration method'. The development of the equations in iterative form, using a modified Newton-Raphson approach, was presented and some simple examples demonstrated the main features of the algorithms. Both methods introduce no amplitude decay, but the linear acceleration method introduces less period elongation into the system when using a timestep within the method's stability limit. However, even with a relatively simple numerical model of a jack-up, the small natural periods of the high modes mean that the Newmark method proves to be a more robust analysis tool for a jack-up analysis.

An advanced method of accounting for the stiffness properties of the structure was incorporated in the dynamic analysis procedure. This method is an Eulerian formulation of beam-column theory as detailed by Oran (1973[a]) and Oran & Kassimali (1976). This method traces the load-deflection path using the linearized incremental approach and therefore results in the formulation of a tangent stiffness matrix. The structural response is therefore path dependent and care must be taken to include suitable equilibrium iterations at each timestep. Several advantages of the

method were discussed. Firstly, the method allows arbitrarily large chord rotations because rigid body rotations are uncoupled from local member deformations. Secondly, accurate solutions to large deformation problems can be obtained using relatively few beam-column elements. The fundamental period of a jack-up model was therefore seen to be unaffected by the level of leg discretization. However, several authors (*e.g* Remseth, 1979; Chan & Kitipornchai, 1987) note that the method is computationally less efficient than the Lagrangian approach for accounting for geometric non-linearity when it is extended to the analysis of space frames. Modifications made to the Eulerian formulation by Martin (1994) to account for deformation due to shear were also incorporated in the analysis procedure.

The feasibility of incorporating a work hardening plasticity model for the soil-structure interaction in a dynamic analysis was demonstrated. In JAKUP, this procedure is incorporated by using the formulation derived and experimentally validated by Martin (1994). This method results in a more realistic prediction of the soil-structure interaction than analyses assuming pinned or fixed joints at the foundation. The important elements of the model are:

1) A realistic failure envelope is defined. For combined force points lying within the envelope, incremental force-displacement behaviour is elastic.
2) A hardening law is defined, so that the pure vertical load capacity can be found for any value of vertical plastic penetration. This vertical load capacity in turn dictates the size of the yield surface.
3) A flow rule is defined, so that plastic displacement increments can be found during yield, and realistic predictions of any post yield behaviour can be made.

One of the major advantages of such a model is that a direct indication of yield at the foundation is given. In addition, the elastic soil stiffnesses allow an appropriate estimate of the fundamental period of the jack-up to be made.

The numerical models developed were applied to the structural analysis of a simplified jack-up model operating in 90.0m water depth. The hydrodynamic load on the structure was accounted for using the Stokes fifth wave theory, in conjunction with the extended Morison equation. This approach is one of the standard deterministic procedures for analysing a frame with slender members. Quasi-static and dynamic analyses were performed with the soil-structure interaction modelled as pinned joints, Model B footings and fixed joints. For quasi-static analyses, the assumption of pinned footings at the soil-structure interface resulted in the largest jack-up response variables at all wave periods considered. However, this was shown not to be the case when dynamic motions were accounted for in the analyses. Instead at certain periods, the assumption of partial fixity gave the largest jack-up response variables. This was acknowledged to be dependent on the system parameters used but demonstrated the importance of accounting for dynamic motions in the structural analysis.

Plots of the variation with frequency of the dynamic hull displacement variables, non-dimensionalized with respect to the corresponding quasi-static results were presented. These demonstrated the similarity in behaviour for analyses with different assumptions of footing behaviour. The response was seen to be dominated by the second harmonic of the wave load in the period range typically used for an assessment analysis. However, the use of the Stokes fifth wave theory to define the particle kinematics was acknowledged to be an important factor in this effect. In addition, the advantage of

the Model B formulation was demonstrated because it gave an indication of stable and unstable yield at the foundation during quasi-static and dynamic analyses with hydrodynamic loading.

7.3 Areas for future research

Because a comprehensive jack-up analysis involves the combination of many numerical methods which can be developed to various levels of sophistication, the results of this thesis provide scope for much future research.

7.3.1 Extension to 3-dimensions

The program JAKUP was developed for the analysis of plane frames only and environmental loads were applied along an axis of symmetry. However, these load directions do not necessarily result in the most critical load case. As a result the extension to 3-dimensional problems would constitute a considerable advance on JAKUP in its present stage of development. Both Oran (1973[b]) and Chan & Kitipornchai (1987), for example, present methods for accounting for geometric non-linearity in problems involving space frames. The approach derived by the former author is the 3-dimensional analogue of the Eulerian beam-column formulation presently implemented in JAKUP.

7.3.2 Modelling of structural detail

The nature of the hull-leg interaction was not considered in this thesis. The platform of a jack-up in its elevated mode is supported by the legs through jacking units and leg guides at the level of the hull. As a result the leg-hull connection is not rigid. Rotational springs could be placed at the hull-leg interface to account for this

interaction. The finite spring stiffness at the hull level would have an effect on the natural period of the jack-up and on the distribution of load between the legs and the hull.

7.3.4 Modelling cyclic behaviour at the footings

The Model B foundation model was derived primarily to predict footing displacements for monotonic loads. The number of physical experiments involving cycles of loading was limited and used mainly for illustrative purposes. Therefore a significant area of research would involve an extensive physical testing program to examine the behaviour of spudcan footings when subjected to cyclic loading.

7.3.5 A footing model in 3-dimensions

The incorporation of a realistic plasticity model within a 3-dimensional analysis is a long term goal. To account for horizontal and moment loading in two orthogonal directions would require experimental work to investigate the shape of the interaction locus and the corresponding flow rule to define plastic displacement increments for the additional displacement vector components.

7.3.6 Wave theories

Additional consideration should be given to the wave theories used in the environmental model. As noted in Chapter 6, much of the jack-up response in the period range typically used for a design analysis was dominated by the second load harmonic. This is partly due to the current load used in conjunction with the Morison equation and partly due to the use of the Stokes fifth wave theory. A comparison with results obtained with a higher order wave theory such as stream function theory is an

area in need of investigation.

The method of accounting for the combined wave-current kinematics should be refined by incorporating a Doppler shift of the wave particle kinematics. In addition, an investigation of the influence of the convective terms in the equations for the particle accelerations on platform response would be an informative area of research

As noted in Chapter 5, true ocean waves are random in nature. Therefore the inclusion of a random wave theory in the structural analysis procedure would be a significant advance on JAKUP in its present condition. This is usually achieved by the summation of linear wave components with amplitudes chosen from the required wave spectrum at the desired frequency. The phase angles are randomly generated using a probability density function uniform between 0 and 2π (SNAME, 1993). Tucker *et al* (1984) note that this process does not truly model a random seastate because the derived surface elevation is not Gaussian. They detail a more sophisticated method where the amplitude coefficients are generated as independent Gaussian distributed random numbers. Because the simulations for random analyses must be carried out over long durations to ensure that the extreme load event is captured, it would also be informative to investigate the maximum timestep size that could be used for a particular jack-up analysis whilst maintaining accuracy in the fundamental mode. In contrast to this approach, 'Newwave theory' for example, (Tromans *et al*, 1991; Elzinga & Tromans, 1992) chooses the amplitude coefficients in a seastate such that the extreme wave is modelled within a deterministic analysis, thereby reducing the analysis time. Inclusion of such a model in JAKUP would also be beneficial.

REFERENCES

Airy, G. B. (1845). Tides and Waves. *Encyclopaedia Metropolitana*. Vol. 5, Art. 192, pp. 241-396.

Al-Bermani, F. G. A. & Kitipornchai, S. (1990). Elasto-plastic large deformation analysis of thin walled structures. *Engng Struct.* Vol. 12, pp. 28-36.

American Petroleum Institute (1993). *Recommended practice for planning, designing and constructing fixed offshore platforms - load and resistance factor design*. RP 2A-LRFD, 1st ed. Washington DC: American Petroleum Institute.

API. (1993). See American Petroleum Institute (1993).

Barltrop, N. D. P. & Adams, A. J. (1991). *Dynamics of fixed marine structures*. Butterworth Heinemann. 3rd ed.

Bathe, K. J. (1982). *Finite element procedures in engineering analysis*. Prentice-Hall Inc.

Bathe, K. J. & Wilson, E. L. (1973). Stability and accuracy analysis of direct integration methods. *Int. J. of Earthquake Engng and Struct. Dynamics*. Vol. 1, pp. 283-291.

Bazant, Z. P. & Cedolin, L. (1991). *Stability of structures. Elastic, inelastic, fracture and damage theories*. Oxford University Press.

Bazant, Z. P. & El-Nimeiri, M. (1973). Large deflection spatial buckling of thin walled beams and frames. *J. Engng Mech. Div.* ASCE. Vol. 99, No. 6, pp. 1259-1281, (Sec. 6.5).

Bell, R. W. (1991). *The analysis of offshore foundations subjected to combined loading*. M.Sc. thesis. University of Oxford.

Bennett Jr, W. T. & Patel, R. K. (1987). *Jack-up behaviour in elevated condition, model test and computer simulation*. In-house report, Freide & Goldman Ltd, New Orleans.

Bhatt, P. (1986). *Programming the matrix analysis of skeletal structures*. Ellis Horwood.

Boswell, L. F. & D' Mello, C. (1993). *The dynamics of structural systems*. Blackwell Scientific Publications.

Breeden, J. O'R. (1990). *The next generation of jack-up drilling units*. Paper presented to SNAME Texas section meeting.

Brekke, J. N., Campbell, R. B., Lamb, W. C. & Murff, J. D. (1990). Calibration of a jack-up structural analysis procedure using field measurements from a North

Sea jack-up. *Proc. 22nd Offshore Technology Conf., Houston, Texas.* OTC 6465.

Brinch Hansen, J. (1970). A revised and extended formula for bearing capacity. *Bulletin No 28, Danish Geotechnical Institute*, Copenhagen, pp. 5-11.

Butterfield, R. & Ticof, J. (1979). Design parameters for granular soils. *Proc. 7th European Conf. Soil Mech. Fndn Engng.* Brighton, Vol. 4, pp. 259-261.

Cambridge University Mechanics databook. (1988). *Department of Engineering Science.* University of Cambridge.

Chan, S. L. & Kitipornchai, S. (1987). Geometric non-linear analysis of asymmetric thin-walled beam-columns. *Engng. Struct.* Vol. 9, No. 4, pp. 243-254.

Chen, W. F. & Atsuta T. (1976). *Theory of beam-columns.* Vol. 1. McGraw-Hill book company.

Chen, Y. N., Chen, Y. K., & Cusack, J. P. (November 1990). *Extreme dynamic response and fatigue damage assessment for self elevating drilling units in deep water.* Paper presented to the Society of Naval Architects and Marine Engineers.

Chiba, S., Onuki, T. & Sao, K. (1986). Static and dynamic measurement of bottom fixity. *Proceedings of the 1st international conference on the jack-up platform, design, construction and operation.* City University

Clough, R. W. & Penzien, J. (1975). *Dynamics of structures.* McGraw-Hill book company.

Connor Jr, J., Logcher, R. D. & Chan S. C. (1968). Nonlinear analysis of elastic framed structures. *J. Struct. Div.* ASCE. Vol. 94 No. ST6, pp. 1525-1547.

Craig Jr, R. R. (1981). *Structural Dynamics-An introduction to computer methods.* John Wiley and Sons Inc.

Dean, R. G. (1965). Stream function representation of non-linear ocean waves. *J. Geophys. Res.* Vol. 70.

Dean, R. G. (1970). Relative validities of water wave theories. *Journal of the Waterways, Harbours and Coastal Engineering Division.* ASCE. Vol. 96, No. 1.

Eatock Taylor, R. & Rajagopalan, A. (1983). Load spectra for slender offshore structures in waves and currents. *Int. J. of Earthquake Engng and Struct. Dynamics.* Vol. 11.

Elzinga, T. & Tromans, P. S. (1992). Validation of 'Newwave' theory and RDWF

predictions against measured global loading on a North Sea jacket. *Proceedings of the sixth international BOSS conference*. Vol. 1.

Frieze, P. A., Bucknell, J., Birkenshaw, M., Smith, D. & Dixon, A. T. (1995). Fixed and jack-up platforms: Basis for reliability assessment. *Proceedings of the 5th international conference on the jack-up platform, design, construction and operation*. City University.

Frish-Fay, R. (1962). *Flexible bars*. London, Butterworths.

Goudreau, G. L. & Taylor, R. L. (1973). Evaluation of numerical integration methods in elastodynamics. *Journal of Computer Methods in Applied Mechanics and Engineering*. Vol. 2, No. 1, pp. 69-97.

Greeves, E. J., Jukui, B.H. & Sliggers, P.G.F. (1993). Evaluating jack-up dynamic response using frequency domain methods and the inertial load set technique. *Proceedings of the 4th international conference on the jack-up platform, design, construction and operation*. City University.

Gudmestad, O. T. (1990). A new approach for estimating irregular deep water wave kinematics. *Applied Ocean Research*. Vol. 12, No. 1.

Gudmestad, O. T. & Connor, J. J. (1986). Engineering approximations to non-linear deepwater waves. *Applied Ocean Research*. Vol. 8, No. 2.

Hahn, G. D. & Sanghvi, J. R. (April 1994). Dynamic modal responses of wave excited offshore structures. *J. Engng Mech. Div*. ASCE. Vol. 120, No. 4, pp. 893-908.

Hambly, E. C., Imm, G. R., & Stahl, B. (May 1990). Jack-up performance and foundation fixity under developing storm conditions. *Proc. 22nd Offshore Technology Conf., Houston, Texas*. OTC 6466.

Hambly, E. C. & Nicholson, B. A. (May 1991). Jack-up dynamic stability under extreme storm conditions. *Proc. 23rd Offshore Technology Conf., Houston, Texas*. OTC 6465.

Hilber, H. M. & Hughes, T. J. R. (1978). Collocation, dissipation and overshoot for time integration schemes in structural dynamics. *Int. J. of Earthquake Engng and Struct. Dynamics*. Vol. 6, pp. 99-117.

Hilber, H. M., Hughes, T. J. R. & Taylor, R. L. (1977). Improved numerical dissipation for time integration algorithms in structural mechanics. *Int. J. of Earthquake Engng and Struct. Dynamics*. Vol. 5, pp. 283-292.

Houbolt, J. C. (1950). A recurrence matrix solution for the dynamic response of elastic aircraft. *Journal of Aeronautical Science*. Vol. 17, pp. 540-550.

Houlsby, G. T. & Martin, C. M. (1992). Modelling of the behaviour of

foundations of jack-up units on clay. *Proc. Wroth Memorial Symp. "Predictive Soil Mechanics"*, Oxford, pp. 339-358. London: Thomas Telford.

Hoyle, M. J. R. (1992). Jack-up dynamics - A review of analysis techniques. In *Recent developments in jack-up platforms* (ed. L. F. Boswell & C. D'Mello). pp. 176-200. Blackwell Scientific Publications.

Jensen, J. J., Mansour, A. E. & Terndrup Pedersen, P. (November 1989). *Reliability of jack-up platforms against overturning*. Internal report, Technical University of Denmark, DCAMM - report No. 399.

Karunakaran, D. & Spidsoe, N. (1995). Verification of methods for simulation of non-linear response of jack-up platforms. *Proceedings of the 5th international conference on the jack-up platform, design, construction and operation*. City University.

Karunakaran, D., Leira, B. J., Spidsoe, N., Gudmestad, O. T. & Moan, T. (1992).Non-linear long term response of dynamically sensitive drag-dominated offshore platforms. *Proceedings of the sixth international BOSS conference*.

Kassimali, A. (August 1983). Large deformation analysis of elastic-plastic frames. *J. Struct. Engng Div.* ASCE. Vol. 109, No. 8.

Kreig, R. D. (June 1973). Unconditional stability in numerical time integration methods. *Journal of applied mechanics*. ASME. pp. 417-421.

Kreig, R. D. & Key, S. W. (1973). Transient shell response by numerical time integration. *Int. J. for Num. Meth. in Engng*. Vol. 7, pp. 273-286.

Kitipornchai, S. & Chan, S. L. (April 1987). Non-linear finite element analysis of angle and tee beam-columns. *J. Struct. Engng Div.* ASCE. Vol. 113, No. 4, pp. 721-739.

Leijten, S. F. & Efthymiou, M. (1989). A philosophy for the integrity assessment of jack-up units. *Society of Petroleum Engineers*. SPE 19236.

Lewis, D., Maison, J. & Mobbs, B. (1992). Analysis of a jack-up unit using super-element techniques. *In Recent developments in jack-up platforms* (ed. L. F. Boswell & C. D'Mello). pp. 1-40. Blackwell Scientific Publications.

Liu, P., Massie, W. W., Wolters, J. G. & Blaauwendraad, J. (1992). Elevated jack-up modelling. *Proceedings of the sixth international BOSS conference*.

Livesley, R. K. (1975). *Matrix methods of structural analysis*. 2nd ed. Pergamon Press.

Loseth, R., Mo, O., & Lotsberg, I. (1990). Probabilistic analysis of a jack-up platform with respect to the ultimate limit state. *Proceedings of the*

European offshore mechanics symposium.

Madsen, O. S. (1986). Force on circular cylinders. *Applied Ocean Research.* Vol. 8, No. 3.

Martin, C. M. (1991). *The behaviour of jack-up rig foundations on clay.* First Year report, University of Oxford.

Martin, C. M. (1994). *Physical and numerical modelling of offshore foundations under combined loads.* D.Phil. thesis. University of Oxford.

Morison, J. R., O'Brien, M. P., Johnson, J. W. & Schaaf, S. A. (1950). The force exerted by surface waves on piles. *Petrol. Trans.* AIME. Vol. 189, pp. 149-154.

NDA. (1987). See Noble Denton & Associates (1987).

Newmark, N. M. (1959). A method of computation for structural dynamics. *J. Engng Mech. Div.* ASCE. Vol. 85, pp. 67-94.

Nickell, R. E. (1971). On the stability of approximation operators in problems of structural dynamics. *Int. J. of Solids and Structures.* Vol. 7, pp. 301-319.

Nickell, R. E. (1973). Direct integration in structural dynamics. *J. Engng Mech. Div.* ASCE. Vol. 99, pp. 303-317.

Nielsen, L. P., Friis Hansen, P., Juncher Jensen, J. & Terndrup Pedersen B. J. (1994). Reliability based inspection planning of a jack-up rig. *Proceedings of the eighth international BOSS conference.*

Nishimura, H., Isoke, M. & Honkawa, H. (1977). Solutions of the Stokes' and cnoidal waves. *J. Fac. Eng. University of Tokyo.* Series B, Vol. 24, pp. 267-293.

Noble Denton & Associates. (1987). *Foundation fixity of jack-up units: A Joint Industry Study.* London: Noble Denton & Associates.

O'Brien, M. D. & Morison, J. R. (1952). The forces exerted by waves on objects. *Transactions of the American Geophysical Union.* Vol. 33, No. 1.

Oran, C. (1973[a]). Tangent stiffness in plane frames. *J. Struct. Engng Div.* ASCE. Vol. 99, No. ST6.

Oran, C. (1973[b]). Tangent stiffness in space frames. *J. Struct Engng Div.* ASCE. Vol. 99, No. ST6.

Oran, C. & Kassimali, A. (1976). Large deformations of framed structures under static and dynamic loads. *Computers and Structures.* Vol. 6, pp. 539-547.

Patel, M. H. (1989). *Dynamics of offshore structures.* Butterworths.

Press, W. H., Flannery, B. P., Teukolsky, S. A., & Vetterling, W. T. (1986). *Numerical recipes - The art of scientific computing*. Cambridge University Press.

Prince-Wright, R. (1988). *A computer program for Skjelbreia and Hendrickson's fifth order wave theory*. Department of Naval Architecture and Ocean Engineering, University of Glasgow. NAOE-89-18.

Przemieniecki, J. S. (1968). *Theory of matrix structural analysis*. McGraw-Hill book company.

Rahman, M. (1995). *Water Waves: Relating modern theory to advanced engineering applications*. Oxford University Press.

Reardon, M. J. (1986). Review of the geotechnical aspects of jack-up unit operations. *Ground Engng*. Vol. 19, No. 7, pp. 21-26.

Remseth, S. N. (1979). Non-linear static and dynamic analysis of framed structures. *Computers and structures*. Vol. 10, No. 6, pp. 879-897.

Saafan, S. A. (1963). Nonlinear behaviour of structural plane frames. *J. Struct. Engng Div*. ASCE. Vol. 89, No. ST4, Proc. Paper 3615, pp. 557-579.

Santa Maria, P. E. L. (1988). *Behaviour of footings for offshore structures under combined loads*. DPhil thesis, University of Oxford.

Sarpkaya, T. & Isaacson, M. (1981). *Mechanics of wave forces on offshore structures*. Van Nostrand Reinhold.

Skjelbreia, L. (1959). *Gravity waves, Stokes' third order approximation, tables of functions*. The Engineering Foundation Council on Wave research, Berkeley, California, U.S.A.

Skjelbreia, L. & Hendrickson, J. (1960). Fifth order gravity wave theory. *Proc. 7th Coastal Eng. Conf*. The Hague, pp. 184-196.

Smith, I. M. & Griffiths, D. V. (1988). *Programming the finite element method*. John Wiley and sons Inc.

Smith, I. M. & Griffiths, D. V. (1990). *Numerical methods for engineers-A programming approach*. Blackwell Scientific.

SNAME. (1993). *Guideline for the site specific assessment of mobile jack-up units*. New Jersey: Society of Naval Architects and Marine Engineers.

Stokes, G. G. (1847). On the theory of oscillatory waves. *Trans. Camb. Philos. Soc*. Vol. 8, pp. 441-455.

Tan, F. S. C. (1990). *Centrifuge and theoretical modelling of conical footings on*

sand. Ph.D. thesis, University of Cambridge.

Tezcan, S. S. & Mahapatra, B. C. (1969). Tangent stiffness matrix for space frame members. *J. Struct. Engng Div.* ASCE. Vol. 95, No. ST6.

Thomson, W. T. (1993). *The theory of vibration with applications*. 4th ed. Chapman & Hall.

Timoshenko, S. P. & Gere, J. M. (1961). *Theory of elastic stability*. 2nd ed. McGraw-Hill book company.

Timoshenko, S., Young, D. H. & Weaver, Jr W. (1974). *Vibration problems in engineering*. John Wiley and Sons.

Tromans, P. S., Anaturk, A. R., & Hagemeijer, D. (1991). *A new model for the kinematics of large ocean waves - Application as a design wave*. Proceedings of the ISOPE-91 conference. Edinburgh, Scotland.

Tucker, M. J., Challenor, P. G. & Carter, J. T. (1984). Numerical simulation of a random sea: a common error and its effect upon wave group statistics. *Applied Ocean Research*. Vol. 6, No. 2.

Vesic, A. S. (1975). Bearing capacity of shallow foundations. In *Foundation Engineering Handbook* (ed. H. F. Winterkorn & H. Y. Fang). pp. 121-147. New York: Van Nostrand.

Vugts, J. H. (1990). Environmental forces in relation to structure design or assessment. A personal view towards integration of the various aspects involved. *Keynote paper presented at the SUT International conference on environmental forces on offshore structures*. London.

Weeks, G. (1972). Temporal operators for non-linear structural dynamics problems. *J. Engng Mech. Div.* ASCE. Vol. 98, No. EM5.

Wheeler, J. D. (March 1970). Method for calculating forces produced by irregular waves. *Journal of Petroleum Technology*. March, pp. 359-367.

Wilson, E. L., Farhoomand, I. & Bathe, K. J. (1973). Non-linear dynamic analysis of complex structures. *Int. J. of Earthquake Engng and Struct. Dynamics*. Vol. 1, pp. 241-252.

Wu, J. S. & Chang, C. Y. (1988). Structural simplification of jack-up rig and its dynamic responses in regular waves. *Journal of Ship Research*. Vol. 32, No. 2, pp. 134-153.

Yang, T. Y. & Saigal, S. (May, 1984). A simple element for static and dynamic response of beams with material and geometric non-linearities. *Int. J of Num. Meth. in Engng*. Vol. 20, No. 5, pp. 851-867.

Young, A. G., Remmes, B. D. & Meyer, B. J. (1984). Foundation performance of offshore jack-up drilling rigs. *J. Geotech. Engng Div.* ASCE. Vol. 110, No. 7, pp. 841-859.

Natural periods calculated by Matlab (s)	Natural periods calculated by JAKUP. Cholesky decomposition. (s)	Natural periods calculated by JAKUP. Spectral decompostion (s)
3.628	3.627	3.628
1.779	1.779	1.779
0.181	0.181	0.181

TABLE 3.1 Natural periods for the beam of Fig 3.6[a]

Eigenvectors calculated by Matlab	Eigenvectors calculated by JAKUP. Cholesky decomposition.	Eigenvectors calculated by JAKUP. Spectral decomposition.
$\begin{bmatrix}1.000\\0.0\\0.0\end{bmatrix}$ $\begin{bmatrix}0.0\\0.726\\1.000\end{bmatrix}$ $\begin{bmatrix}0.0\\0.131\\1.000\end{bmatrix}$	$\begin{bmatrix}1.000\\0.0\\0.0\end{bmatrix}$ $\begin{bmatrix}0.0\\0.726\\1.000\end{bmatrix}$ $\begin{bmatrix}0.0\\0.131\\1.000\end{bmatrix}$	$\begin{bmatrix}1.000\\0.0\\0.0\end{bmatrix}$ $\begin{bmatrix}0.0\\0.726\\1.000\end{bmatrix}$ $\begin{bmatrix}0.0\\0.131\\1.000\end{bmatrix}$

TABLE 3.2 Eigenvectors for the beam of Fig 3.6[a]

Natural periods calculated by JAKUP. (s)
3.899
1.786
1.116
0.283
8.360×10^{-2}
2.880×10^{-2}

TABLE 3.3 Natural periods for the beams of Fig 3.6[b] and Fig 3.7[b]

Eigenvectors calculated by JAKUP. Cholesky decomposition

$$\begin{bmatrix} 0.707 \\ O(-7) \\ O(-5) \\ 1.000 \\ O(-5) \\ O(-6) \end{bmatrix} \begin{bmatrix} -0.707 \\ O(-7) \\ O(-5) \\ 1.000 \\ O(-5) \\ O(-5) \end{bmatrix} \begin{bmatrix} O(-6) \\ 0.247 \\ 0.848 \\ O(-7) \\ 0.727 \\ 1.000 \end{bmatrix} \begin{bmatrix} O(-7) \\ -0.150 \\ 0.090 \\ O(-7) \\ 0.208 \\ 1.000 \end{bmatrix} \begin{bmatrix} O(-9) \\ -0.010 \\ -0.794 \\ O(-9) \\ 0.104 \\ 1.000 \end{bmatrix} \begin{bmatrix} O(-13) \\ 0.013 \\ 0.269 \\ O(-12) \\ 0.052 \\ 1.000 \end{bmatrix}$$

Eigenvectors calculated by JAKUP. Spectral decomposition

$$\begin{bmatrix} 0.707 \\ O(-8) \\ O(-7) \\ 1.000 \\ O(-7) \\ O(-7) \end{bmatrix} \begin{bmatrix} -0.707 \\ O(-10) \\ O(-9) \\ 1.000 \\ O(-10) \\ O(-10) \end{bmatrix} \begin{bmatrix} O(-8) \\ 0.247 \\ 0.848 \\ O(-8) \\ 0.727 \\ 1.000 \end{bmatrix} \begin{bmatrix} O(-8) \\ -0.150 \\ 0.090 \\ O(-8) \\ 0.208 \\ 1.000 \end{bmatrix} \begin{bmatrix} O(-10) \\ -0.010 \\ -0.794 \\ O(-9) \\ 0.104 \\ 1.000 \end{bmatrix} \begin{bmatrix} O(-10) \\ 0.013 \\ 0.269 \\ O(-10) \\ 0.052 \\ 1.000 \end{bmatrix}$$

TABLE 3.4 Eigenvectors for the beam of Fig 3.6[b]

Period (s)	d/gT^2	H_d (m)	H_{max} (m)
4.6	0.43	5.0	5.6
6.0	0.25	7.6	8.7
6.6	0.21	10.1	11.5
7.6	0.15	13.2	15.1
8.3	0.13	14.9	18.0
11.0	0.075	21.0	31.0
12.0	0.063	22.1	34.5
14.0	0.047	22.5	44.96
16.0	0.036	22.5	50.23
18.0	0.028	22.2	54.35
20.0	0.023	20.5	58.67

Table 6.1 Approximate limiting wave heights for Stokes fifth wave theory

footing model	Ω	T (s)	Variation of the dynamic maximum hull displacement (%)	Variation of the dynamic double amplitude of hull displacement (%)	Variation of the quasi-static maximum hull displacement (%)	Variation of the quasi-static double amplitude of hull displacement (%)	Variation of the maximum hull displacement amplification factor (%)	Variation of the double amplitude amplification factor (%)
pinned	0.49	17.0	1.6	1.9	-1.6	-3.3	3.25	5.34
pinned	0.52	16.0	1.9	3.9	-1.7	-3.36	-0.24	-0.62
pinned	0.61	13.5	8.3	-2.6	-0.9	-1.93	9.2	-0.73
Model B	0.41	16.0	2.05	0.301	-1.42	-3.25	3.5	3.67
Model B	0.49	13.5	4.4	8.7	-0.64	-1.73	5.07	10.6
Model B	0.6	11.0	-0.98	-2.54	-2.26	-4.38	1.31	1.9
fixed	0.29	16.0	0.79	4.6	-1.37	-3.346	0.59	-1.12
fixed	0.5	9.0	8.9	14.5	-3.7	-8.2	13.07	24.8
fixed	0.62	7.5	-4.2	-8.0	-5.2	-10.0	1.05	2.2

TABLE 6.2 Percentage differences of response variables compared to a more detailed numerical model

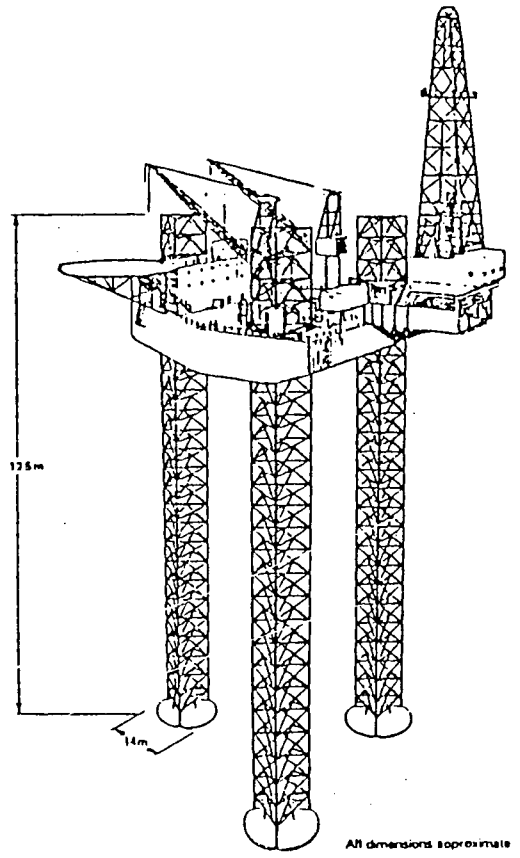

FIGURE 1.1 A typical three legged jack-up unit (from Reardon, 1986)

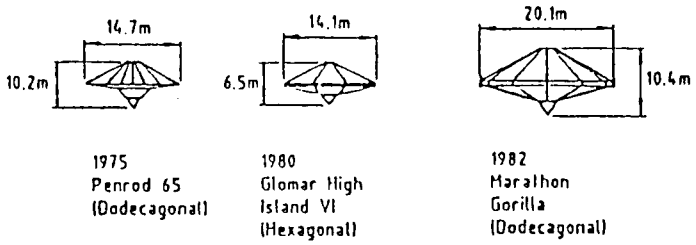

FIGURE 1.2 Some typical spudcan footings (from Young *et al*, 1984)

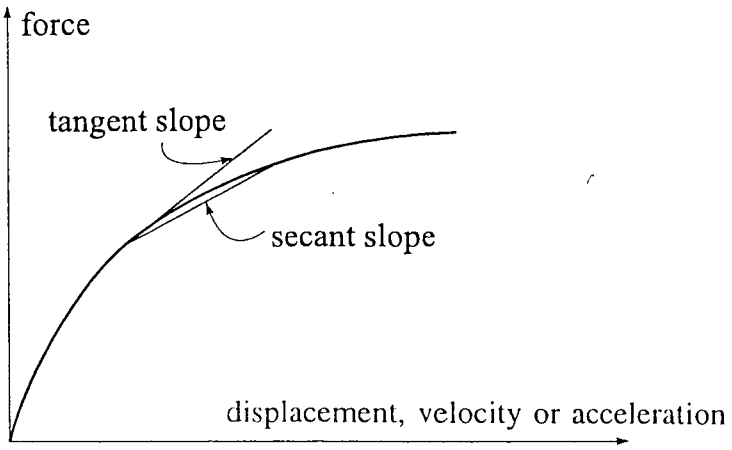

FIGURE 2.1 Secant and tangent slopes on a non-linear response path

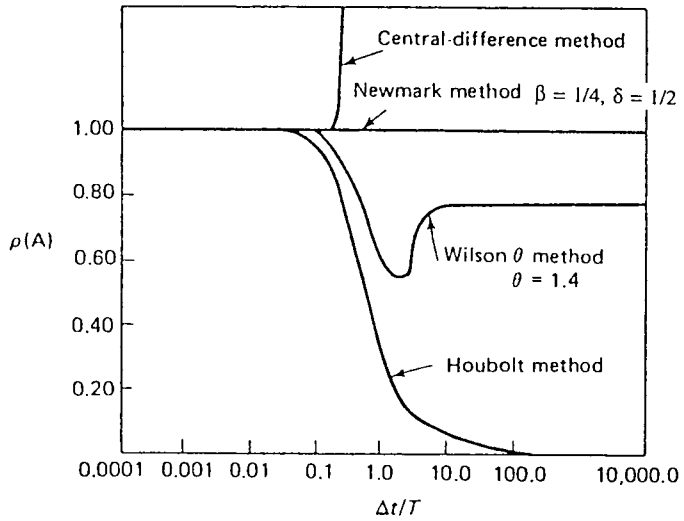

FIGURE 2.2 Spectral radii of approximation operators (from Bathe, 1982)

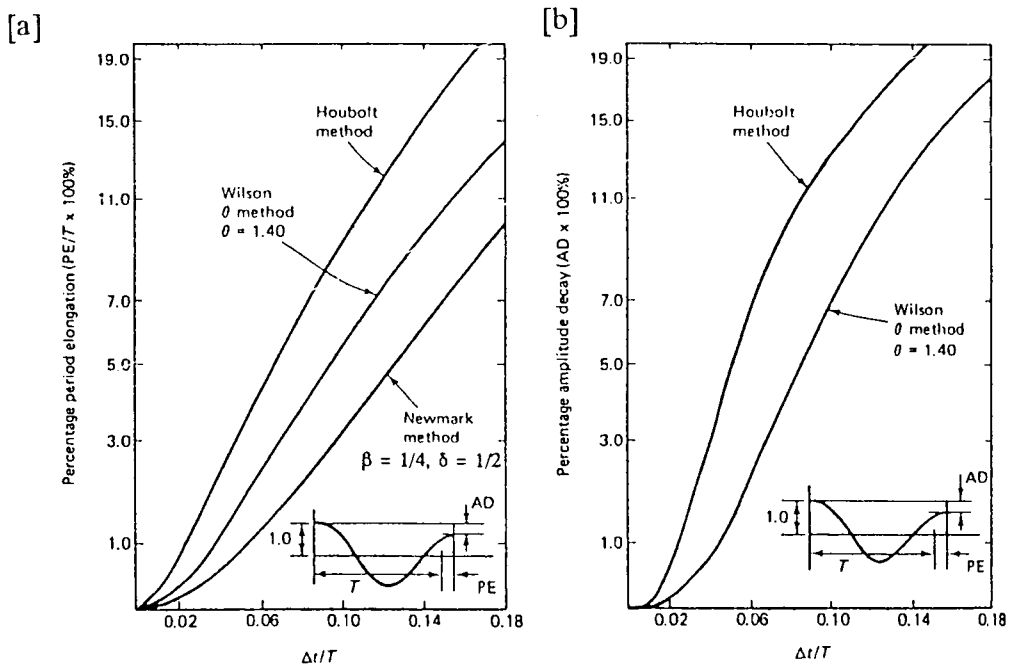

FIGURE 2.3 Percentage period elongation and amplitude decays (from Bathe, 1982)

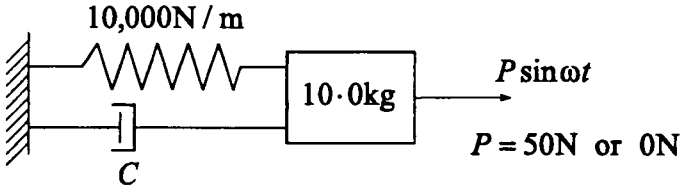

FIGURE 2.4 Linear mass-spring-damper system

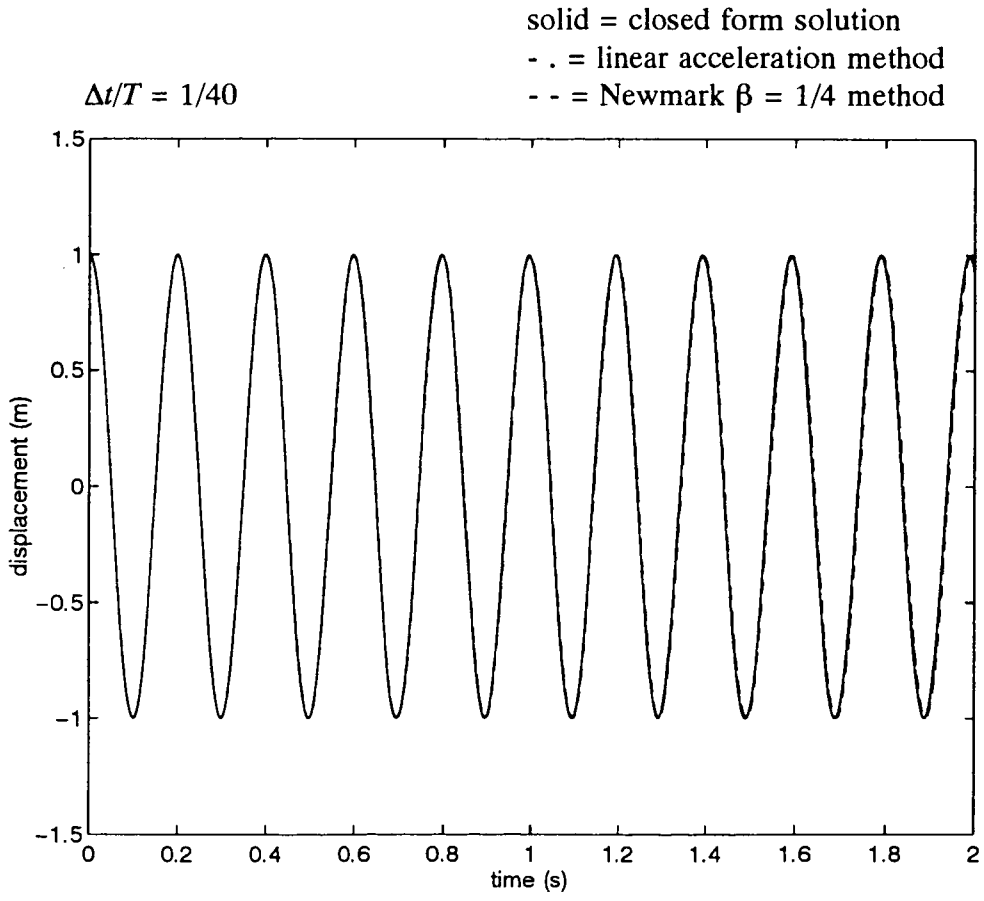

FIGURE 2.5 Undamped displacement response

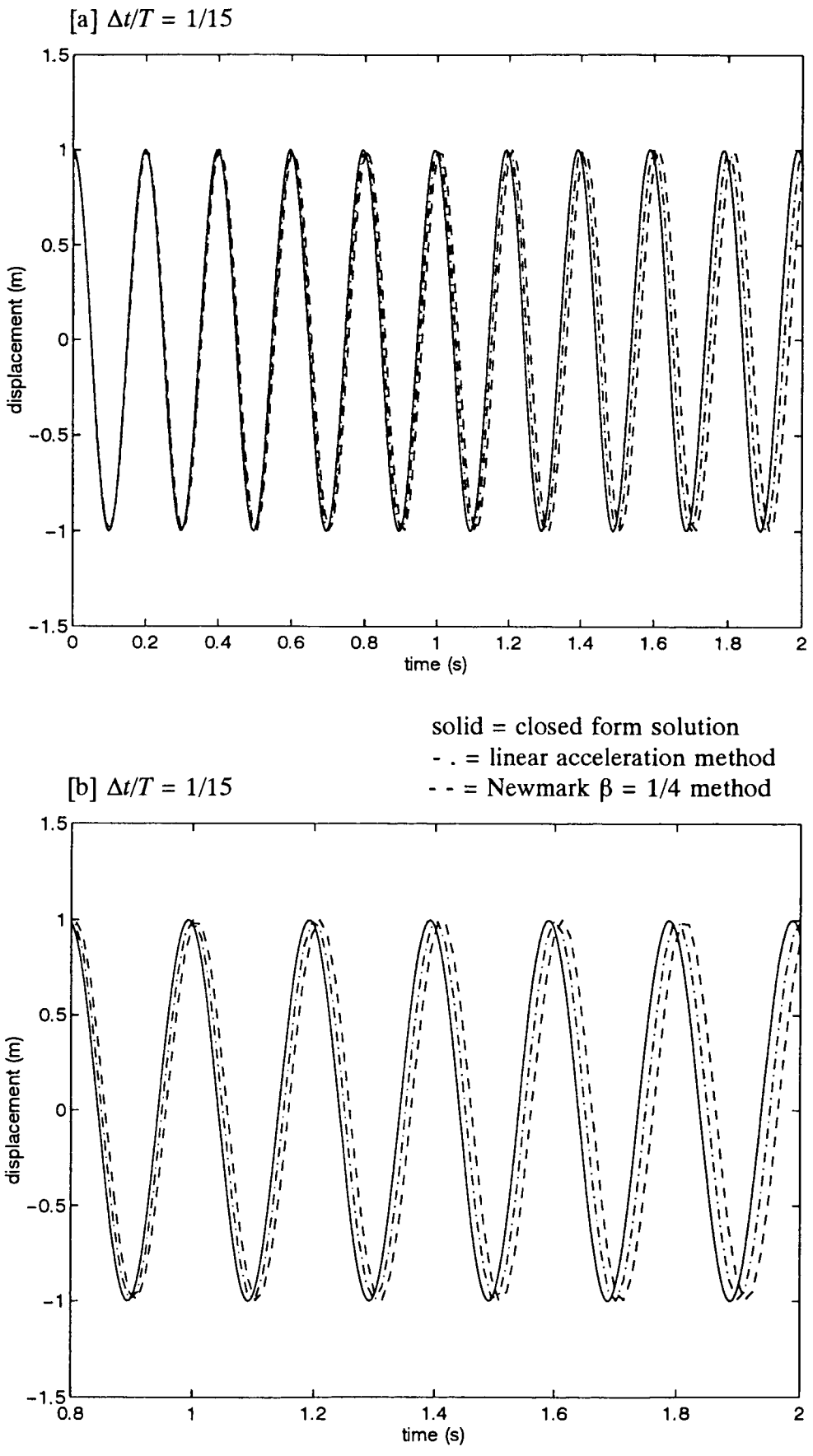

FIGURE 2.6 Undamped displacement response

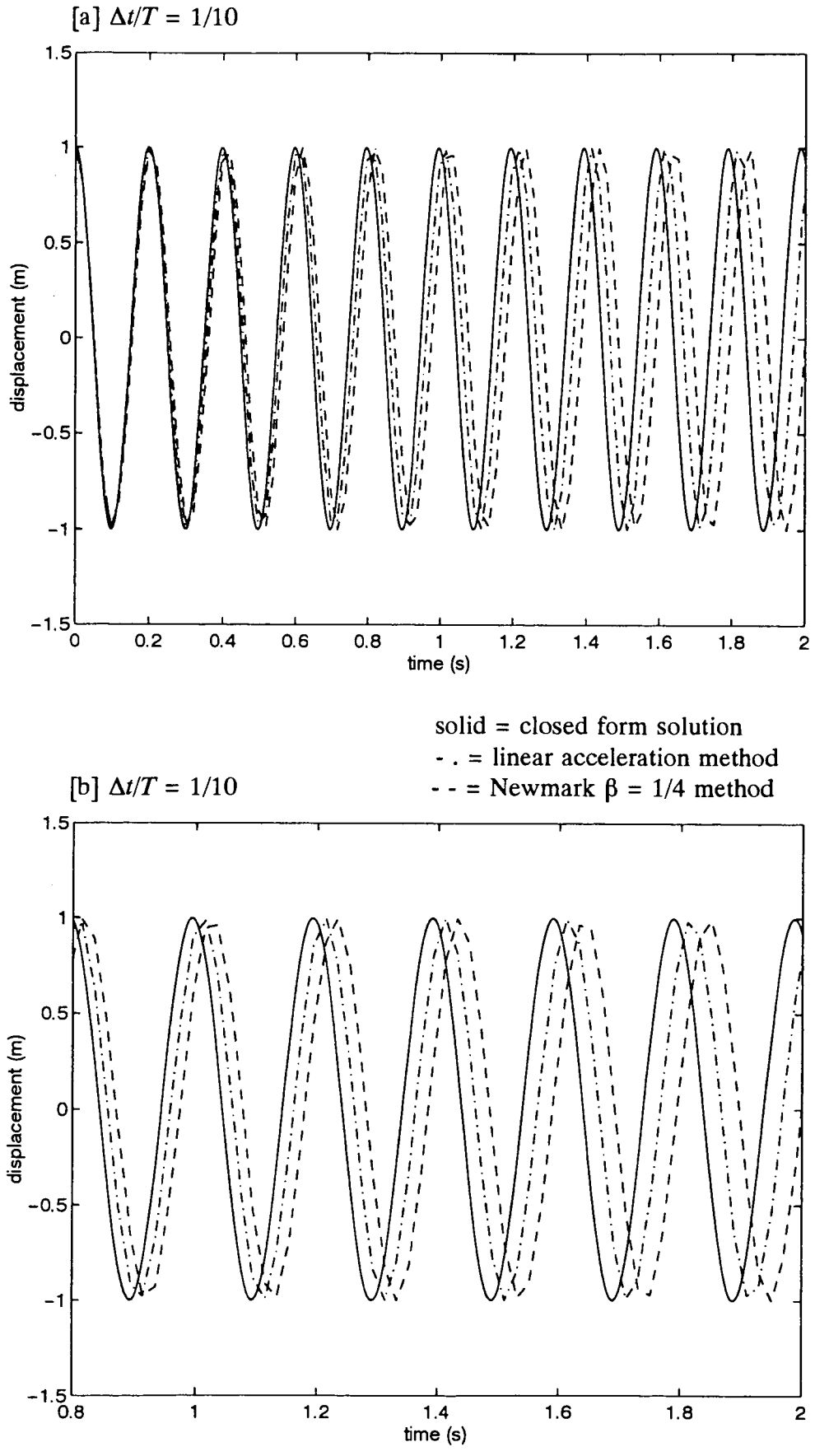

FIGURE 2.7 Undamped displacement response

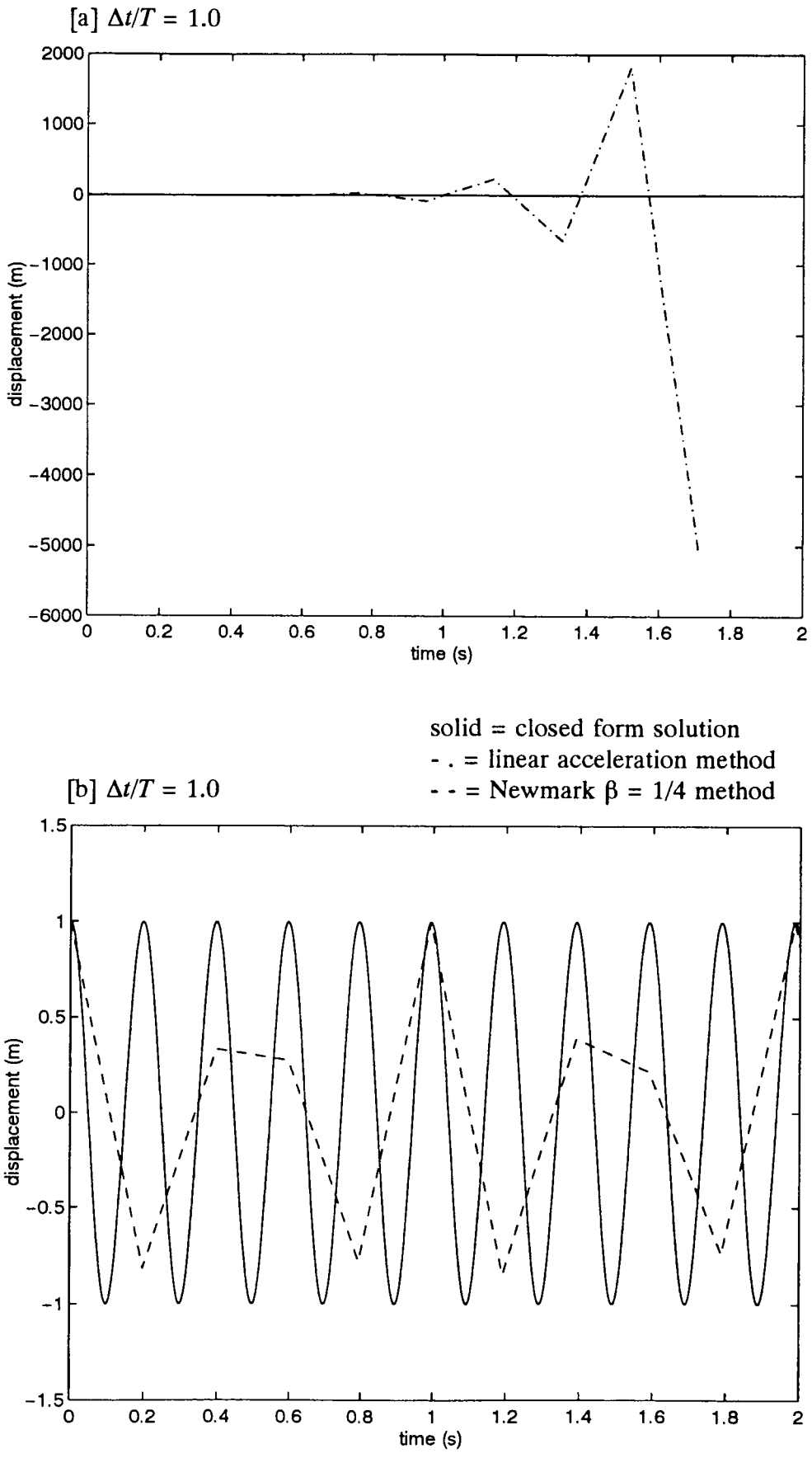

FIGURE 2.8 Undamped displacement response

[a] $\xi = 0.05$

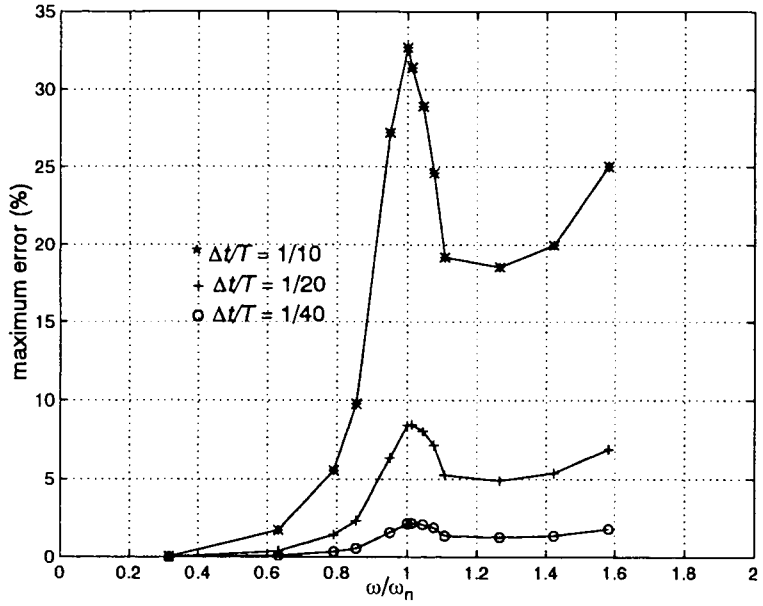

[b] $\xi = 0.5$

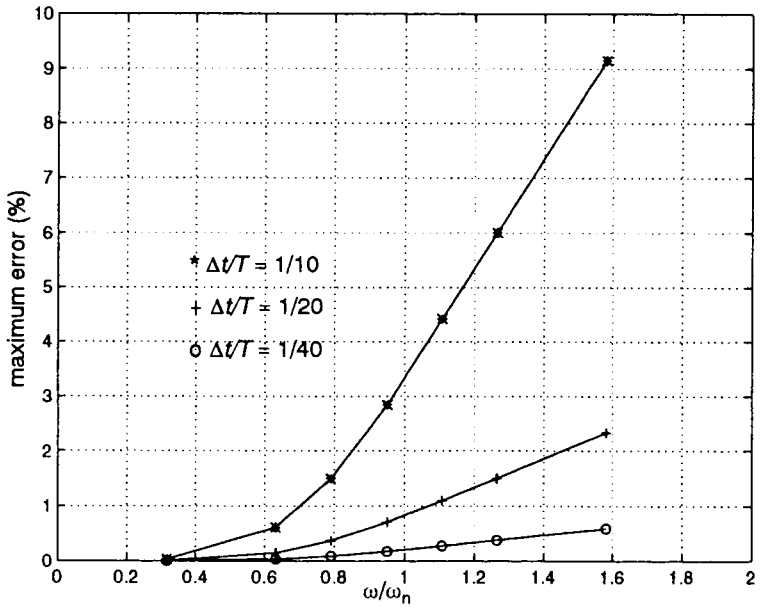

FIGURE 2.9[a] and **[b]** Error curves for the linear acceleration method

[c] ξ = 1.0

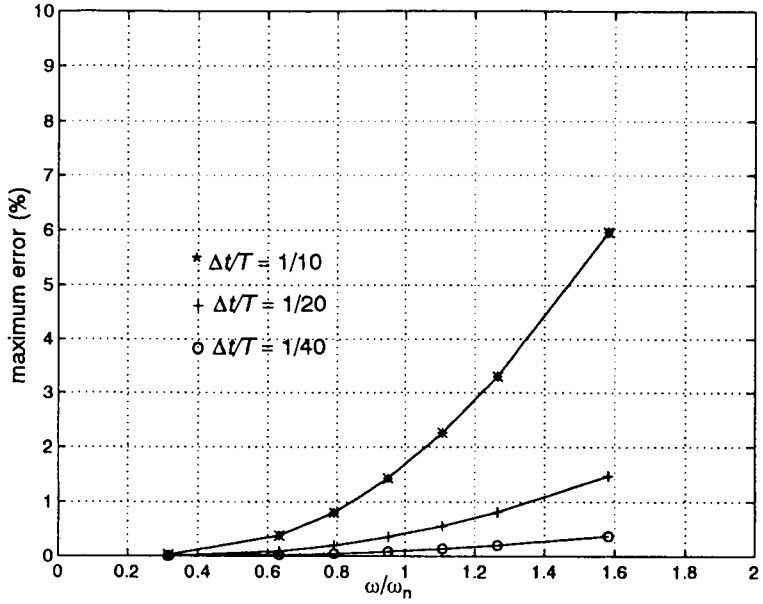

[d] ξ = 1.2

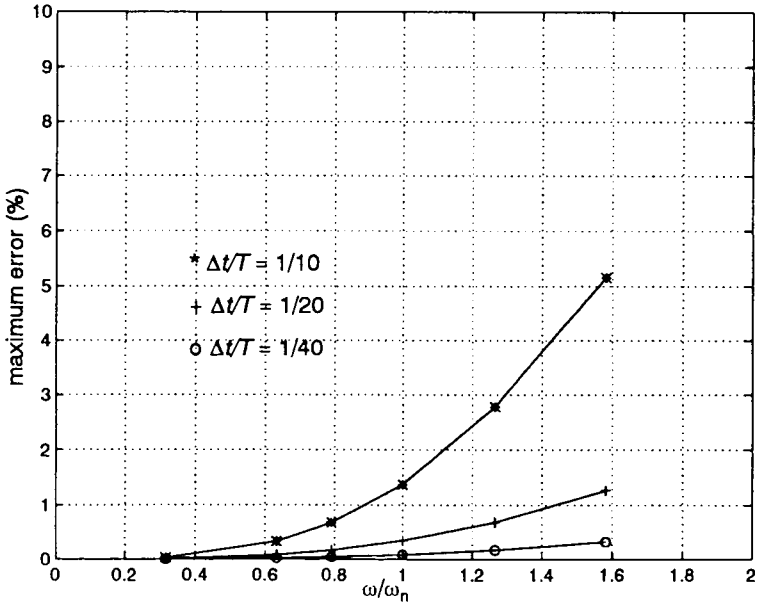

FIGURE 2.9[c] and **[d]** Error curves for the linear acceleration method

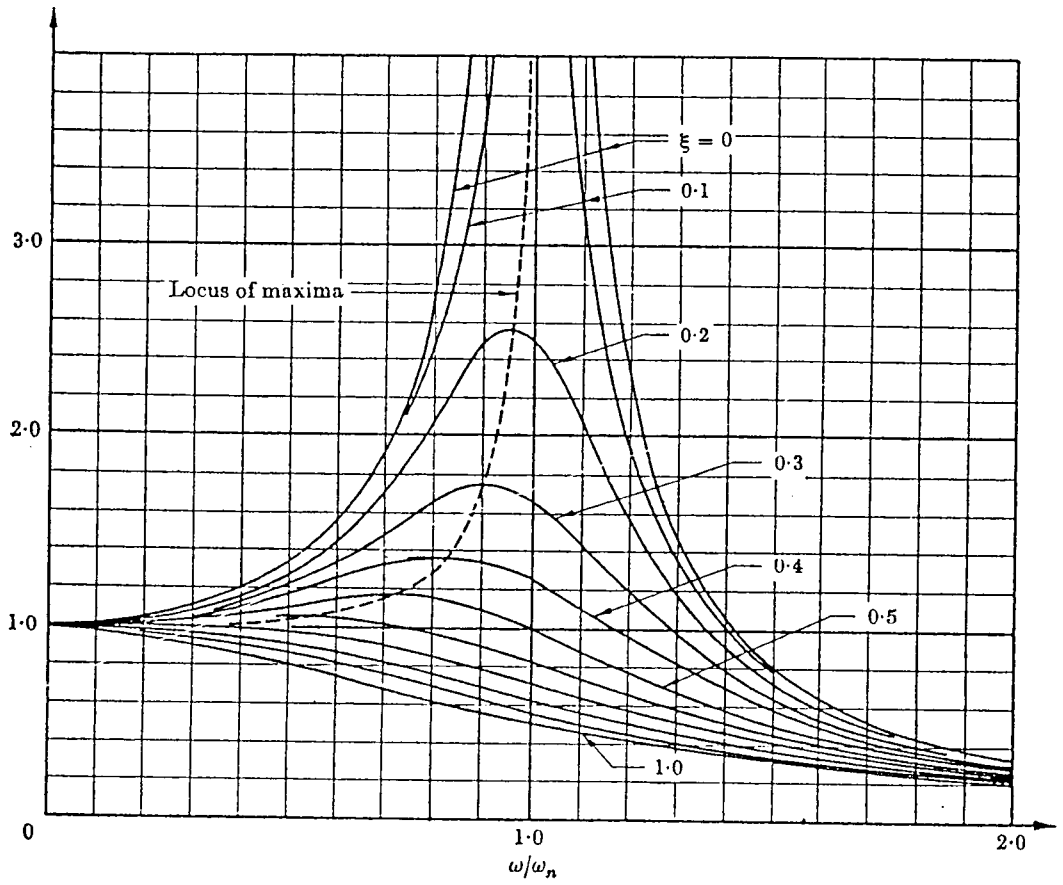

FIGURE 2.10 Variation of dynamic amplification factor with frequeny ratio (from Cambridge University Mechanics databook, 1988)

[a] $\xi = 0.05$

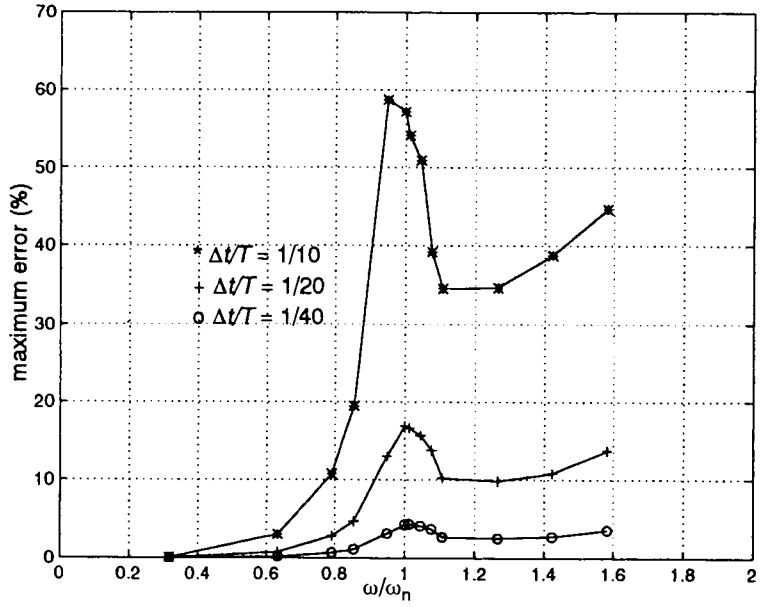

[b] $\xi = 0.5$

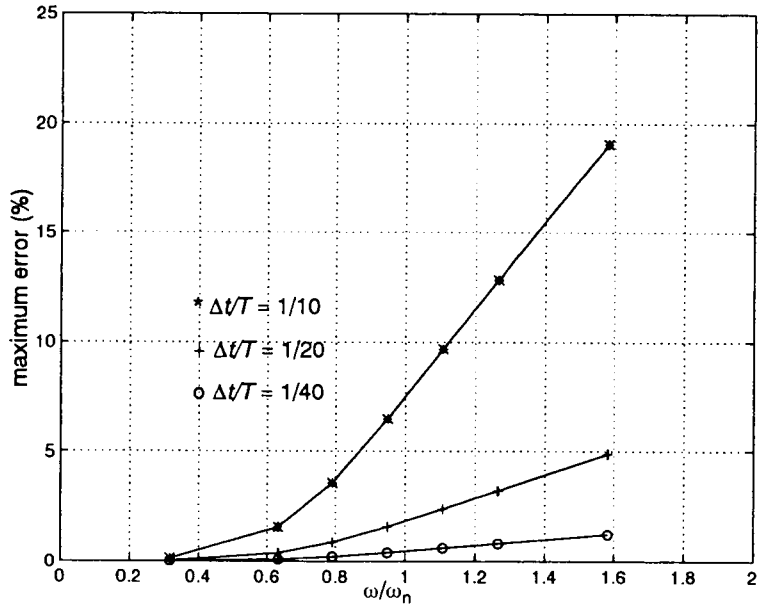

FIGURE 2.11[a] and **[b]** Error curves for the Newmark $\beta = 1/4$ method

[c] ξ = 1.0

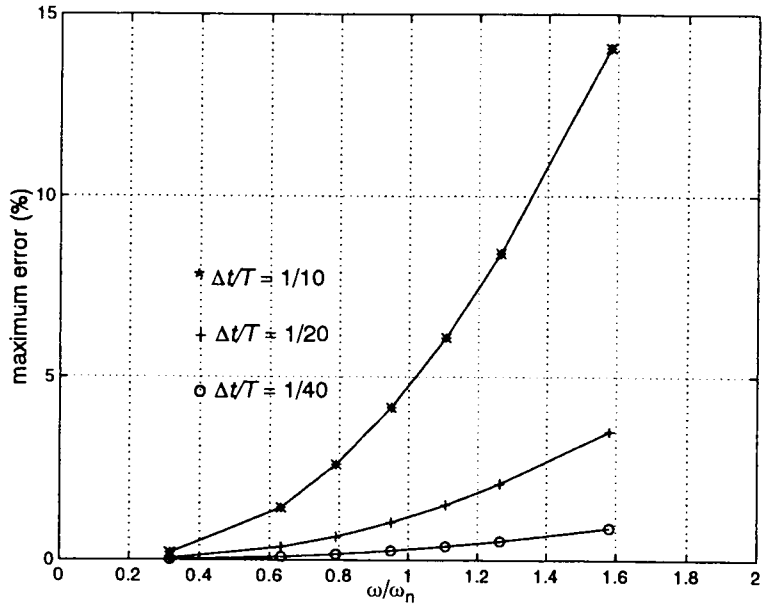

[d] ξ = 1.2

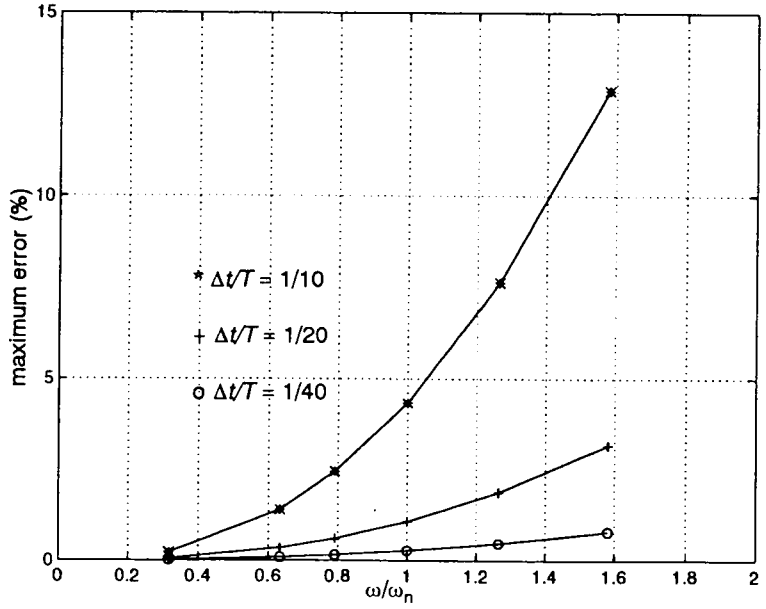

FIGURE 2.11[c] and **[d]** Error curves for the Newmark β = 1/4 method

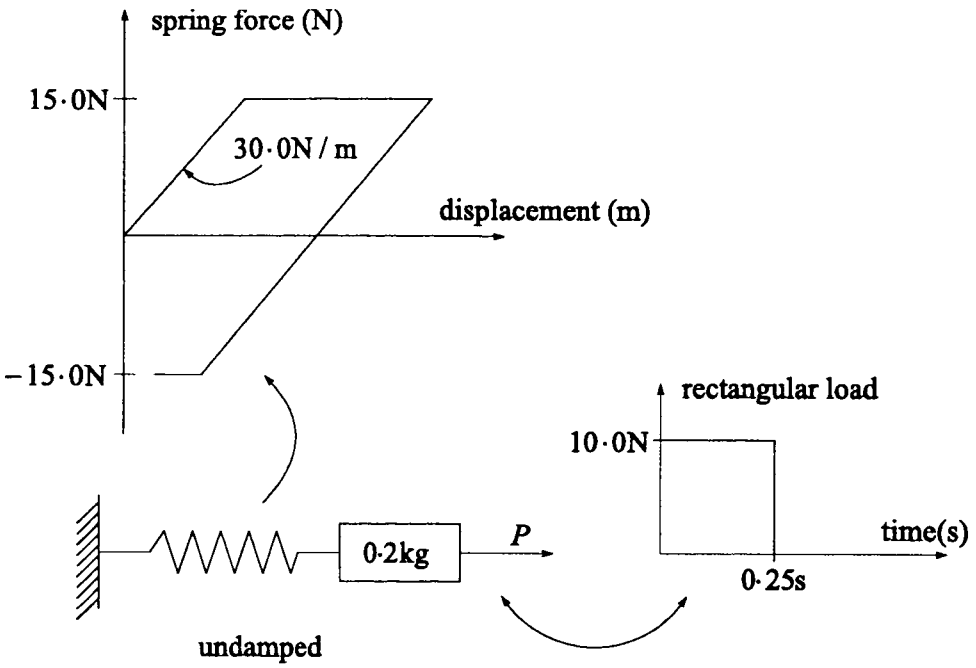

FIGURE 2.12 Non-linear single degree of freedom system (after Craig, 1981)

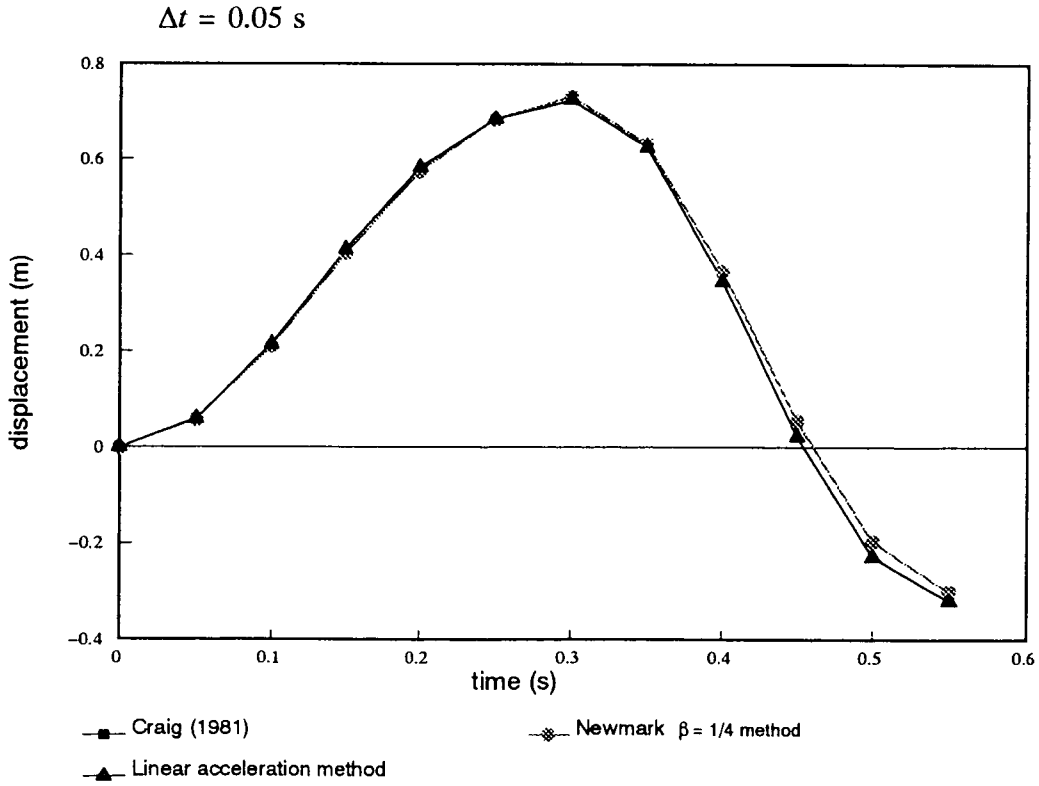

FIGURE 2.13 Non-linear displacement response

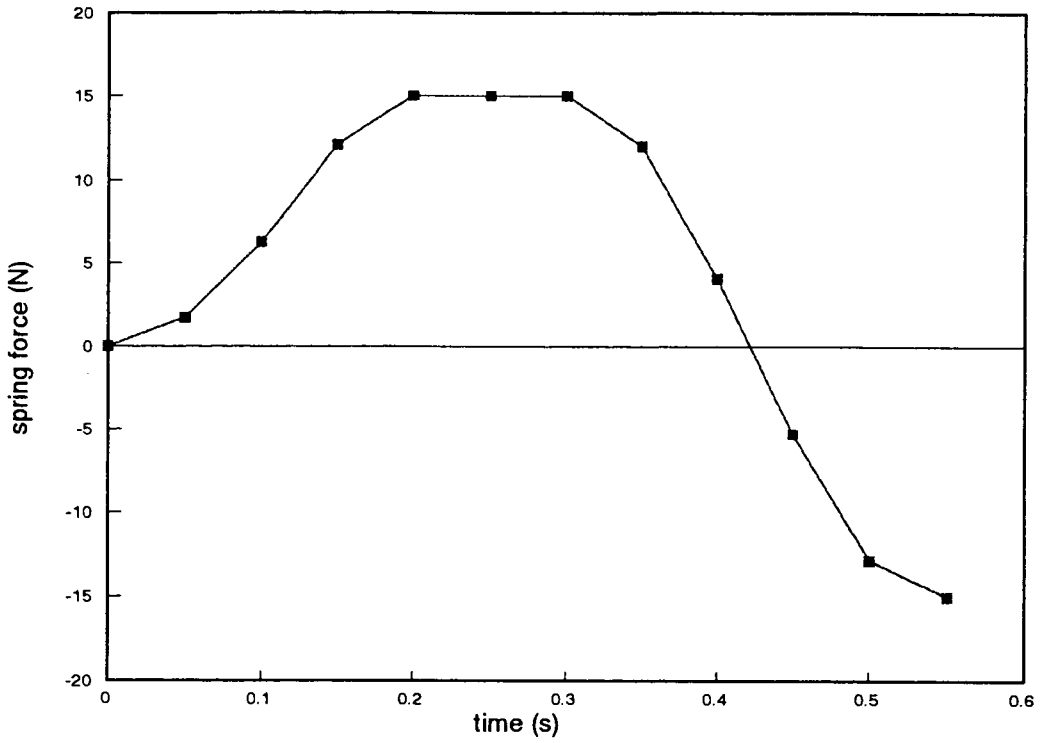

FIGURE 2.14 Non-linear spring force response

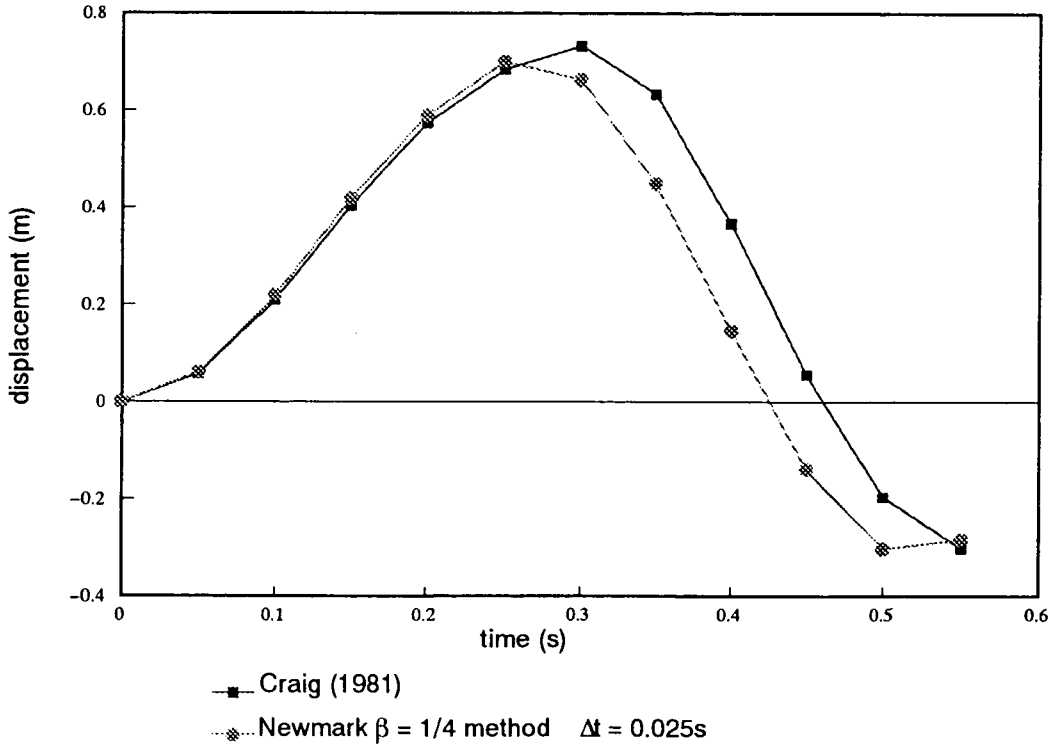

FIGURE 2.15 Displacement response

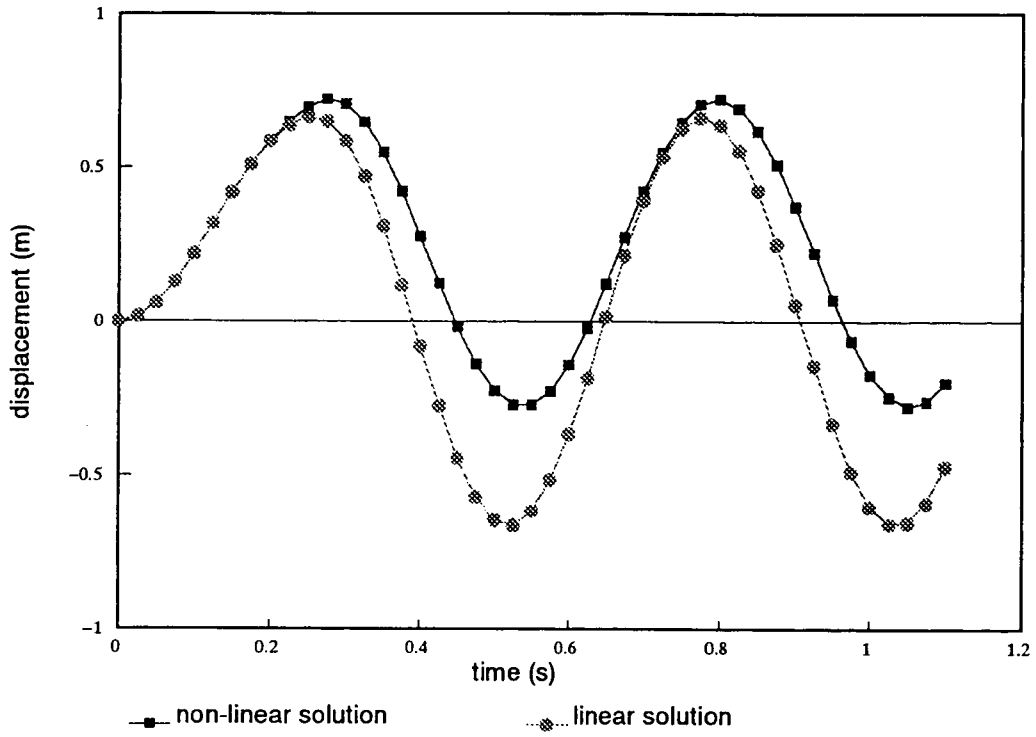

FIGURE 2.16 Linear and non-linear displacement responses predicted by JAKUP

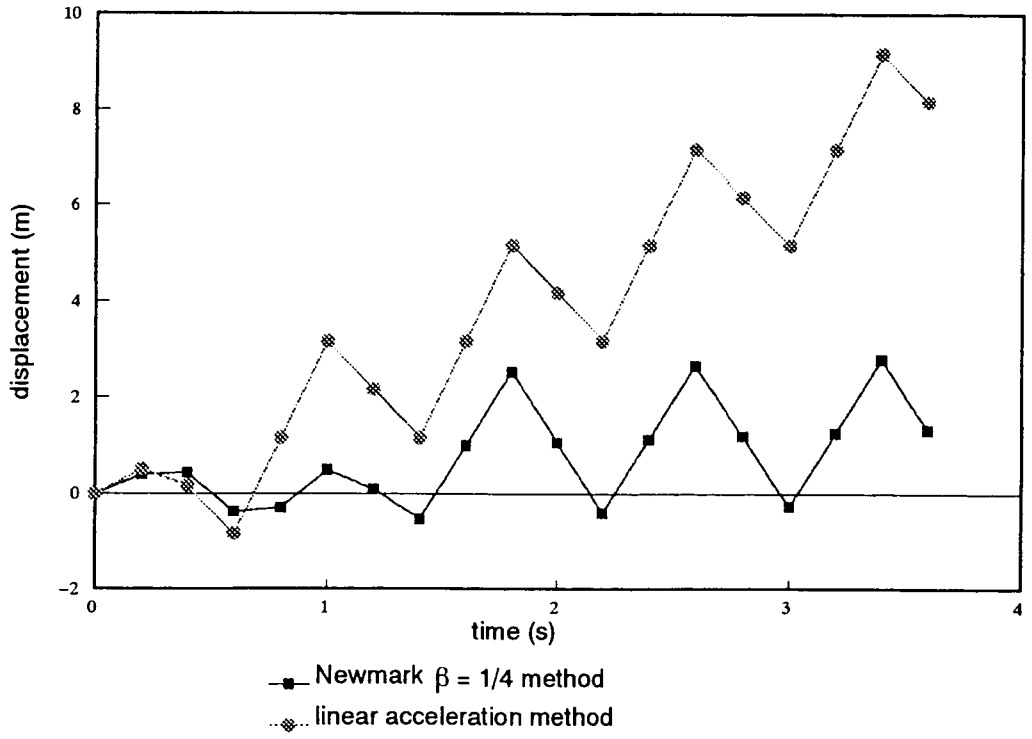

FIGURE 2.17 Displacement response with a large timestep

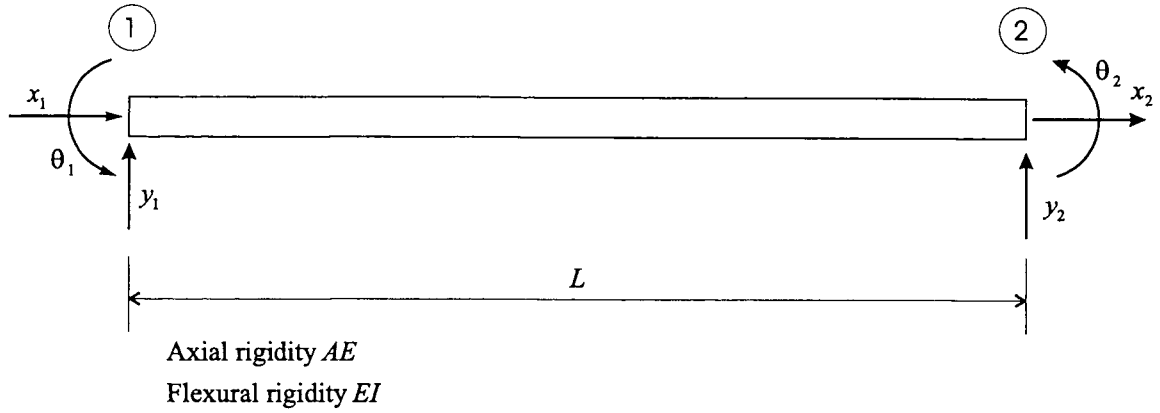

FIGURE 3.1 Uniform beam in local coordinate system

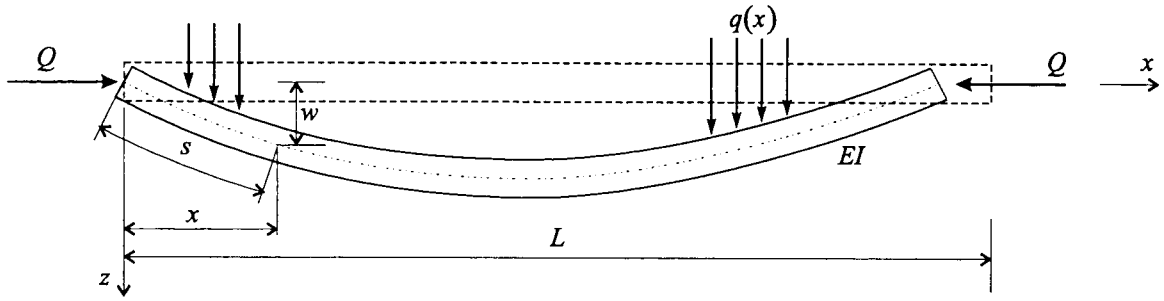

FIGURE 3.2 Local beam-column element

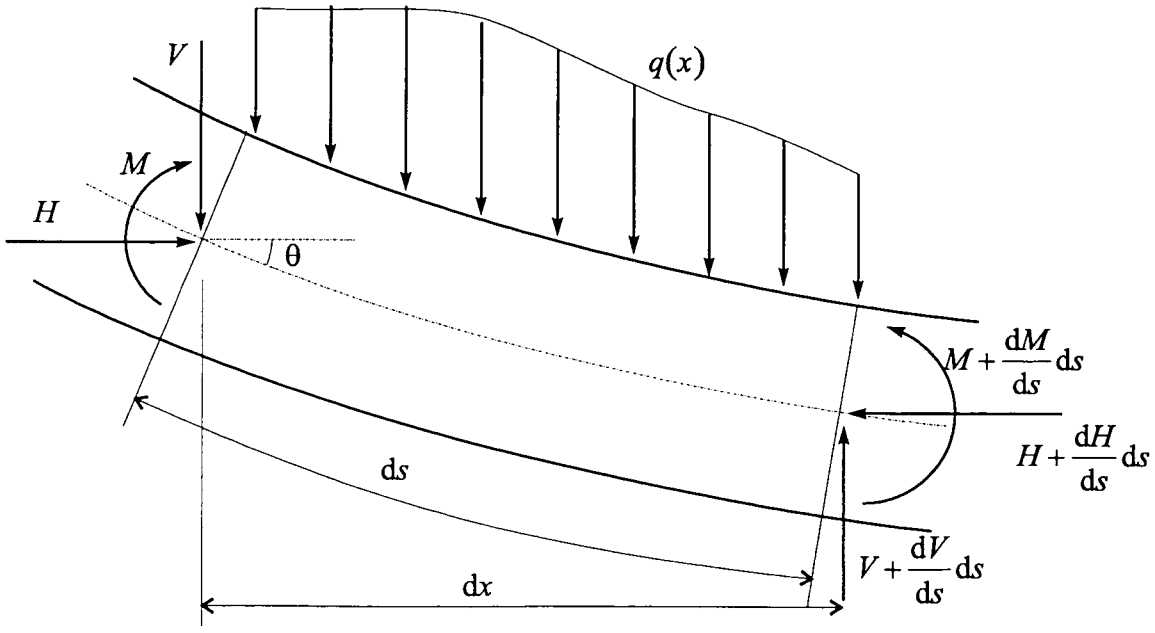

FIGURE 3.3 Equilibrium of an incremental beam-column section (after Chen & Atsuta, 1976)

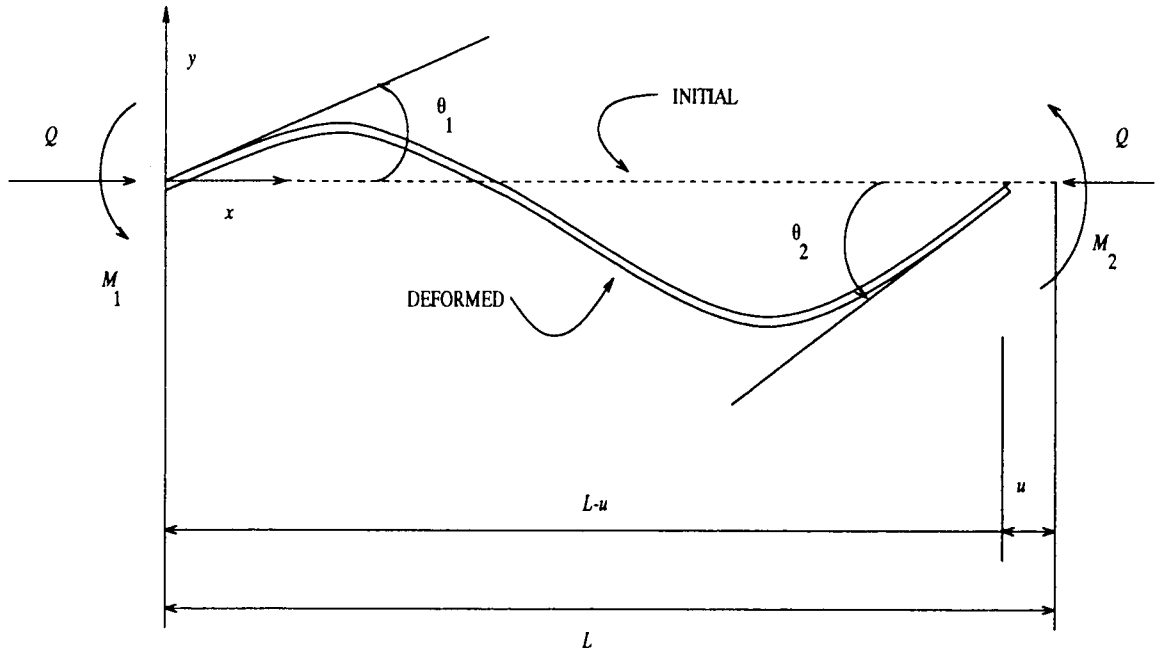

FIGURE 3.4 End forces and displacements on a local beam-column element

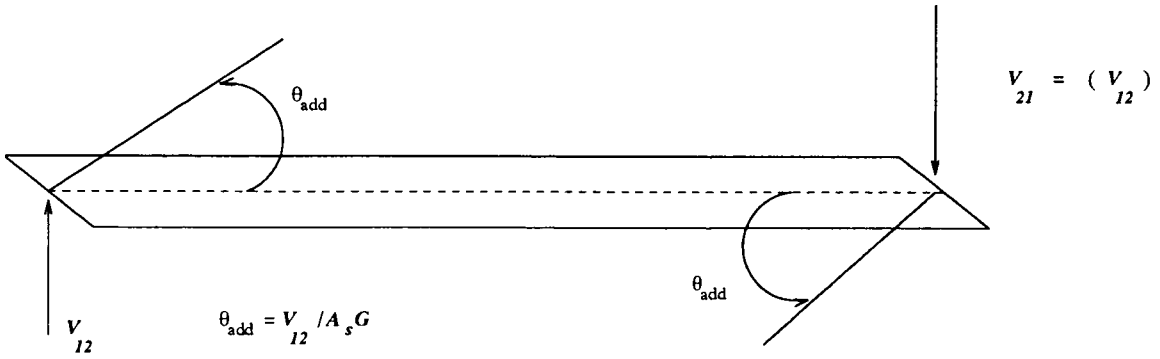

FIGURE 3.5 Additional end rotation due to shear (after Martin, 1994)

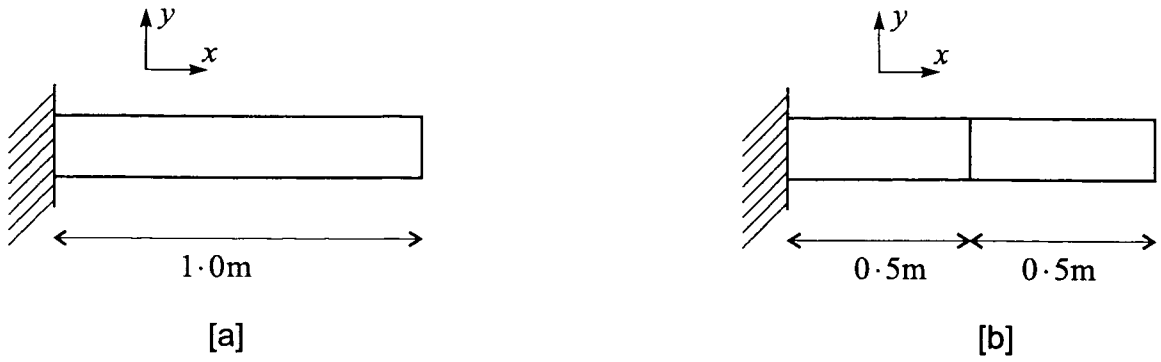

FIGURE 3.6 Beam used in eigensystem test

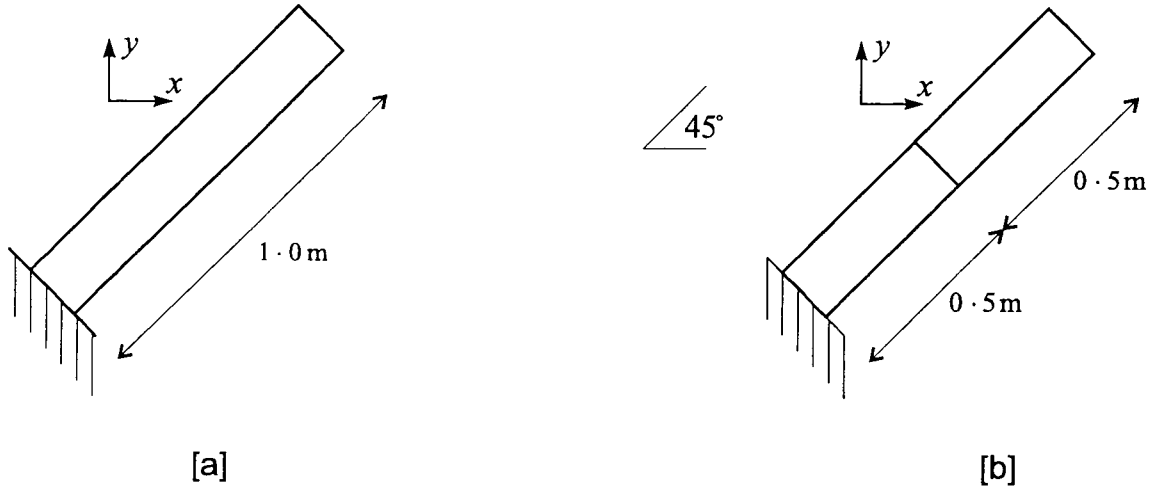

FIGURE 3.7 Beam rotated through 45^0

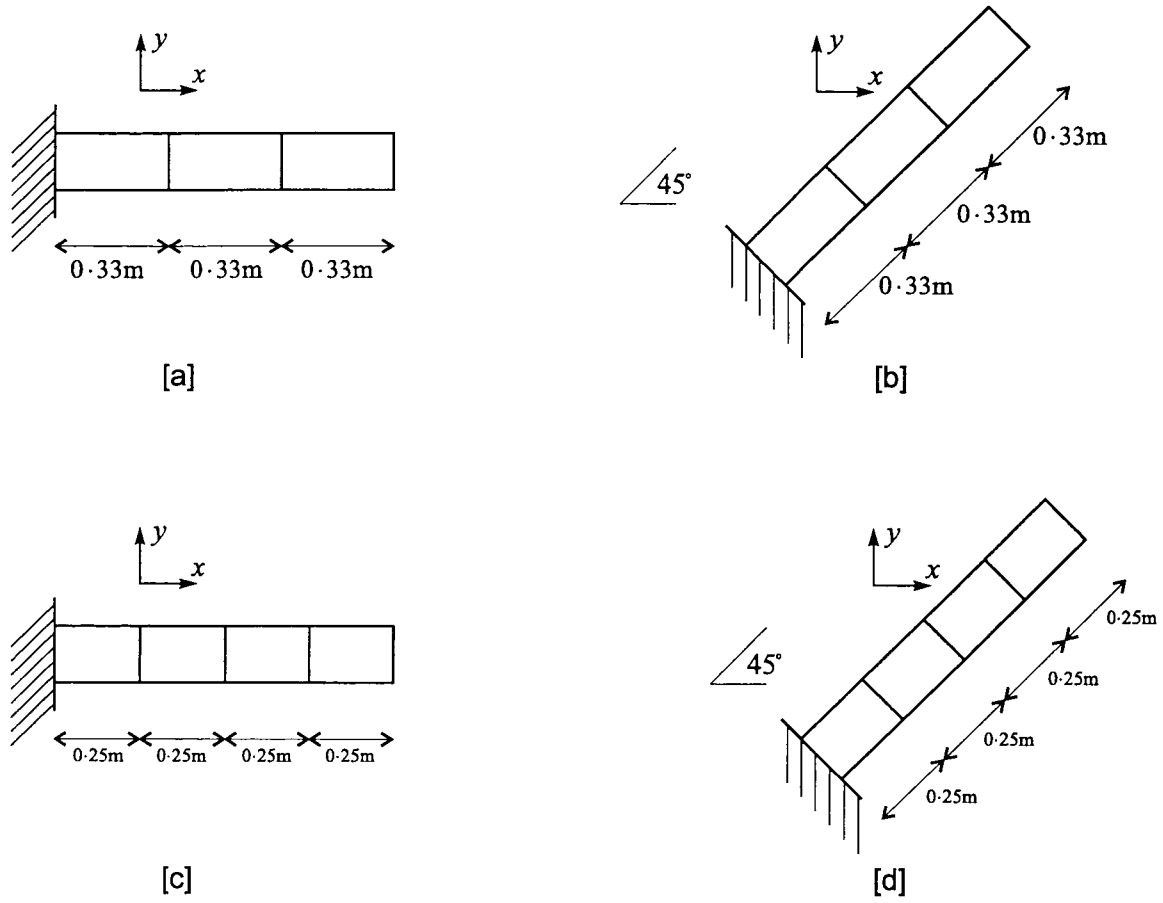

FIGURE 3.8 Beams used in further eigensystem tests

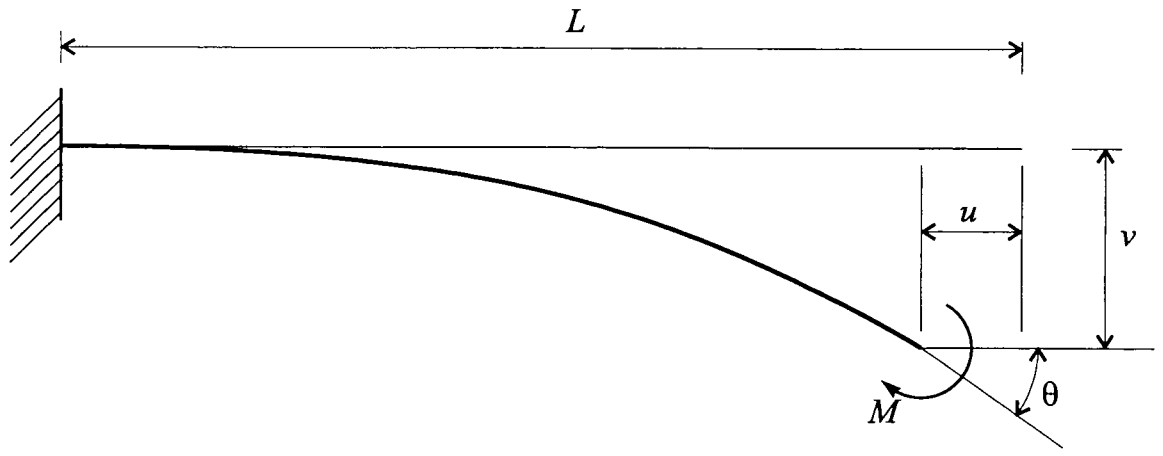

FIGURE 3.9 Cantilever subjected to an end moment

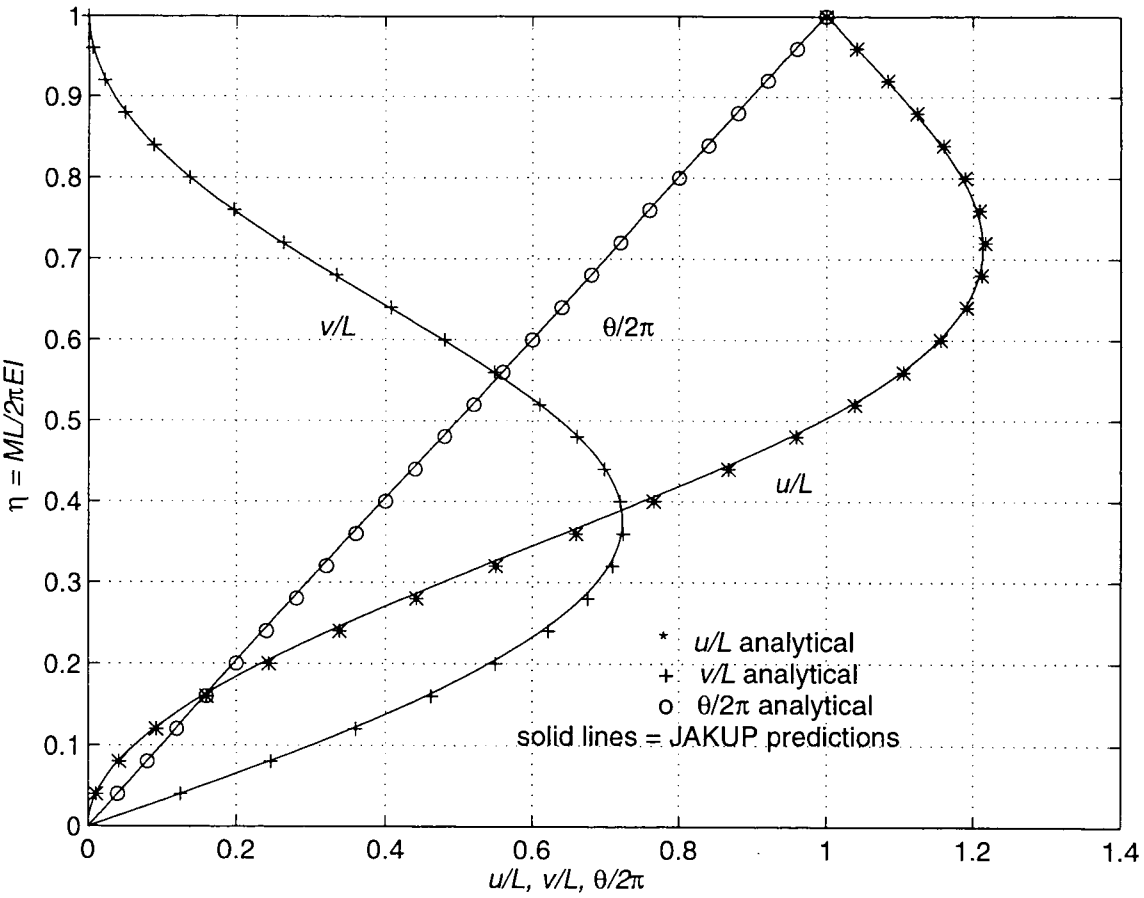

FIGURE 3.10 Cantilever end displacements

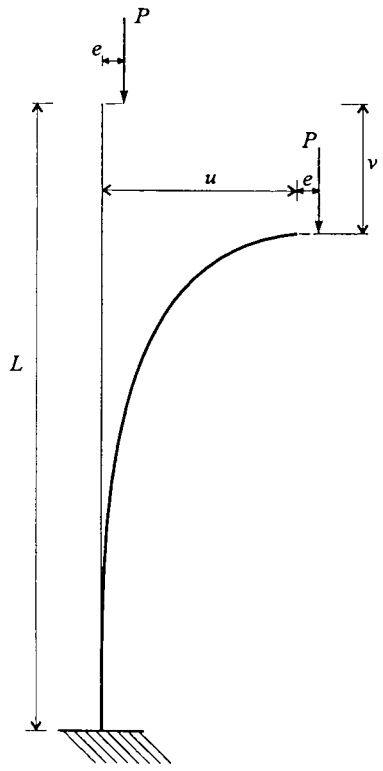

FIGURE 3.11 Axially loaded strut

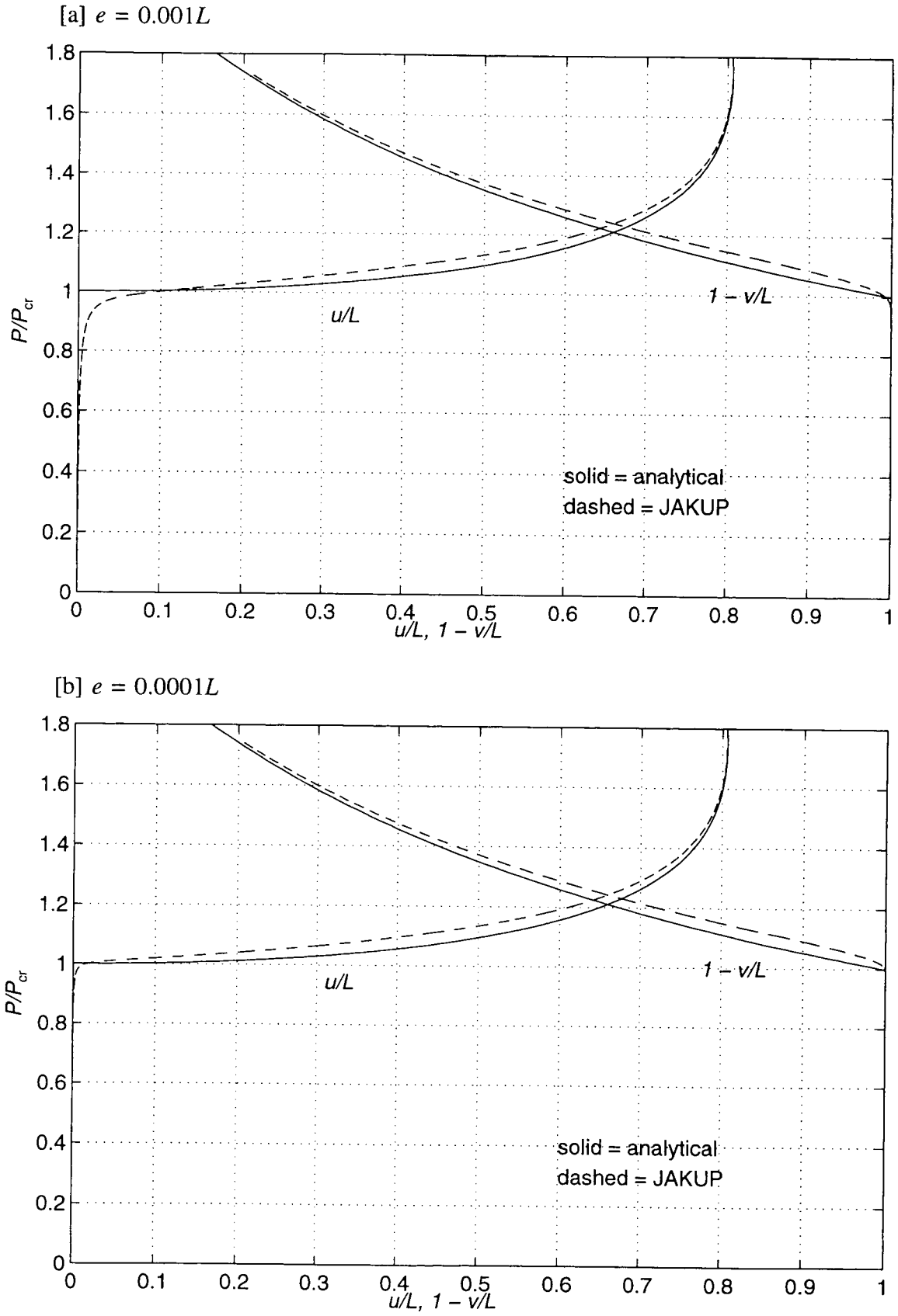

FIGURE 3.12 Deformation path of an axially loaded strut

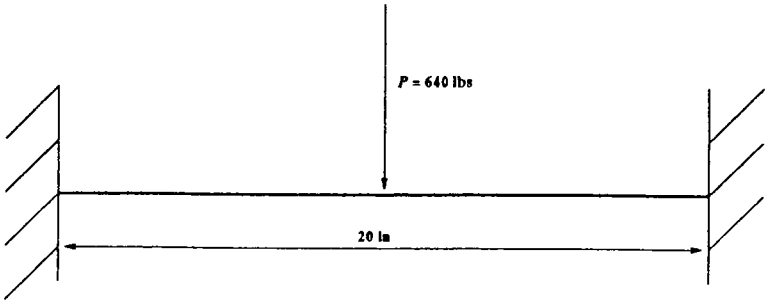

FIGURE 3.13 Undamped beam with suddenly applied load

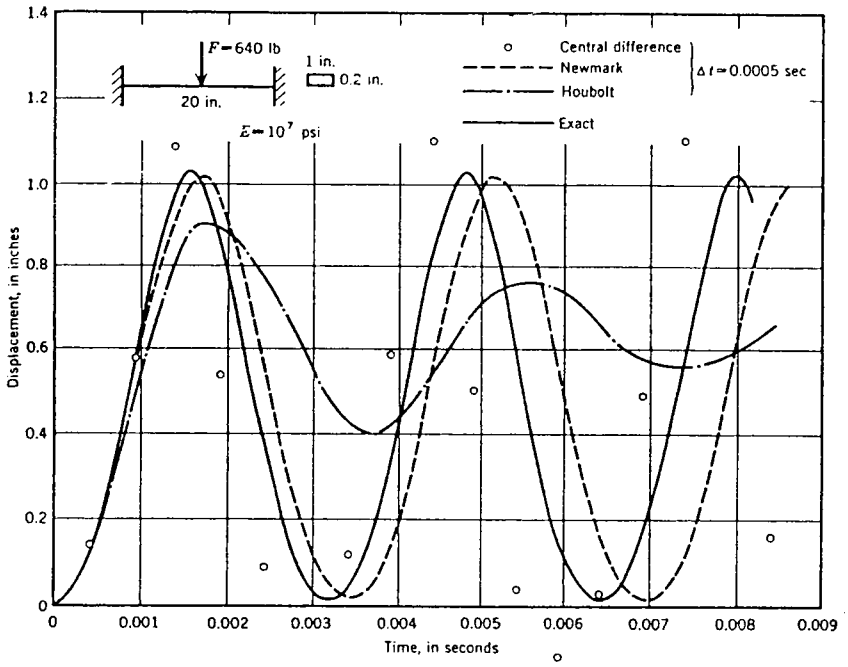

FIGURE 3.14[a] Midspan vertical displacement predicted by Weeks (1972)

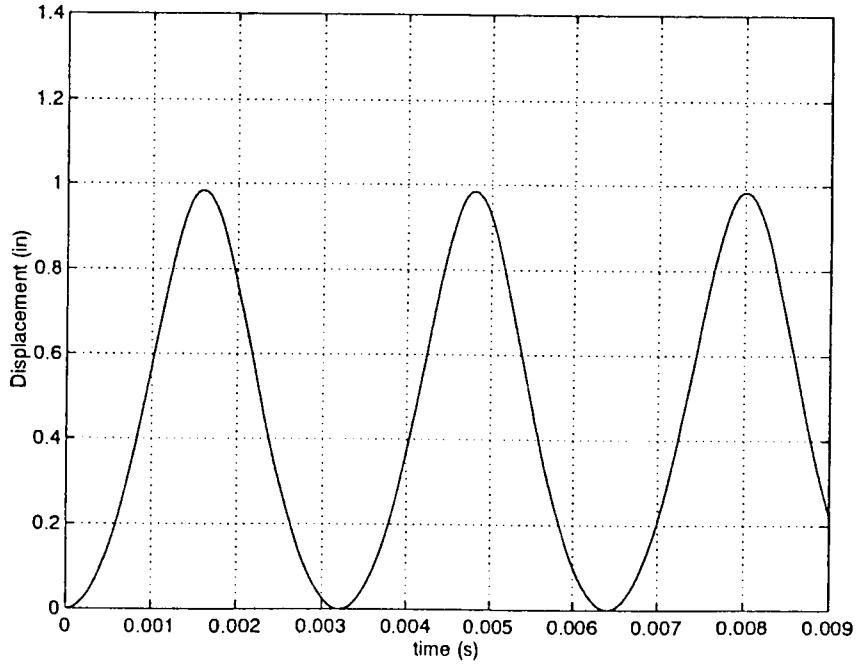

FIGURE 3.14[b] Midspan vertical displacement predicted by JAKUP

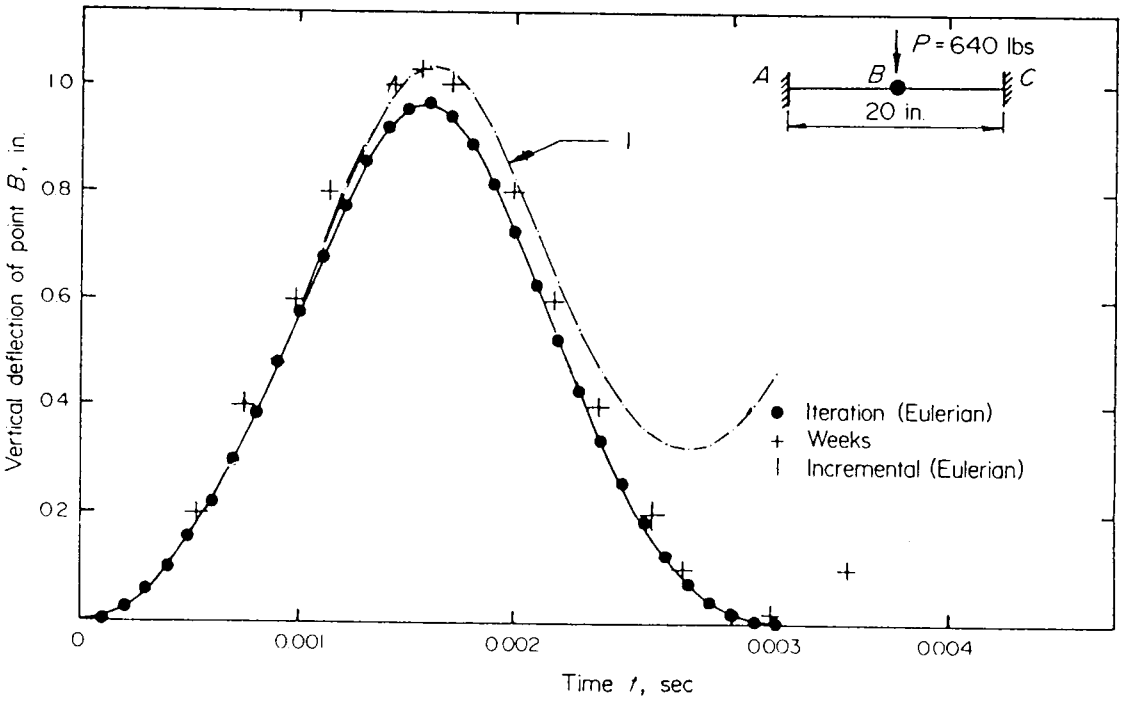

FIGURE 3.15 Midspan vertical displacement predicted by Oran & Kassimali (1976)

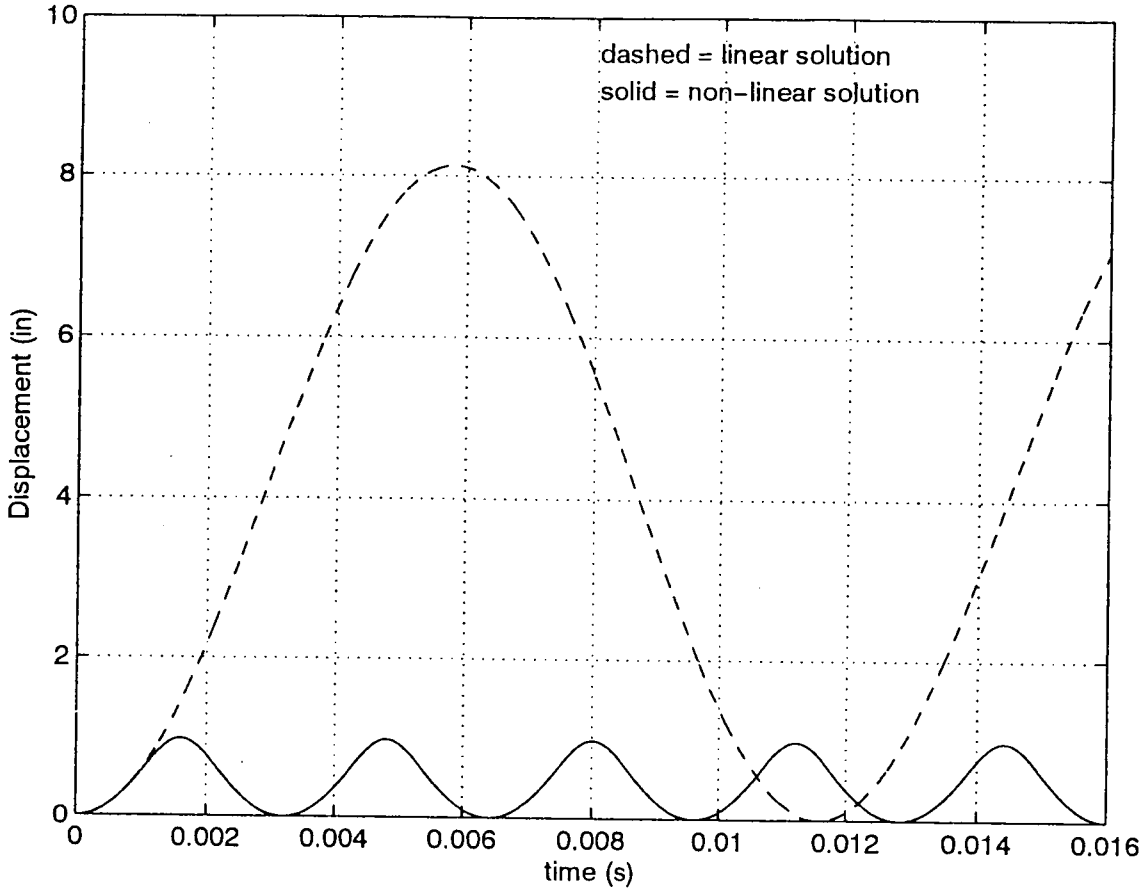

FIGURE 3.16 Linear midspan vertical displacement predicted by JAKUP

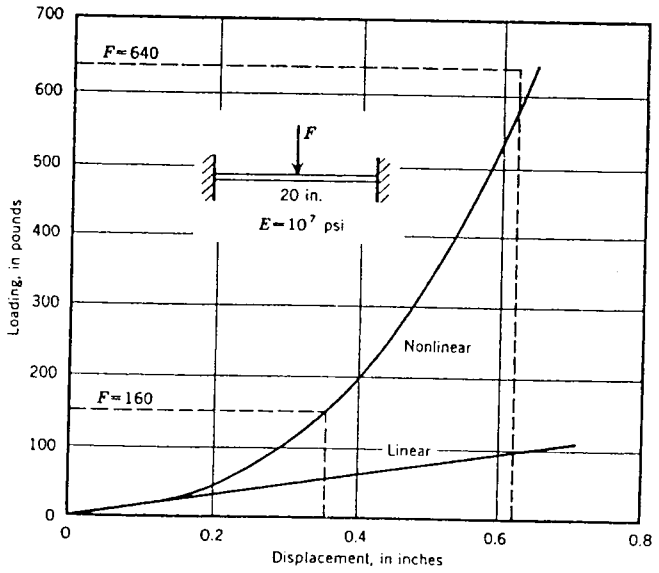

FIGURE 3.17 Linear and non-linear quasi-static load-displacement paths predicted by Weeks (1972)

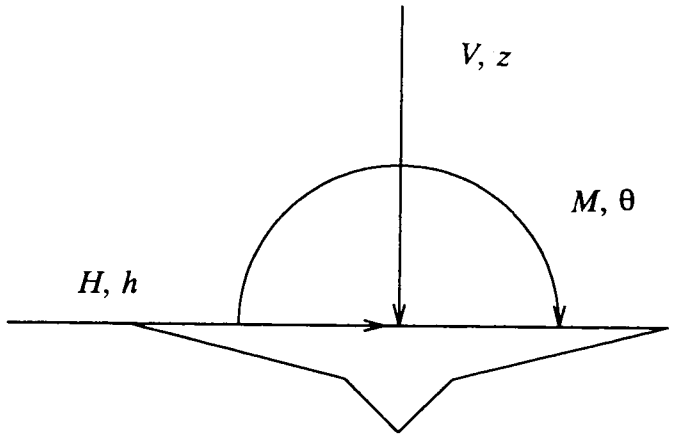

FIGURE 4.1 Loads and displacements in the local coordinate system at the footing

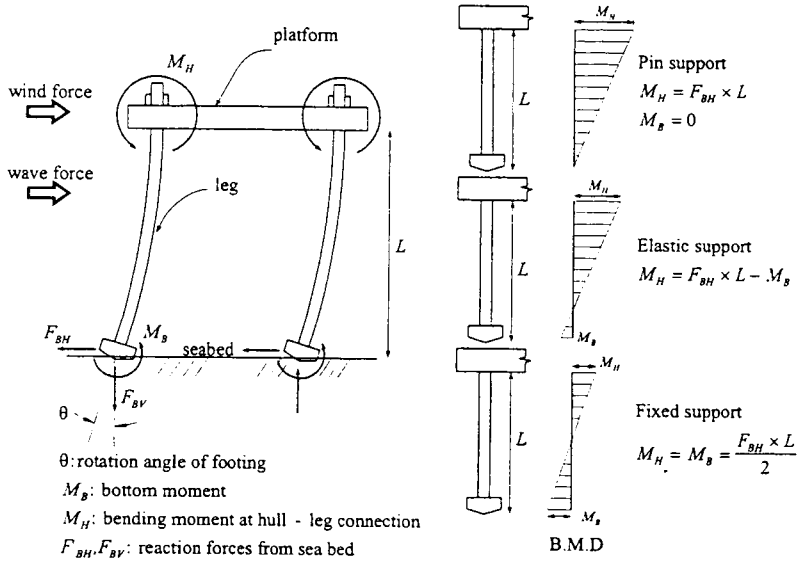

FIGURE 4.2 Influence of foundation fixity on leg bending moments (after Chiba *et al*, 1986)

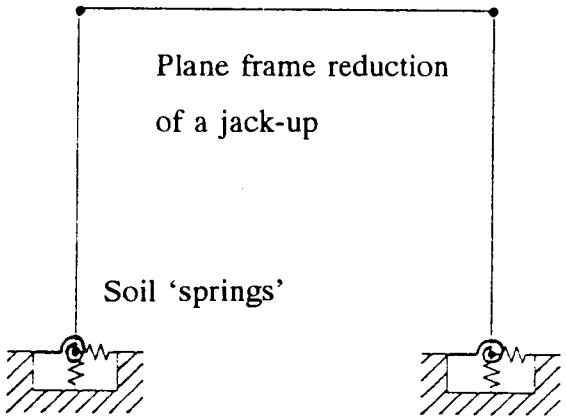

FIGURE 4.3 Linear springs at the soil-structure interface

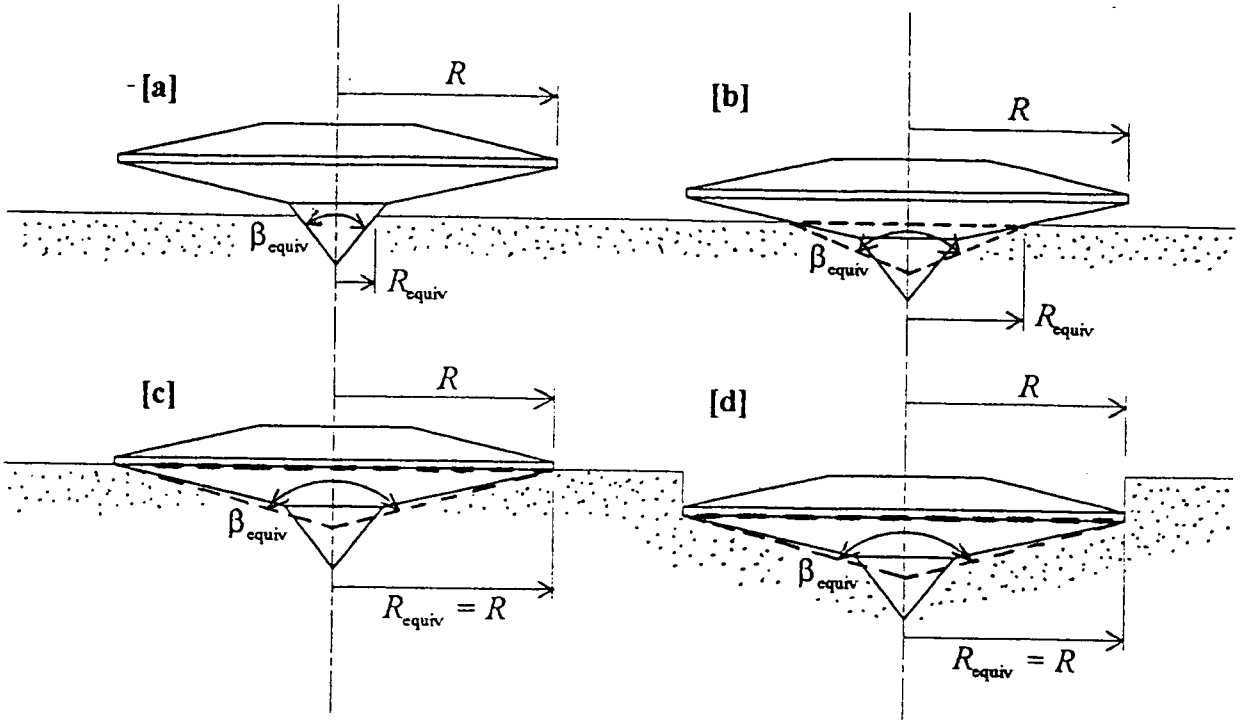

FIGURE 4.4 Spudcan represented as an equivalent cone
(volume of equivalent cone = volume of penetrated portion of spudcan)

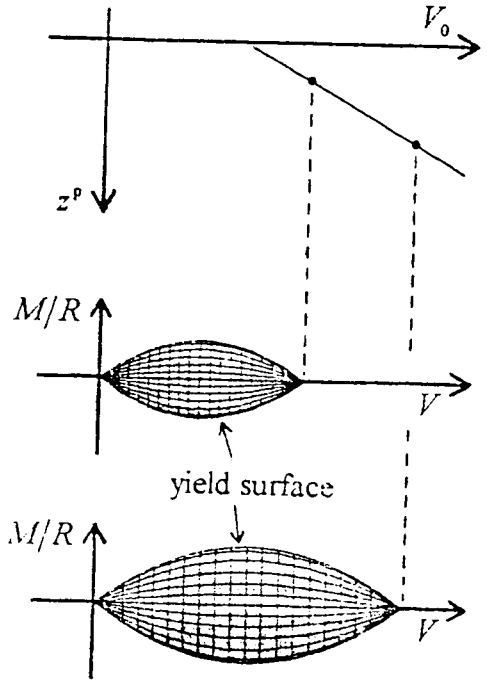

FIGURE 4.5 Yield surface reforming through
new V_0 apex point (from Martin, 1994)

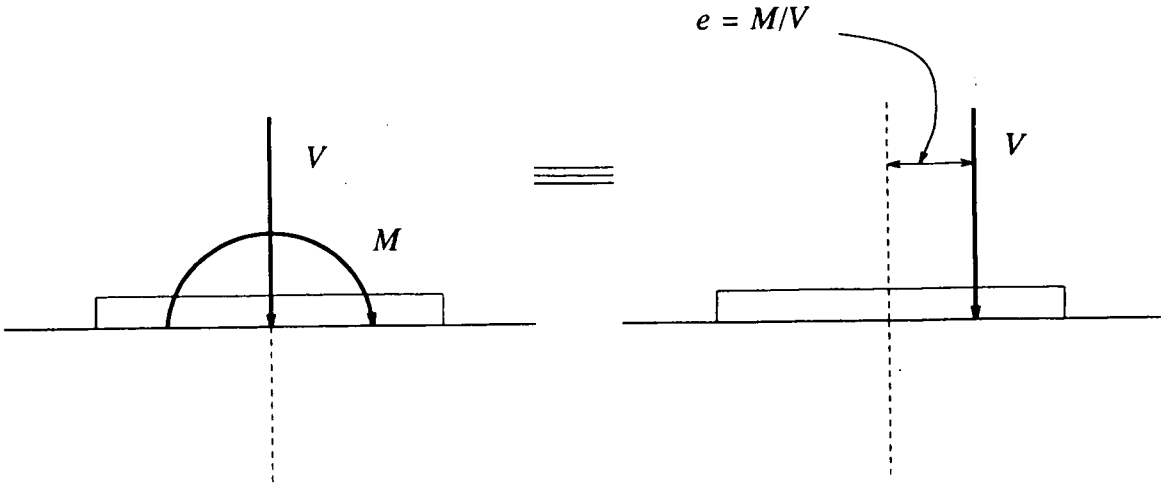

FIGURE 4.6 Vertical load and moment treated as statically equivalent eccentric load

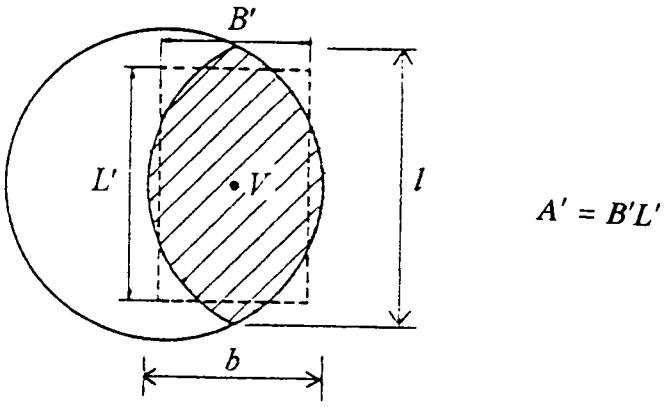

FIGURE 4.7 Eccentric load acting on a reduced effective area

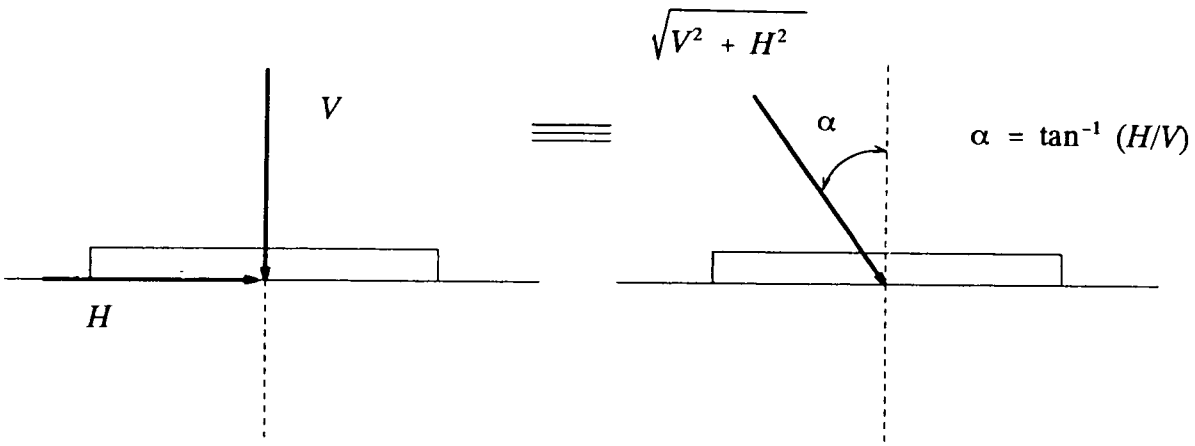

FIGURE 4.8 Horizontal and vertical load treated as a central inclined load

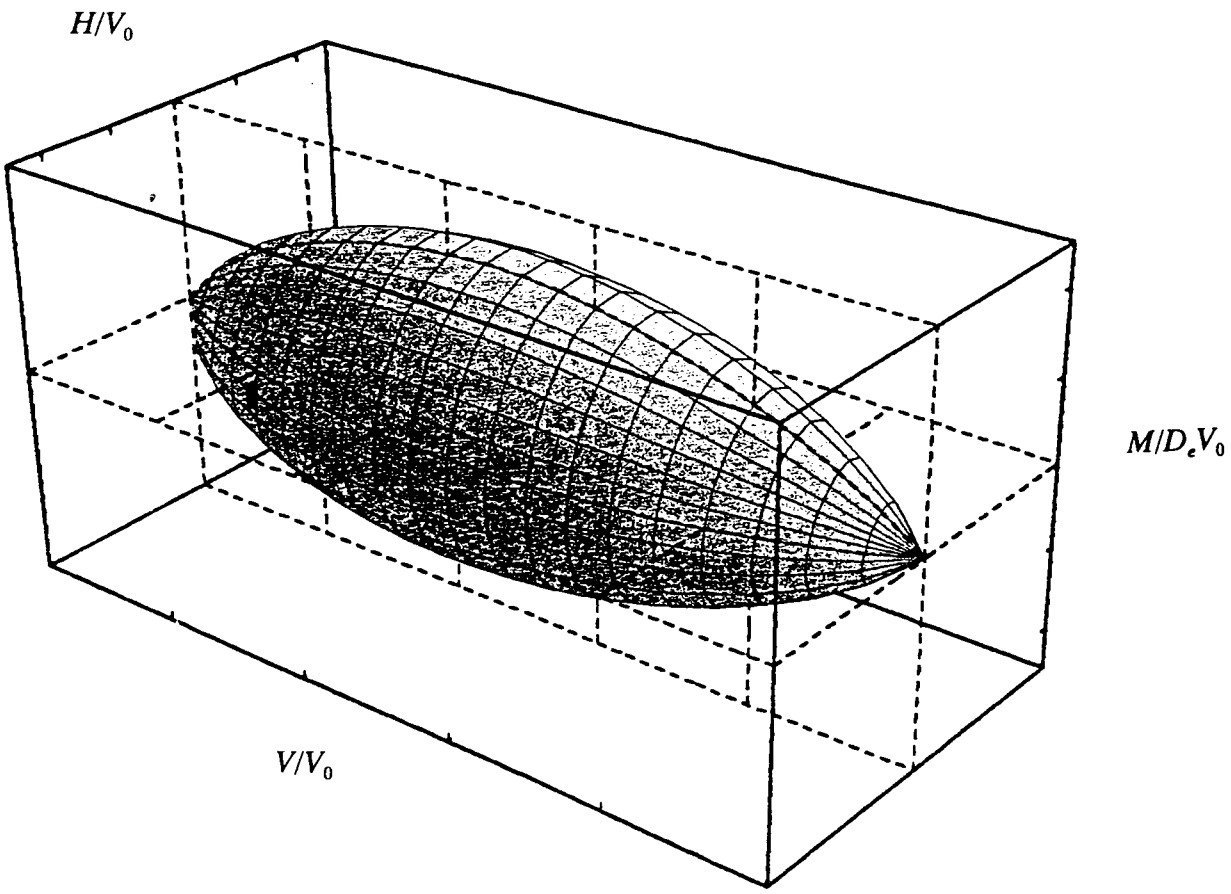

FIGURE 4.9 Cigar shaped yield surface (from Martin, 1994)

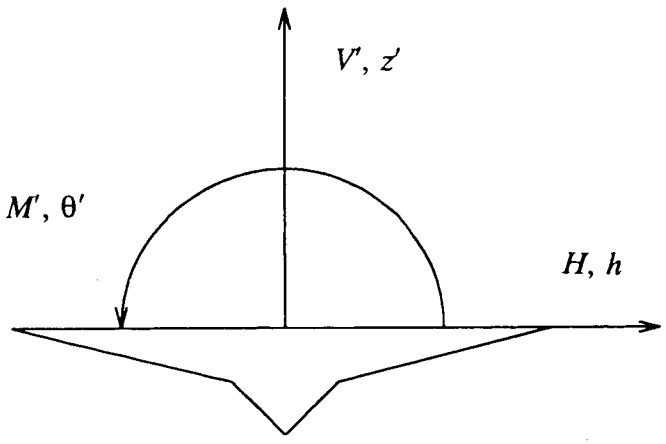

FIGURE 4.10 Forces and displacements in the global coordinate system

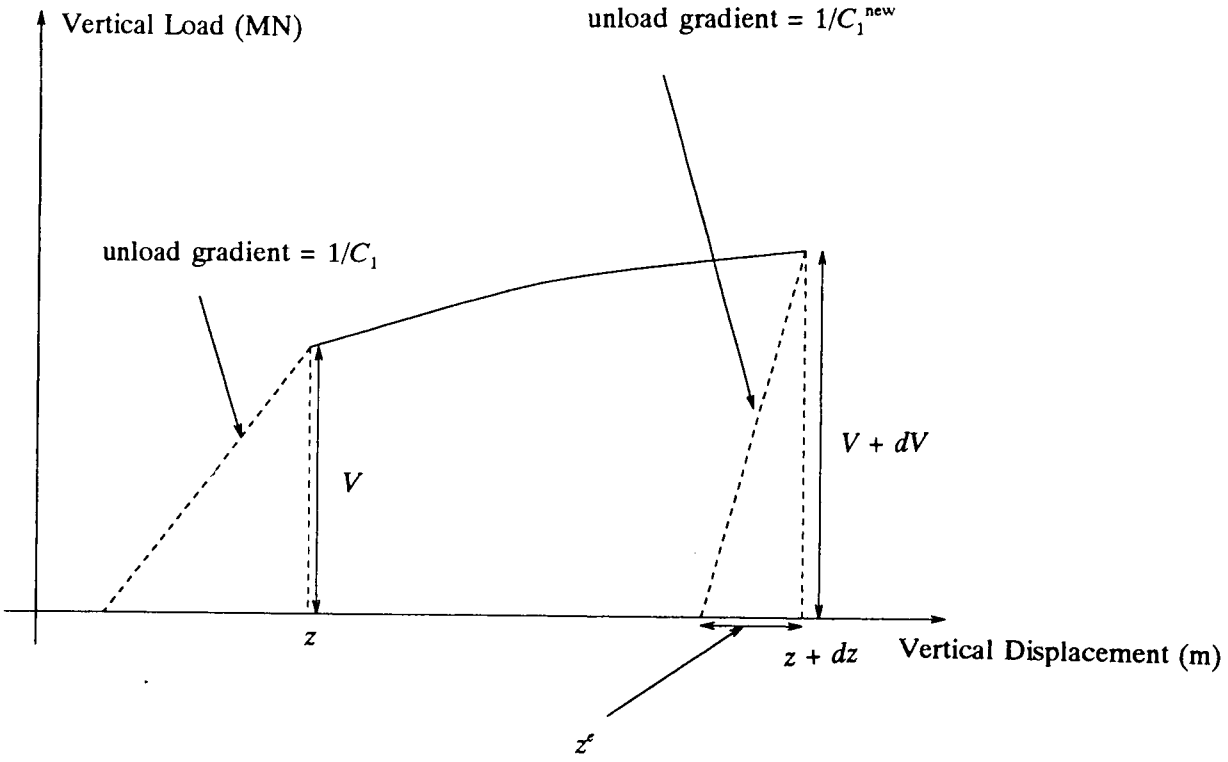

FIGURE 4.11 Incremental elastoplastic vertical footing displacement

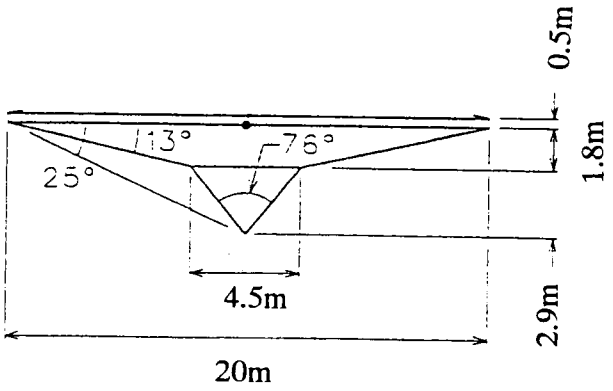

FIGURE 4.12 Dimensions of reference spudcan footing

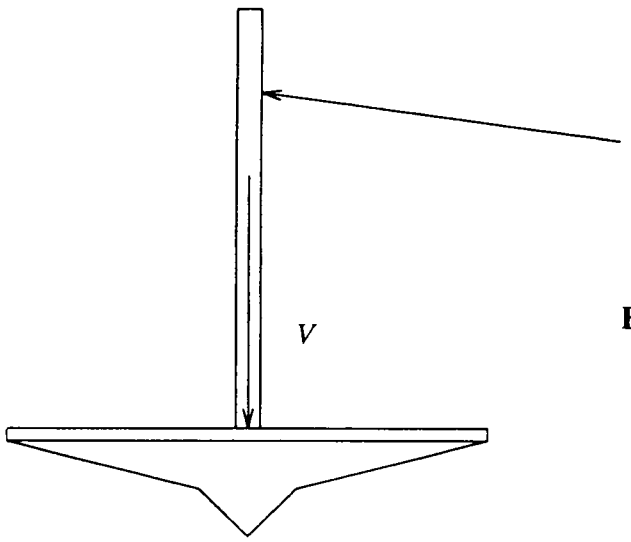

FIGURE 4.13 Footing/structure system analysed by JAKUP

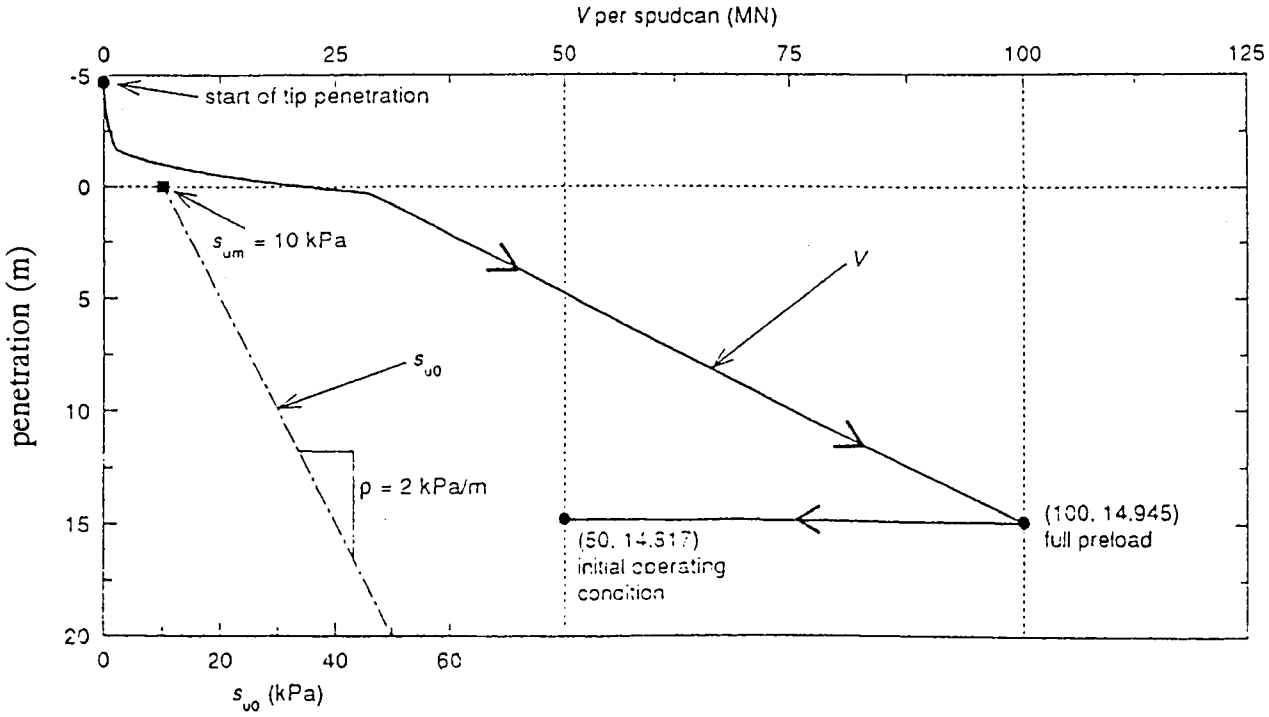

FIGURE 4.14[a] Spudcan penetration during installation (after Martin, 1994)

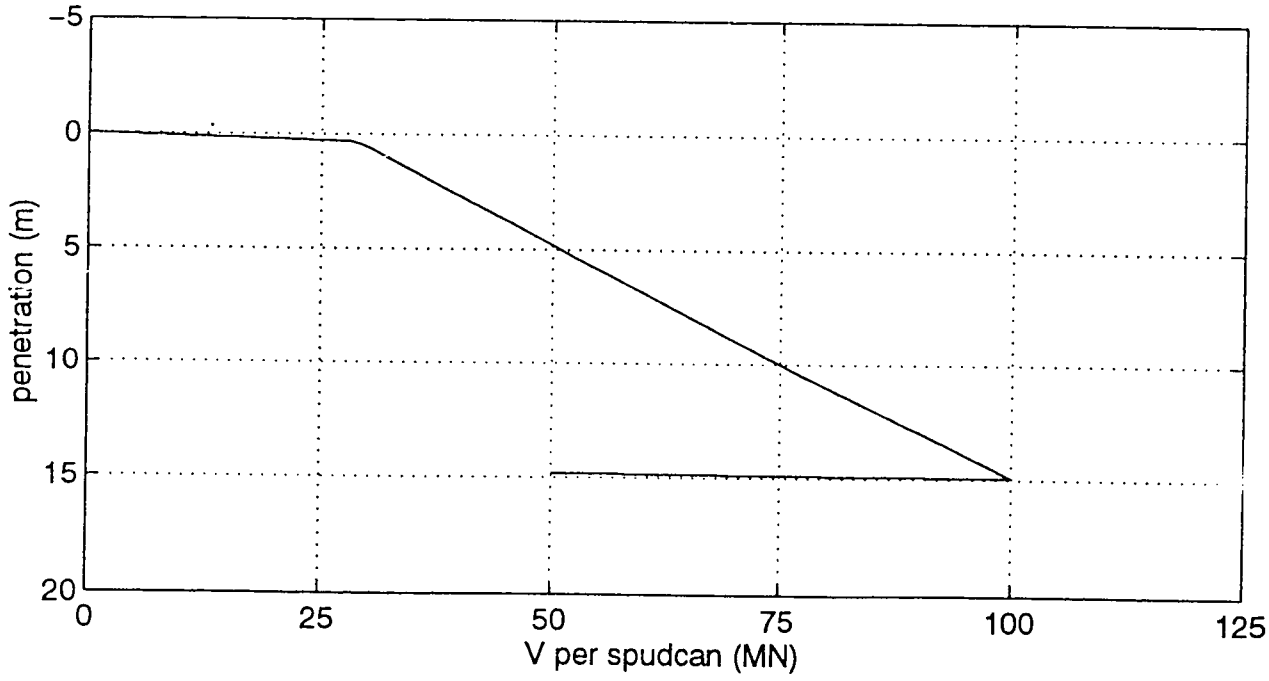

FIGURE 4.14[b] Spudcan penetration during installation (from JAKUP)

H_{env} = environmental load per leg

W = hull self-weight per leg

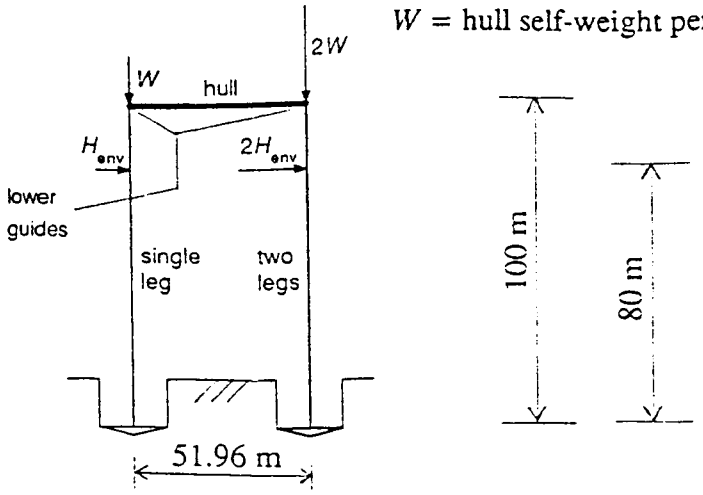

single leg to windward

spudcan diameter	20 m
single leg equivalent I	7.5 m^4
single leg equivalent A	0.6 m^2
single leg equivalent A_s	0.04 m^2
hull equivalent I	10 × single leg I
hull equivalent A	50 × single leg A
hull equivalent A_s	50 × single leg A_s

E of structure	200000 MPa
G of structure	80000 MPa
total preload weight $3W$	300 MN
total operating weight $3W$	150 MN

Clay seabed properties:

undrained strength at mudline s_{um}	10 kPa
strength increase with depth ρ	2 kPa/m
rigidity index G/s_u	100

FIGURE 4.15 Plane frame jack-up analysed by Martin (1994)

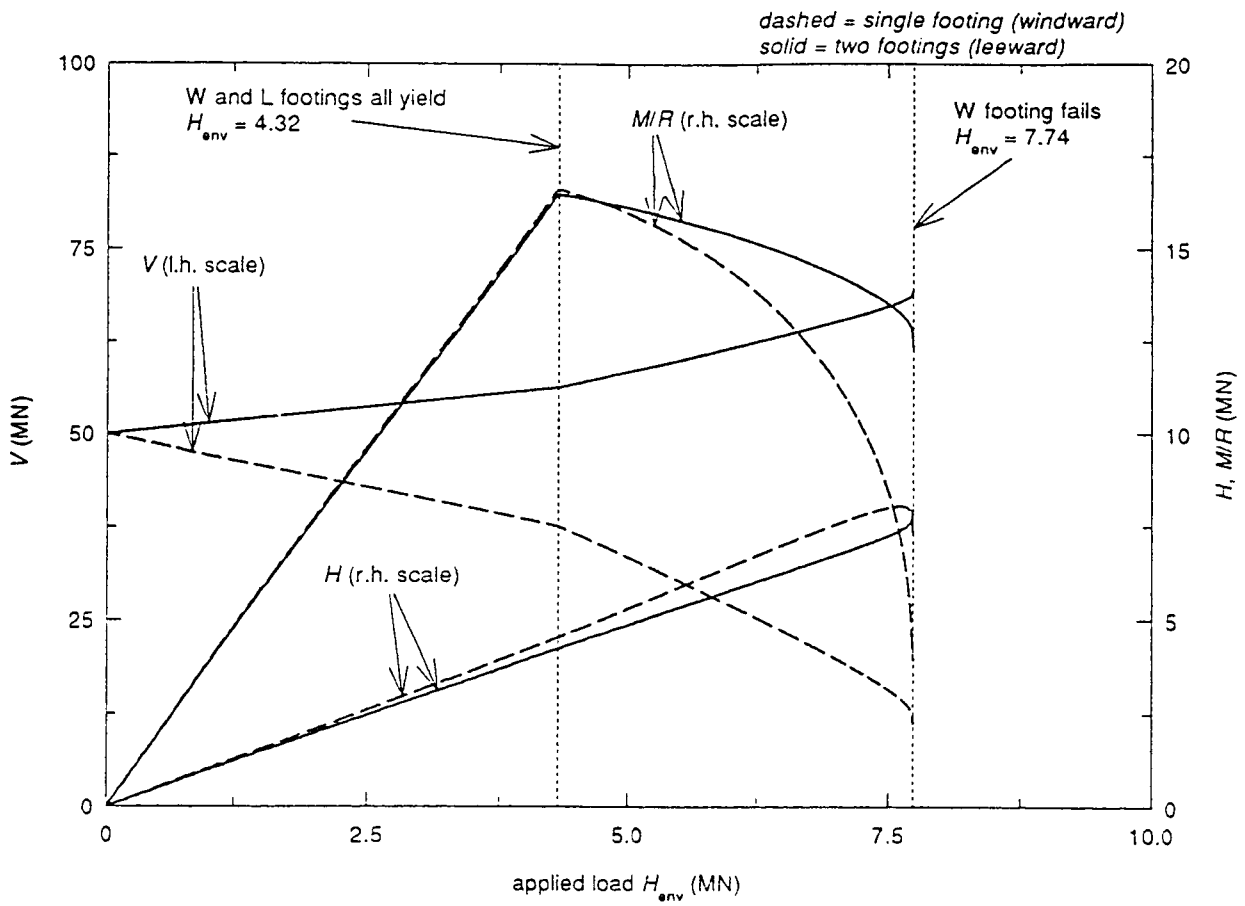

FIGURE 4.16[a] Spudcan reactions (after Martin, 1994)

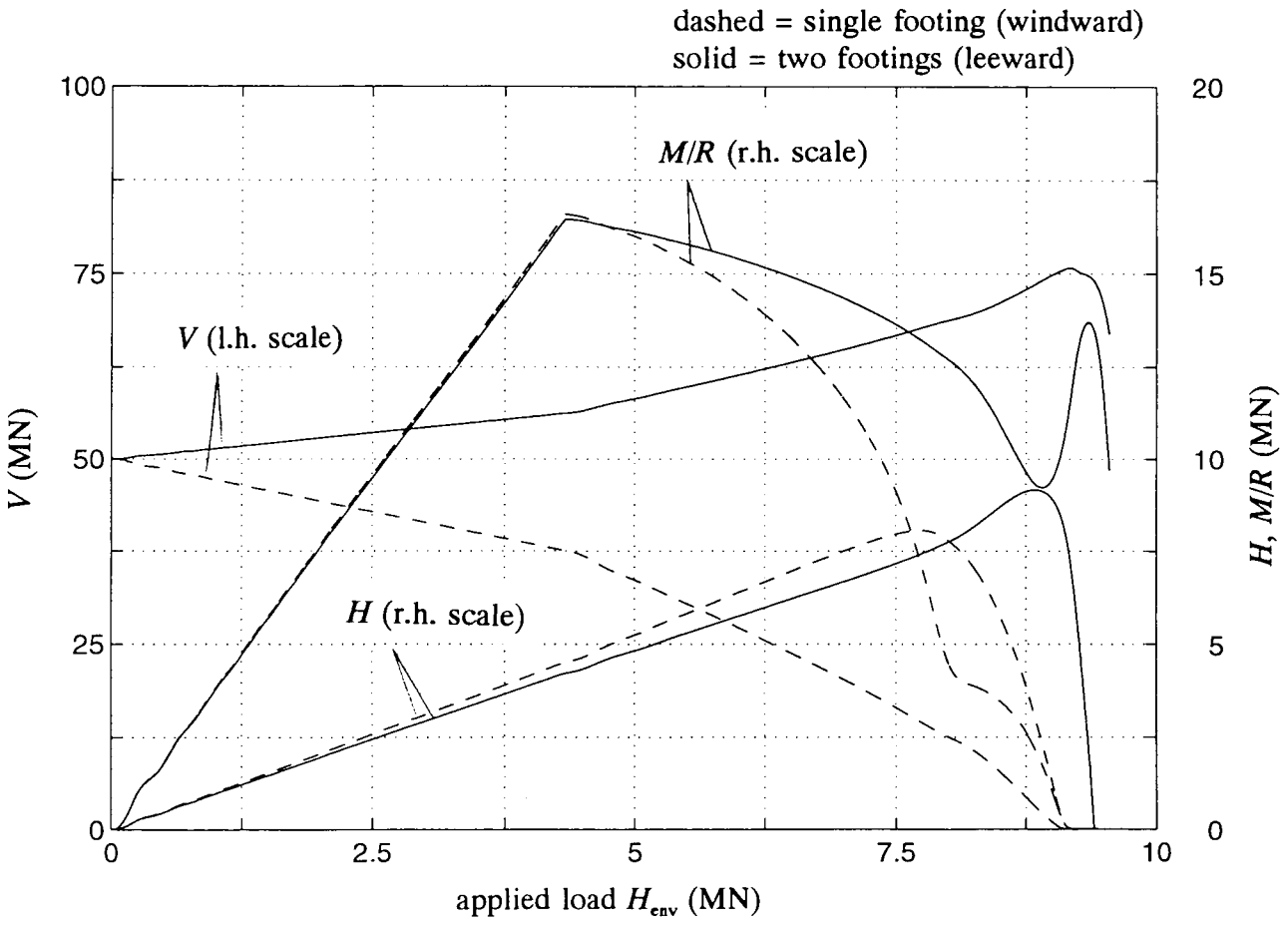

FIGURE 4.16[b] Spudcan reactions from JAKUP

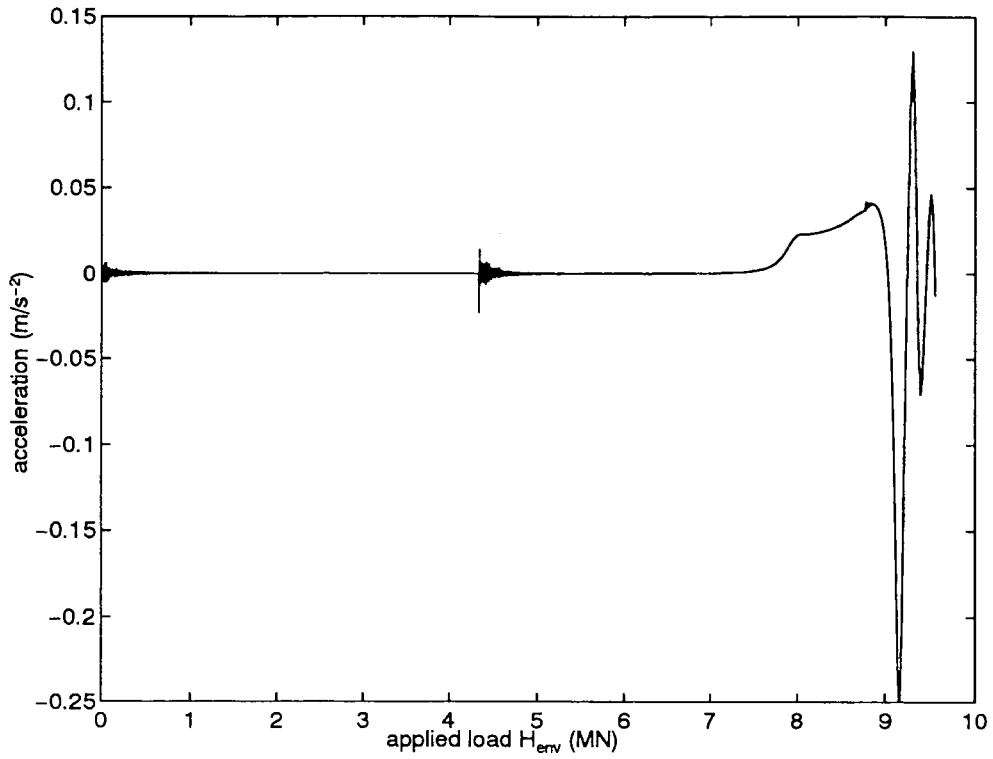

FIGURE 4.17 Hull acceleration predicted by JAKUP

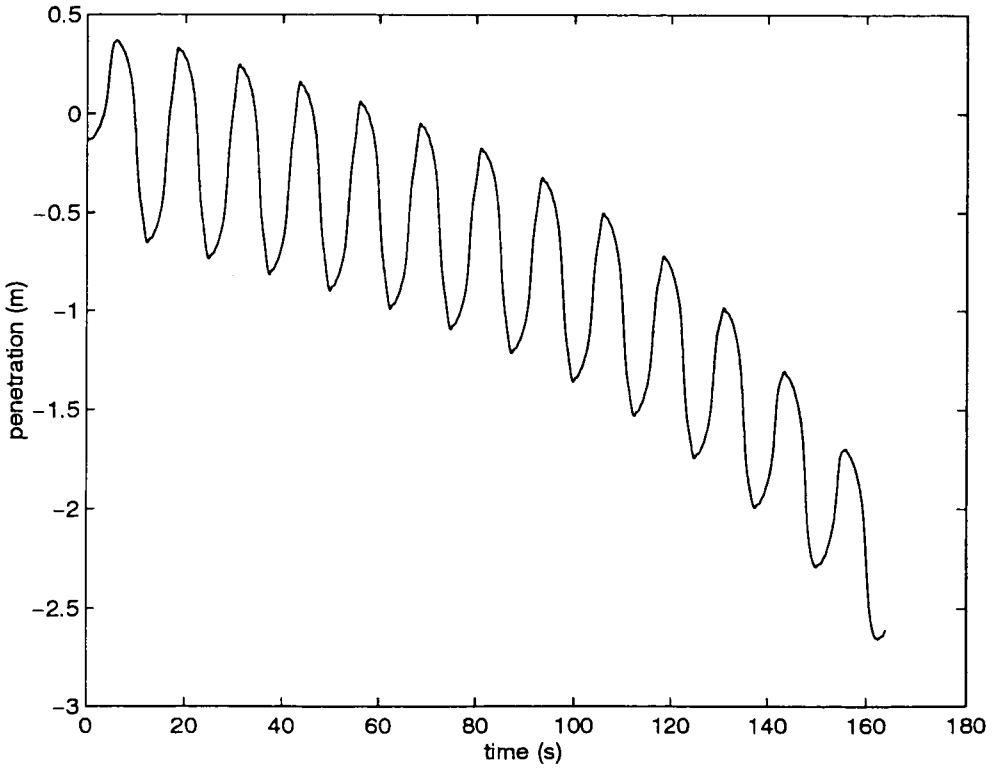

FIGURE 4.18 Vertical footing displacement for the windward footing

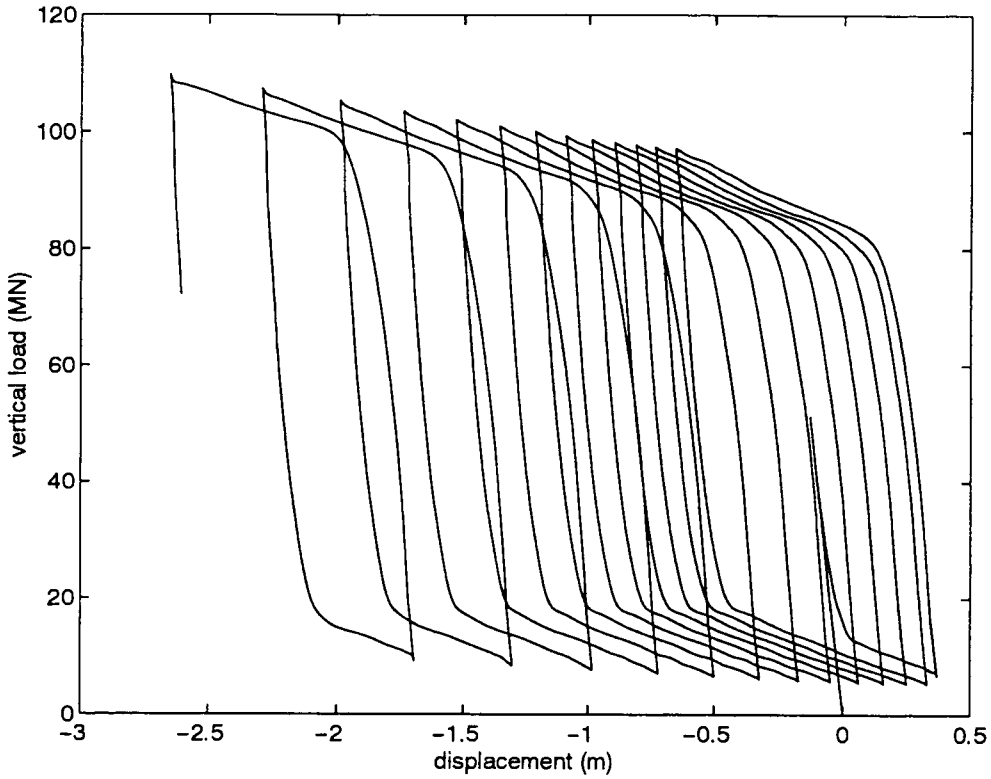

FIGURE 4.19 Vertical load-displacement path for the windward footing

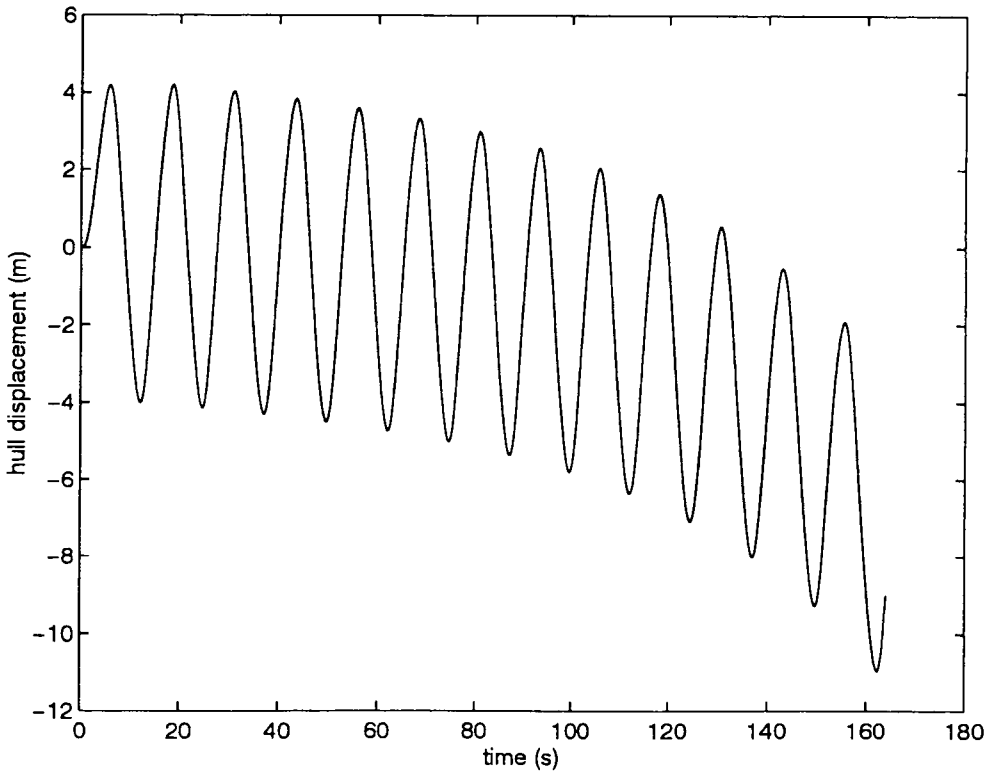

FIGURE 4.20 Horizontal displacement at the hull level

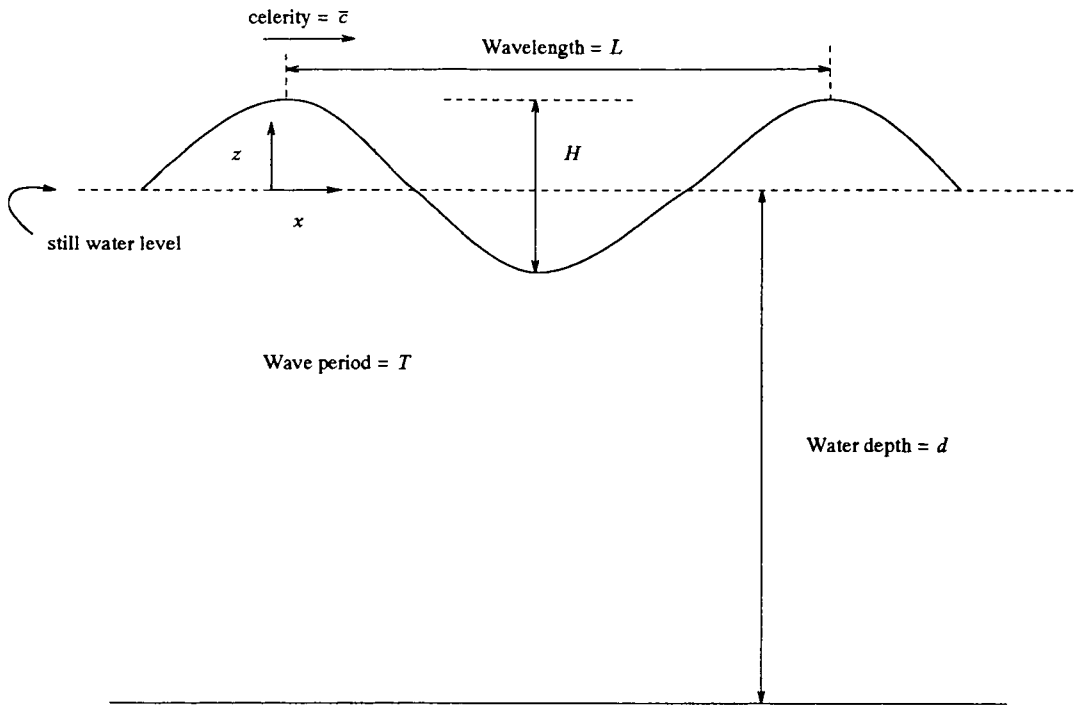

FIGURE 5.1 Regular wave coordinate system

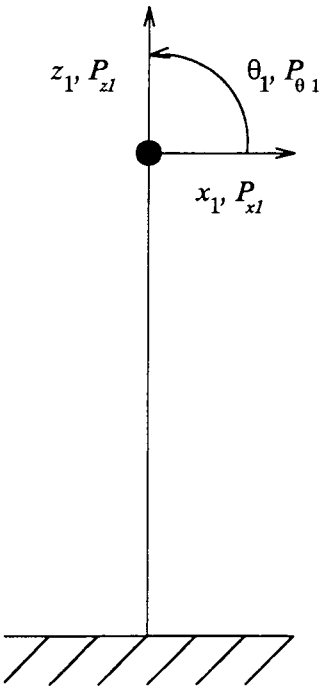

FIGURE 5.2 Nodal loads and displacements for a three degree of freedom beam

[a]

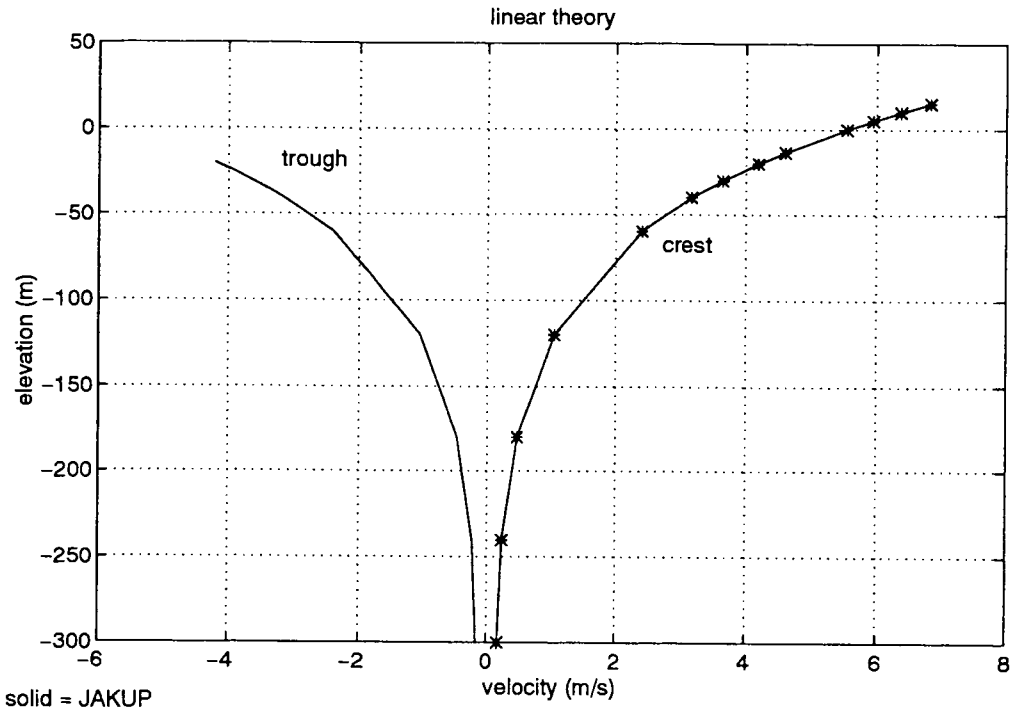

[b]

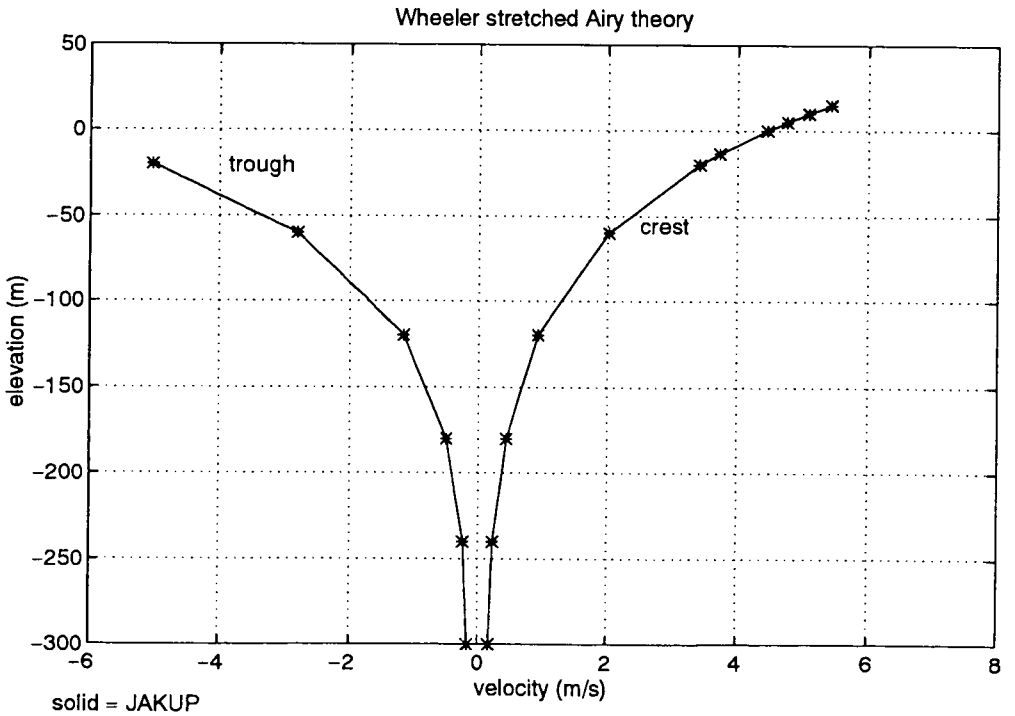

FIGURE 5.3[a] and **[b]** Velocity predictions for linear theory and Wheeler stretched Airy theory

[c]

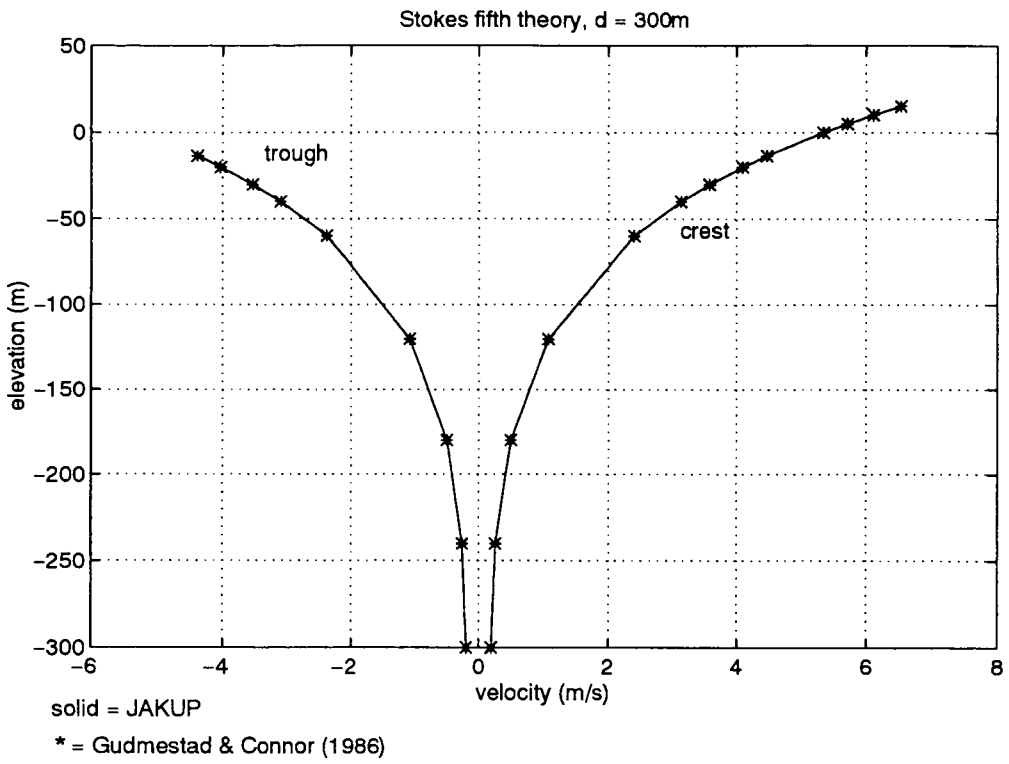

[d]

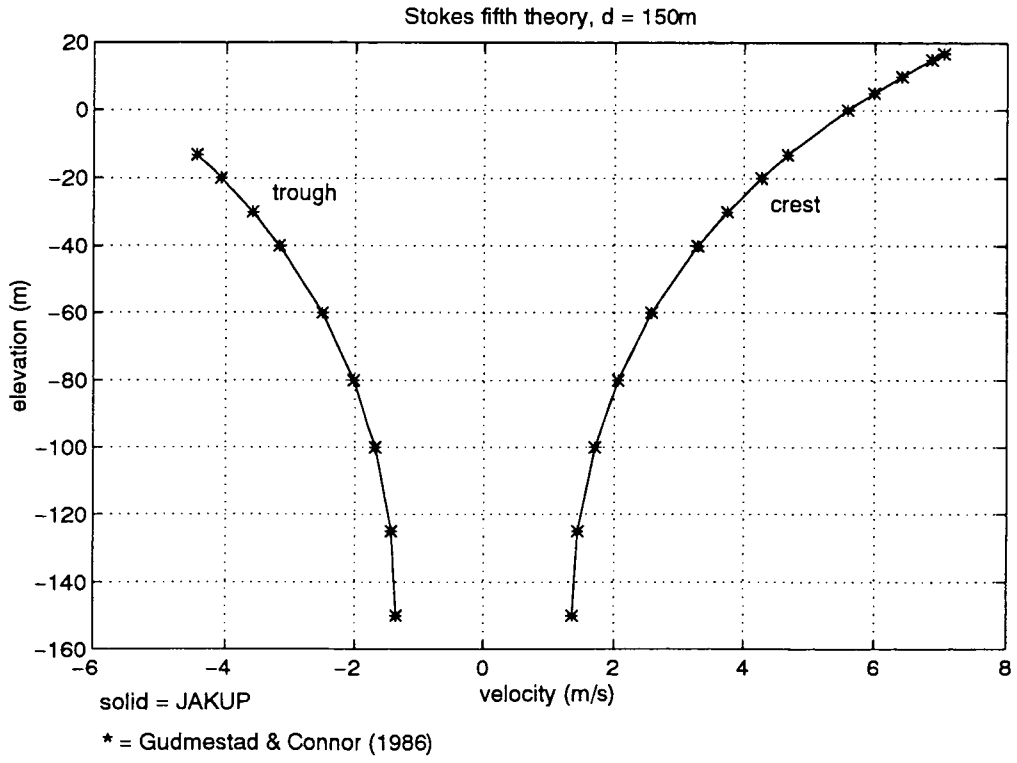

FIGURE 5.3[c] and **[d]** Velocity predictions for Stokes fifth wave theory

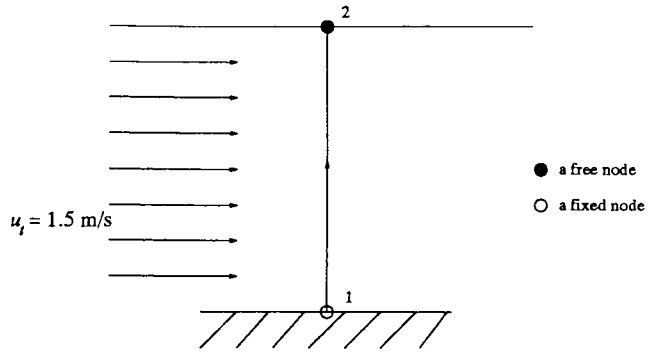

FIGURE 5.4 A uniform current passing a linear beam

[a]

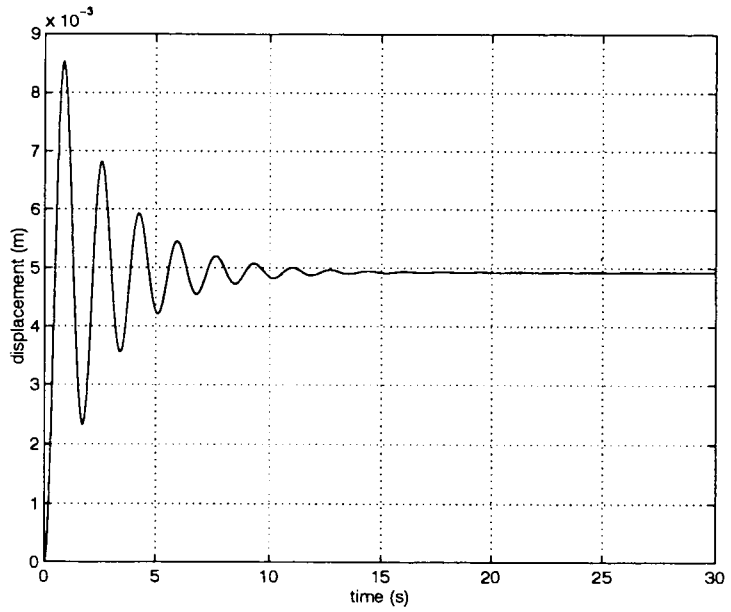

[b]

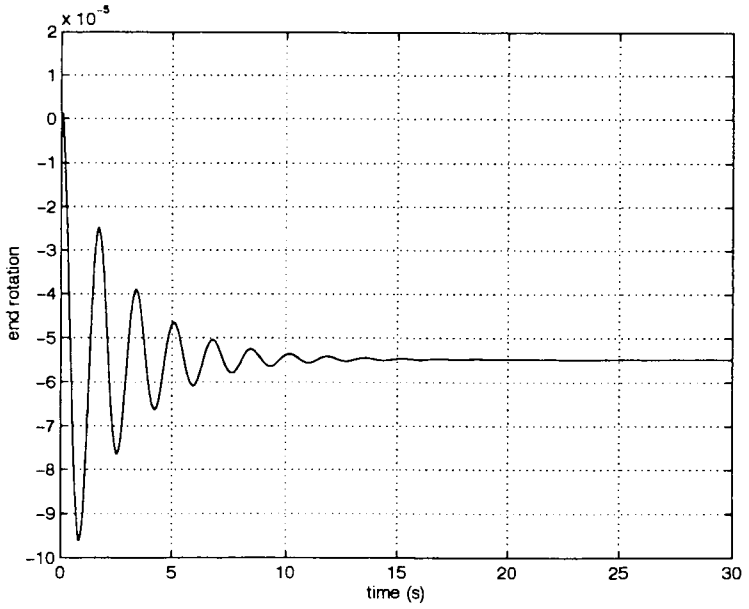

FIGURE 5.5 Lateral tip displacement and end rotation as predicted by JAKUP

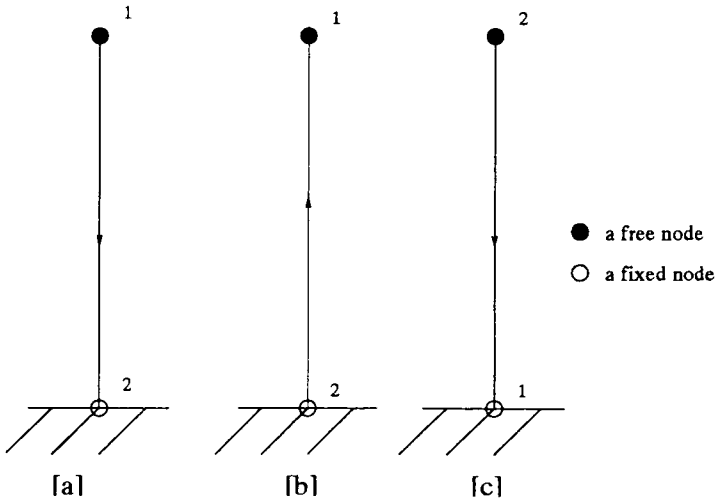

FIGURE 5.6 Linear beams used in JAKUP tests

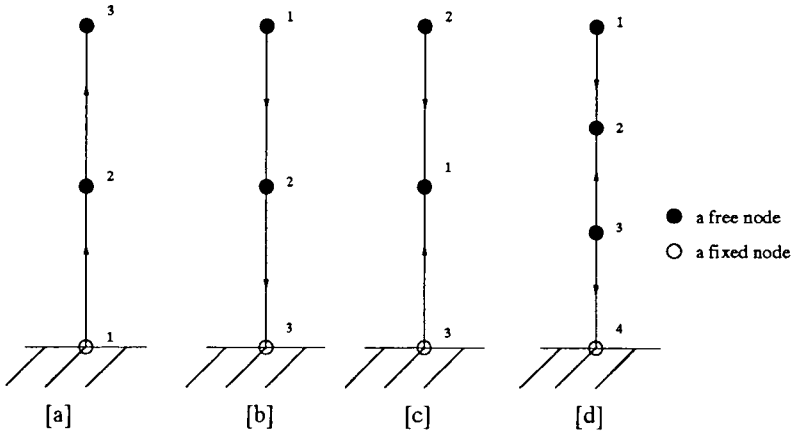

FIGURE 5.7 Linear beam modelled with two and three elements for JAKUP tests

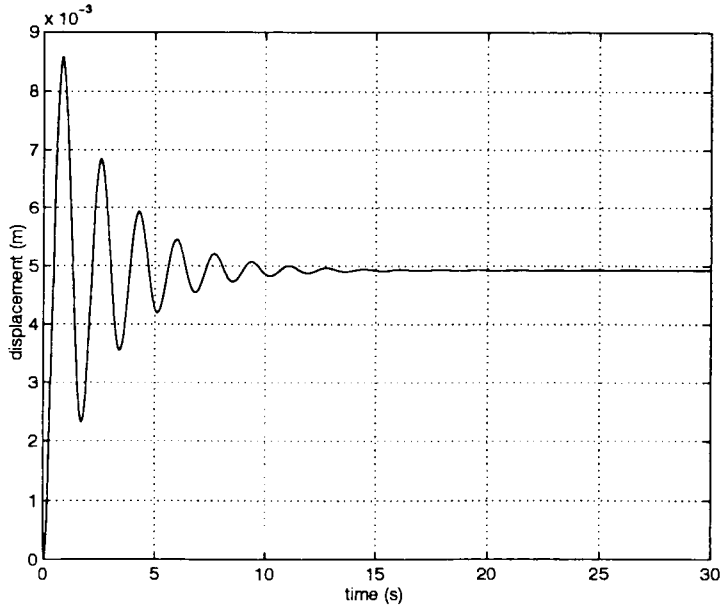

FIGURE 5.8 Tip deflection predicted by JAKUP for the three beam elements case

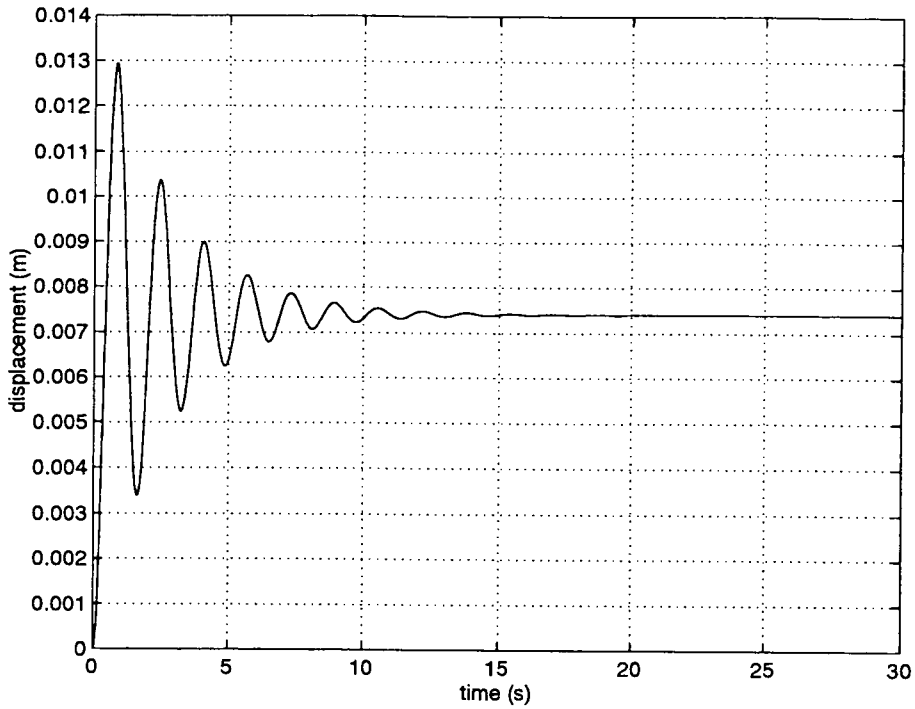

FIGURE 5.9 Lateral tip displacement predicted by JAKUP for a single beam element

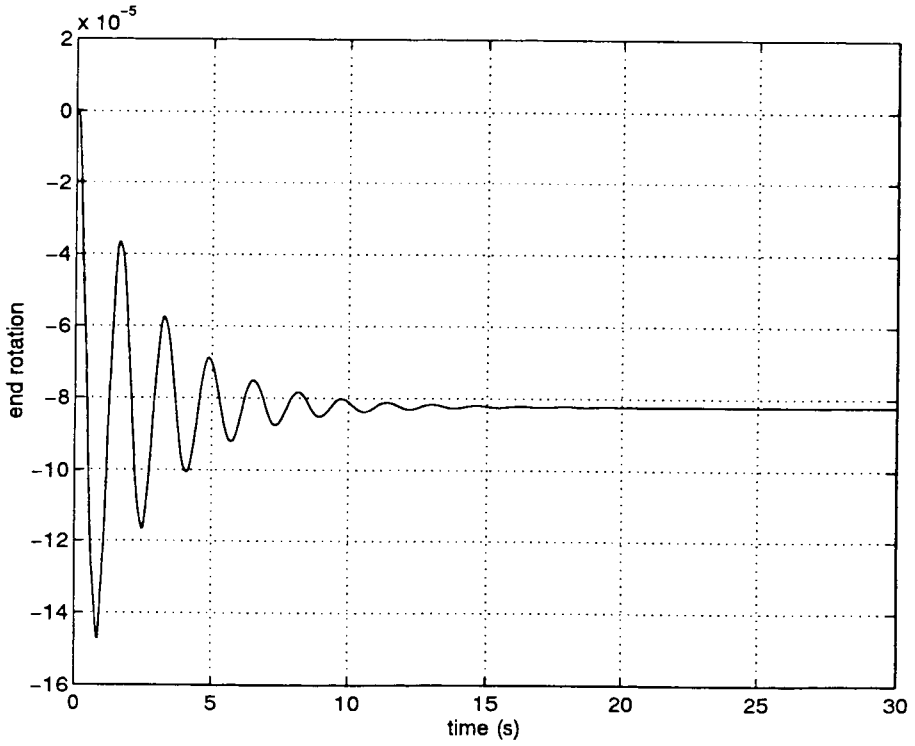

FIGURE 5.10 End rotation predicted by JAKUP using three beam elements

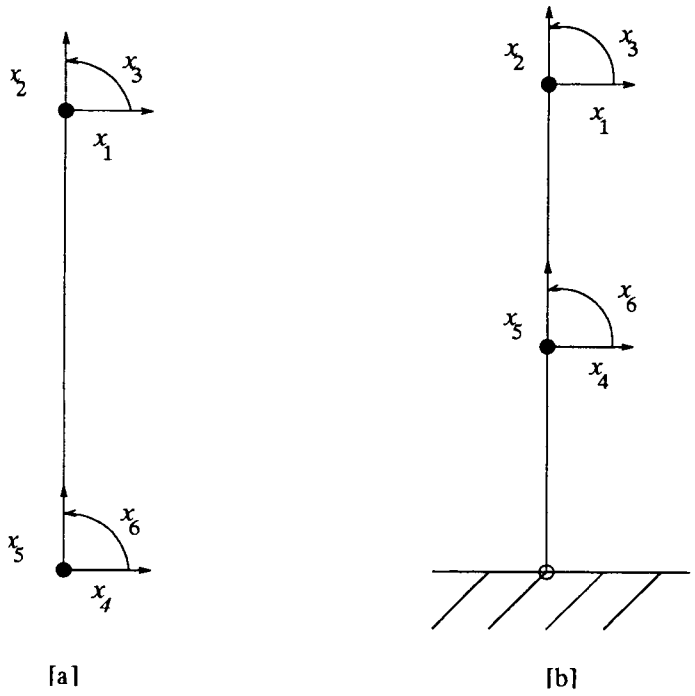

FIGURE 5.11 Sign convention for the six degree of freedom test case

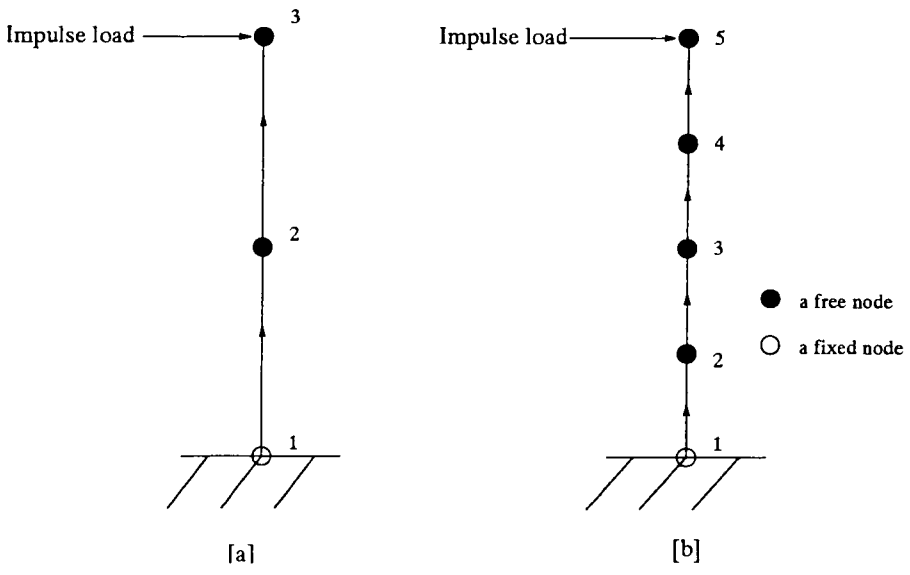

FIGURE 5.12 Test cases for the non-linear hydrodynamic damping term

[a]

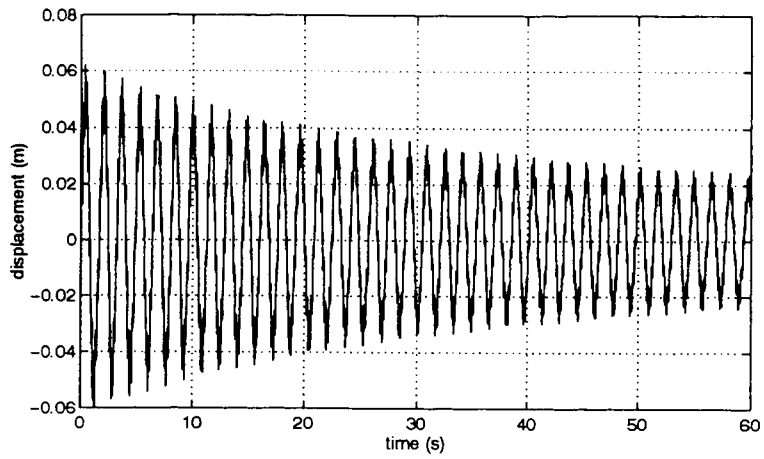

[b]

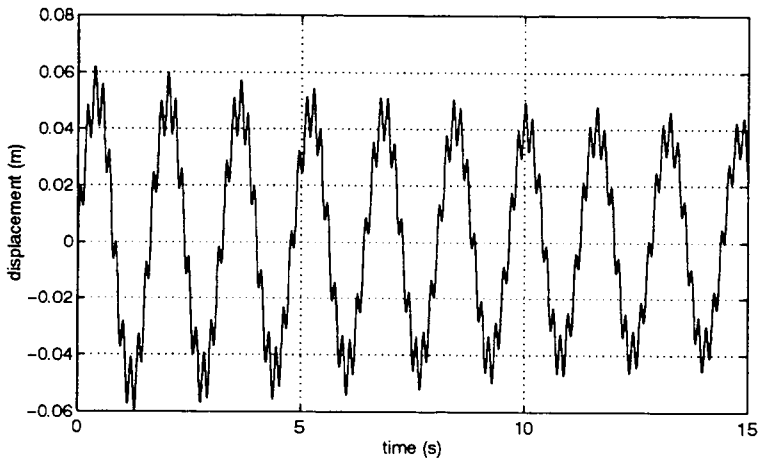

FIGURE 5.13 Response to an impulse load in stagnant water with no structural damping

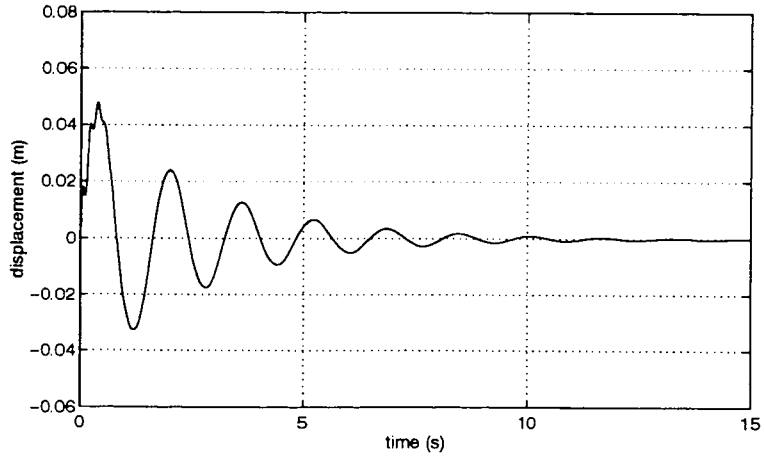

FIGURE 5.14 Response to an impulse load in stagnant water with 10% structural damping

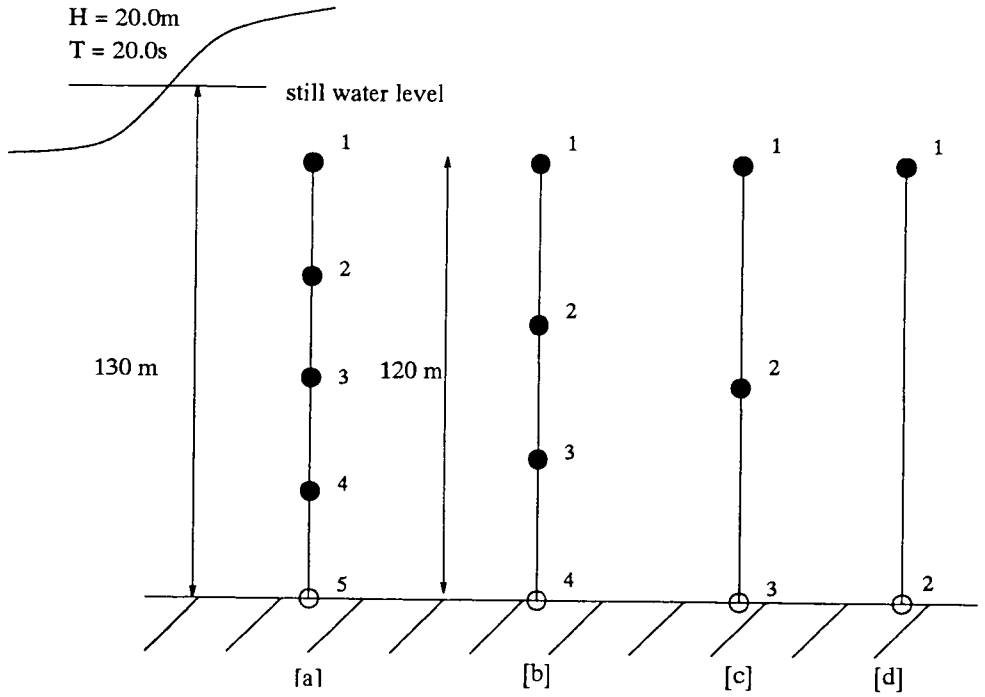

FIGURE 5.15 Test cases used with a finite amplitude wave

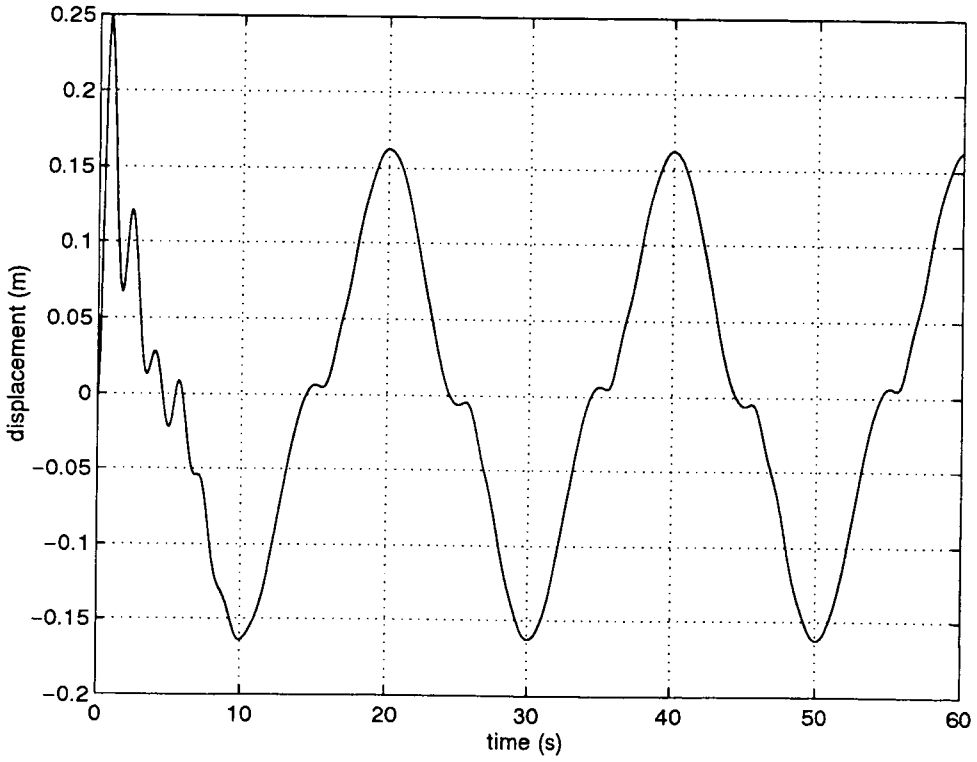

FIGURE 5.16 Superimposition of the lateral tip deflections for the test cases of Fig 5.15

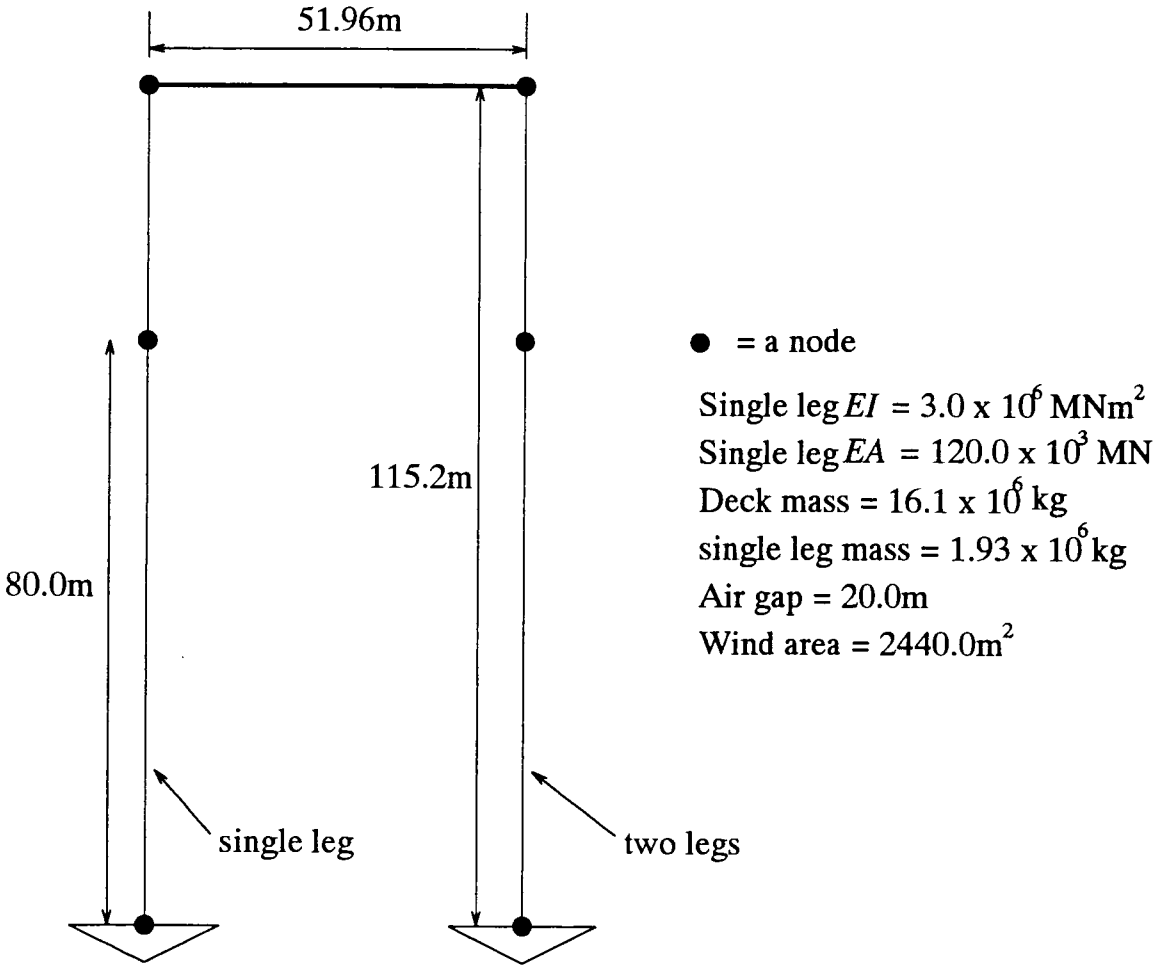

FIGURE 6.1 Jack-up numerical model

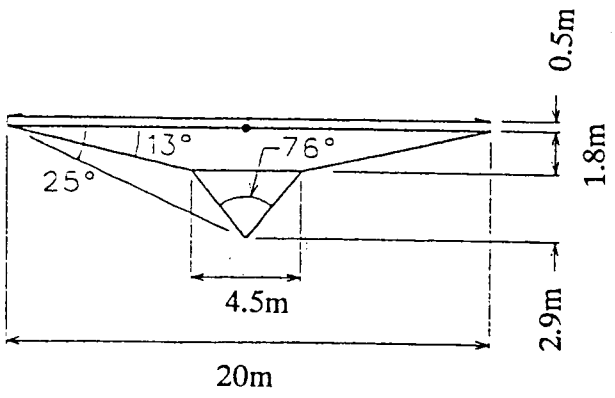

FIGURE 6.2 Spudcan footing

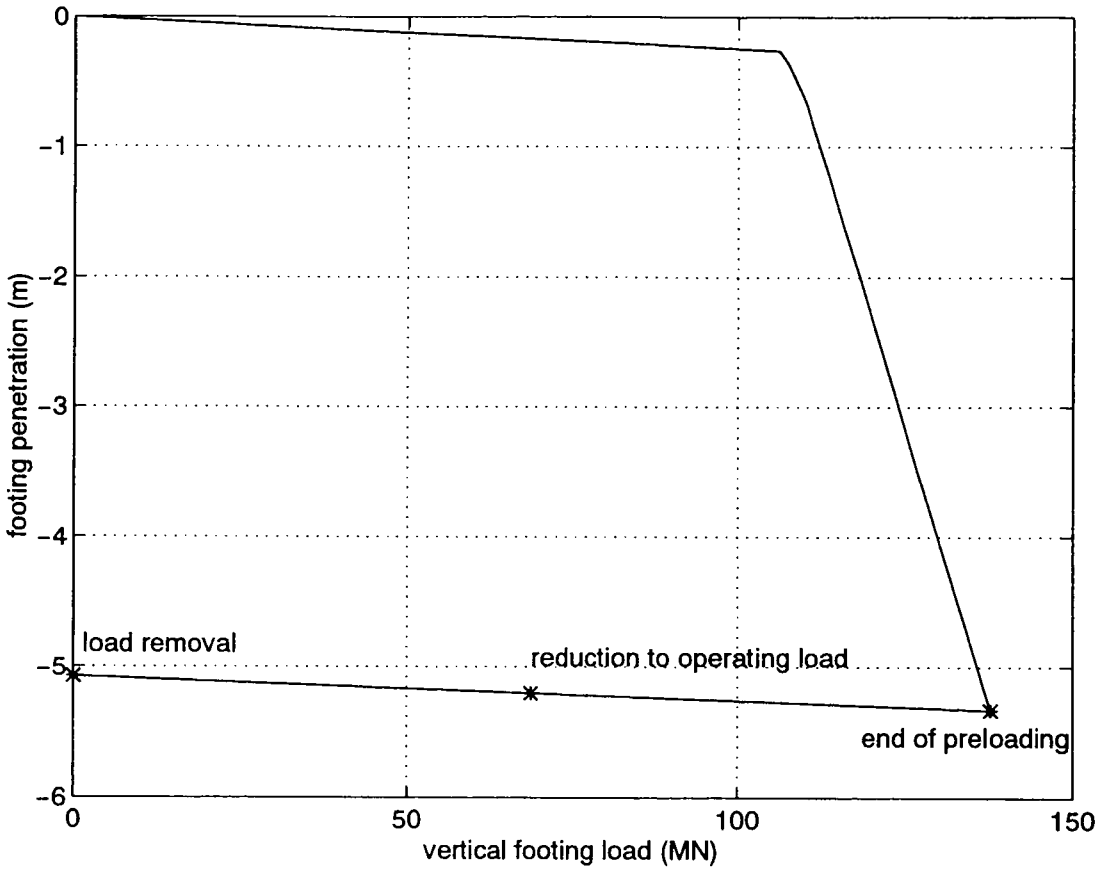

FIGURE 6.3 Vertical load-penetration path for spudcan footing

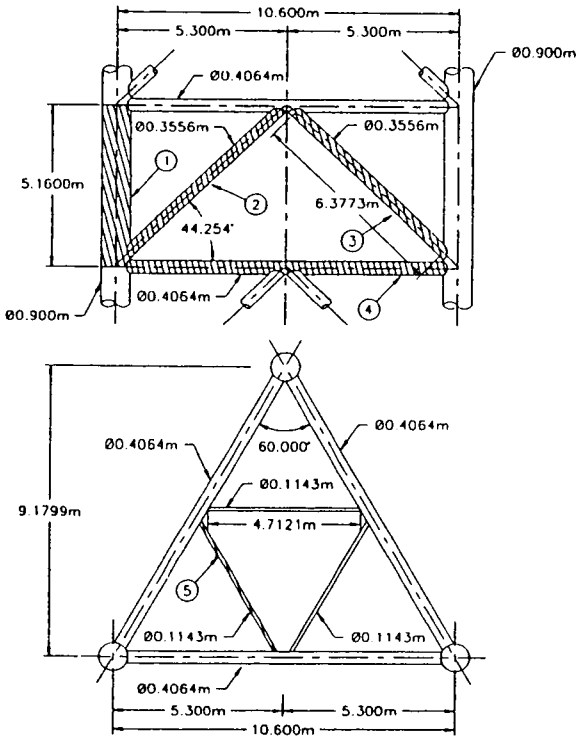

FIGURE 6.4 Jack-up leg bay section (from Nielsen *et al*, 1994)

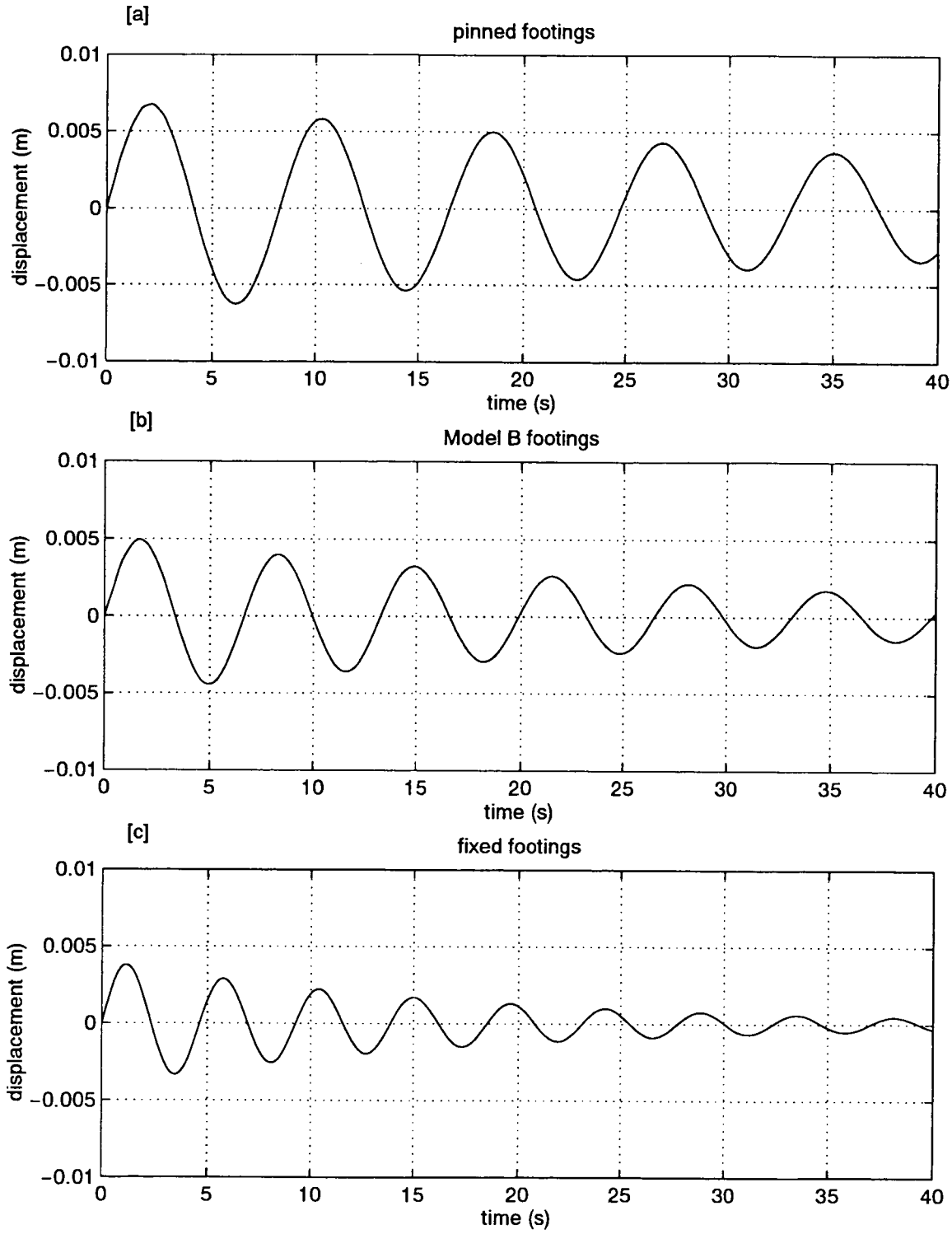

FIGURE 6.5 Horizontal hull displacement due to an impulse load at the deck level

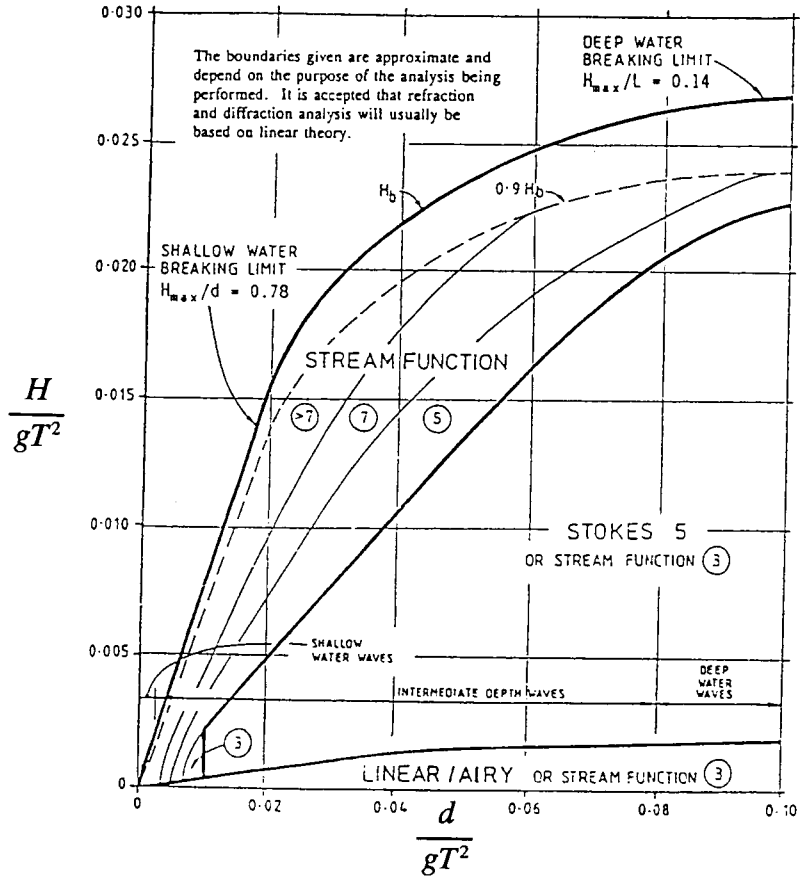

FIGURE 6.6 Wave theory selection diagram (from SNAME, 1993)

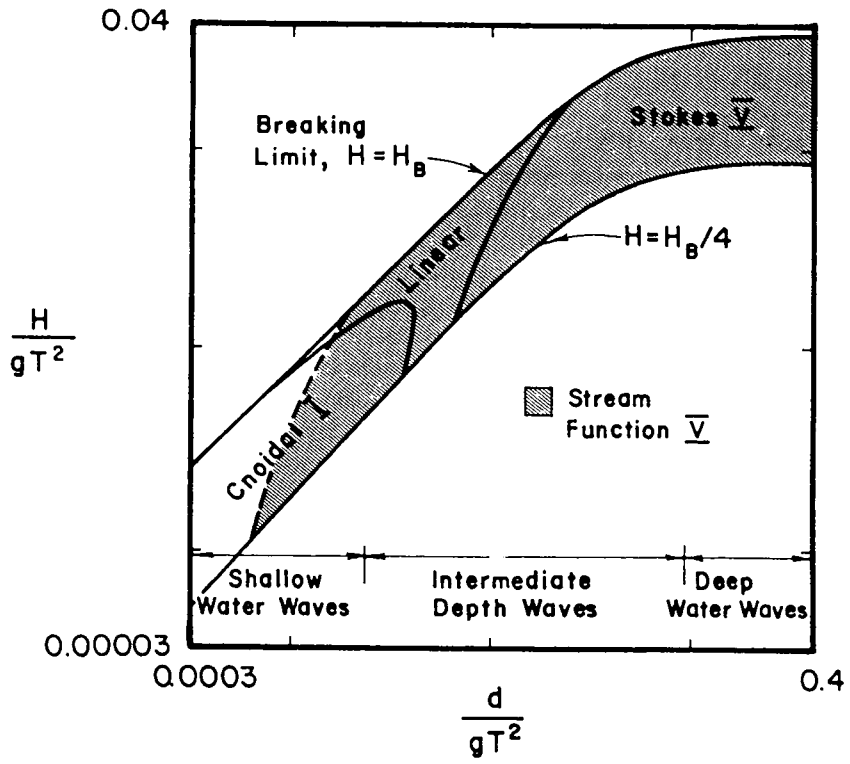

FIGURE 6.7 Range of wave theories giving the best fit to the dynamic free surface boundary condition (after Dean, 1970)

[a] maximum values

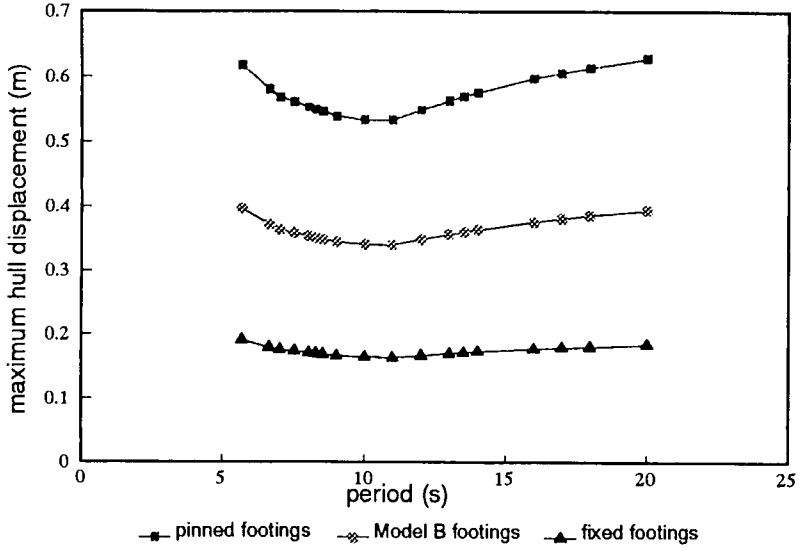

[b] maximums as percentages of pinned analyses

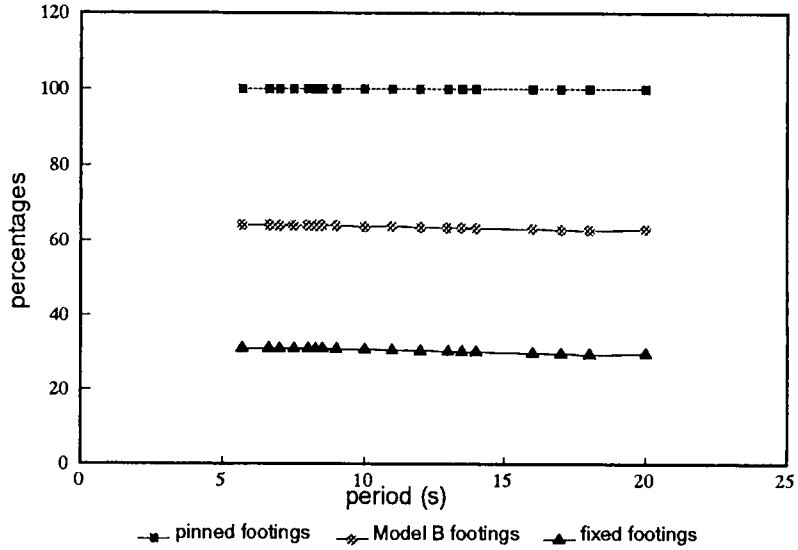

[c] double amplitudes

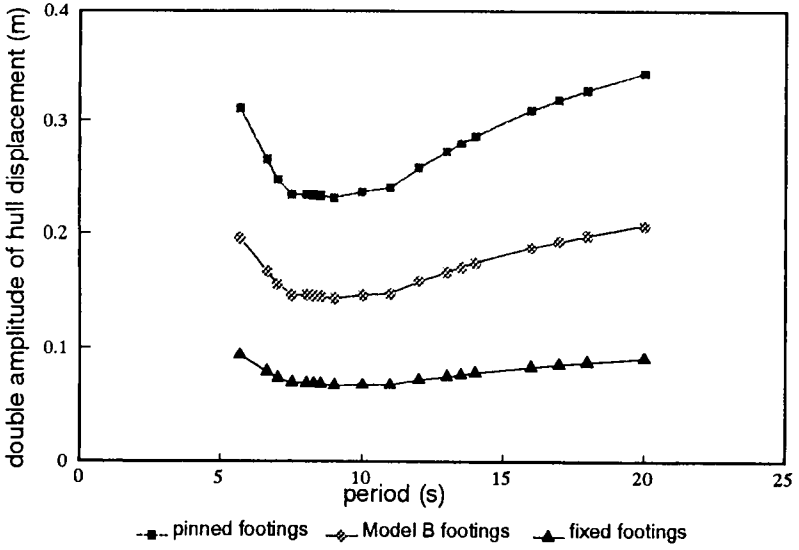

[d] double amplitudes as percentages of pinned analyses

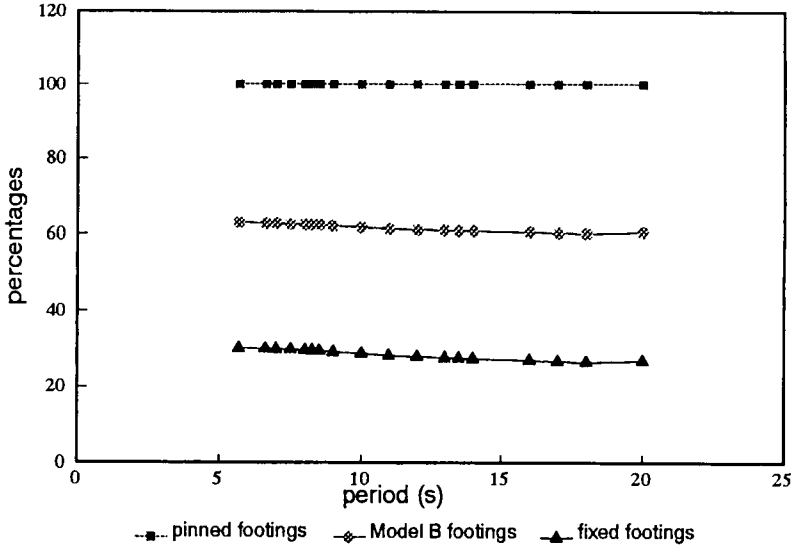

FIGURE 6.8 Quasi-static hull displacements

[a] hydrodynamic leg load

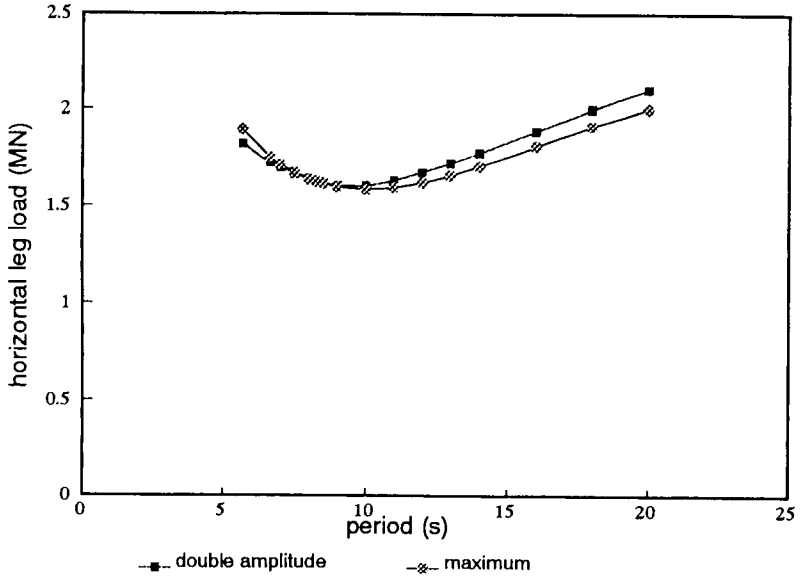

[b] hydrodynamic leg overturning moment

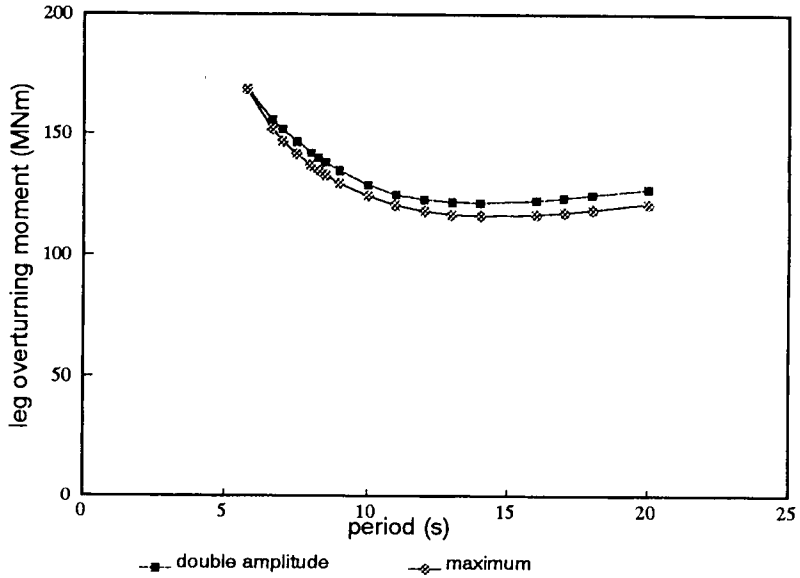

[c] global platform base shear (excluding wind load)

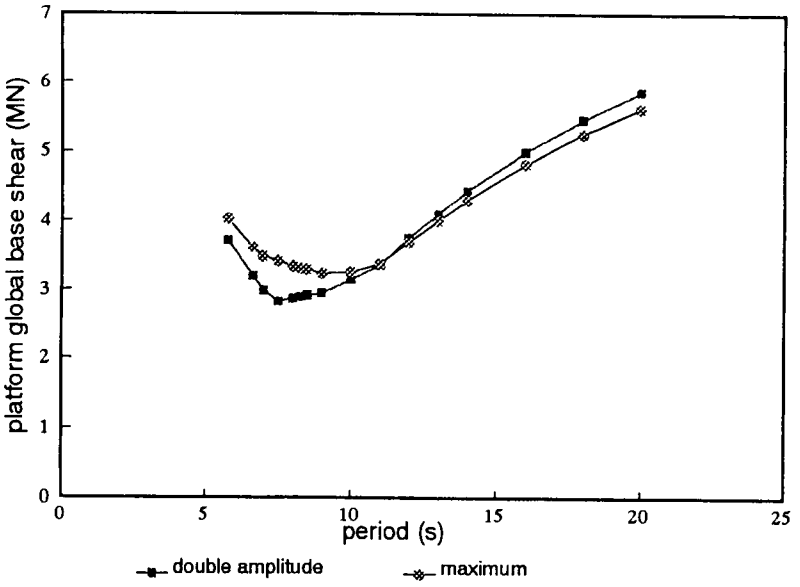

[d] global platform overturning moment (excluding wind moment)

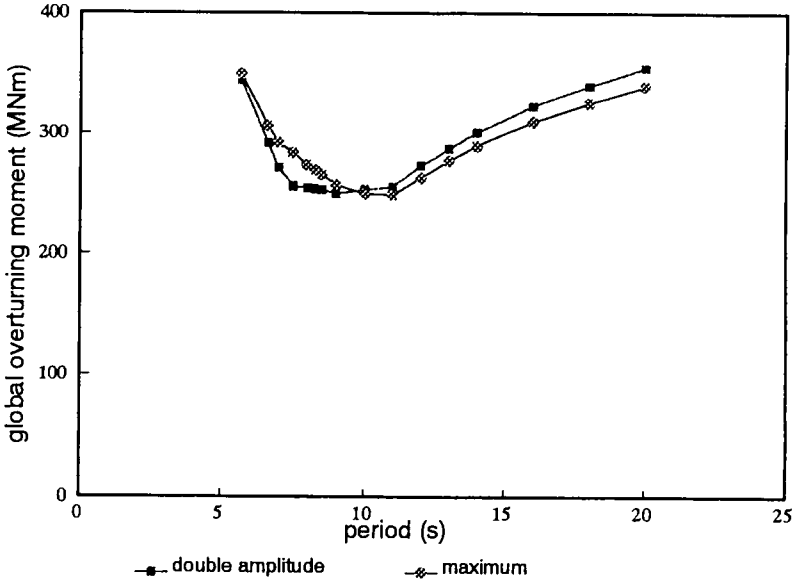

FIGURE 6.9 Variation of platform loads

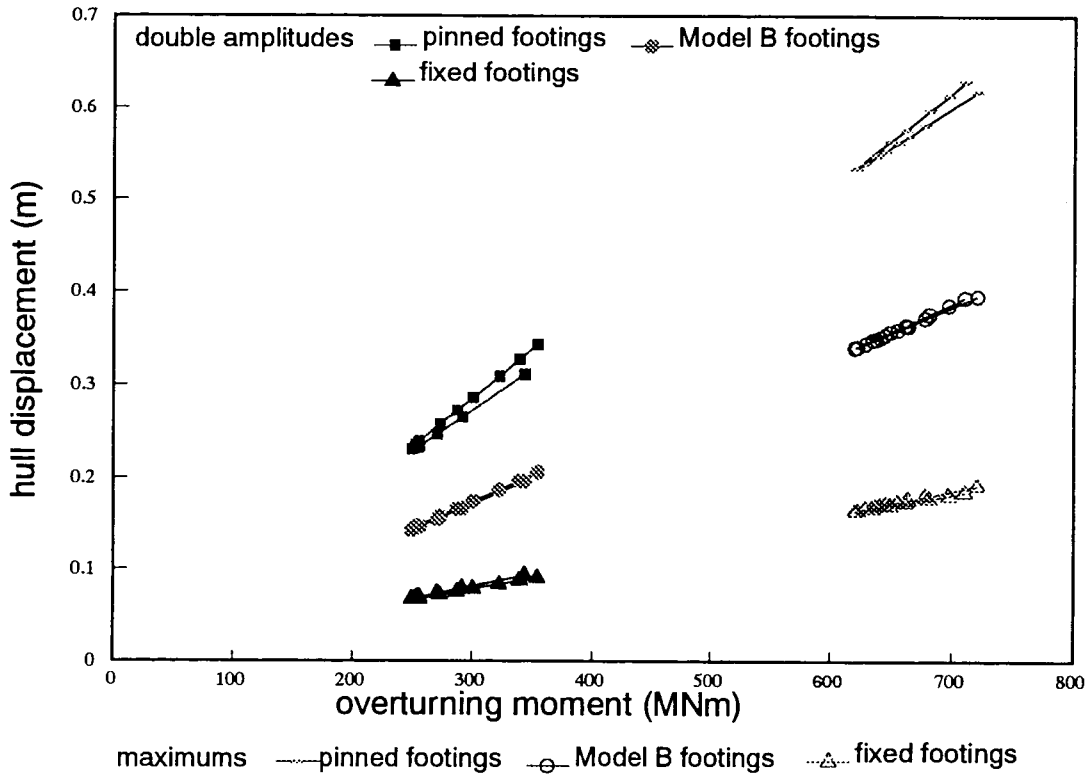

FIGURE 6.10 Variation of hull displacement with overturning moment

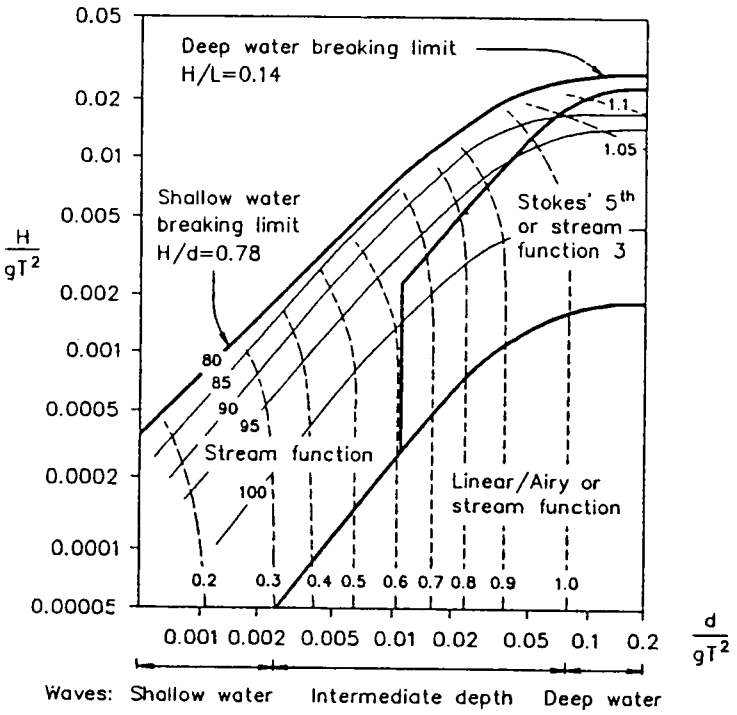

FIGURE 6.11 Wavelength predictions from linear theory (solid lines) as a percentage of the shown higher order theory (from Barltrop & Adams, 1991)

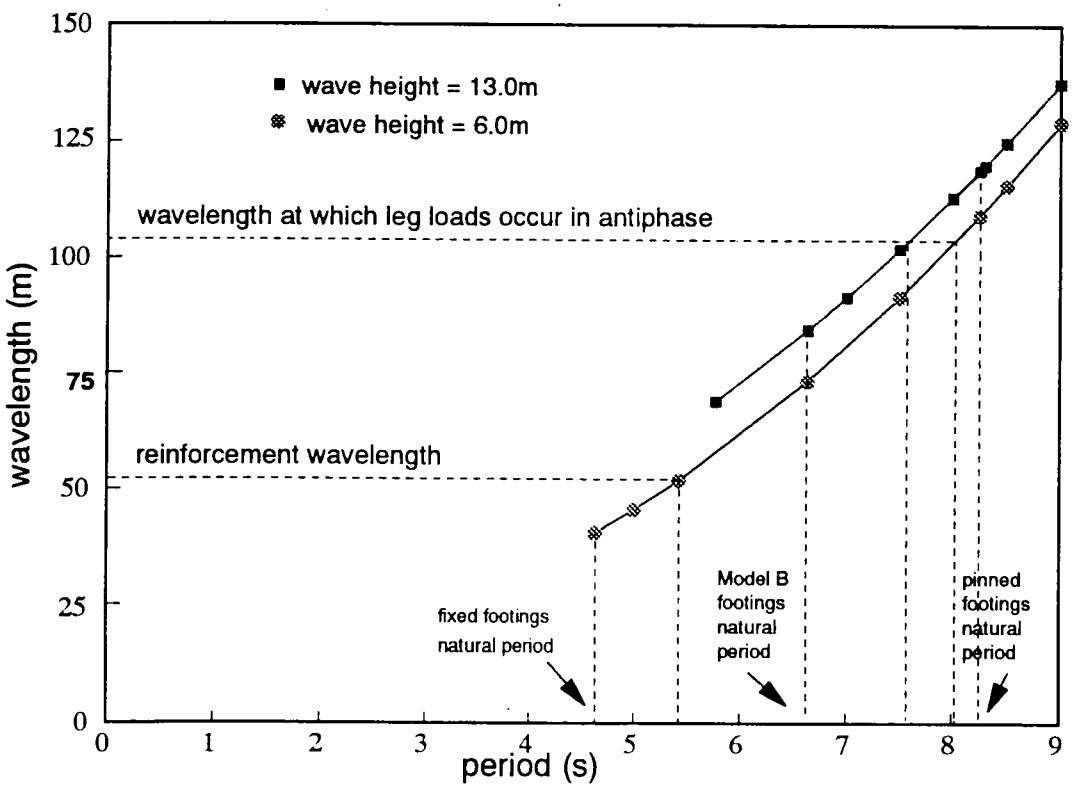

FIGURE 6.12 Variation of wavelength with period

[a]

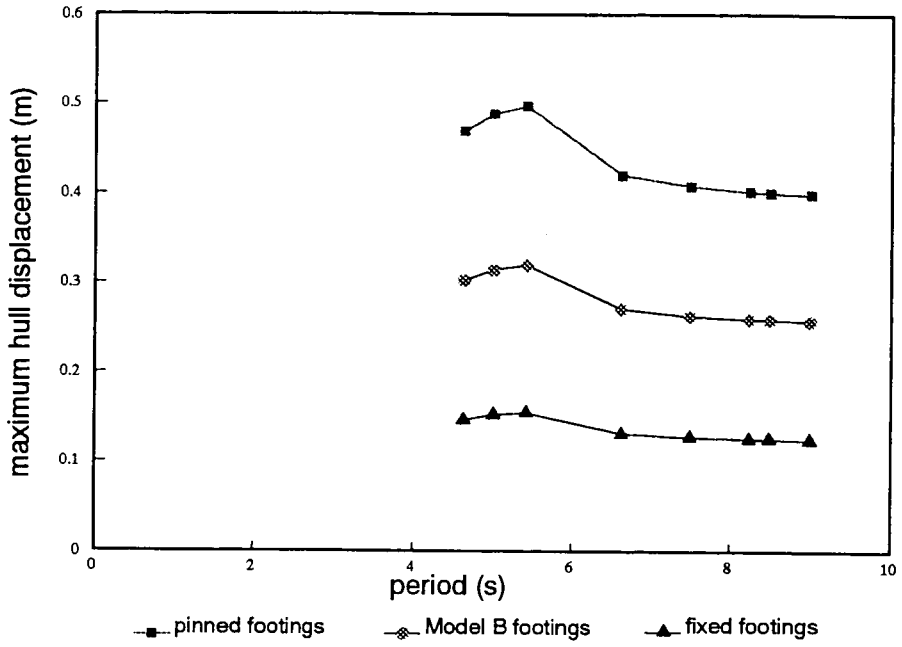

[b]

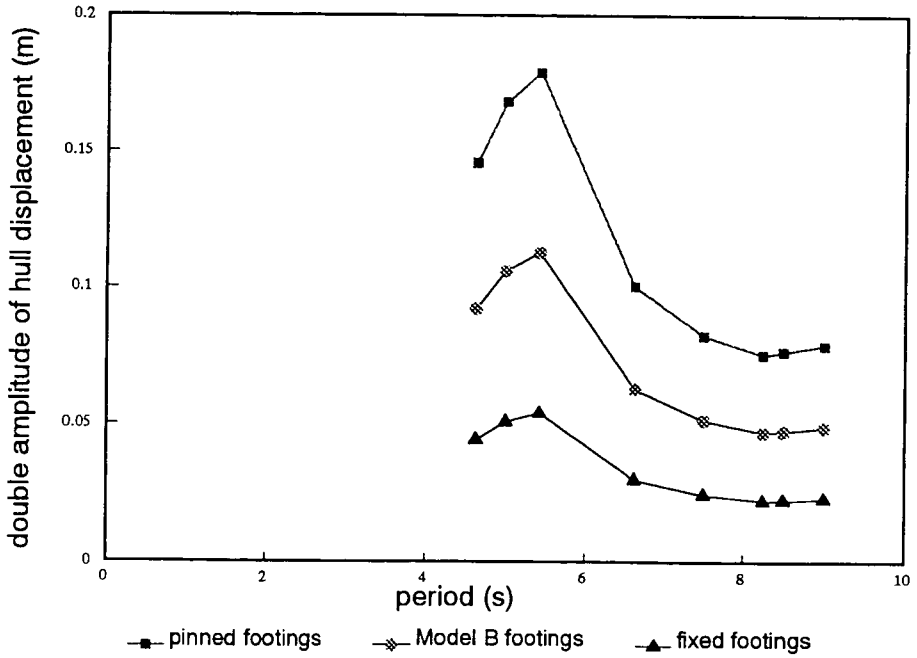

FIGURE 6.13 Quasi-static hull displacements at low periods

[a] maximum values, windward leg

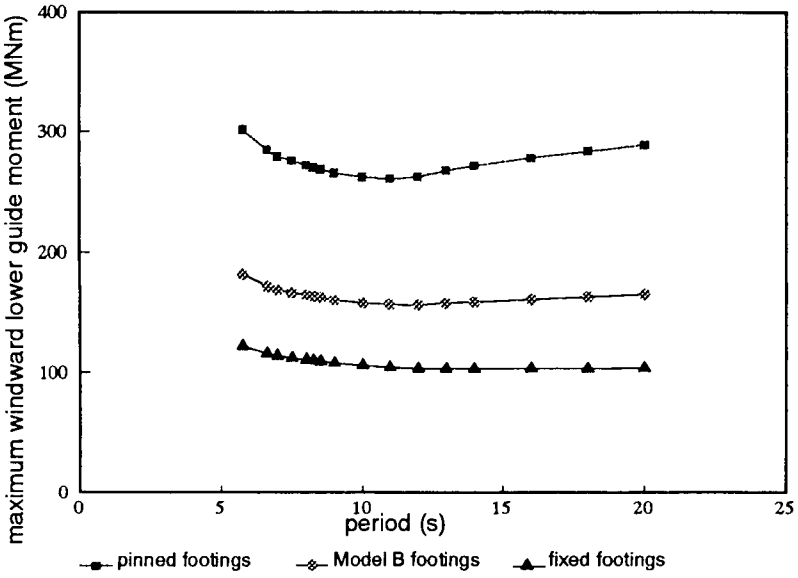

[b] double amplitude values, windward leg

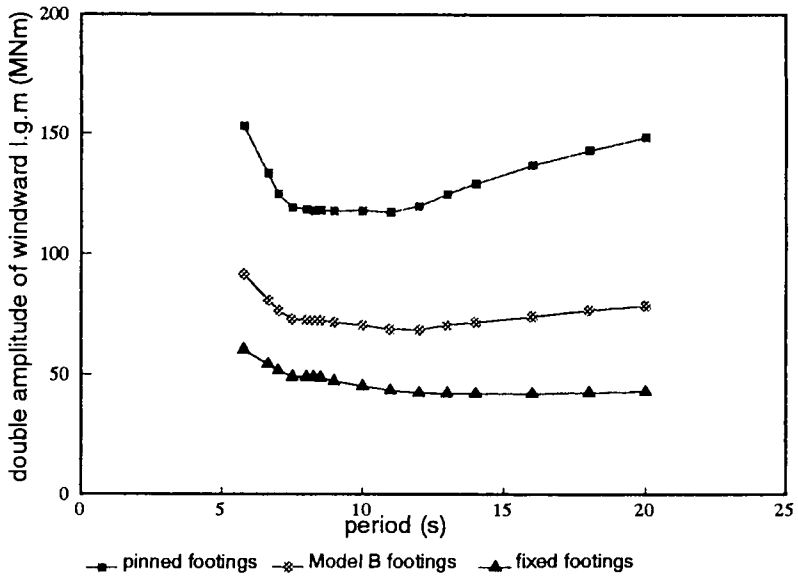

[c] maximum values, leeward leg

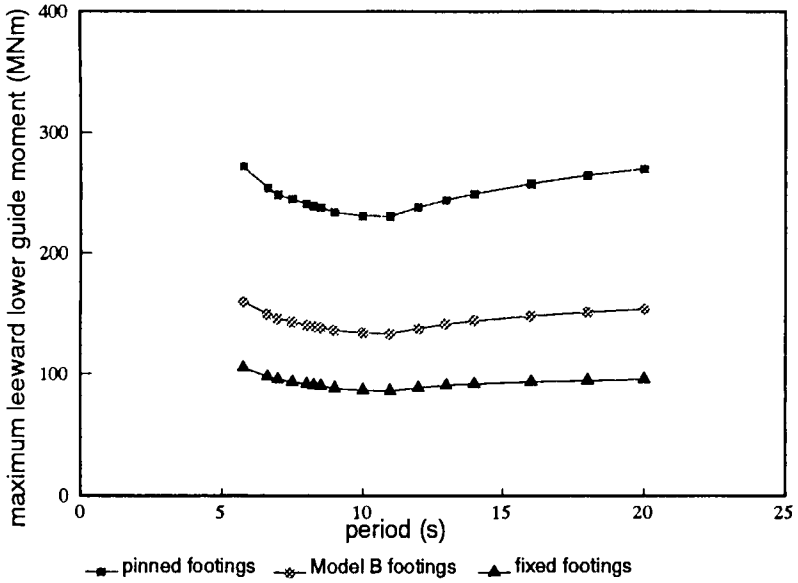

[d] double amplitude values, leeward leg

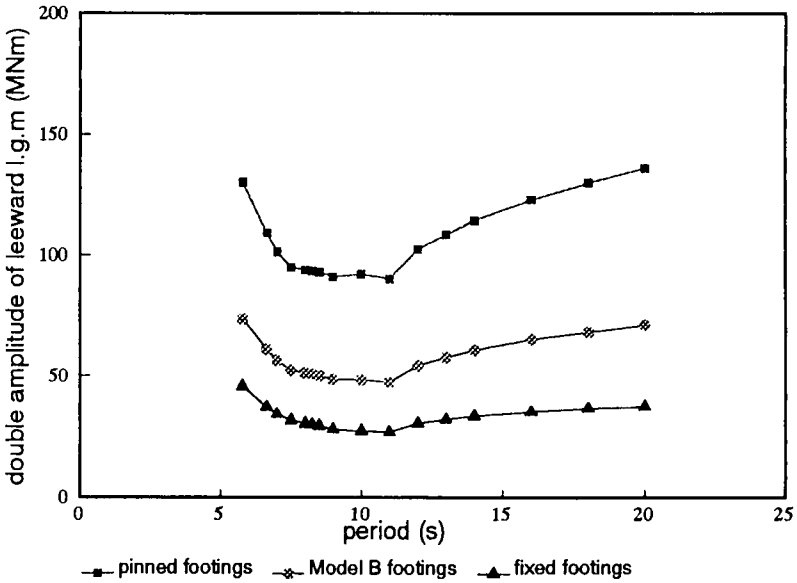

FIGURE 6.14 Quasi-static lower guide moments

[a]

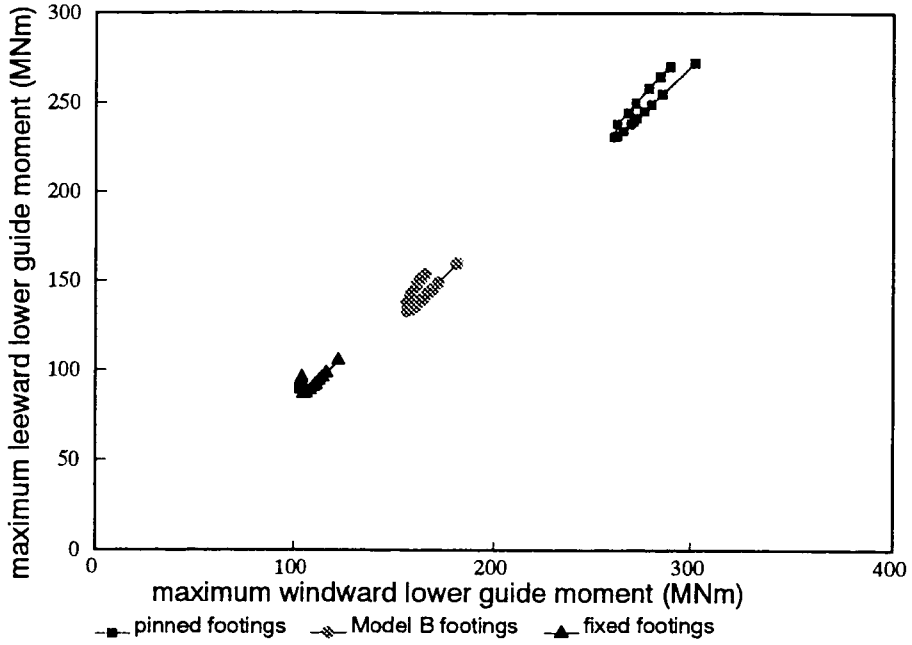

[b]

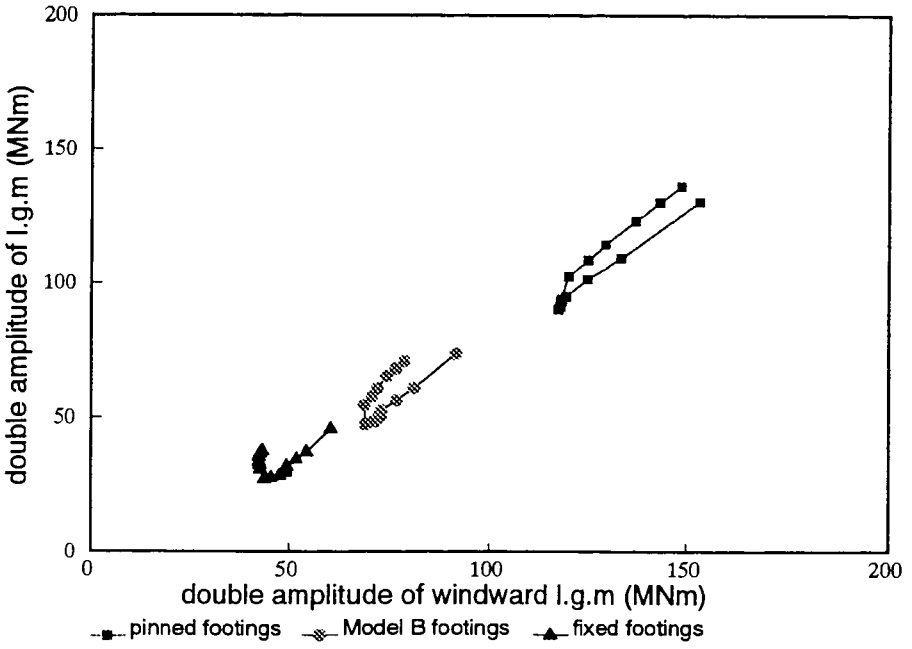

FIGURE 6.15 Variation of the lower guide moments

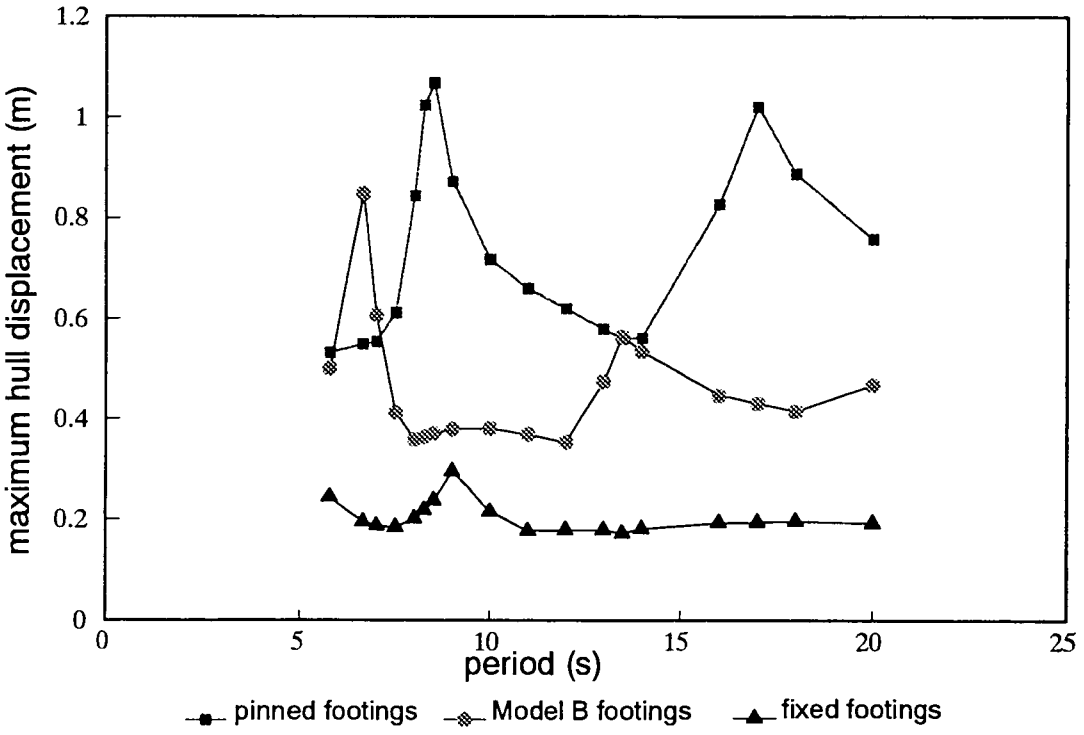

FIGURE 6.16 Maximum dynamic hull displacement

[a] hull displacement

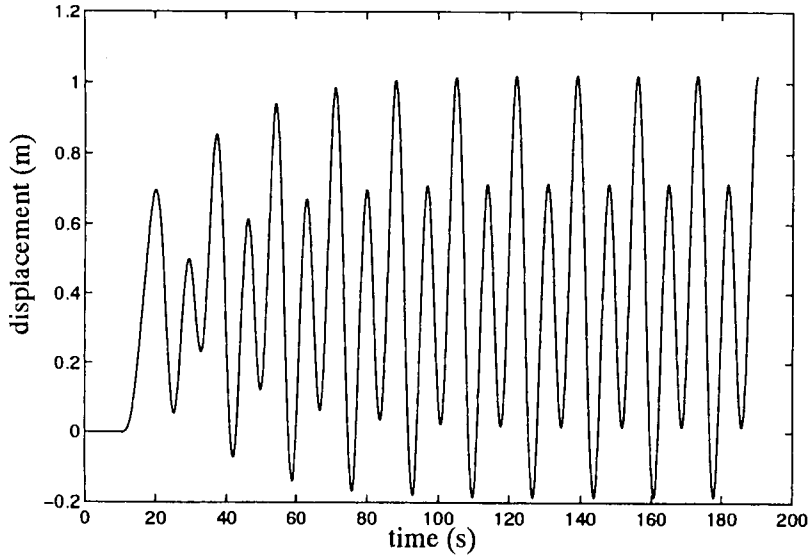

[b] amplitude spectrum of hull displacement

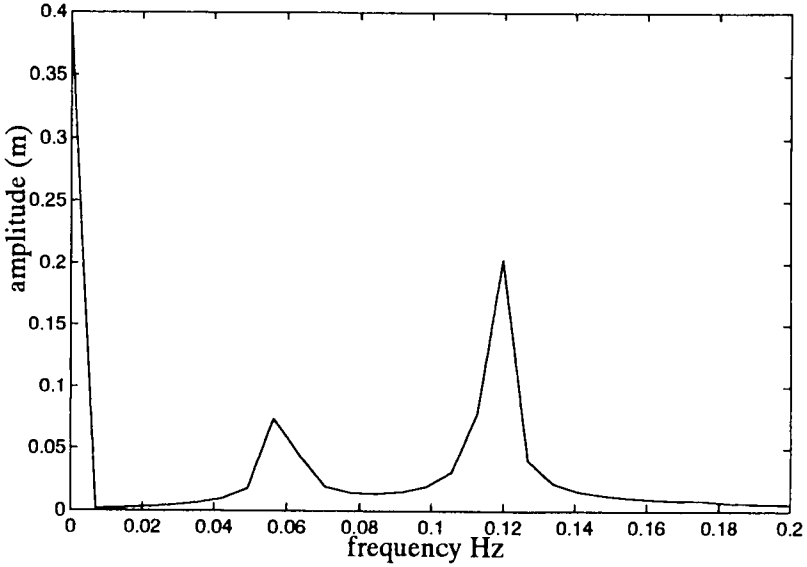

[c] amplitude spectrum of hydrodynamic load

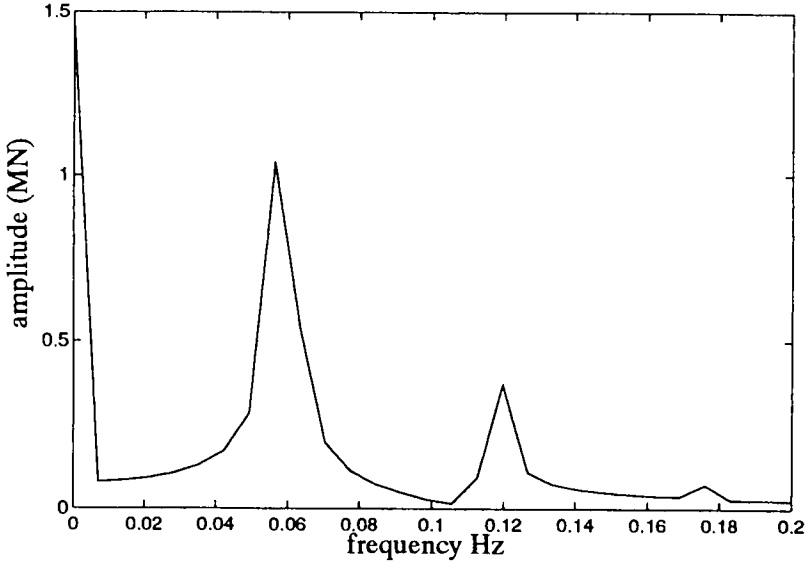

FIGURE 6.17 Hull displacement and amplitude spectra for a 17.0s wave

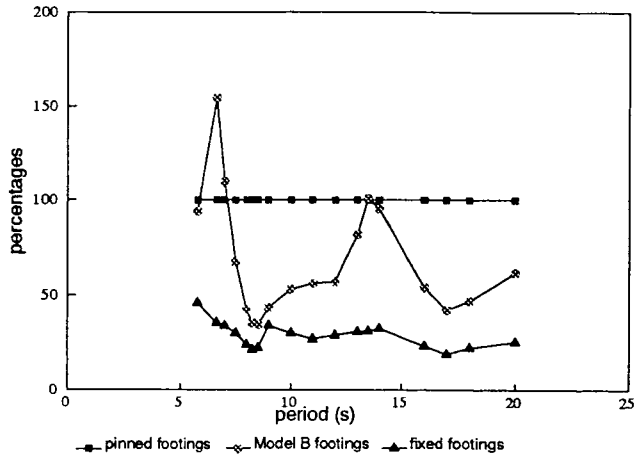

FIGURE 6.18 Hull displacements as a percentage of the pinned analyses

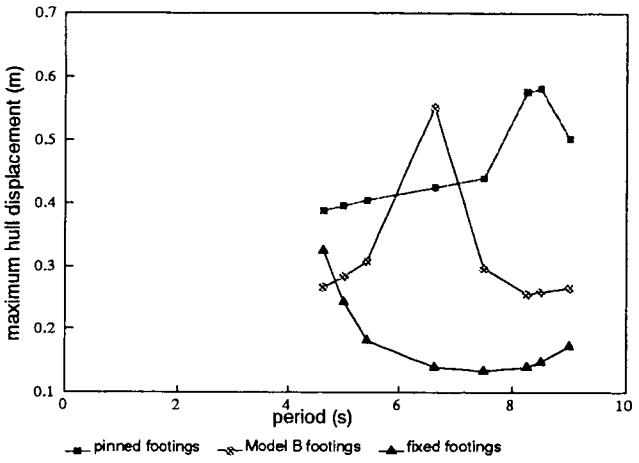

FIGURE 6.19 Dynamic hull displacements at low periods

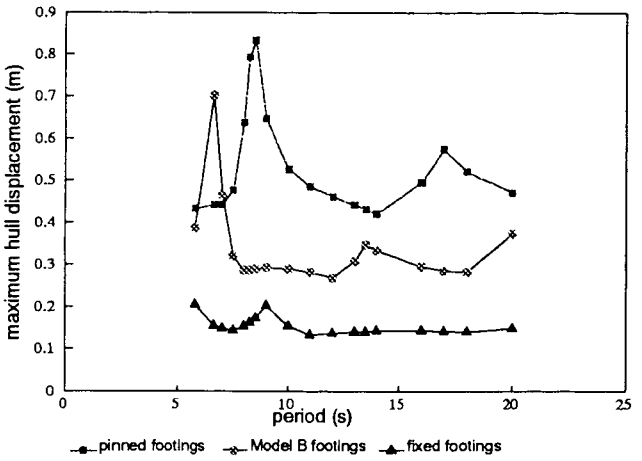

FIGURE 6.20 Maximum hull displacements with no current

[a] maximum values, windward leg

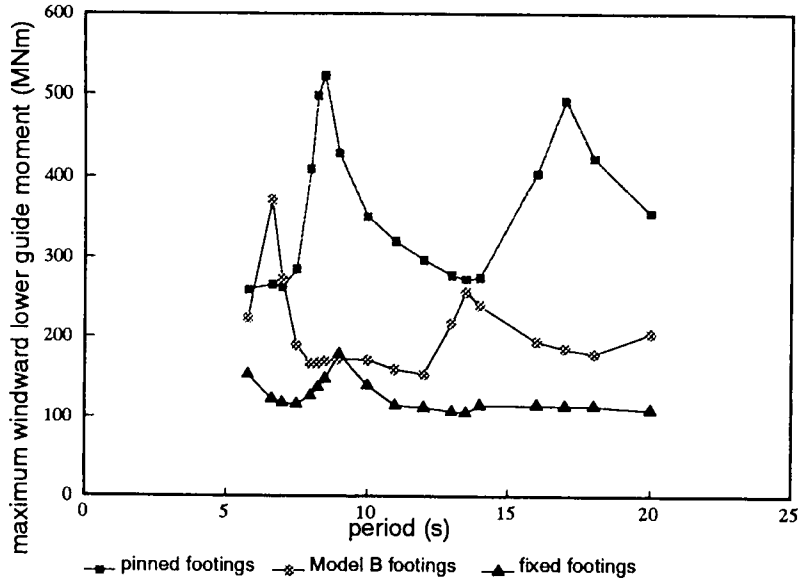

[b] windward values as percentage of pinned analysis

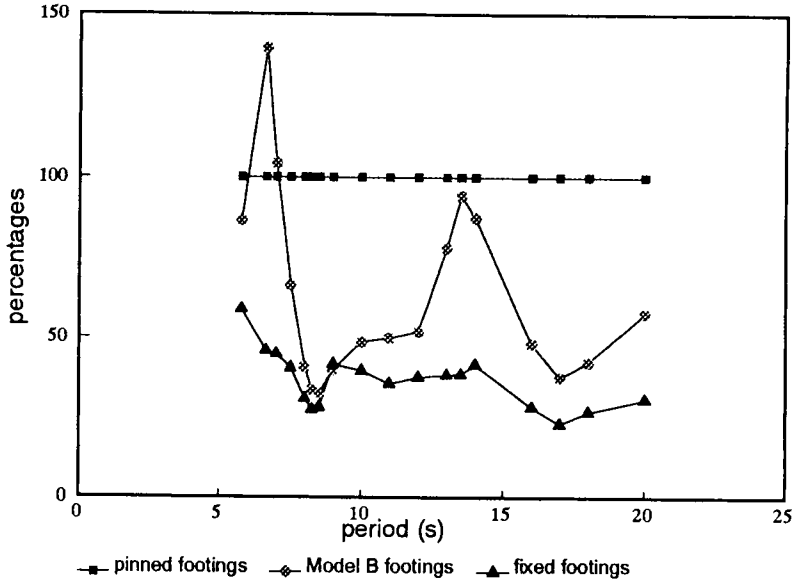

[c] maximum values, leeward leg

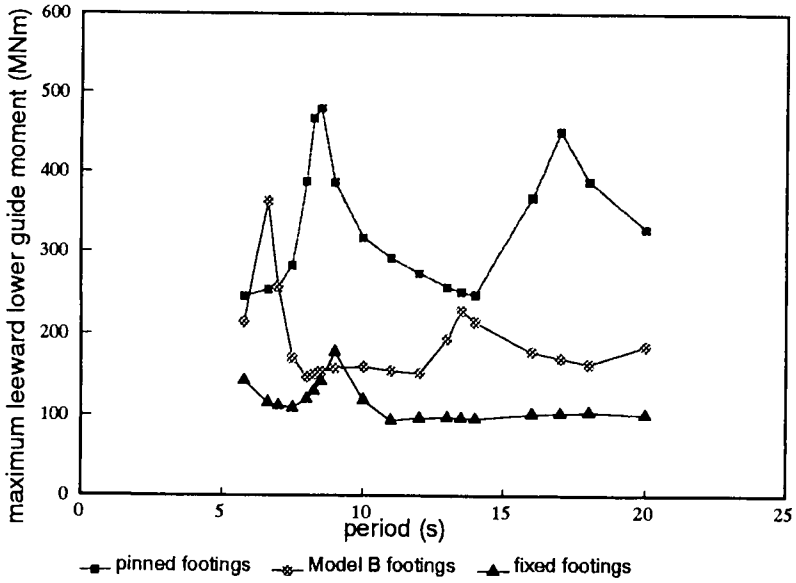

[d] variation of lower guide moments

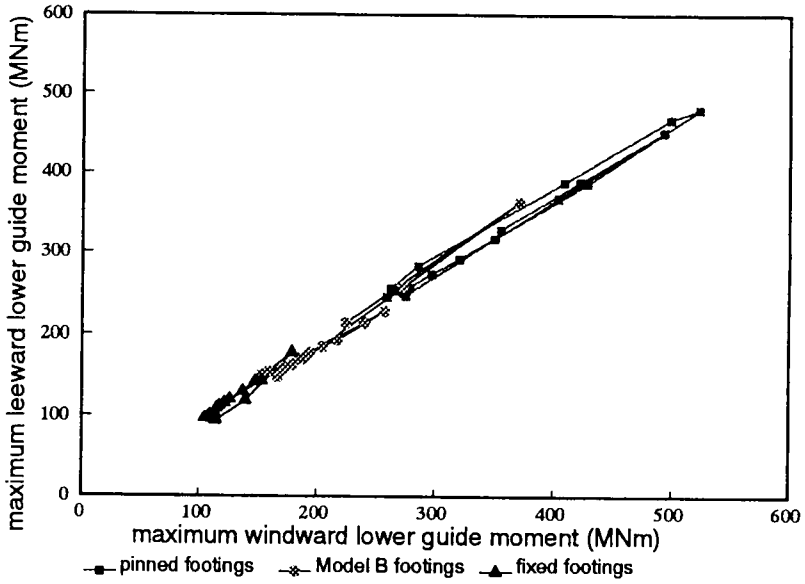

FIGURE 6.21 Dynamic maximum lower guide moments

[a] double amplitude of hull displacement

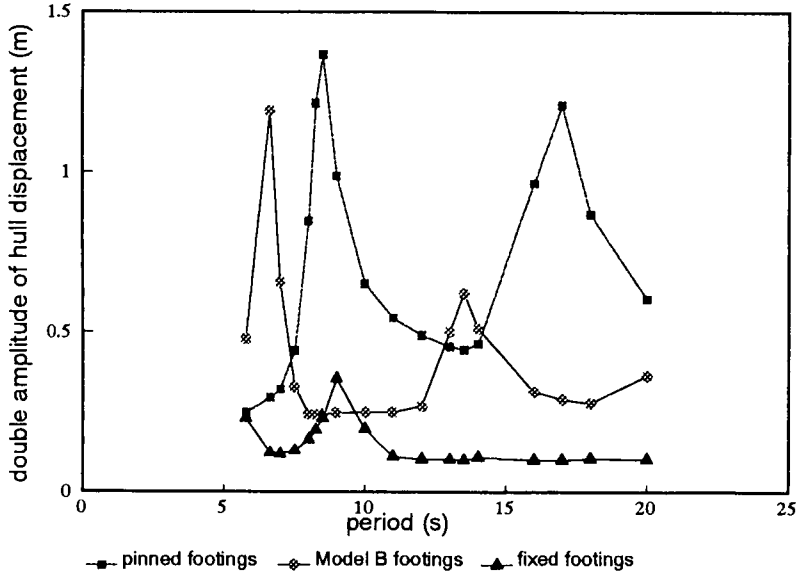

[b] double amplitude of windward lower guide moment

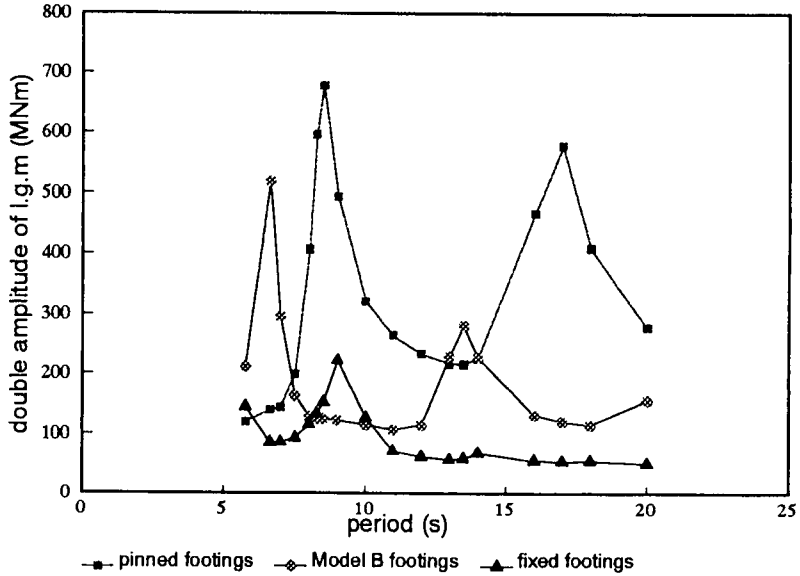

[c] double amplitude of leeward lower guide moment

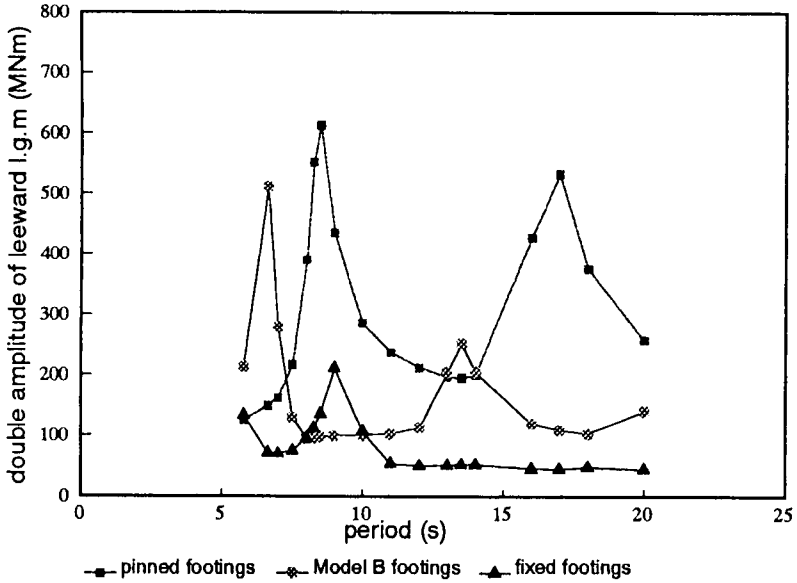

[d] variation of lower guide moments

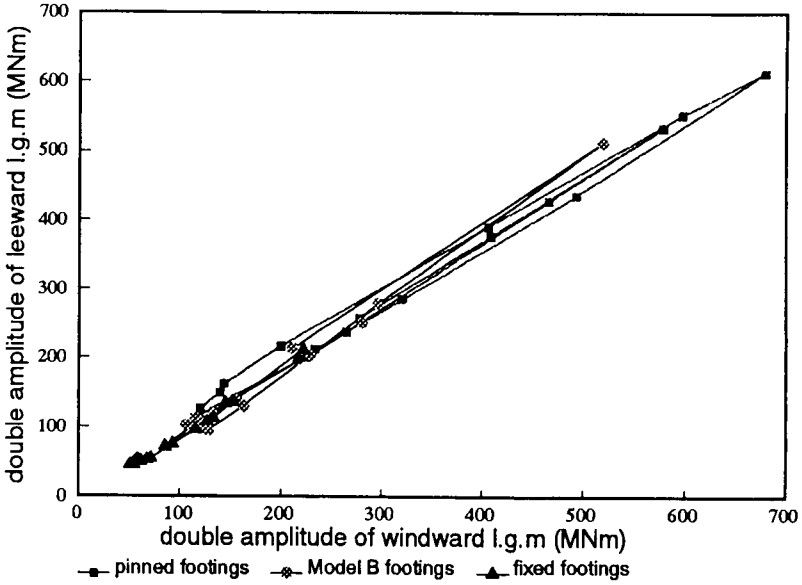

FIGURE 6.22 Dynamic maximum lower guide moments

[a]

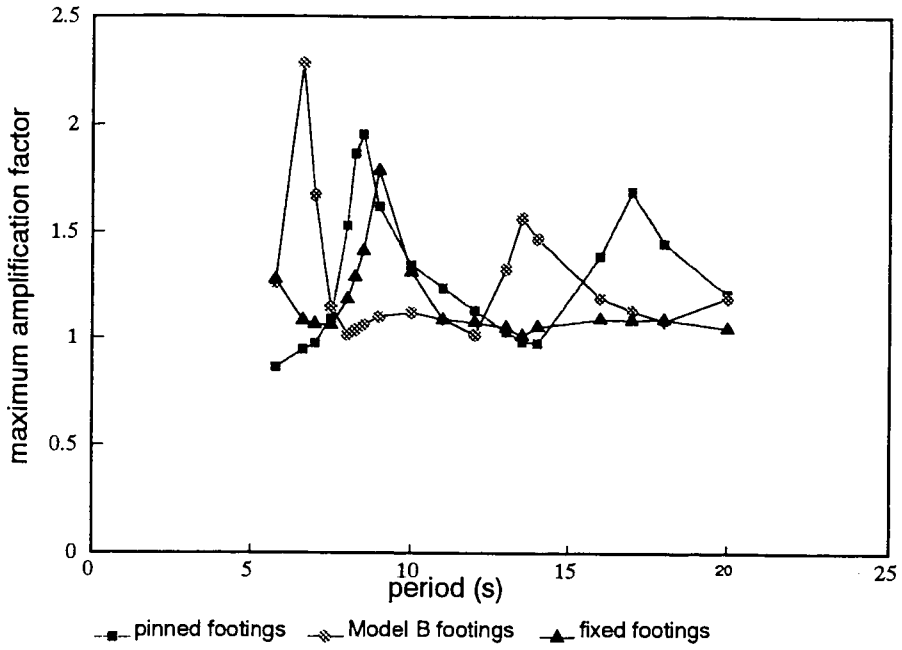

[b]

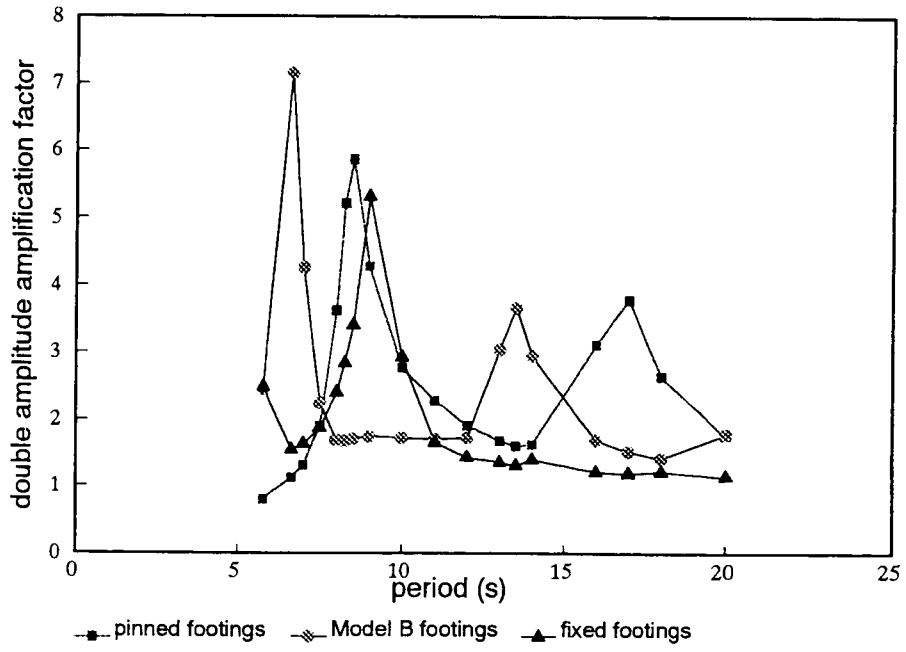

FIGURE 6.23 Hull displacement variables non-dimensionalized with respect to the quasi-static hull displacement variables

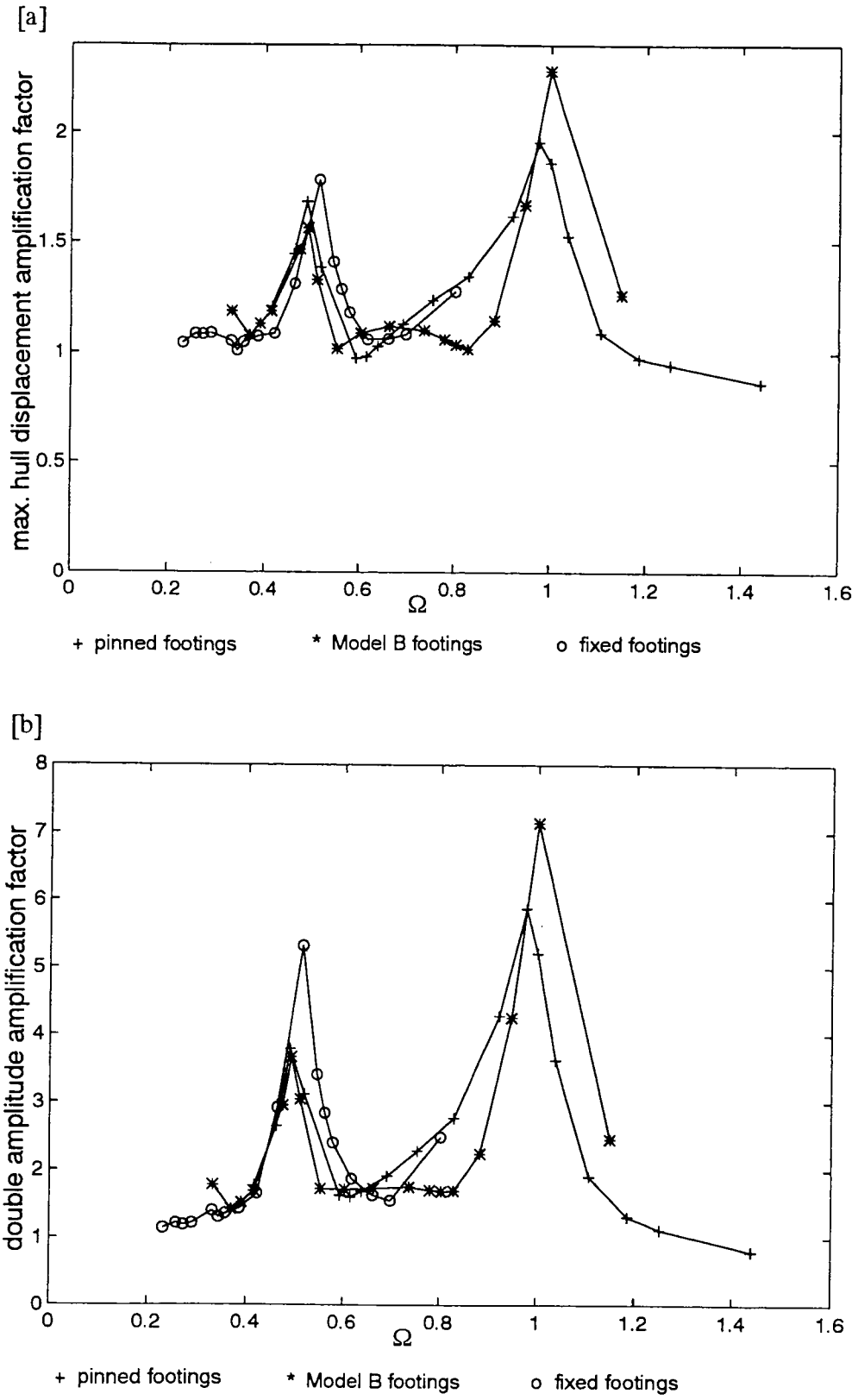

FIGURE 6.24 Variation of amplification factors with frequency ratio

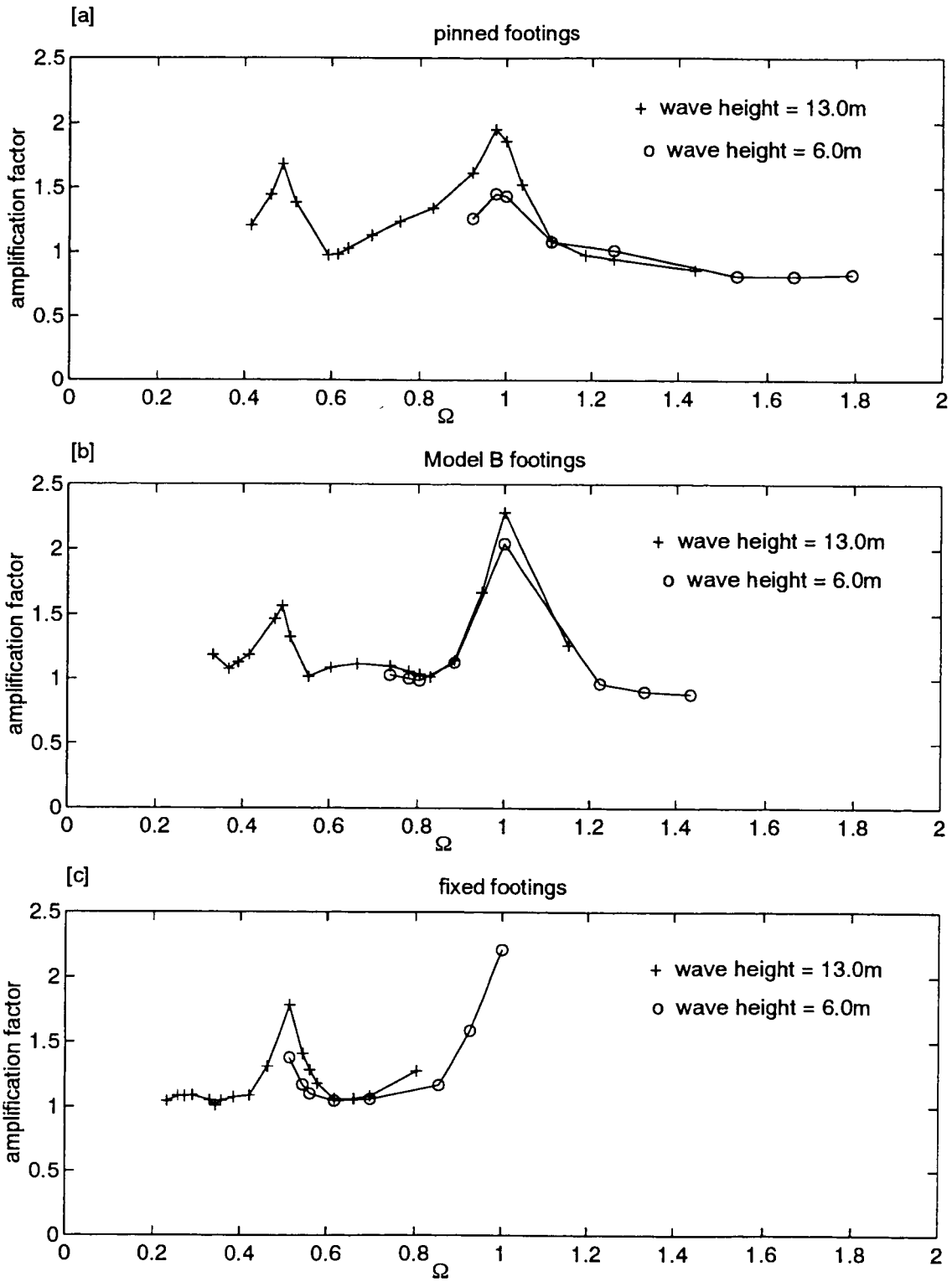

FIGURE 6.25 Maximum hull displacement amplification factors with an extended frequency range

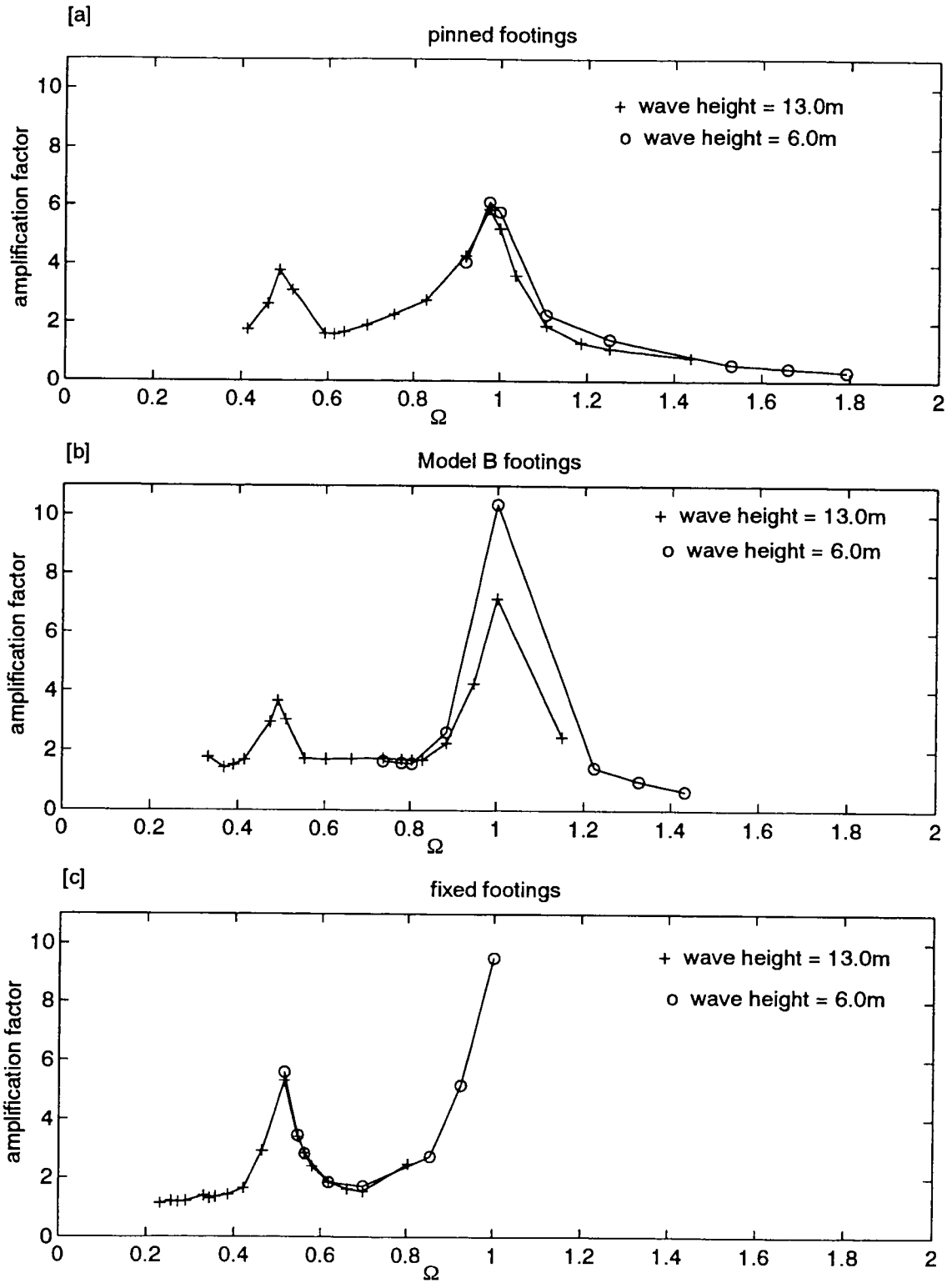

FIGURE 6.26 Double amplitude amplification factors with an extended frequency range

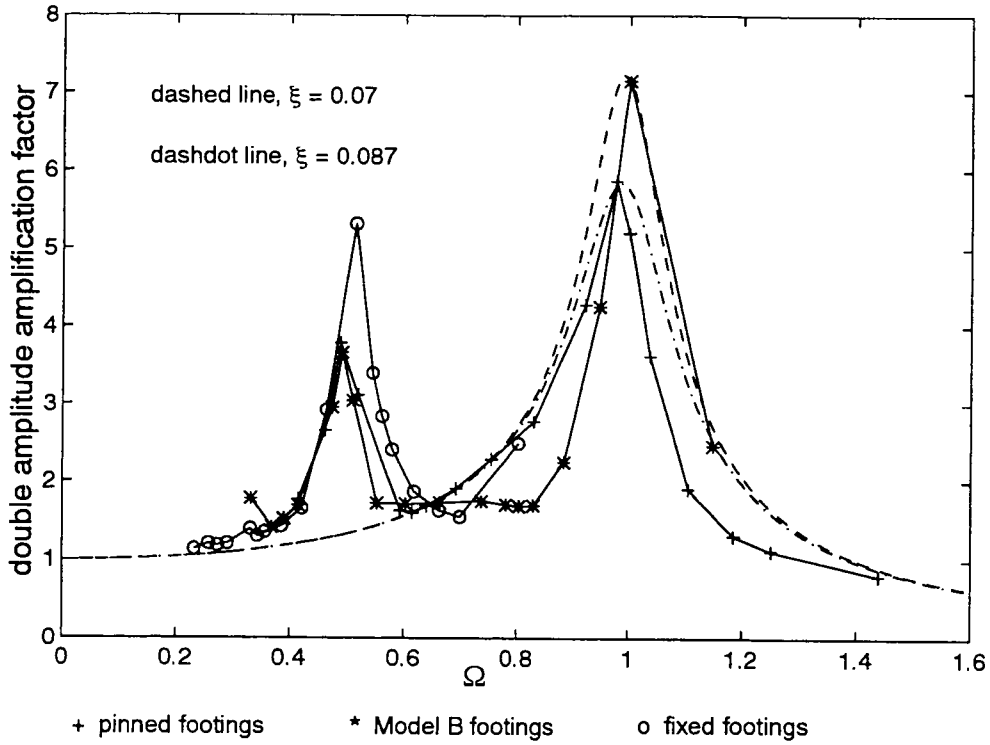

FIGURE 6.27 Amplification curves compared to the dynamic amplification factor for a linear single degree of freedom system

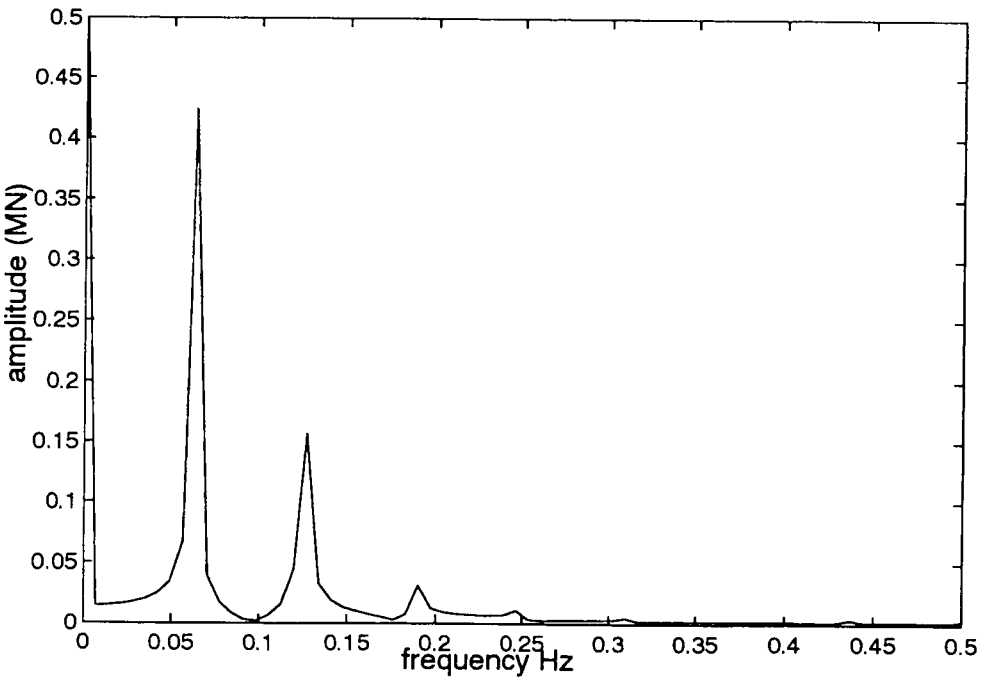

FIGURE 6.28 Amplitude spectrum of the hydrodynamic load on a leg at T = 16.0s

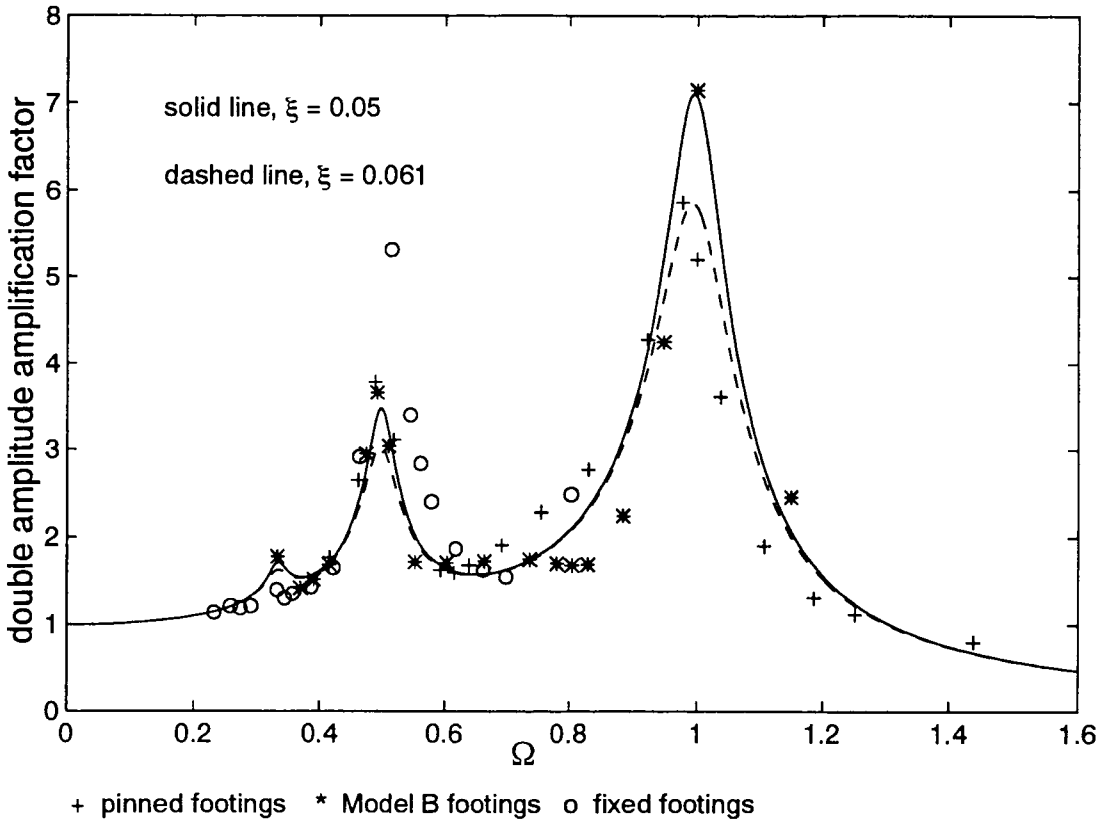

FIGURE 6.29 Amplification curves with multiple harmonics

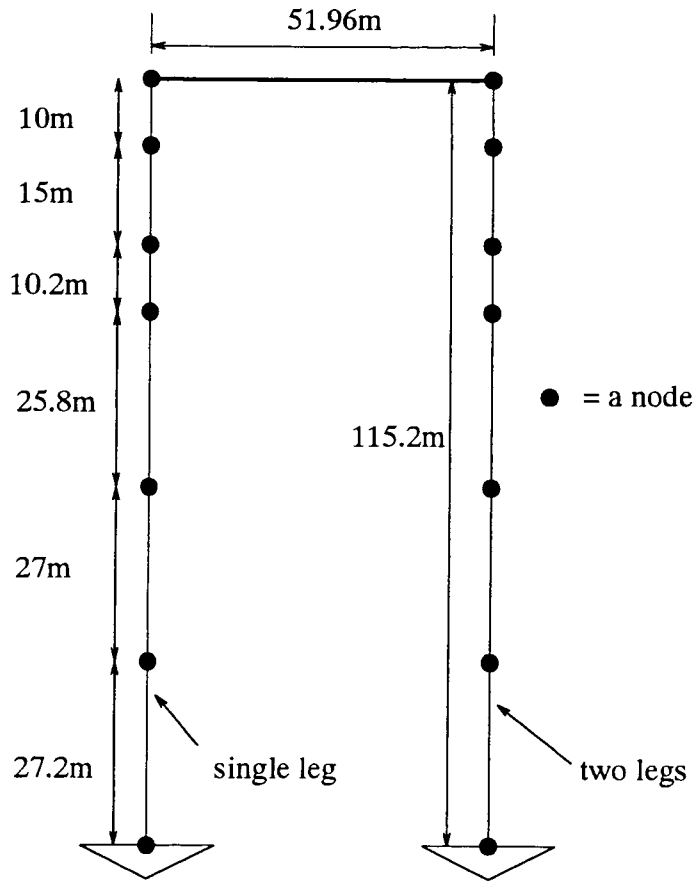

FIGURE 6.30 Jack-up numerical model with increased number of nodes

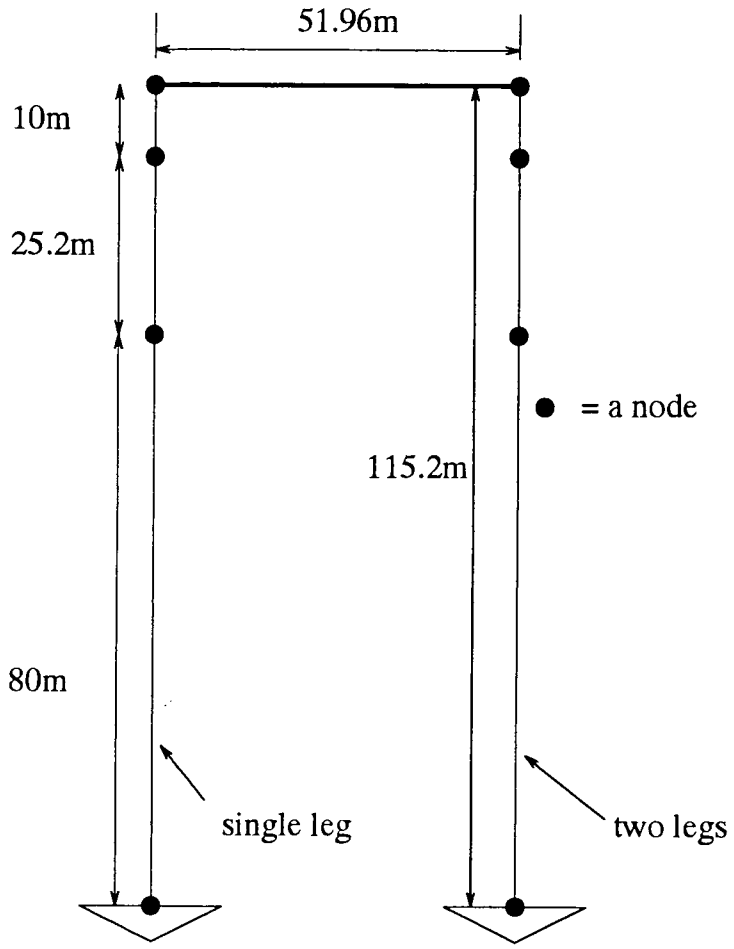

FIGURE 6.31 Jack-up numerical model used for analyses at a fixed period

[a] quasi-static analyses

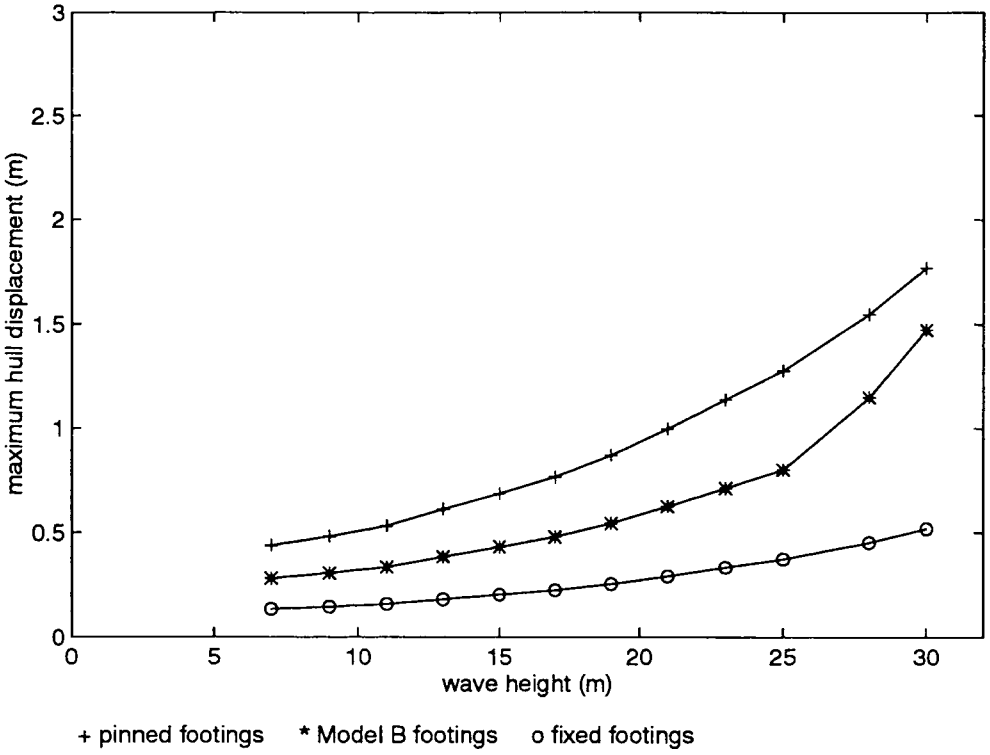

[b] dynamic analyses

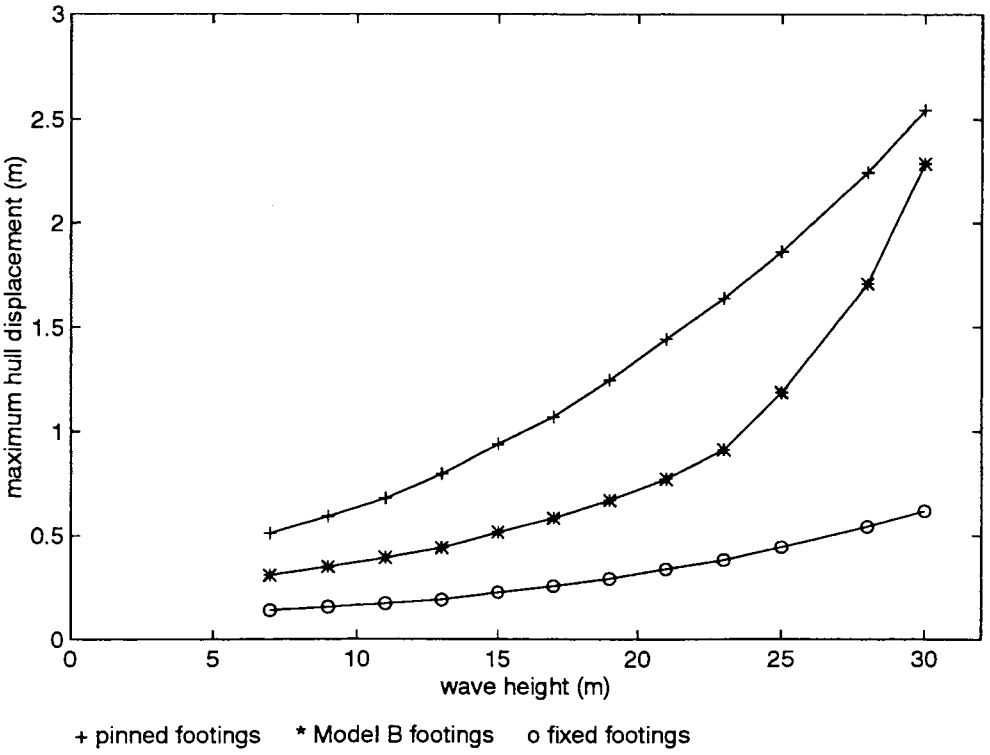

FIGURE 6.32 Variation of the maximum hull displacement with wave height

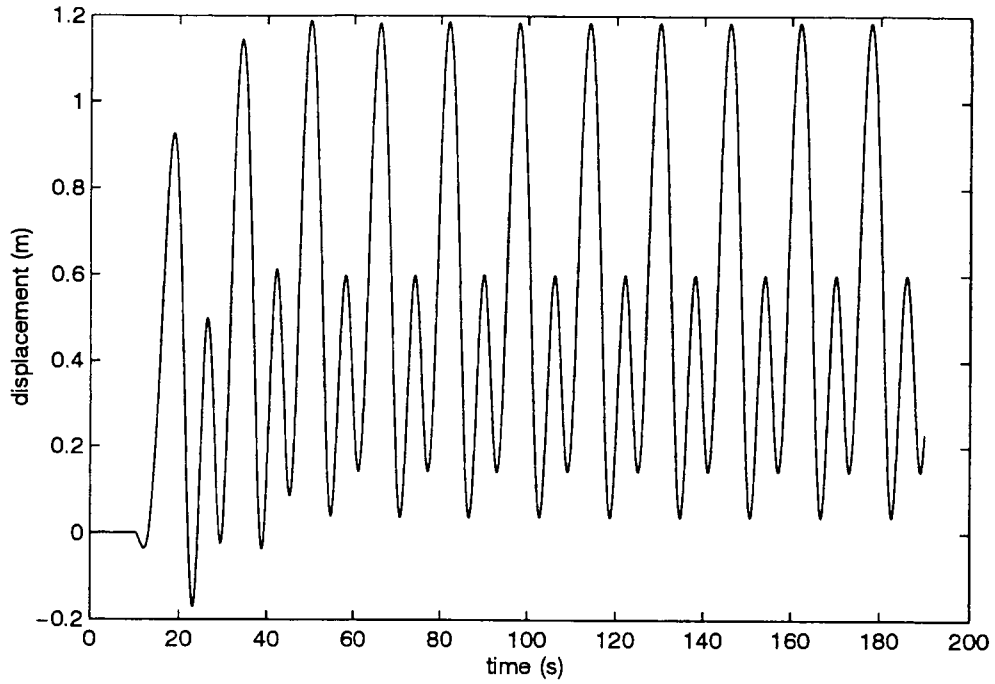

FIGURE 6.33 Dynamic hull displacement for a wave height of 25.0m

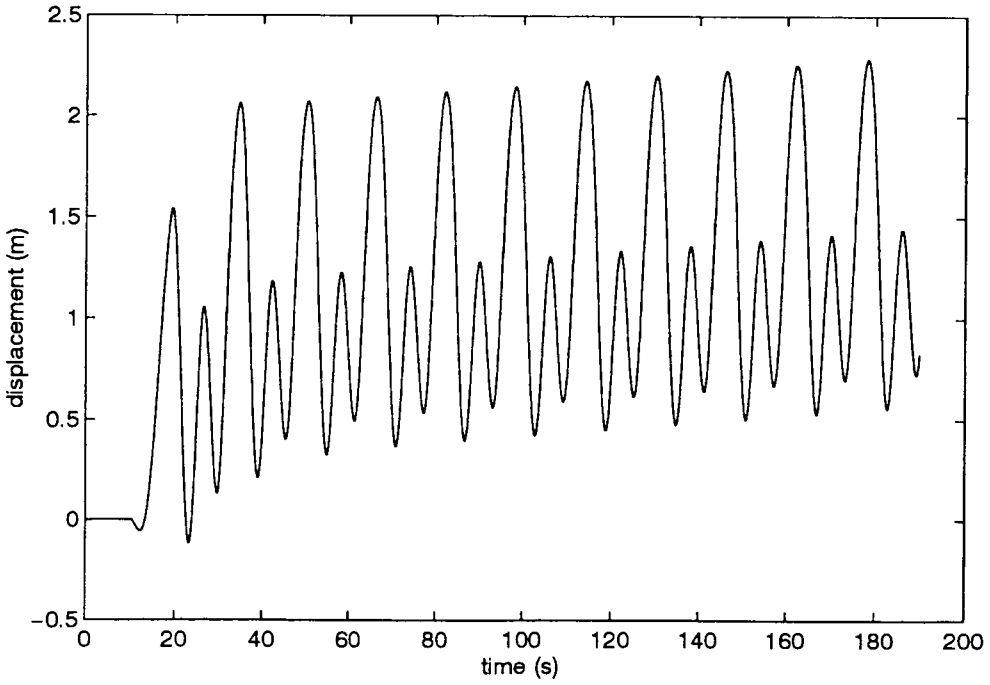

FIGURE 6.34 Dynamic hull displacement for a wave height of 30.0m

[a] quasi-static analyses

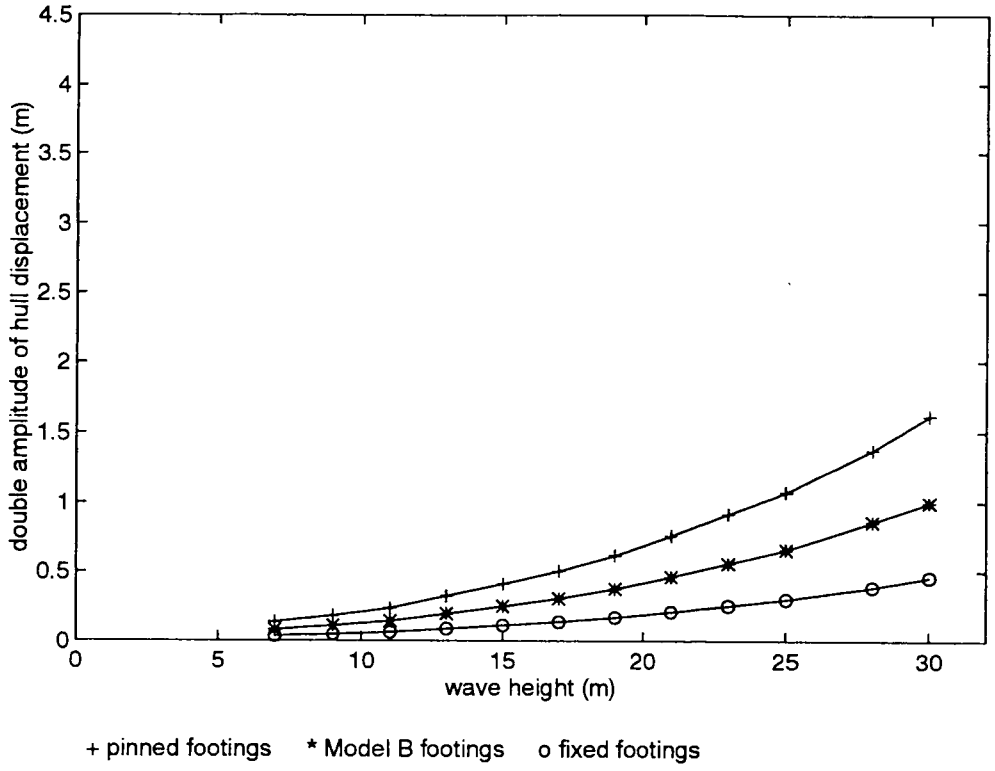

[b] dynamic analyses

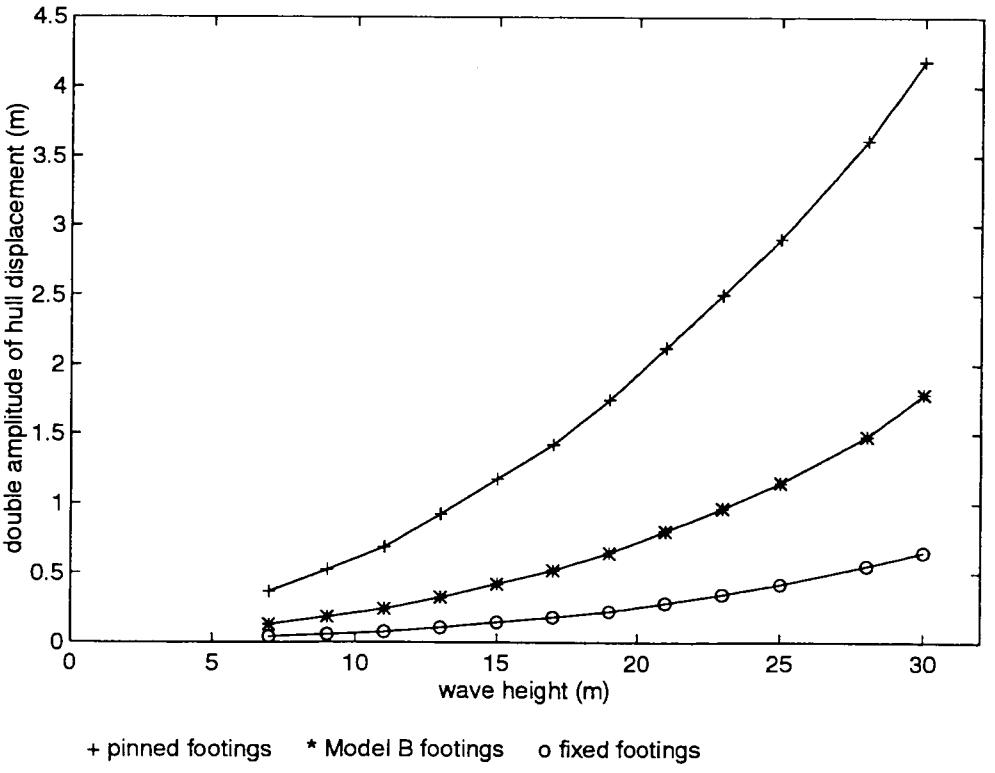

FIGURE 6.35 Variation of the double amplitude of hull displacement with wave height

[a] maximum hull displacement amplification factor

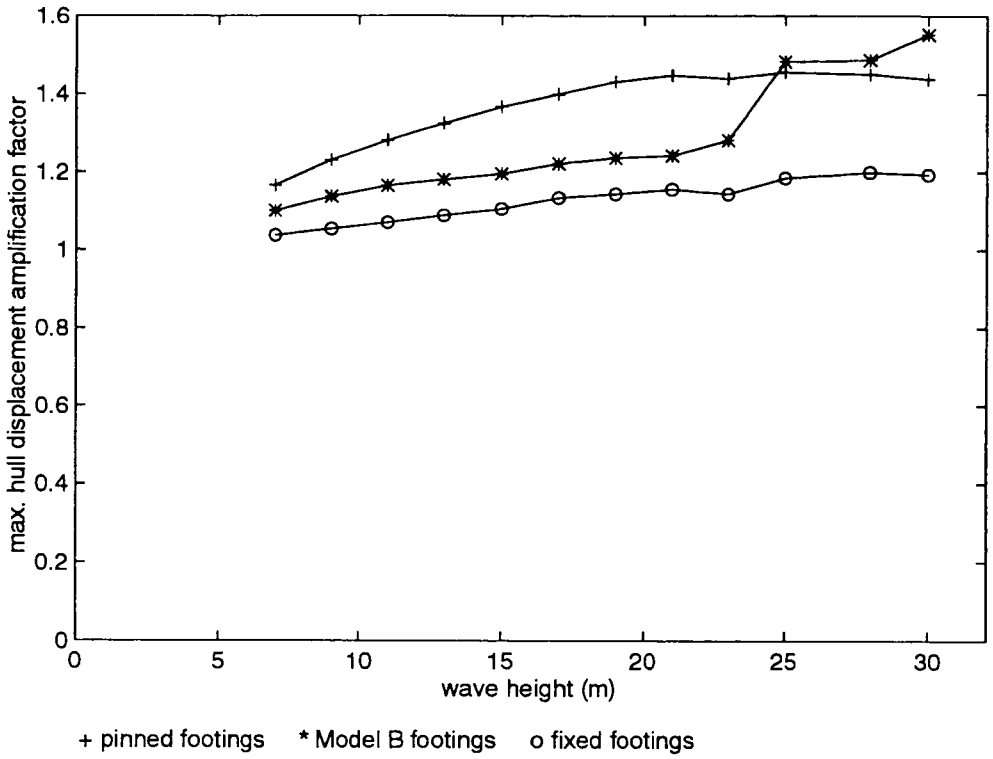

[b] double amplitude amplification factor

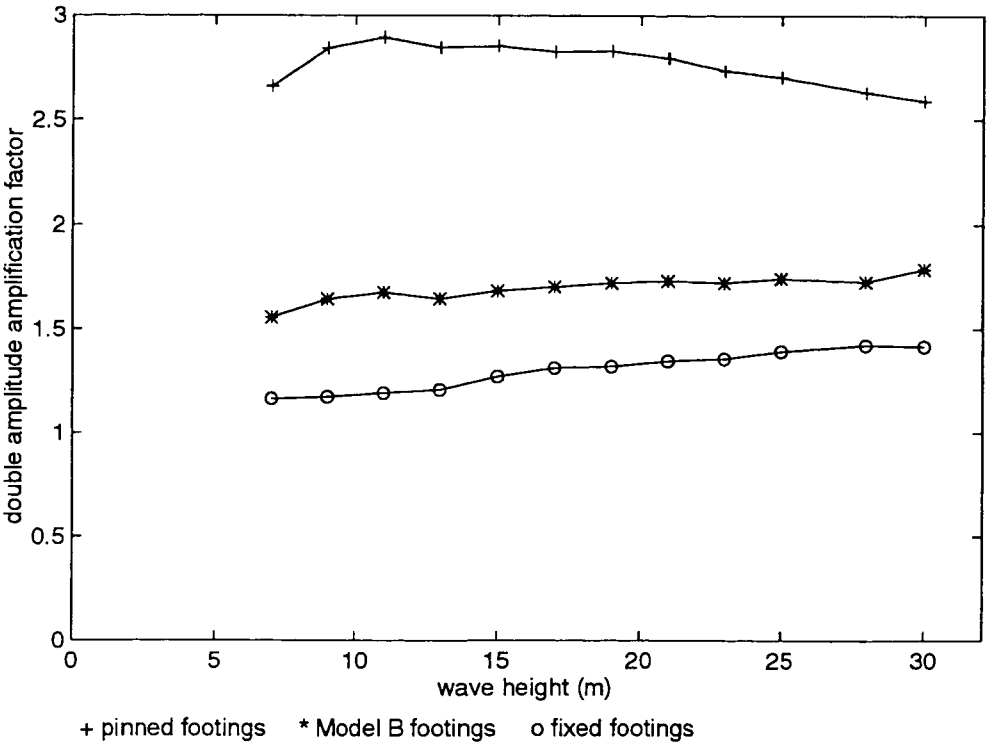

FIGURE 6.36 Variation of the amplification factors with wave height

[a] power index for the maximum quasi-static hull displacement

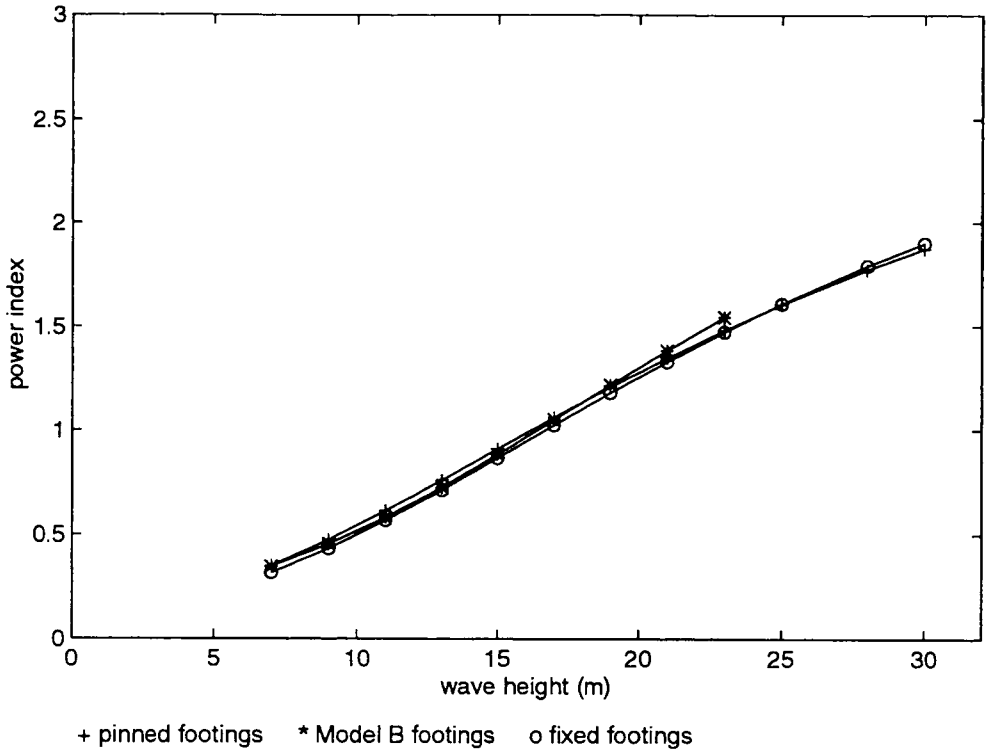

[b] power index for the double amplitude of quasi-static hull displacement

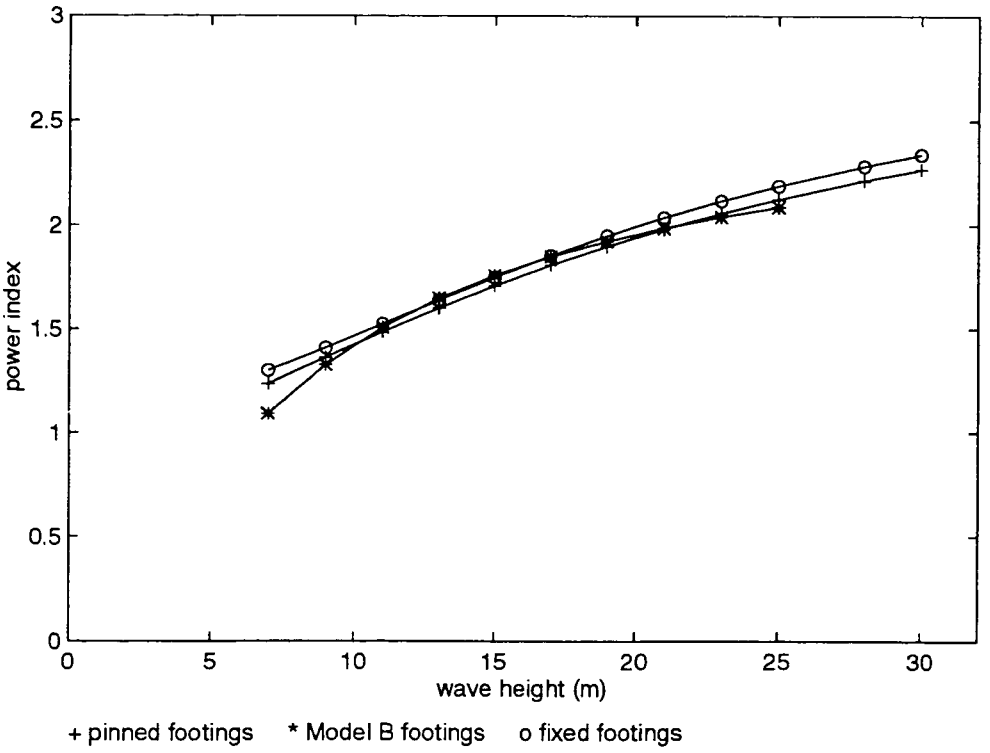

FIGURE 6.37 Variation of the quasi-static power index with wave height

[a] power index for the maximum dynamic hull displacement

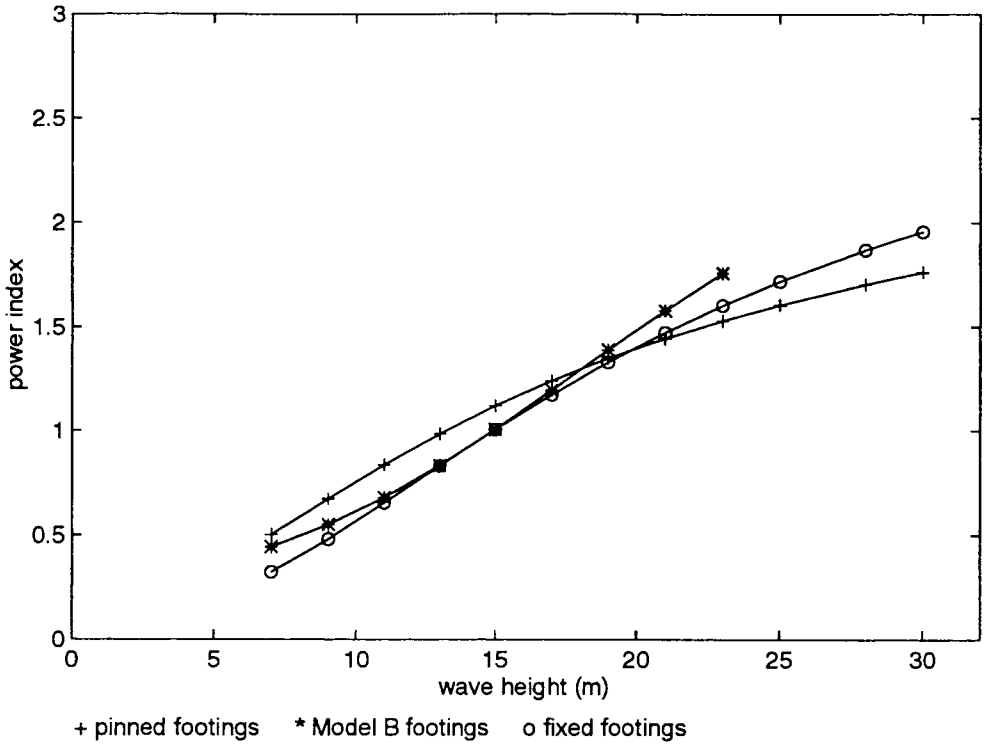

[b] power index for the double amplitude of dynamic hull displacement

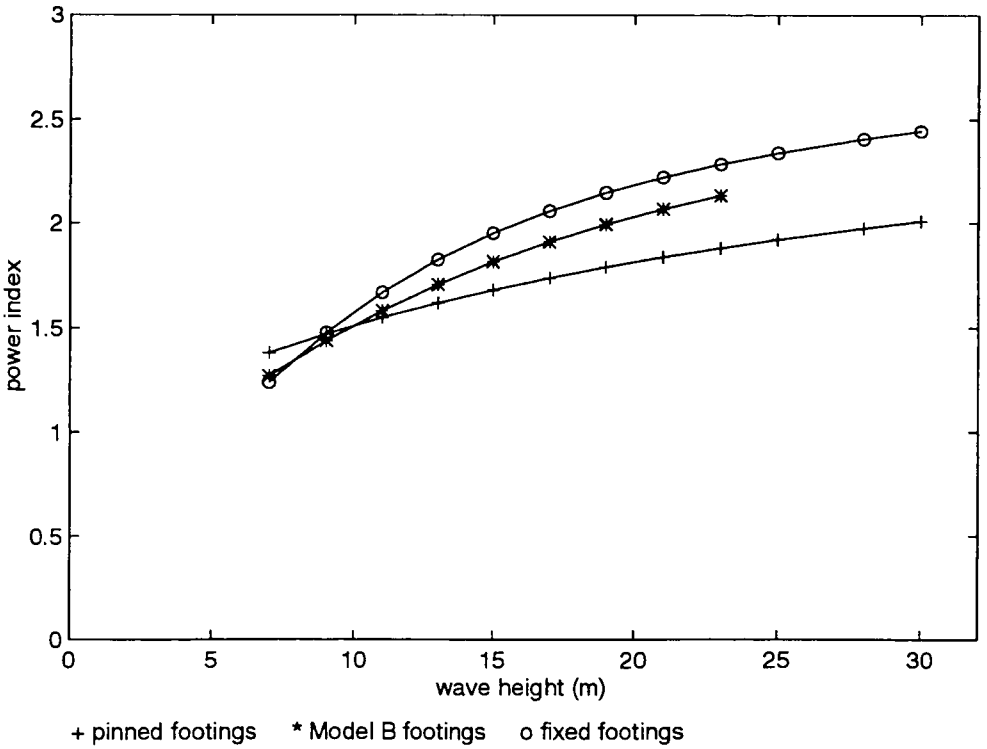

FIGURE 6.38 Variation of the dynamic power index with wave height